

ANNUAL REPORT



FR9704841

9



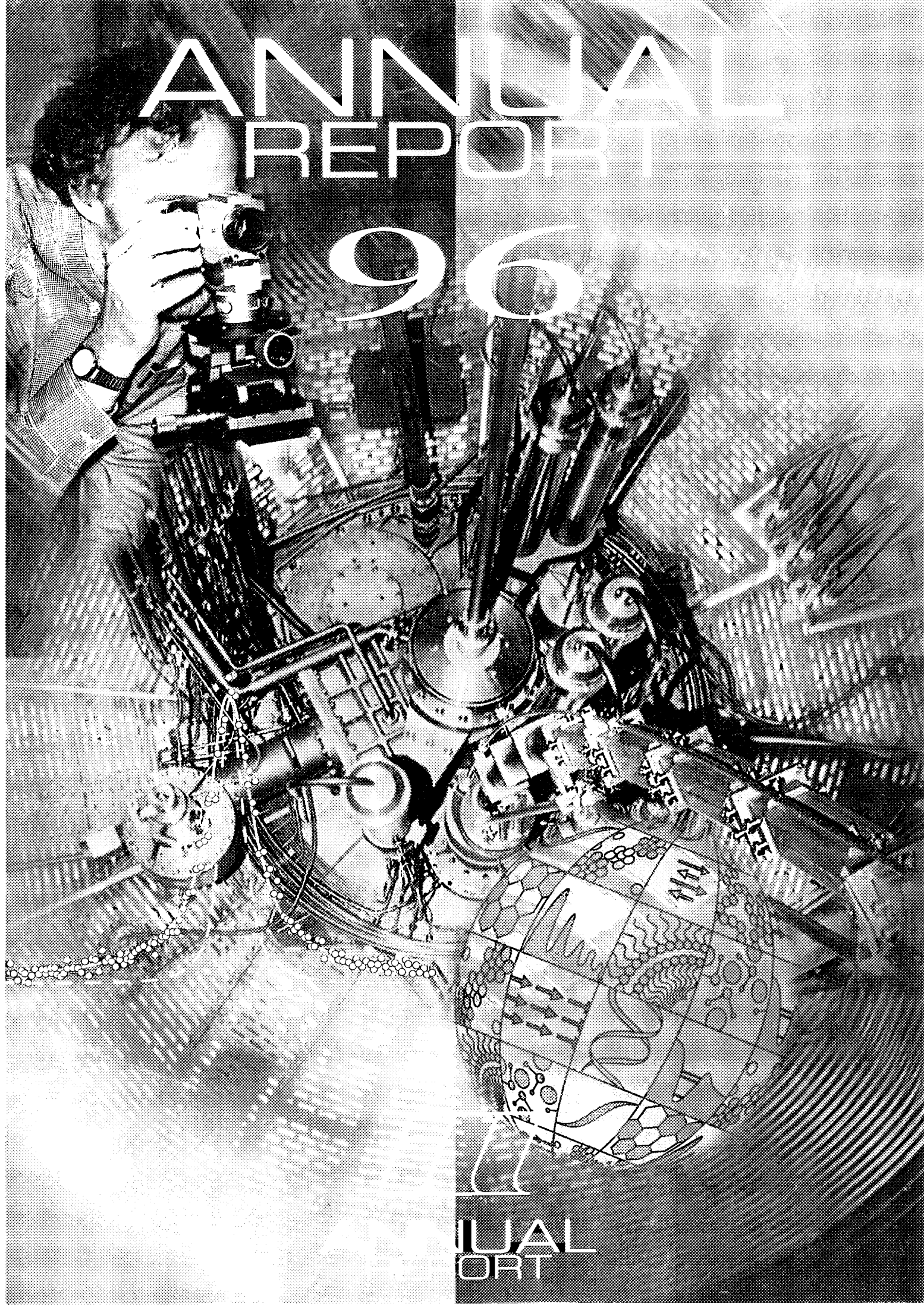
Cession INIS
enreg. le :
N° TRN : F.R. 3. 7. 6. 6. 7
Destination : I.R.E.C.

29 09

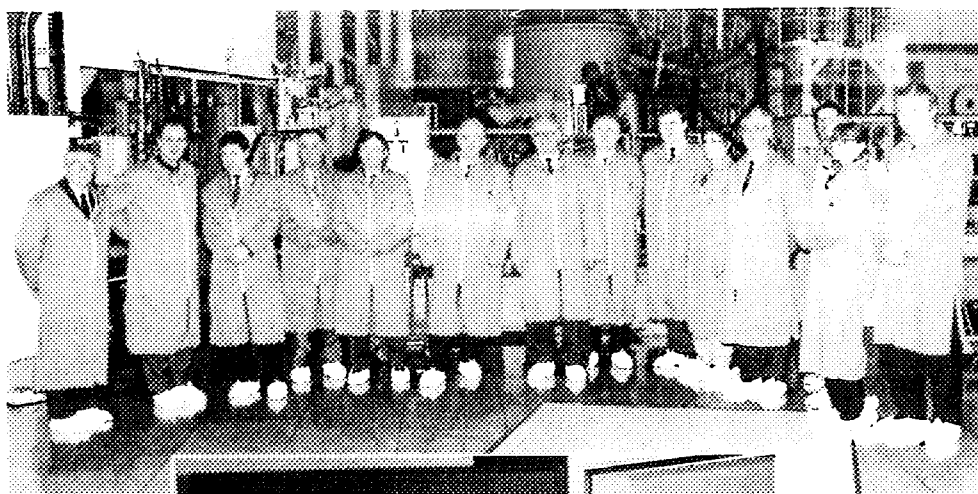


ANNUAL
REPORT

ANNUAL REPORT 96



ANNUAL
REPORT



Visit of Russian delegation headed by V.G. Vinogradov (March 1996).











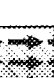


*Coffee break at the Colloquium in honour of Heinz Maier-Leibnitz's 85th birthday (June 1996).
From left: Heinz Maier-Leibnitz, Erwin Bertaut.*



Visit of the Préfet de l'Isère, Jean-René Garnier, in August 1996. From left: Jean-Marie Astruc, Alan Leadbetter, Jean-René Garnier, Reinhard Scherm.

CONTENTS

	DIRECTOR'S MESSAGE	4
1	SCIENTIFIC REVIEWS	7
	MATERIALS SCIENCE	8
	LIQUIDS AND GLASSES	16
	SOFT MATTER	22
	BIOLOGY	28
	SURFACES AND THIN FILMS	34
	MOLECULAR SPECTROSCOPY	37
	QUANTUM SYSTEMS	44
	FUNDAMENTAL PHYSICS	48
	STRONGLY CORRELATED ELECTRON SYSTEMS	54
	MAGNETISM - STRUCTURE	59
	MAGNETISM - DYNAMICS	66
2	WORKSHOPS	73
3	NEW REVIEWS	77
4	EXPERIMENTAL REVIEWS	99
5	FACTS REVIEWS	105
6	PUBLICATIONS	109

.....
■ In 1996 ILL completed its second year of operation since the refurbishment of the reactor. It was also a year in which, for the first time ever, the reactor functioned without a single « chute de barres » (i.e. unforeseen shutdown). The nominal complement of 25 ILL instruments is now fully operational and in addition a total of 11 CRG instruments are either under construction or already being operated by eight Collaborating Research Groups (CRG) from research institutes and universities in the member countries. Some of these instruments are already partially included in the ILL experimental user programme.

The demand for beam time and the quality of the many proposals received were both as high as ever. Some 800 experiments were conducted on the Institut's suite of scheduled instruments, including the ILL share of time on the CRG instruments. In 1996 two new instruments came into full operation: a second high-resolution back-scattering spectrometer, IN16, and a second small-angle neutron scattering instrument, D22, which has been fully operational since the middle of the year when problems with the new detector were eventually overcome.

The most notable event of the year was undoubtedly the accession of two new Scientific Members to the Institut. On 7 June 1996, a general agreement was signed between the Russian Minister of Atomic Energy (MinAtom), Prof. V. Mikhailov, the CEA and ILL. This agreement includes Russian scientific membership of ILL, which officially came into effect on 14 November 1996 with the signing of a commercial contract for the delivery of uranium for ILL's high-flux reactor. On 28 October 1996, a further agreement was signed with INFN of Italy which thereby joined the ranks of the Institut's Scientific Members on 1 January 1997, thus bringing the total number of countries participating in ILL to eight. We are extremely pleased to welcome these two new member countries and their scientists to participate in the scientific life of ILL.

1996 also brought us a major step forward towards ensuring the reactor fuel cycle on a long-term basis, thanks not only to the above-mentioned contract with MinAtom but also to the positive outcome of negotiations to have spent fuel elements reprocessed in France. The Associates have had to make great efforts to find the additional funding needed to meet the fuel cycle requirements and their success in doing so is a measure of the continuing support for ILL in difficult financial times. On a less optimistic note, however, ILL has to reduce its normal annual operating budget (i.e. excluding the fuel cycle) by 6 MF for the years to come. In the short term this will cause delays in planned instrument upgrades, the longer term effects are currently being examined.

On a personal note, I wish to record two honours conferred recently on ILL staff and offer my congratulations: Ekkehardt Bauer, Head of the Reactor Division, has been nominated « Chevalier de l'Ordre National du Mérite » by the President of the French Republic, and Anton Oed has been awarded the 1997 Robert-Wichard-Pohl prize by the Deutsche Physikalische Gesellschaft (the German Physical Society) for his work in the field of microstrip detectors.

As you can see, ILL's Annual Report has been given a fresh new look. There is always such an embarrassment of riches that it is impossible to cover everything. We have therefore decided to emphasise some of the scientific highlights of the year and to give brief descriptions of some of the more important technical developments, while at the same time significantly reducing the length of the Report and trying to make it more easily readable. The facts and figures concerning operations, users, personnel and finance can be found towards the end of the Report and, last but very importantly, comes the list of publications, which is growing towards previous levels now that we are well and truly back in full operation.

I express my gratitude to all those who have contributed to ILL's success in 1996, in particular the ILL staff and, of course, our users who continue to come and perform experiments which produce the kind of exciting results you will find in what follows.

.....
■ Avec 1996 s'achève la deuxième année de fonctionnement de l'ILL depuis la remise en état du réacteur. Pour la première fois cette année, le réacteur a fonctionné sans aucune chute de barre. Les 25 instruments officiels de l'ILL sont maintenant entièrement opérationnels. A ceux-ci viennent s'ajouter 11 instruments, en cours de construction ou déjà exploités par 8 Groupes de Collaboration Scientifique (CRG) en provenance des instituts de recherche et des universités des pays membres. Une partie du temps de faisceau ILL de certains des instruments CRG est déjà inclus dans le programme expérimental des utilisateurs.

La demande de temps de faisceau et la qualité des nombreuses propositions présentées restent aussi élevées que par le passé. 800 expériences ont été réalisées sur les instruments de l'ILL officiellement programmés, en incluant le temps de faisceau mis à la disposition de l'ILL sur les instruments CRG. En 1996, deux nouveaux instruments ont été mis en service : un deuxième spectromètre à rétrodiffusion et haute résolution, IN16, et un deuxième instrument de diffusion aux petits angles, D22, qui est entièrement opérationnel depuis le second semestre 1996, malgré les problèmes initialement rencontrés avec le nouveau détecteur et qui ont pu être surmontés.

L'événement le plus important de l'année a sans aucun doute été l'adhésion de deux nouveaux Membres Scientifiques à l'ILL. Le 7 juin 1996, un accord général, qui incluait la participation de la Russie à l'ILL en tant que membre Scientifique, était signé entre le Ministre Russe de l'Energie Atomique (MinAtom), Prof. V. Mikhailov, et le CEA/ILL. La participation de la Russie est officiellement entrée en vigueur le 14 novembre 1996 avec la signature d'un contrat commercial relatif à la livraison d'uranium pour le réacteur à haut flux de l'ILL. Le 28 octobre 1996, un second accord était signé à Rome avec l'INFN d'Italie qui rejoint le cercle des partenaires scientifiques à compter du 1er janvier 1997, portant ainsi à huit le nombre des pays partenaires de l'ILL. Nous sommes heureux d'accueillir ces deux nouveaux membres ainsi que leurs chercheurs au sein de la vie scientifique de l'ILL.

L'année 1996 aura également été une année importante pour l'Institut, puisqu'une étape décisive a été franchie pour garantir à long terme la totalité du cycle du combustible pour le réacteur, d'une part grâce au contrat avec MinAtom mentionné ci-dessus, mais également grâce aux résultats positifs des négociations qui permettront le retraitement en France des éléments combustibles irradiés. Les Associés ont eu à faire d'importants efforts pour trouver les fonds supplémentaires nécessaires pour garantir le cycle du combustible. Leur succès témoigne de leur volonté de continuer à apporter un ferme soutien à l'ILL dans cette période de difficultés financières.

Cependant, tout n'est pas positif : l'ILL doit réduire son budget de fonctionnement normal (hors cycle combustible) de 6 MF pour les prochaines années. A court terme, cette réduction aura pour conséquence des retards dans le programme prévu pour l'amélioration des instruments. Les conséquences à long terme sont en cours d'étude.

C'est avec plaisir que je mentionne ici les distinctions qui ont été attribuées à deux membres du personnel ILL : Ekkehardt Bauer, Responsable de la Division réacteur, a été nommé « Chevalier de l'Ordre National du Mérite » par le Président de la République Française, et Anton Oed a reçu le Prix « Robert-Wichard-Pohl » de la Deutsche Physikalische Gesellschaft (Société Allemande de Physique) pour ses travaux sur le développement des détecteurs microstrip. Nous leur adressons toutes nos félicitations.

Comme vous pouvez le constater, le rapport annuel se présente cette année sous une forme nouvelle. Vu le nombre important d'expériences de haute qualité réalisées à l'ILL, il était difficile de toutes les mentionner. Nous avons donc décidé de mettre l'accent sur certains événements scientifiques majeurs et de décrire brièvement les développements techniques les plus importants, tout en réduisant sensiblement la longueur du rapport afin qu'il soit, nous l'espérons, plus facile à lire. Les faits et chiffres relatifs au fonctionnement, aux utilisateurs, au personnel et aux finances se trouvent à la fin du rapport, suivis par la liste des publications, dont le nombre est en augmentation et se rapproche de celui atteint dans le passé maintenant que l'Institut fonctionne à nouveau normalement.

Je voudrais adresser mes remerciements à tous ceux qui ont contribué au succès de l'ILL en 1996, en particulier aux membres du personnel de l'ILL, et, bien sûr, à nos utilisateurs qui viennent à l'ILL pour réaliser leurs expériences. C'est à eux tous que nous devons les résultats passionnants décrits ci-après.

.....
☛ 1996, das zweite Jahr seit der Erneuerung des Reaktors, war auch das erste Jahr, in dem der Reaktor ohne « chute de barres » (= Schnellabschaltung) gelaufen ist. Die offiziellen 25 Instrumente sind inzwischen in vollem Betrieb. Hinzu kommen noch 11 Instrumente, die von acht verschiedenen « Collaborating Research Groups » aus Forschungsinstituten und Universitäten in den Mitgliedsländern gebaut oder betrieben werden. Einige dieser CRG-Instrumente tragen auch schon zum Nutzer-Programm bei.

Nachfrage und Qualität der zahlreichen Proposals waren so hoch wie je zuvor. So wurden denn 800 Experimente an den offiziell programmierten Instrumenten des ILL - inklusive der ILL Strahlzeit an CRG-Instrumenten - durchgeführt. Im Berichtsjahr gingen schließlich zwei neue Instrumente in Betrieb: das zweite Rückstreuспекrometer IN16 sowie die zweite Kleinwinkel-Camera D22, letztere erst in der zweiten Jahreshälfte, nachdem ernste Probleme mit dem Multidetektor gelöst waren.

Als herausragendes Ereignis des Jahres ist der Beitritt von zwei neuen wissenschaftlichen Mitgliedsländern zu berichten. Am 7. Juni 1996 unterzeichneten der russische Minister für Atomenergie (MinAtom), Prof. V. Mikhailov, sowie das CEA und ILL ein allgemeines Abkommen, das auch die wissenschaftliche Mitgliedschaft enthält. Letztere trat offiziell am 14. November 1996 mit der Unterzeichnung eines Handelsabkommens zur Lieferung von Uran für den Hochflußreaktor des ILL in Kraft. Des Weiteren wurde am 28. Oktober 1996 in Rom ein Vertrag mit dem italienischen INFN unterzeichnet. Somit sind mit dem Beitritt Italiens vom 1. Januar 1997 an acht Länder am ILL beteiligt. Mit großer Freude begrüßen wir die beiden neuen Mitgliedsländer und laden ihre Wissenschaftler ein, am wissenschaftlichen Leben des Instituts teilzuhaben.

Das Jahr 1996 brachte uns dem Ziel, den Brennstoff-Kreislauf für den Reaktor langfristig zu sichern, einen großen Schritt näher: einmal der schon erwähnte Vertrag mit MinAtom, zum anderen konnten Verhandlungen abgeschlossen werden, abgebrannte Brennelemente in Frankreich zu entsorgen. Die Gesellschafter des ILL hatten große Anstrengungen unternommen, um hierfür zusätzliche Geldmittel bereitzustellen. Dieser Erfolg zeugt auch vom festen Willen, das ILL in finanziell schwierigen Zeiten zu stützen. Allerdings geht dies nicht ohne Wermutstropfen vorüber: für die kommenden Jahre mußte das ILL sein Normalbudget (ohne Brennstoffkosten) um 6 MF reduzieren. Dadurch wird sicher die geplante Modernisierung einiger Instrumente verzögert; die langfristigen Auswirkungen werden derzeit überprüft.

Mit Vergnügen berichte ich über die Ehrung zweier Mitarbeiter: Ekkehardt Bauer, Leiter des Reaktors, wurde zum « Chevalier de l'Ordre National du Mérite » ernannt und Anton Oed wird von der DPG (Deutsche Physikalische Gesellschaft) der Robert-Wichard-Pohl Preis 1997 für « seine bedeutenden Leistungen bei der Entwicklung des Mikrostrip-Gasdetektors » verliehen. Herzliche Glückwünsche!

Wie Sie sehen wurde der Jahresbericht diesmal neu gestaltet. Es ist unmöglich, über alle Ergebnisse zu berichten. Statt dessen werden wir einige der wissenschaftlichen Glanzlichter des vergangenen Jahres beleuchten und kurz über besondere technische Entwicklungen berichten. Der Bericht wird so kürzer und - hoffentlich - auch leichter lesbar. Zum Abschluß finden Sie noch Fakten und Zahlen über Betrieb, Nutzer, Personal und Finanzen. Es schließt sich die Publikationsliste an, die jetzt, da das Institut wieder voll in Betrieb ist, zum gewohnten Umfang anschwillt. Meinen tiefen Dank spreche ich allen aus, die zum Erfolg des ILL im Jahre 1996 beitrugen, zu allererst dem Personal des Instituts, aber auch unseren Nutzern, die hierherkommen und experimentieren. Sie erzielten alle die schönen Ergebnisse, die im folgenden beschrieben sind.

REINHARD SCHERM

DIRECTOR'S



The Deutsche Physikalische Gesellschaft has awarded the 1997 Robert-Wichard-Pohl prize to Anton Oed for his work in the field of microstrip detectors.



Reinhard Scherm has been awarded the 1997 Gentner-Kastler prize (a joint prize of the Deutsche Physikalische Gesellschaft with the Société Française de la Physique) for his outstanding contributions to explain the dynamical structure of quantum liquids using thermal neutron scattering.



Ekkehardt Bauer, Head of the Reactor Division, has been nominated « Chevalier de l'Ordre National du Mérite » by the President of the French Republic.

SCIENTIFIC HIGHLIGHTS

1

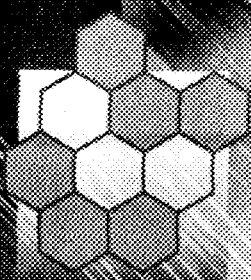
IN 1996 THE REACTOR OPERATED FOR 225 DAYS AND ABOUT 800 EXPERIMENTS WERE SCHEDULED FOR ILL USERS. THESE EXPERIMENTS RANGE FROM EXPERIMENTS WHICH MAY LAST FOR MANY YEARS, LIKE THE SEARCH FOR THE NEUTRON ELECTRIC DIPOLE-MOMENT, TO ONE OR TWO-DAY EXPERIMENTS USING POWDER DIFFRACTION OR SMALL-ANGLE SCATTERING. THE SUBJECT MATTER OF THE EXPERIMENTS COVERS AN ENORMOUS RANGE OF SCIENTIFIC DISCIPLINES FROM BIOLOGY TO FUNDAMENTAL PHYSICS, INCLUDING EXPERIMENTS ON CRYSTALS, QUASI-CRYSTALS, GLASSES, LIQUIDS, GASES AND INTERFACES AND IN THE MANY DIFFERENT KINDS OF EXPERIMENT, NEUTRONS PROBE DISTANCE SCALES OF LESS THAN 10^{-5}\AA TO MORE THAN 1000\AA AND TIME-SCALES OF GREATER THAN 10^{-7}s TO CA. 10^{-15}s .

IT IS CLEAR THAT PRESENTING AN ANNUAL REPORT WHICH ADEQUATELY DESCRIBES THIS BREADTH OF ACTIVITY PRESENTS CERTAIN DIFFICULTIES. THE ULTIMATE MEASURE OF THE SCIENTIFIC QUALITY OF THE RESEARCH CARRIED OUT AT THE ILL MUST BE THE RESULTING PUBLICATIONS AND THESE DO NOT GENERALLY APPEAR IN THE SAME YEAR AS THAT IN WHICH THE EXPERIMENTS ARE CARRIED OUT — THEY ARE THEN OF COURSE ACCESSIBLE TO ALL BUT ARE SPECIALISED. ON THE OTHER HAND, SHORT REPORTS ARE REQUIRED ON ALL EXPERIMENTS CARRIED OUT AT THE ILL AND THESE ARE PUBLISHED IN THE ANNEX TO THE ANNUAL REPORT. WE HAVE THEREFORE DECIDED TO PRESENT HERE SELECTED HIGHLIGHTS FROM THE LAST YEAR TO TRY TO GIVE A FLAVOUR OF THE QUALITY AND BREADTH OF THE RESEARCH CARRIED OUT ON THE WIDE VARIETY OF ILL INSTRUMENTS, IN A FORM WHICH IS ACCESSIBLE TO A WIDE SCIENTIFIC READERSHIP. IT IS CLEAR THAT SELECTING SOME 30 HIGHLIGHTS FROM SUCH A LARGE RANGE AND QUANTITY OF ACTIVITY MEANS THAT NOT ALL AREAS OF RESEARCH ARE INCLUDED BUT WE WILL TRY FROM YEAR TO YEAR TO GIVE COVERAGE TO ALL THE MAIN AREAS. TO THIS END WE INVITE OUR USERS TO SUBMIT HIGHLIGHTS OF THEIR OWN RESEARCH WHICH THEY FEEL MERIT INCLUSION IN FUTURE REPORTS.

SCIENTIFIC HIGHLIGHTS



FR9704842



STRUCTURAL CHANGES IN IRRADIATED STEELS: AN EXAMPLE OF INDUSTRIAL STUDIES

■ R. MAY (ILL),
■ S. MILOUDI (EDF/DER).

THE SECURITY OF NUCLEAR REACTORS DEPENDS ON KNOWLEDGE ABOUT THE DEGRADATION OF SOME OF THEIR COMPONENTS BY NEUTRON IRRADIATION. THIS PHENOMENON IS WELL KNOWN ON THE BASIS OF INTERNATIONAL STUDIES AND ON RESULTS FROM RESEARCH REACTORS. IT IS ANTICIPATED IN THE DESIGN OF POWER REACTORS SO AS TO ENSURE THEIR SAFE OPERATION. THE LONG-TIME BEHAVIOUR OF REACTOR COMPONENTS IS THE OBJECT OF INTENSIVE STUDIES DIRECTED BY ÉLECTRICITÉ DE FRANCE (EDF), THE FRENCH NATIONAL ELECTRICITY COMPANY. THESE STUDIES SERVE TO VERIFY THAT THE PREDICTIONS CONCERNING MECHANICAL PROPERTIES OF REACTORS HOLD, BUT ALSO TO BETTER UNDERSTAND THE PROCESSES LEADING TO DEGRADATION IN ORDER TO FIND MEANS FOR SAFELY INCREASING THE LIFETIMES OF POWER PLANTS.

INTRODUCTION

The reactor vessel as the central part of a reactor is one of its most irradiated components. In French reactors, it has dimensions of 4.4 m diameter and nearly 12 m height; the outer wall is 23 cm thick. The lower part of the vessel is embedded in concrete; its replacement would be very expensive and can be considered as nearly impossible.

Steel, an alloy containing mainly iron and a few additional elements depending on the purpose it is made for, but also unwanted impurities (for example copper from recycled automobile steel), becomes harder when it is irradiated.

As a consequence, irradiated steel is less extensible, and the transition from elasticity to rupture is more abrupt and less predictable (Fig. 1a).

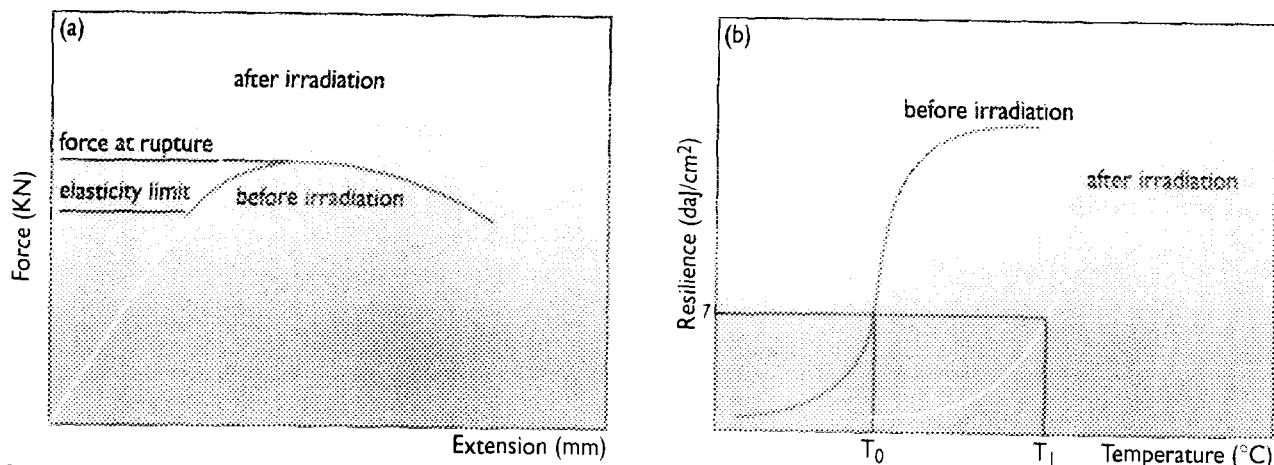


FIGURE 1: a) Traction resistance : Force as a function of extension, b) Ductile-to-brittle transition curves: Resilience as a function of temperature.

Another worrying aspect is that the ductile to brittle transition temperature is increased under irradiation (Fig. 1b). Normally, this temperature is relatively low; virgin steel is ductile even at room temperature.

After irradiation, steel may be adequately ductile at working temperatures (about 300°C), but when the reactor is switched off and the temperature of the vessel drops, it could get into a state where it cannot resist residual mechanical tensions. The sensitivity of steel to irradiation depends on its composition. Elements that are known to increase it are copper, nickel and phosphorus. Steels used in French power plants are particularly low in copper (< 800 ppm) contrary to American steels (> 2000 ppm).

The metallurgical properties of the vessel material are constantly monitored by the use of specimens that are contained in capsules which are fixed within the reactor vessel at a distance closer to the core than the reactor wall. The radiation dose in the capsules is therefore two to three times higher than in the vessel steel. The samples age correspondingly faster and thus allow one to study the «future» of the wall material. A multitude of techniques is applied including mechanical tests, field emission microscopy and also small-angle neutron scattering.

THE ROLE OF NEUTRON SCATTERING

The increase of the brittleness of steel by irradiation is due to the formation of clusters. The clusters are very small (in the range of 10 Å) and have a very low contrast for optical and electron microscopy; they contain different amounts of different elements. All of these contribute to a potential mixture of particles giving a highly convoluted pattern with the usual scattering methods. Neutrons are ideal for small-angle scattering studies of steels, because they easily penetrate relatively thick samples (up to several millimetres).

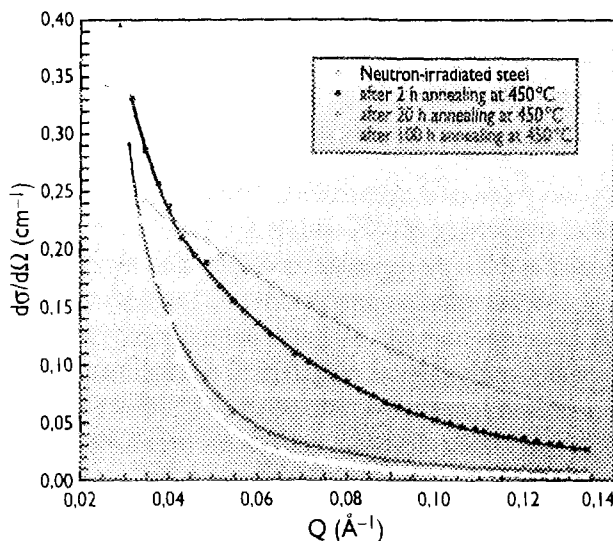


FIGURE 2: Difference intensities of irradiated steels before and after annealing for different times as a function of momentum transfer. The curves show the neutron small-angle scattering curves in the direction perpendicular to a magnetic field (1.4 T) after subtraction of that from a non-irradiated reference sample. The scattering contrast is mainly between the magnetic matrix and less magnetic clusters.

They also sense magnetic fields which can be used to enhance the contrast of the clusters with respect to the matrix: The iron in the matrix is ferromagnetic, contrary to the elements which, according to atom probe measurements, are found most frequently in the clusters (copper) and around them (phosphorus). This creates two phases of different scattering density.

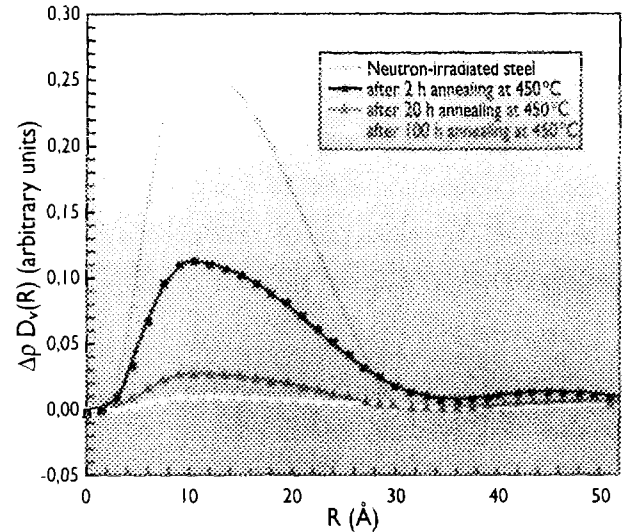


FIGURE 3: Contrast-weighted volume distribution functions (Fourier transforms of the curves in Fig. 2) of irradiated steels before and after annealing for different times. The oscillations at larger dimensions are artifacts caused by the mathematical procedure.

When one subtracts the scattering perpendicular to a strong magnetic field (1.4 Tesla) of a reference sample that has not been irradiated from that of samples that have been irradiated and annealed (heated at high temperatures, about 450°C) for 2 to 100 h, one can observe the disappearance of a relatively flat difference scattering pattern (Fig. 2). On the basis of the magnetic-contrast argument above, one can make the assumption that one deals with a mixture of simple homogeneous particles (spheres in our model) that disappear upon annealing. Fig. 3 shows the development of the contrast-weighted volume distribution of the particles with annealing time. This indicates that irradiation produces precipitates in the 10 Å size range which get redissolved by annealing. The scientists involved in this work hope that in the future such results, combined with those of other techniques, will allow them to develop suitable thermal treatment techniques which will enable reactors to be used safely for longer times, i.e. more economically.



The EDF experimental team from left: Salem Miloudi, Patrick Miguet, Jean-Paul Massoud, Arnaud Hennion.



RESIDUAL-STRESS MEASUREMENTS

- A.N. EZEILO, G.A. WEBSTER (IMPERIAL COLLEGE),
- P.J. WEBSTER (SALFORD UNIVERSITY).

BECAUSE NEUTRONS CAN PENETRATE DISTANCES OF UP TO 50 MM IN MOST ENGINEERING MATERIALS, THIS MAKES THEM UNIQUE FOR ESTABLISHING RESIDUAL-STRESS DISTRIBUTIONS NON-DESTRUCTIVELY. D1A IS PARTICULARLY SUITED FOR THROUGH-SURFACE MEASUREMENTS AS IT DOES NOT SUFFER FROM INSTRUMENTAL SURFACE ABERRATIONS COMMONLY FOUND ON MULTI-DETECTOR INSTRUMENTS, WHILE D20 IS BEST FOR FAST INTERNAL-STRAIN SCANNING.

TWO EXAMPLES ARE PRESENTED OF RESIDUAL-STRESS MEASUREMENTS, IN A SHOT-PEENED MATERIAL, AND IN A WELD, TO DEMONSTRATE THE ATTRACTIVE FEATURES OF BOTH INSTRUMENTS.

Residual stresses can exist in engineering components in the absence of externally applied loads. As these stresses can be large and influence the load carrying capacity and resistance to fracture of components, it is necessary for engineers to know their magnitude and distribution. In general compressive stresses at surfaces provide resistance to fracture, while tensile stresses tend to promote fracture. Residual stresses can be introduced into components during manufacture, for example by welding, forging, heat and surface treatment processes, and also by loading during service. Several methods are available for measuring these stresses including X-ray diffraction, neutron diffraction, hole drilling, sectioning and magnetic techniques. However, because neutrons can penetrate distances of up to around 50 mm in most engineering materials, this makes them unique for establishing residual stress distributions non-destructively throughout the interior of components.

In diffraction techniques the measured quantity is the lattice d -spacing which varies according to the level of stress and location within the component. Stresses need to be known to within 20-30 MPa, which is typically an accuracy in $\Delta d/d$ of $1 \cdot 10^{-4}$. Other measuring considerations include: masking the neutron beam to produce small sampling volumes; accurate automated positioning of the specimen; stress gradients; measuring in at least 3 orientations; counting efficiency to keep measuring times low (< 2 hrs) and choice of a suitable reflection, preferably near $90^\circ 2\theta$. Strains are obtained by comparing the measured d -spacings with the unstressed d_0 value. Diffraction elastic constants are used to convert strains to stress.

Two instruments at the ILL are used for residual-stress measurements, D1A which provides moderate flux with medium resolution and D20 which provides high flux at relatively low resolution. D1A is particularly suited for the important through-surface measurements, as it does not appear to suffer from severe instrumental surface aberrations commonly found on multidetector instruments. D20 is best for fast internal-strain scanning.



FIGURE 1: D1A in stress configuration.

D1A, as seen in Fig. 1, is equipped for residual-stress measurements with a theodolite, laser, closed circuit television, computer controlled sample manipulation system and masking slits in the beam paths. Manufacturing processes that have been studied on D1A and D20 include cold hole expansion, autofrettage, manufacturing and service stresses in railway rails, shot peening, laser surface remelting, laser cladding, extrusion and welds.

SHOT-PEENING RESIDUAL STRESS

Most engineering failures initiate at the surface of a component as this is the region that is usually most highly stressed, contains manufacturing defects or is exposed to a harsh chemical environment. Although polishing and chemical treatment may improve resistance to crack initiation, the presence of compressive residual-stresses is beneficial. An effective surface-treatment process for introducing compressive residual-stresses is shot peening. This is a mechanical process involving the bombardment of the surface with small spherical particles, plastic deformation of the surface layers and the production of a steep residual-stress field which is compressive at the surface. It is a process widely used in the aerospace industry to improve fatigue life. A variety of shot-peened materials have been successfully examined on D1A.

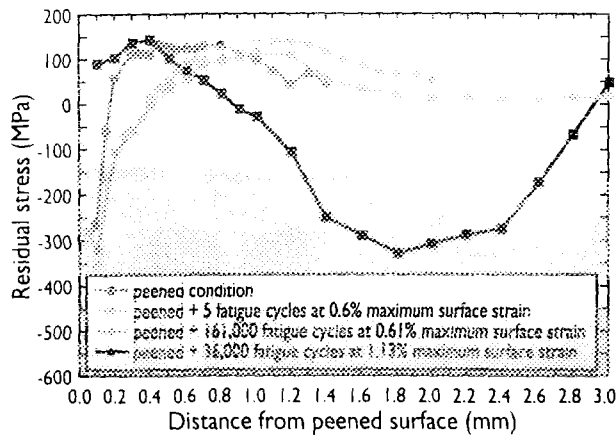


FIGURE 2: In-plane shot-peening residual stresses.

Shot-peened residual stresses have been examined before and after cycles of fatigue load. Results are presented in Fig. 2, of measurements made on D1A, showing the beneficial effect of the shot-peening process. The effect of fatigue cycling is seen to redistribute the initial residual-stress profile.

RESIDUAL STRESSES IN FLASH-BUTT WELDED RAILWAY RAILS

Railway rails are made in various lengths, typically around 40 m. They may be bolted together, but bolting has its disadvantages. The joints are relatively expensive to make and maintenance costs are high. Rail hammer occurs as a wheel passes over the expansion gap - generating the traditional sound of moving trains - and the repeated impacts can initiate and propagate horizontal web cracks from defects and tensile 'hot-spots' at the rail ends. Fretting at bolt holes can lead to cracks and broken end pieces.

Although it will always be necessary to bolt together some sections of rail, wherever possible rails are now joined by welding. Welding is generally a cheaper process and usually produces a superior joint. As a welded rail, continuous hammer and impact noise and the related fatigue problems are eliminated, as also are bolt holes and their associated problems. However, residual-stress patterns arise due to the various welding processes and these can, in rare cases, lead to particular types of weld-induced failures. The few failures that do occur are invariably transverse, in contrast to the angled or horizontal crack failures of bolted joints.

Typically, sections of rail are flash-butt welded together in the factory by passing large current through the rails sufficient to cause the ends to melt as they are brought together. Excess material is removed and the top surface is ground

to the rail profile. Lengths of about 300 m are then transported for laying in track where they are usually joined, by an aluminio-thermic welding process, under tension to avoid buckling on hot days. Typically about 80-90% of weld tracks are flash-butt welds. They are usually very reliable, as they must be, because even occasional failure could have serious consequences. Neutron strain scanning has been used to study the residual-stress patterns generated by flash-butt welding in a rail. D20 was employed as a fast-area scanner to determine the residual strains in the principal directions over a longitudinal/vertical central plane through a weld. The rail section was 400 mm long and the weld was at the centre, at the 200 mm position. The longitudinal residual-strain contours, which are the most significant, are shown in Fig. 3. The pattern shows the influence of the welding process, which extends to about 50 mm either side of the weld itself. Away from the weld the pattern is typical of unwelded rail, with tension in the head and foot (shown in red) balanced by compression (green) in the web. In the weld region, the pattern is reversed with strong compression (green > blue) in the head and foot and strong tension (deeper red) in the web. Fortunately this longitudinal strain pattern is generally desirable as compression at the upper and lower bearing surfaces will tend to inhibit crack propagation from surface defects. On the other hand cracks would be encouraged to grow in the web region if there were internal material defects such as inclusions or porosity. Modern welding techniques are designed to ensure that such defects are very rare as evidenced by the generally high reliability of welded rails.

Neutron strain scanning is now being adopted by advanced industries as a non-destructive technique for residual-stress determination, but industry must be assured that measurements are always made to an agreed standard.

The ILL is actively participating in an international project under the auspices of VAMAS (Versailles Project on Advanced Materials and Standards), aimed at establishing accurate and reliable procedures for making neutron diffraction residual-strain/stress measurements. VAMAS will provide the technical basis for the drafting of an international standard. The VAMAS project, designated TWA20, held its inaugural meeting on Jan 9-10, 1996 at the ILL and was attended by leading practitioners and representatives from Canada, Europe, Japan and the USA.

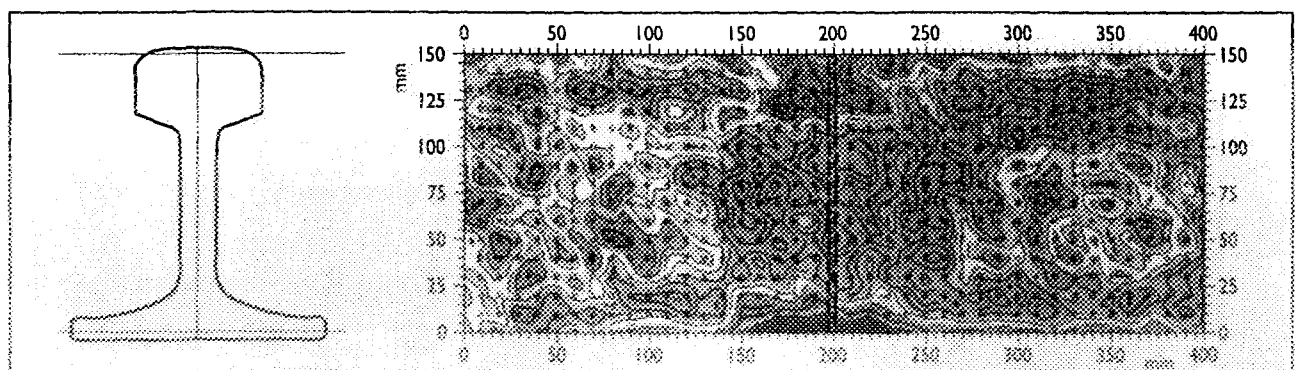


FIGURE 3: Longitudinal strain in flash-butt welded rail.



FR9704844

THE HEALING OF FRACTURED BONES

■ G.E. BACON (CHELTENHAM).

NEUTRON BEAMS OF WIDTH 1 MM HAVE BEEN USED ON D1B (2.4 Å) AND D20 (1.3 Å) TO STUDY THE HEALING OF FRACTURED BONES. IT IS FOUND THAT THE CALLUS BONE UNITING THE FRACTURED TIBIA OF A SHEEP, WHOSE HEALING HAD BEEN ENCOURAGED BY DAILY MECHANICAL VIBRATION OVER A PERIOD OF THREE MONTHS, SHOWED NO TRACE OF THE LARGE PREFERENTIAL VERTICAL ORIENTATION OF THE APATITE CRYSTALS WHICH IS CHARACTERISTIC OF THE NORMAL BONE. NEVERTHELESS THE BONE HAD REGAINED ABOUT 60% OF ITS MECHANICAL STRENGTH AND THE CALLUS BONE, ALTHOUGH NOT ORIENTED, WAS WELL CRYSTALLISED. IT IS NOW PLANNED TO STUDY FRACTURES AFTER 1 OR 2 YEARS REHABILITATION. IT IS CONSIDERED THAT THE NEW MONOCHROMATOR FOR D20, EXPECTED TO GIVE INCREASED INTENSITY AT 2.5 Å, WILL BE OF CONSIDERABLE ADVANTAGE.

Bone is a composite material of collagen and slightly impure hydroxyapatite. The c-axes of the apatite crystals and the collagen fibres are preferentially oriented - very substantially in long bones - in the directions of the stresses which the bones need to withstand. Over a lifetime these stresses change in magnitude and a constant process of bone renewal takes place; this can be studied with neutrons which can accurately determine the configuration of the apatite crystals in samples of bone of millimetre or centimetre size [1]. In a recent experiment we have studied the renewal process

in bones which have been fractured and subsequently healed. We have used the tibia bone of a sheep, with particular interest also in assessing the effect of mechanical vibration [2] on the healing process. After such treatment for 3 months the bone has recovered about 60% of its mechanical strength but neutrons show that the callus bone, which unites the two sections, displays no trace of preferential orientation. We conclude that a much longer period than 3 months is required before the bone is restored to its original texture.

The details of the neutron data, and their unequivocal nature,

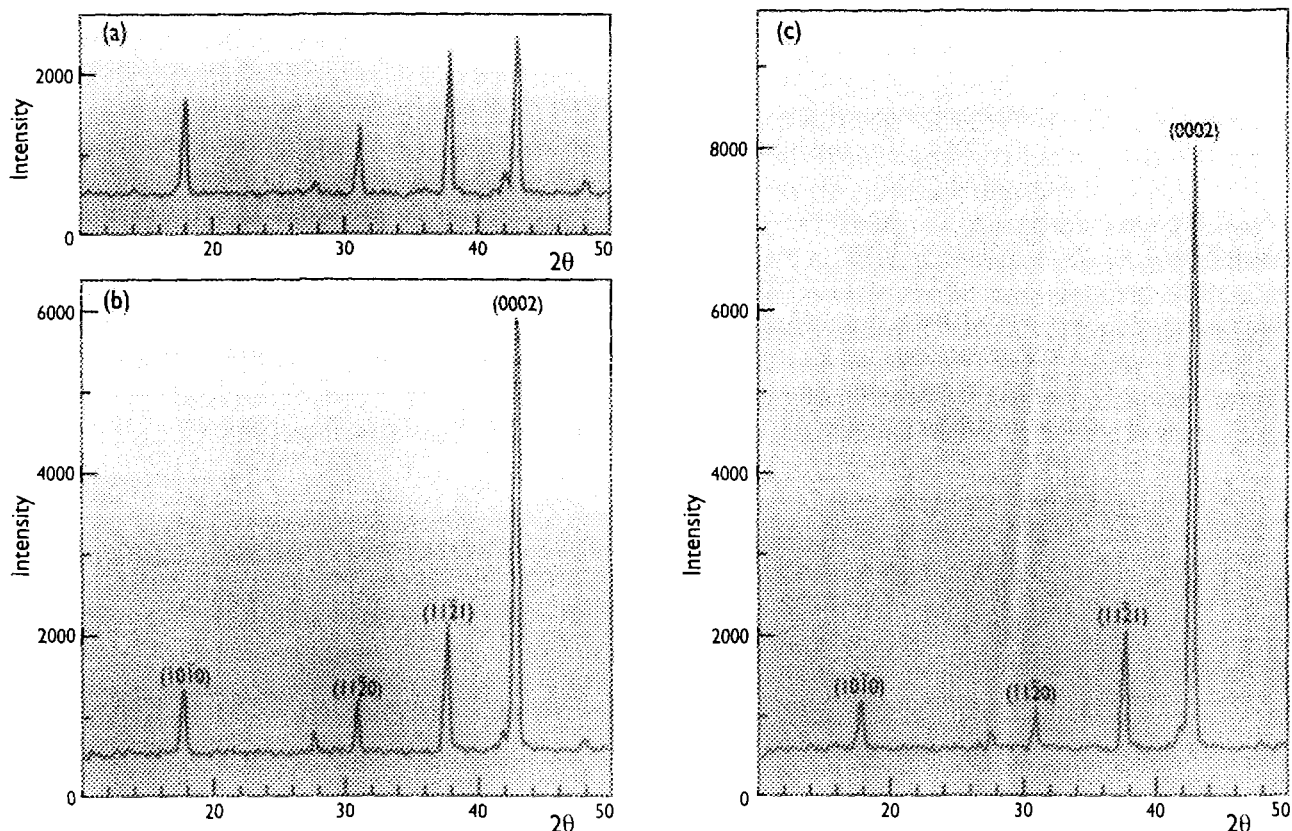
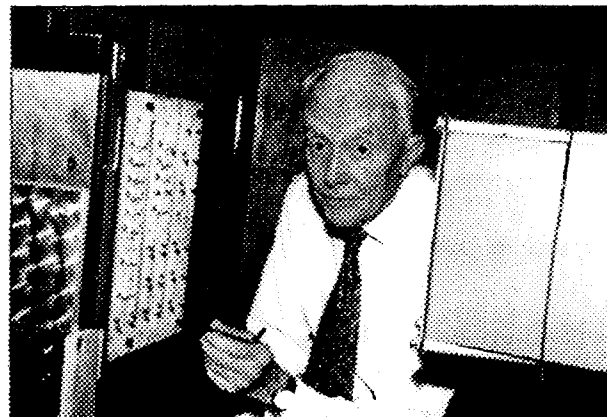


FIGURE 1: Neutron diffraction patterns of the tibia bone of a sheep, healed after fracture. The indices identify the reflecting planes of hydroxyapatite. In a) the neutron beam is centred on the position of fracture; in b) the beam is displaced by 1 mm and in c) by 2 mm.

can be followed with the aid of the figures. A 5 cm length of the front cortex of the sheep tibia (including the healed fracture) was placed horizontally on the centre table of D1B and viewed successively at 1 mm intervals with a neutron beam of width 1 mm at 2.4 Å. Fig. 1(a) is the lower angle portion of the diffraction pattern when the beam was centred on the position of fracture: Fig. 1(b) was recorded at 1 mm away from the fracture and Fig. 1(c) at 2 mm, and this last pattern is indeed representative of those taken at greater distances. In assessing the preferential orientation the crucial diffraction lines are $11\bar{2}1$ and 0002 . When hydroxyapatite crystals are unoriented - as in a powdered sample - these two lines are approximately equal in intensity, whereas in a normal « undamaged » tibia the 0002 line is 6 or 7 times greater than the $11\bar{2}1$, because of the vertical orientation in the bone. We have not observed such near equality of the $11\bar{2}1$ and 0002 lines, which Fig. 1(a) displays, in any sheep tibia which we have ever examined. Even in a foetus 80 days after conception the $0002/11\bar{2}1$ intensity ratio has not been less than 1.8.

More dramatically the results are shown in Fig. 2 where the diffraction pattern is displayed as a function of the position along the bone, with the fracture position at 13 mm. The rapid fall of the 0002 line at the fracture is very evident and is accompanied by a small rise in $11\bar{2}1$ which, otherwise,

remains largely constant over the picture. The two lines in the foreground, which have significant values only in the neighbourhood of the fracture, arise from prism planes $10\bar{1}0$ and $11\bar{2}0$ in the hydroxyapatite structure and their variation is accordingly the converse of the behaviour of 0002 , which comes from the basal planes. A similar result was obtained with the rear and side cortices of the tibia.



George Bacon: hands on D20.

Acknowledgement:

I am very grateful for the continued assistance of Pierre Convert with this work, for which he has now been my Local Contact for 20 years.

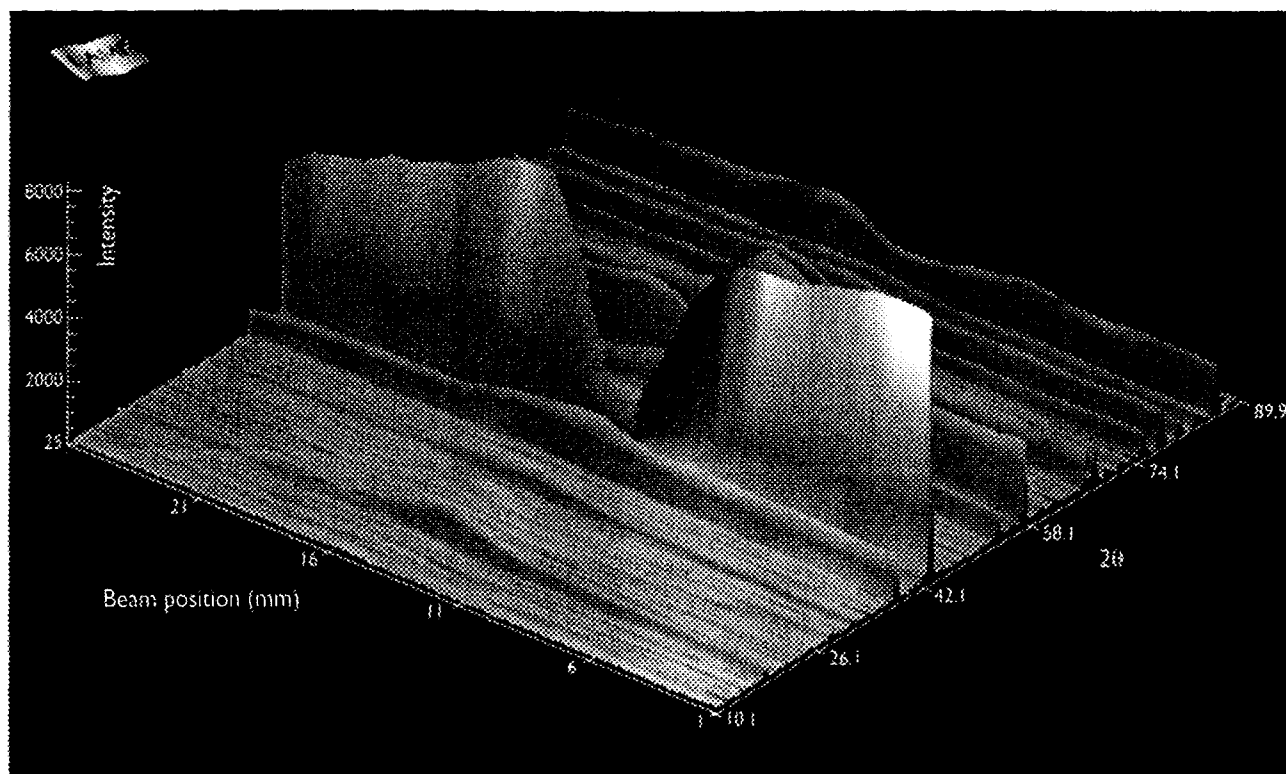


FIGURE 2: A 3-dimensional representation of the variation of the diffraction pattern of a healed tibia as a function of the distance of the neutron beam from the position of fracture. The left-hand horizontal scale gives the beam position in mm, the position of fracture being 13 mm; the right-hand scale, reading from 10.1 to 89.9 degrees, is the value of 2θ . The first four lines in the pattern are $10\bar{1}0$, $11\bar{2}0$, $11\bar{2}1$ and 0002 , as indexed in figure 1.

STRUCTURE / PROPERTY RELATIONSHIPS IN NON-LINEAR OPTICAL MATERIALS



FR9704845

- J. M. COLE (ILL/UNIV. DURHAM),
- J. A. K. HOWARD (UNIV. DURHAM),
- G. J. MCINTYRE (ILL).

THE APPLICATION OF NEUTRONS TO THE STUDY OF STRUCTURE/PROPERTY RELATIONSHIPS IN ORGANIC NON-LINEAR OPTICAL MATERIALS (NLOs) IS DESCRIBED. IN PARTICULAR, CHARGE-TRANSFER EFFECTS AND INTERMOLECULAR INTERACTIONS ARE INVESTIGATED. CHARGE-TRANSFER EFFECTS ARE STUDIED BY CHARGE-DENSITY ANALYSIS AND AN EXAMPLE OF ONE SUCH INVESTIGATION IS GIVEN. THE STUDY OF INTERMOLECULAR INTERACTIONS CONCENTRATES ON THE EFFECTS OF HYDROGEN-BONDING AND AN EXAMPLE IS GIVEN OF TWO STRUCTURALLY SIMILAR MOLECULES WITH VERY DISPARATE NLO PROPERTIES, AS A RESULT OF DIFFERENT TYPES OF HYDROGEN-BONDING.

An NLO material is a compound in which a non-linear polarisation is invoked on application of an intense electric-field. This electric field results from the external application of an intense laser-source.

Mathematically, the NLO effect can be described on the molecular scale by the equation:

$$P_{\text{TOT}} = \mu + \alpha E + \beta E^2 + \gamma E^3 + \dots (*)$$

and macroscopically by the equation:

$$P_{\text{TOT}} = P_0 + \epsilon_0 [\chi^{(1)} E + \chi^{(2)} E^2 + \chi^{(3)} E^3 + \dots]**$$

The most important term is the quadratic and the related phenomenon known as second harmonic generation (SHG). This is essentially a frequency-doubling process: two waves, each of frequency ω , simultaneously superimpose constructively. The resulting wave excites an electron from the ground state to a virtual excited state. On relaxation, one wave of frequency 2ω is emitted.

In order to optimise the SHG effect on a molecular scale, one must optimise β and to optimise the effect on a macroscopic scale, one must optimise $\chi^{(2)}$. Various structural features of compounds have been found to influence the value of β . Crystallographically, the compound must be *non-centrosymmetric* by nature of SHG being an even (second) order tensorial effect. Within the molecule, *charge-transfer* is deemed the most dominant factor affecting β . In turn, high charge-transfer requires strong donor-to-acceptor interactions, extended conjugation (and hence planarity), aromaticity and a large transition dipole-moment. In order to achieve successful propagation of the SHG effect through the crystal, the three-dimensional lattice should pack very closely and efficiently with *intermolecular interactions* as strong as possible.

Our investigations are concentrating on both charge-transfer processes and intermolecular interactions. Two series of organic compounds (Fig. 1) were investigated primarily using neutron diffraction.

(*) P_{TOT} = the total polarisation of the molecule; μ = the permanent dipole moment; E = the electric field; α = the linear polarisability; β , γ , ... = the first, second, ... hyperpolarisability coefficients.

(**) P_0 = any permanent polarisation in the medium; ϵ_0 = the dielectric constant; $\chi^{(1)}$, $\chi^{(2)}$, ... $\chi^{(n)}$ = the n th order susceptibility to polarisation.

Firstly, charge-density studies have been performed. These use the positional and vibrational information, especially of the important hydrogen atoms, obtained from a low-temperature neutron structure of a compound as an *a priori* model in a multipolar refinement of the charge deformation against a complementary X-ray data set (performed at the same temperature). The results enable one to observe, in detail, the exact nature of charge-transfer effects ensuing in terms of polarisation of electrons. Moreover, it has been found [1] that one can obtain a direct measure of the solid-state molecular hyperpolarisability, β , by determining from the structure refinement, the relevant multipolar moments of the molecule in different directions.

7,7-Dicyano-8,8-bis(diethyl-1-amino)quinodimethane, 1a, has been studied in this manner and preliminary results are given in Fig. 2. This shows a deformation density map (i.e. an indication of the polarisation of valence electrons) of the benzenoid ring. Once these results have been finalised, we will proceed to the calculations of β_{ijk} .

Secondly the nature of intermolecular interactions was investigated. In particular, a comparison of 5-nitro-2-

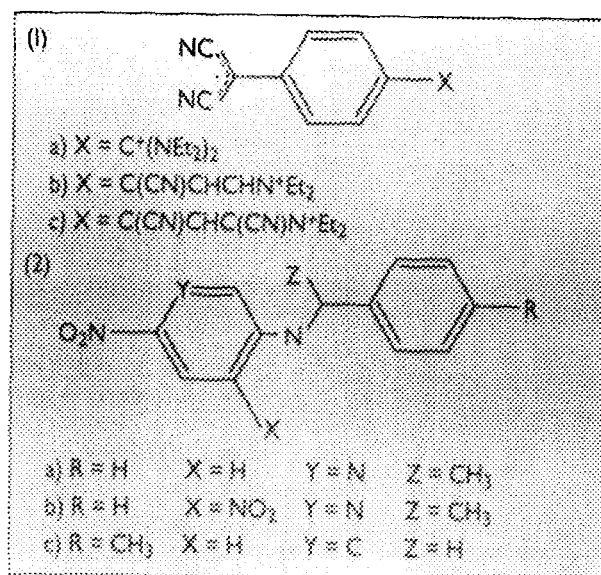


FIGURE 1: The two series of compounds studied.

[(1-phenylethyl)amino]pyridine, 2a and 3,5-dinitro-2-[(1-phenylethyl)amino]pyridine, 2b gave some interesting results.

Compound 2b was deemed more optimal than 2a, in terms of β , due to the extra charge-transfer resulting from the additional NO_2 group in 2b. Crystallographically, the two compounds are very alike: they both crystallise in the non-centrosymmetric space group, $P2_1$, and pack in a semi-layer like fashion whereby the exact nature of the three-dimensional lattice is determined by several types of hydrogen-bonds. However, powder SHG measurements for the two compounds gave very unexpected macroscopic values of $\chi^{(2)}$. $\chi^{(2)}$ for 2a was circa 5 times that of 2b.

This discrepancy was explained by neutron diffraction. This showed compound 2a to possess one very strong intermolecular hydrogen-bond, $\text{N}(3\text{C})\cdots\text{H}(4\text{NC})\cdots\text{O}(1\text{A})$ ($2.029(8)\text{\AA}$) and one secondary intermolecular hydrogen-bond, $\text{N}(2\text{A})\cdots\text{O}(2\text{A})\cdots\text{H}(4\text{D})$ ($2.517(9)\text{\AA}$). This arrangement used all possible hydrogen-bond donors and acceptors. Furthermore, the planes were found to stack almost on top of each other with an interplanar spacing of only 5.4\AA .

This very efficient and close packing is ideal for effective propagation of the SHG phenomenon throughout the solid. Compound 2b was found to contain one intramolecular

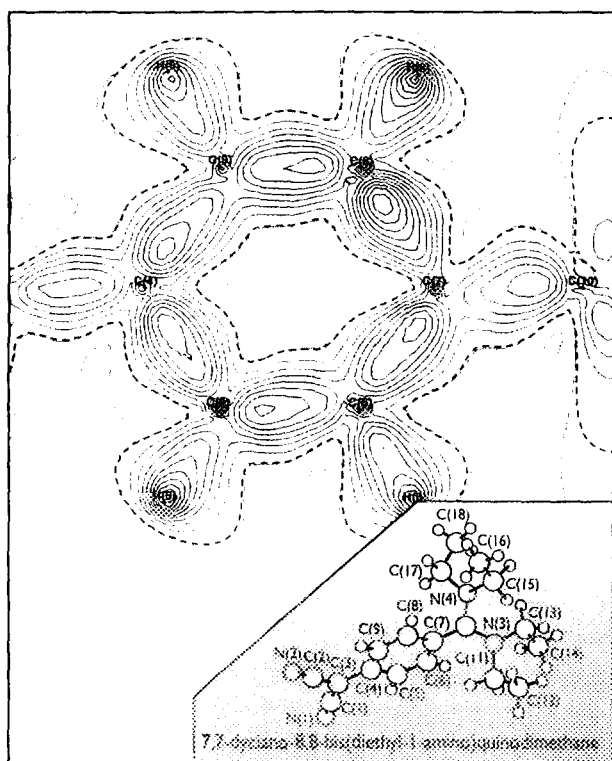


FIGURE 2: An electron-deformation density (EDD) map of the benzoid ring in compound 1a. Blue lines indicate positive EDD and red lines indicate negative EDD. The zero contour is black.

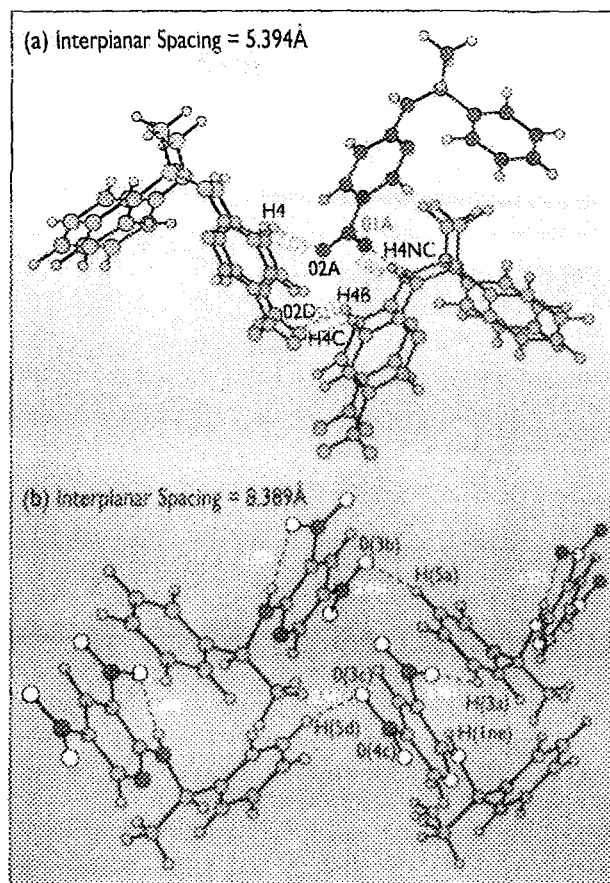


FIGURE 3: An illustration of the packing of a) compound 2a, b) including all inter/intramolecular contacts.

hydrogen-bond as well as three intermolecular ones. The intramolecular hydrogen-bond, $\text{N}(3)\cdots\text{O}(1)\cdots\text{H}(1\text{n})$ ($1.971(7)\text{\AA}$) is very strong and as the molecule adjusts to try and best accommodate it, a twist in the chain between the two rings is invoked. This twist precludes ideal herringbone formation in the three-dimensional lattice and disrupts the layer-like close packing as found in compound 2a. This results in an interplanar spacing (8.4\AA) noticeably larger than in compound 2a.

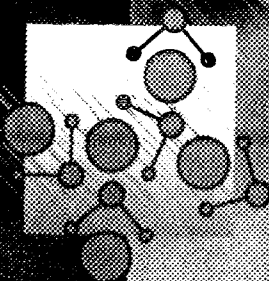
The intermolecular hydrogen-bonding is also affected. The twist deters the molecules from slotting over each other efficiently (in contrast to compound 2a) so less close contacts ensue. Not all hydrogen-bond donors and acceptors are utilised and the three intermolecular hydrogen-bonds which do exist, $\text{N}(4\text{b})\cdots\text{O}(3\text{b})\cdots\text{H}(5\text{a})$ ($2.441(8)\text{\AA}$), $\text{C}(3\text{a})\cdots\text{H}(3\text{a})\cdots\text{O}(1\text{c})$ ($2.561(7)\text{\AA}$) and $\text{N}(1\text{e})\cdots\text{H}(1\text{ne})\cdots\text{O}(4\text{c})$ ($2.332(7)\text{\AA}$) are all of weak-intermediate strength. The formation of the one strong intramolecular hydrogen-bond is therefore at the expense of the efficiency of intermolecular packing. We believe that this, in turn, is the cause of the much lower efficiency of SHG propagation through the three-dimensional solid.

- A. FKYERAT, A. GUELZIM, F. BAERT, W. PAULUS, G. HEGER, J. ZYSS & A. PERIGAUD, ACTA CRYSTALLOGR. B51 (1995) 197
 ■ R. TWIEG, A. AZEMA, K. JAIN AND Y.Y. CHENG CHEM. PHYS. LETT. 92 (1982) 208 ■ J.M. COLE, J.A.K. HOWARD AND J.A.H. MACBRIDE, (SUBMITTED TO ACTA CRYSTALLOGR. C).

LIQUIDS AND GLASSES



FR9704846



NEUTRON BRILLOUIN SCATTERING IN DENSE FLUIDS

P. VERKERK (DELFT UNIVERSITY) ON BEHALF OF THE FINGO (FRANCE, ITALY, NETHERLANDS, GERMANY, ONTARIO) COLLABORATION.

THERMAL NEUTRON SCATTERING IS A TYPICAL MICROSCOPIC PROBE FOR INVESTIGATING DYNAMICS AND STRUCTURE IN CONDENSED MATTER. IN CONTRAST, LIGHT (BRILLOUIN) SCATTERING WITH ITS THREE ORDERS OF MAGNITUDE LARGER WAVELENGTH IS A TYPICAL MACROSCOPIC PROBE. IN A SERIES OF EXPERIMENTS USING THE IMPROVED SMALL-ANGLE FACILITY OF IN5 A SIGNIFICANT STEP FORWARD IS MADE TOWARDS REDUCING THE GAP BETWEEN THE TWO. FOR THE FIRST TIME THE TRANSITION FROM THE CONVENTIONAL SINGLE LINE IN THE NEUTRON SPECTRUM SCATTERED BY A FLUID TO THE RAYLEIGH-BRILLOUIN TRIPLET KNOWN FROM LIGHT-SCATTERING EXPERIMENTS IS CLEARLY AND UNAMBIGUOUSLY OBSERVED IN THE RAW NEUTRON DATA WITHOUT APPLYING ANY CORRECTIONS.

Since its very beginning thermal neutron scattering has been an invaluable tool in the development of theories for the dynamics and structure of fluids. The reason is that the wavelength as well as the energy perfectly match the structure and dynamics of a fluid on a microscopic scale. In contrast, light scattering and in particular Brillouin scattering is a typical macroscopic probe suitable for the investigation of hydrodynamics.

Our aim is the understanding of thermodynamics and hydrodynamics on the basis of the molecular-interaction forces. Therefore, our present understanding of fluids would be further enhanced if we had a probe for investigating the transition from the microscopic to the macroscopic region. In contrast to SANS there is an upper limit to the wavelength of the neutrons which may be used, because their energy must be sufficiently large to permit interaction with the dynamic processes in the fluid. For observation of propagating modes, like for instance phonons, the neutron velocity v must be larger than the sound velocity c_s . In fluids c_s ranges from about 400 ms^{-1} for rare gases to about 5000 ms^{-1} for molten lithium, so, the minimum neutron energy is about 4 meV in the first case and about 400 meV in the second case.

In the hydrodynamic regime the wavelength λ_d of the density fluctuations in the fluid that interact with the scattered radiation (usually light) is large compared with the mean free path l (we regard the fluid for a moment as a collection of moving and colliding hard spheres). Because $\lambda_d = 2\pi/Q$ with $\hbar Q$ the momentum transfer in the scattering event, the hydrodynamic regime is approached if $Ql \ll 1$, which can be realised either by increasing the wavelength of the incident radiation or by measuring at very small scattering angles. As stated before, the first possibility does not work for neutrons if we want to obtain information on the dynamics.

Obviously, in a small-angle experiment very good angular resolution is mandatory. In the hydrodynamic limit the spectrum of scattered radiation consists of the Rayleigh-Brillouin triplet. The width of the peaks is proportional Q^2 and the position of the inelastic Brillouin peaks is proportional to Q , so with decreasing scattering angle increasingly good energy resolution is required. This can only be achieved at the cost of a considerable reduction in count rate and, therefore, neutron Brillouin-scattering requires the world's most intense neutron sources. To the best of our knowledge two instruments are available today for such experiments:

IN5 at ILL for thermal and cold neutrons and PHAROS for hot neutrons at the spallation source of the Neutron Scattering Center, Los Alamos National Laboratory. A third instrument is under construction at the cold source of the Hahn-Meitner Institute, Berlin.

Egelstaff et al. [1] used IN5 modified with a temporarily installed position-sensitive detector with time-of-flight analysis for the first time in an experiment on nitrogen at room temperature. An international team was then set up involving groups from France, Italy, the Netherlands, Germany, and Ontario, hence called FINGO (Latin for "I invent"), to further develop the technique and applications of neutron Brillouin scattering. A few more experiments were done on argon and krypton before the small-angle facility was improved during the reactor shut-down with a permanently installed position-sensitive detector and a vacuum flight-path. In April 1996 FINGO used the new facility in a series of experiments on high-density krypton at room temperature and on liquid argon (using ^{86}Kr and ^{36}Ar for pure coherent scattering). We used an incident wavelength of 5 \AA (3.3 meV), resulting in an energy resolution for the scattered neutrons of 0.13 meV FWHM. Figs. 1 and 2 present the result for ^{86}Kr at room temperature and 800 bar, only corrected for background and container scattering. The sound dispersion is very clearly visible as well as the increasing damping with increasing wave-vector. In Fig. 3 we compare the fully corrected (except for resolution) data for $Q = 0.085 \text{ \AA}^{-1}$ with the hydrodynamic Rayleigh-Brillouin triplet folded with the experimental resolution.

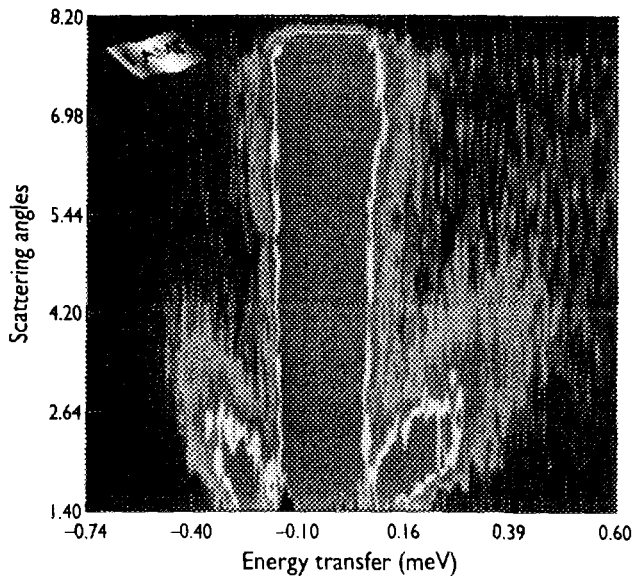


FIGURE 1: Contour map (produced by the LAMP software) of the scattered neutron spectrum for krypton at room temperature and 800 bar after correction for background and container scattering.

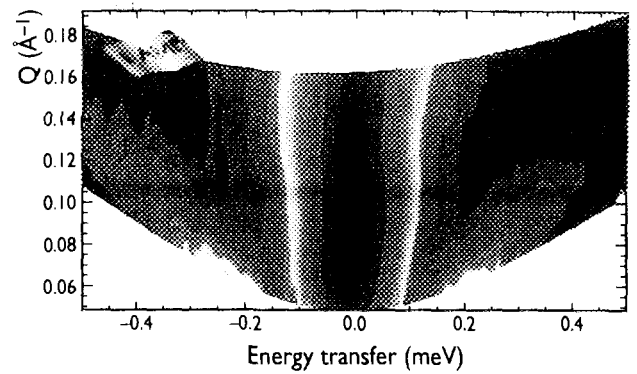


FIGURE 2: Same data as Fig. 1, now plotted as function of wave vector Q and energy transfer ΔE in order to show the limits of the kinematic region. The hydrodynamic sound velocity is 572 ms^{-1} or 3.81 \AA meV .

Although $Ql = 0.02$, which was expected to be well within the hydrodynamic range, the experimental data still deviate considerably from pure hydrodynamics.

This surprising result deserves further analysis; comparison with similar experiments on argon may shed new light on the relation between the interparticle interactions and the transport coefficients.

Reasonable agreement with the experiment may however, be obtained by using the hydrodynamic model but with transport coefficients used as fitting parameters (see Fig. 3). The members of FINGO are or have been Fabrizio Barocchi and Ubaldo Bafle (Florence), James Youden, Chris Benmore and Peter Egelstaff (Guelph, Ontario), Hannu Mutka (ILL) and Jens Suck (ILL / Chemnitz), Leo de Graaf, Barry Mos and Peter Verkerk (Delft).

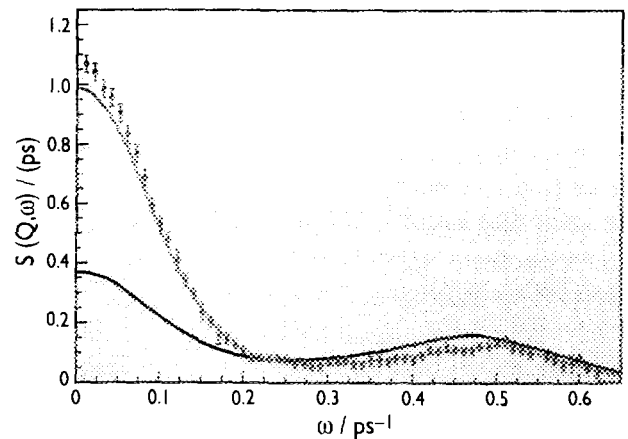


FIGURE 3: Experimental $S(Q, \omega)$ (not corrected for resolution) at $Q = 0.085 \text{ \AA}^{-1}$ (green dots with error bars) compared with the hydrodynamic Rayleigh-Brillouin triplet if the parameters are determined from the experimental thermodynamic and transport coefficients (blue) and if the parameters are fitted (red).

POLYMORPHIC ETHYL ALCOHOL AS A MODEL SYSTEM FOR THE QUANTITATIVE STUDY OF GLASSY BEHAVIOUR



FR9704847

H.E. FISCHER, H. SCHÖBER, M.A. GONZÁLEZ (ILL),
F.J. BERMEJO, R. FAYOS, J. DAWIDOWSKI (CSIC MADRID),
M.A. RAMOS, S. VIEIRA (U. AUTÓNOMA, MADRID).

THE PAST 25 YEARS HAVE WITNESSED A STRONG SCIENTIFIC EFFORT TOWARDS AN UNDERSTANDING OF THE NEARLY UNIVERSAL TRANSPORT AND DYNAMICAL PROPERTIES OF AMORPHOUS MATERIALS OR GLASSES. REASONABLY SUCCESSFUL PHENOMENOLOGICAL MODELS HAVE BEEN DEVELOPED TO ACCOUNT FOR THESE PROPERTIES AS WELL AS THE BEHAVIOUR NEAR THE GLASS-TRANSITION, BUT QUANTITATIVE MICROSCOPIC MODELS HAVE HAD LIMITED SUCCESS. ONE HINDRANCE TO THESE INVESTIGATIONS HAS BEEN THE LACK OF A MATERIAL WHICH EXHIBITS GLASS-LIKE PROPERTIES IN MORE THAN ONE PHASE AT A GIVEN TEMPERATURE. THIS REPORT PRESENTS RESULTS OF NEUTRON-SCATTERING EXPERIMENTS FOR ONE SUCH MATERIAL, ORDINARY ETHYL ALCOHOL, WHICH PROMISES TO BE A MODEL SYSTEM FOR FUTURE INVESTIGATIONS OF GLASSY BEHAVIOUR.

Since the discovery of universality in the low-temperature specific heat and thermal conductivity of amorphous materials [1], the term "glassy" has come to describe any material exhibiting these thermal properties or other behaviour associated with glasses, such as particular elastic properties [2] and excess vibrational modes at low temperature, as well as characteristic relaxation behaviour [3] observed near the glass-transition temperature T_g . A phenomenological model of two-level systems (TLS) [4] has been reasonably successful in explaining the low-temperature ($T < 1$ K) properties of glasses, in particular the time-dependent linear term in the specific heat C_p and the T^2 dependence of the thermal conductivity. In this model, the glassy TLS consist of asymmetric double-well potentials which are thermally activated at high temperature and become tunnelling systems at low temperature. A Gaussian distribution of barrier heights and a flat distribution of the TLS energy splittings can account for the observed low-temperature properties, but the microscopic nature of these TLS has never been identified for an amorphous system.

Low-temperature "glassy behaviour" has also been found in crystalline materials such as orientational glasses (randomly oriented molecules at crystal lattice-sites) and rotator-phase crystals (rotating molecules at lattice sites). The presence of a lattice makes such "glassy crystals" amenable to quantitative modelling. In particular, the glassy properties of the mixed crystal $(\text{KBr})_{1-x}(\text{KCN})_x$ have been intensively studied [5], and a microscopic model involving rotational tunnelling of the CN^- ions has been developed [6] which explains quantitatively (albeit approximately) the observed low-temperature thermal and elastic properties. Despite this reasonable success in the modelling of glassy behaviour in disordered crystals, these materials cannot generally be prepared in amorphous form (due to insufficient quenching rates), thereby frustrating a comparison between the predictions of lattice-based microscopic models and the observed glassy behaviour of amorphous solids.

If one could find a system which can exhibit both amorphous and glassy crystal phases at low-temperature, a microscopic model for the glassy tunnelling systems in the disordered crystal-phase could lead to an identification of those responsible for glassy behaviour in the amorphous phase. It has recently been shown [7] that ordinary ethyl alcohol, or ethanol, satisfies this criterion.

Fig. 1 gives a schematic diagram for the phases of ethanol. To the best of our knowledge, ethanol is the only molecular system capable of existing at the same temperature both as an orientational glass (positional order but orientational disorder) and as a structural glass or amorphous solid (both positional and orientational disorder).

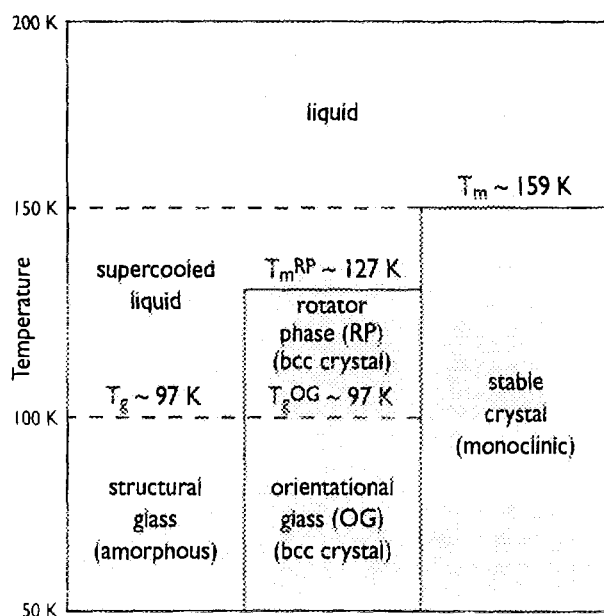


FIGURE 1: The phases of ethanol ($\text{C}_2\text{H}_5\text{OH}$). Cooling the liquid at > 6 K/min produces the glass/amorphous phase. Annealing the glass at 110 K for several hours produces the RP (with an activation energy of $E_A \approx 0.4$ eV). The $\text{RP} \rightarrow \text{OG}$ transition involves a freezing of molecular rotations. At $T \approx 127$ K the RP melts and immediately forms the stable crystal. For $\text{C}_2\text{D}_5\text{OD}$ the transition temperatures increase by about 2 K.

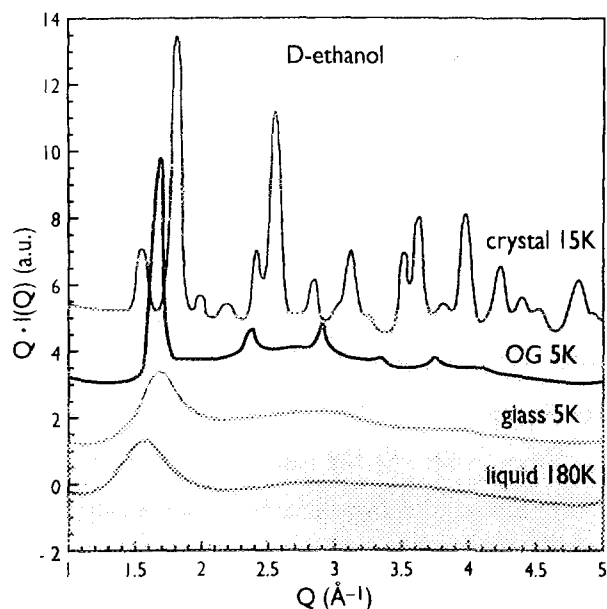


FIGURE 2: The reduced intensity functions $Q \cdot I(Q)$ for 4 of the 5 phases of (deuterated) ethanol studied. The incoherent and self-scattering contributions have been subtracted, and all but the curve for the liquid have been shifted upward for clarity. The curve for the RP crystal at 105 K was basically the same as that for the OG (taking into account the temperature difference), and is not shown.

Ethanol has an additional advantage over mixed-crystal orientational glasses (e.g. $(\text{KBr})_{1-x}(\text{KCN})_x$) in being stoichiometrically homogeneous, but has the disadvantage of having both *trans* and *gauche* isomers.

Fig. 2 shows the reduced intensity functions $Q \cdot I(Q)$ for 4 phases of ethanol, as measured using the D4 diffractometer for liquid and amorphous materials at nominal wavelengths of $\lambda = 0.7 \text{ \AA}$ and 0.5 \AA .

The same sample of fully-deuterated ethanol (D-ethanol) was used for all the measurements, the phases having been prepared *in situ* using a standard orange-cryostat. The data of Fig. 2 were subsequently Fourier transformed (not shown) to produce the pair-pair correlation functions $D(r)$.

In spite of being crystalline, the orientational glass (OG) phase shows a $D(r)$ which is remarkably similar to that for the glass, aside from the expected larger damping of the long-range order oscillations in the latter.

Fig. 3 shows a set of cold-neutron TOF spectra averaged over all detector angles ($Q_{\text{max}} \approx 2 \text{ \AA}^{-1}$) for a sample of D-ethanol in its OG, amorphous and stable crystal phases (all at $T = 30 \text{ K}$), using the IN6 time-focussing spectrometer. The feature at $\sim 2 \text{ meV}$, customarily called the “boson peak” in the glass literature, is absent in the crystal’s spectrum (we also confirmed that the rotator-phase (RP) at 105 K shows a similar peak). These excess vibrational

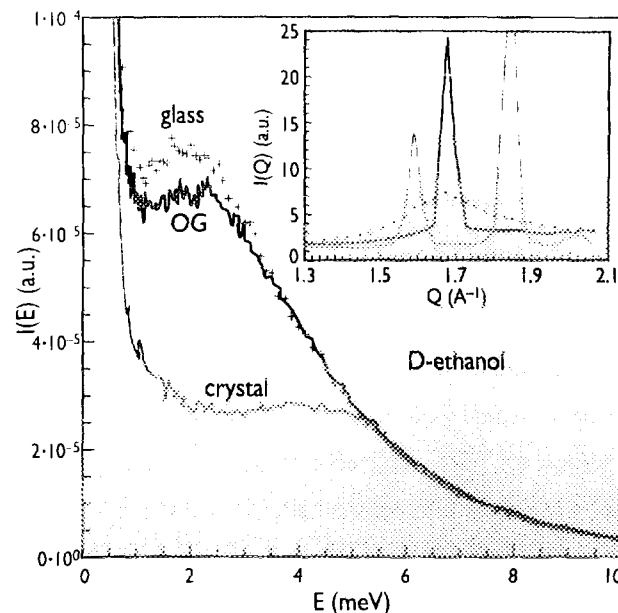


FIGURE 3: TOF spectra at 30 K in the frequency range of the “boson peak” characteristic of glassy systems, obtained using the IN6 spectrometer. The inset shows the *in situ* TOF diffraction results, which confirm production of the 3 phases (the curves are resolution limited due to a grouping of detector banks).

modes, characteristic of glassy behaviour and corresponding to the “excess T^3 term” in specific heat, are therefore limited in ethanol to $\sim 6 \text{ meV}$, where the OG and glass spectra converge to the crystal’s.

The near equivalence of the glass and OG spectra constitutes the clearest indication, to the authors’ knowledge, of the close similarity between the vibrational excitations of an orientationally-disordered crystal and those of an amorphous solid at the same stoichiometry and temperature, and suggests that the glassy behaviour in these two phases is due more to orientational disorder (present in both) rather than positional disorder (present only in the glass). It is therefore tempting to identify the low-temperature glassy two-level systems in ethanol as molecular-rotation tunnelling sites.

In conclusion, ethanol appears to be unique in exhibiting glassy behaviour in 3 different phases which are easily produced at ambient pressure: the structural glass, the orientational glass and the rotator-phase crystal. Having therefore two types of glass transitions (both structural and orientational) as well as a simple molecular nature, ethanol promises to be a nearly ideal system for testing both phenomenological and microscopic models of glassy behaviour, and may also permit the first-ever identification of glassy TLS in an amorphous solid.

- R.C. ZELLER AND R.O. POHL, *PHYS. REV. B* 4 (1971) 2029 ■ K.A. TOPP AND DAVID G. CAHILL, *Z. PHYS. B* 101 (1996) 235
 ■ D. RICHTER, *J. PHYS. CONDENS. MATTER* 8 (1996) 9177 AND REFERENCES WITHIN ■ P.W. ANDERSON, B.I. HALPERIN AND C.M. VARMA *PHILOS. MAG.* 25 (1972) 1 ■ J.J. DEYOREO, W. KNAACK, M. MEISSNER AND R.O. POHL, *PHYS. REV. B* 34 (1986) 8828
 ■ E.R. GRANNAN, M. RANDERIA, J.P. SETHNA, *PHYS. REV. B* 41 (1994) 7799 ■ R. FAYOS, F.J. BERMEJO, J. DAWIDOWSKI, H.E. FISCHER AND M.A. GONZALEZ, *PHYS. REV. LETT.* 77 (1996) 3823 AND REFERENCES WITHIN ■ M.A. RAMOS, S. VIEIRA, F.J. BERMEJO, J. DAWIDOWSKI, H.E. FISCHER, H. SCHÖBER, M.A. GONZALEZ, C.K. LOONG AND D.L. PRICE, *PHYS. REV. LETT.* 78 (1997) 82.

SEPARATION OF COHERENT AND INCOHERENT SCATTERING IN LIQUID PARA-H₂ BY POLARISATION ANALYSIS

M. GARCIA-HERNANDEZ AND F.J. MOMPEÁN (UNIV. MADRID),
O. SCHARPF AND K.H. ANDERSEN (ILL),
B. FÁK (CEA GRENOBLE).



FR9704848

IN THE 1960 IAEA SYMPOSIUM ON NEUTRON SCATTERING, SARMA PRESENTED HIS THEORETICAL STUDY ON THE SCATTERING OF COLD NEUTRONS BY LIQUID HYDROGEN AND DEMONSTRATED HOW THE INTIMATE COUPLING BETWEEN NUCLEAR AND ROTATIONAL DEGREES OF FREEDOM FINALLY RESULTS IN THE POSSIBILITY OF OBSERVING COLLECTIVE MODES FROM THIS MATERIAL, WHICH TO MANY NEUTRON SCATTERERS IS SYNONYMOUS WITH 'INCOHERENT'. IN THE DISCUSSION THAT FOLLOWED SARMA'S PAPER, HE AND MAIER-LEIBNITZ AGREED ON THE INTEREST OF LOOKING INTO THIS PROBLEM WITH POLARISED NEUTRONS. NOW, 35 YEARS LATER, IT IS POSSIBLE TO PERFORM SUCH AN EXPERIMENT TO GAIN ACCESS TO A LIMITED REGION OF THE (Q,E) SPACE WHERE THE COLLECTIVE RESPONSE FROM THIS LIQUID IS FOUND.

Neutron polarisation analysis offers the possibility to separate the coherent and spin-incoherent contributions of nuclear scattering. At ILL, the D7 spectrometer combines this kind of analysis with the time-of-flight technique and a wide angular range of detectors. In our study we have applied this tool to measure the coherent scattering from liquid H₂, the lightest molecular liquid. In molecules where identical nuclei occupy equivalent positions, the corresponding quantum statistics impose requirements on the total molecular wavefunction. H₂ is an extreme example: the fermion nature of the protons requires that the total molecular wavefunction be antisymmetric to their exchange. In the ground electronic and vibrational states, rotational states with even (odd) quantum numbers can only couple to antisymmetric (symmetric) molecular-nuclear spin-states giving rise to *para* (*ortho*) molecular states. Due to the light mass of the H atoms, these two types of states have large separations in their lower energy-levels (14.7 meV) and this fact conditions a large amount of the physics of the condensed phases of H₂. From the neutron scattering point of view, it opens the possibility of sampling regions of the momentum – energy-transfer space (Q, E) with predominantly coherent scattering (Fig. 1).

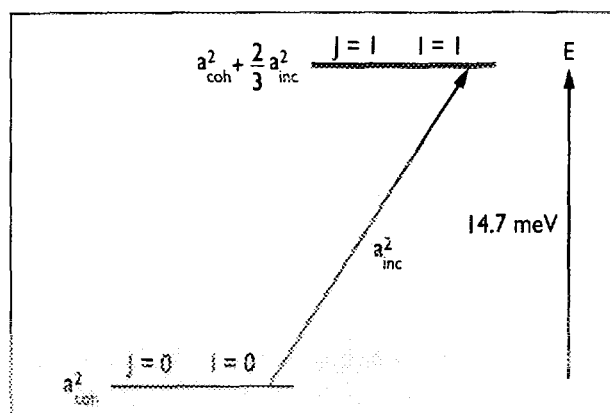


FIGURE 1: Lower energy-level diagram for H₂. *Para* molecules ($J = 0, I = 0$) scatter coherently, while *ortho* molecules ($J = 1, I = 1$) contribute both to coherent and incoherent scattering. In our experiment, neutrons did not have enough energy to cause $\Delta J = \pm 1$ transitions, which would have resulted in additional incoherent contributions.

In the scale of conventional quantum liquids, H₂ occupies the third position right after ⁴He. At the low temperatures (13-33 K) characteristic of its liquid range, collisions between *ortho* molecules convert them to the thermodynamically favoured *para* molecules with a time constant of the order of tens to hundreds of hours. With catalysers, however, it is possible to perform experiments with samples of stable composition and to increase to the thermodynamic-equilibrium limit the fraction of *para*-H₂ molecules, which scatter neutrons coherently. More than 20 years ago, experiments of this kind were reported on three-axes spectrometers with unpolarised neutrons in order to study the collective response from H₂.

While the striking difference found between non-catalysed and catalysed samples cannot be questioned, three-axes measurements on these systems are very sensitive to errors of a different nature. In particular, with incident neutron energies very close to the *ortho*–*para* conversion energy, strong second order contamination of the spectra arise which are difficult to eliminate by filtering.

With polarised neutrons and time-of-flight energy analysis it is possible not only to circumvent this problem but to discriminate between coherent scattering and the incoherent scattering which arises from the presence of a fraction of *ortho* molecules. Figs. 2 and 3 show the basic result from our experiment on a liquid mixture enriched in *para*-H₂ at 16 K. Fig. 2 contains the coherent dynamical structure-factor $S_{\text{coh}}(Q, E)$. The scattering intensity concentrates in the region around $Q = 2 \text{ \AA}^{-1}$, corresponding to a maximum in the structure factor $S(Q)$. In a single-mode approximation, one should expect a minimum in the energy of the collective excitations at this wavevector. Fig. 4 shows the variation with Q of $S_{\text{coh}}(Q, E)$ around $Q = 2 \text{ \AA}^{-1}$.

An asymmetric peak broader than the instrumental resolution is seen, which shows a minimum in energy width near the structure factor maximum, as expected for collective excitations.

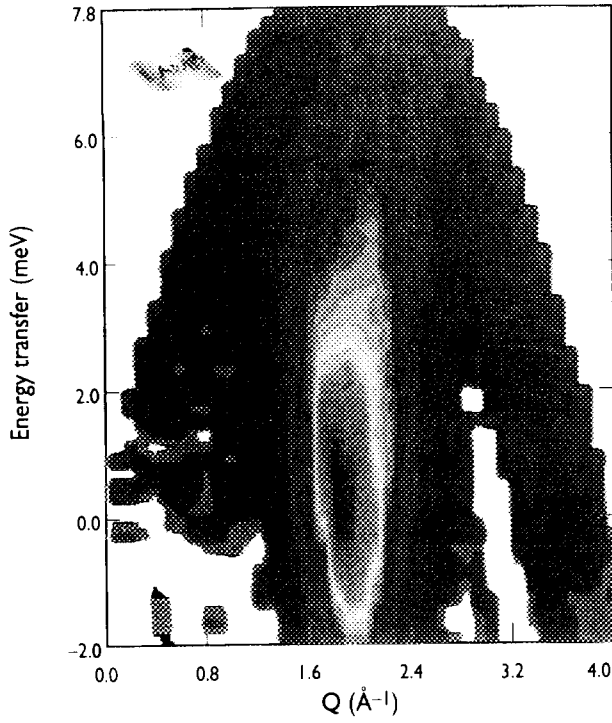


FIGURE 2: $S_{coh}(Q, E)$ from liquid H_2 enriched in para- H_2 at 16 K under saturated vapour pressure. The white area at the elastic energy around $Q = 3 \text{ \AA}^{-1}$ arises from a slight oversubtraction of an Al Bragg peak from the sample cell.

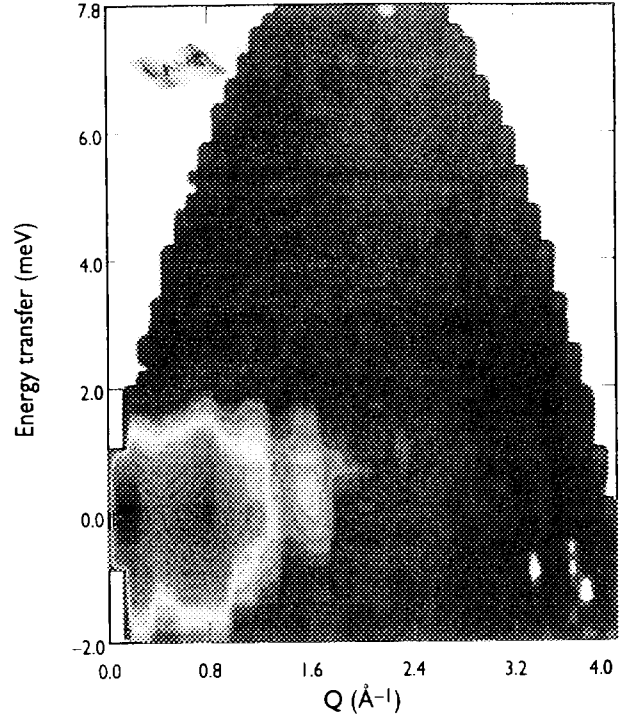


FIGURE 3: $S_{inc}(Q, E)$ from liquid H_2 enriched in para- H_2 at 16 K at saturated vapour pressure. The scale of the colour coding showing the scattering intensity is identical in Figs. 2 and 3.

Fig. 3 offers a different perspective of the collective excitations. Here, the incoherent scattering, $S_{inc}(Q, E)$ contains, at low Q values, contributions from the diffusive motion of the molecules (shown as a quasielastic feature).

For higher Q (corresponding to smaller values of the neutron-molecule classical interaction time), the inelastic features observed reflect the projection on the single-molecule dynamics of the collective modes as a density of states, which does not vary appreciably with Q . The colour coding of the intensity is identical in Figs. 2 and 3.

It is seen that the ortho- H_2 , despite being present at a relative density of only 3%, gives a similar scattering intensity to the para- H_2 due to its high incoherent scattering cross-section.

Our results are limited by the region of (Q, E) accessible on D7 with an incident energy of 8.6 meV. In particular, we are not able to sample the region near $Q = 1 \text{ \AA}^{-1}$ with energy transfers near 7 meV, which should correspond to the maximum in the dispersion relation of the excitations.

Despite this kinematic constraint, we believe that the data shown in Fig. 4 provide new evidence on the dispersion behaviour of the collective excitations in this liquid.

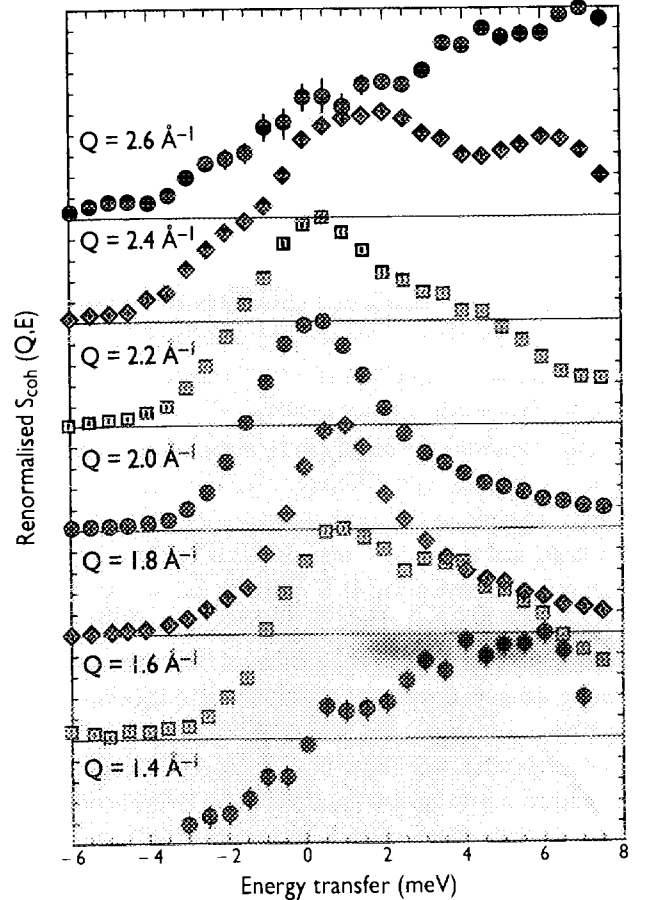
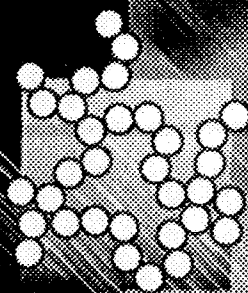


FIGURE 4: $S_{coh}(Q, E)$ from liquid H_2 enriched in para- H_2 at 16 K at saturated vapour pressure shown at 7 different Q -values around the minimum of the dispersive collective excitations. Since $S(Q)$ peaks vary sharply at $Q = 2 \text{ \AA}^{-1}$, the data have been normalised separately to unit height at each value of Q . The dispersion of the collective excitations is clearly seen.



THE SEGMENTAL DYNAMICS OF A MISCIBLE POLYMER BLEND

- A. ALEGRIA, I. CENDOYA, J. COLMENERO, J.M. ALBERDI (UNIV. PAIS VASCO SAN SEBASTIAN),
- B. FRICK (ILL).

THE SEGMENTAL DYNAMICS OF POLY(VINYL METHYL ETHER) (PVME) IN A BLEND CONTAINING 65 WT% PVME AND 35 WT% D-POLYSTYRENE WAS INVESTIGATED ON THE BACKSCATTERING SPECTROMETER IN10. A QUASIELASTIC BROADENING OF THE SPECTRA IS APPARENT AT $T > 350$ K AND SHOWS A STRONG DEPENDENCE ON THE MOMENTUM TRANSFER. WE SHOW THAT AN APPROACH WHICH IS NORMALLY USED TO DESCRIBE THE BLEND DYNAMICS ON A MACROSCOPIC TIME SCALE ALSO DESCRIBES WELL THE NEUTRON RESULTS. WE ALSO FIND A GOOD AGREEMENT WITH NUCLEAR MAGNETIC RESONANCE AND DIELECTRIC SPECTROSCOPY.

The segmental dynamics of a miscible polymer blend are different from those corresponding to each of its components. This fact is usually ascribed to fluctuations of concentration (FC) present in such systems [1,2].

In this framework the blend can be regarded as a superposition of regions with different relaxation behaviour and which depends on the local concentration of the components ϕ_A and ϕ_B in these regions. Usually, the relaxation function of a pure polymer is found to follow a stretched exponential function. Thus in the blend one might try to superimpose the relaxation functions of the components by taking the concentration fluctuations into account. This approach is in agreement with observations from macroscopic relaxation techniques [3,4]. From macroscopic measurements it is found that the effect of FC is less noticeable for high temperatures where the characteristic times approach the mesoscopic range ($T > T_g + 50$ K) [5,6]. However, there is not much direct experimental information available on the mesoscopic and microscopic time or spatial scales. This range can be explored by quasielastic neutron scattering. Using partial deuteration the dynamics of a single component of a blend can be investigated by neutron scattering. Similarly, in dielectric experiments mainly the relaxation

of the component with the higher dipole moment can be observed. Thus, both techniques explore the relaxation function $\Phi(t)$ of one blend component. Within the FC picture $\Phi(t)$ can be regarded as a superposition of distributed relaxation processes, each of these accounting for the pure polymer relaxation $\Phi_{\text{pure}}(t)$.

At temperatures far above T_g , the distribution of relaxation times is well approximated by a log-normal one, so the relaxation of one component in the blend can be written as:

$$\Phi(t) = \int_{-\infty}^{\infty} \exp \left[-\frac{\log^2 \left(\frac{\tau}{\tau_m} \right)}{2\sigma^2} \right] \Phi_{\text{pure}}(t) d \log \tau \quad (1)$$

where τ_m is the most probable relaxation time, depending on the average concentration of the investigated component, and σ accounts for the distribution width.

The system poly(vinyl methyl ether)/polystyrene (PVME/PS) is one of the most extensively studied miscible polymer blends.

The contribution of PVME to the segmental dynamics of this blend has been studied by means of dielectric relaxation (DR) [7] and nuclear magnetic resonance (NMR) techniques, among others.

We performed QENS on the IN10 backscattering spectrometer investigating a blend ($T_g = 260$ K) with protonated PVME (65 wt%) and deuterated PS (dPS) (T-range 350-430 K; energy window ± 10 μ eV and momentum transfer $0.2 \text{ \AA}^{-1} < Q < 2 \text{ \AA}^{-1}$). Therefore, after data correction, we were looking mainly at the protonated PVME.

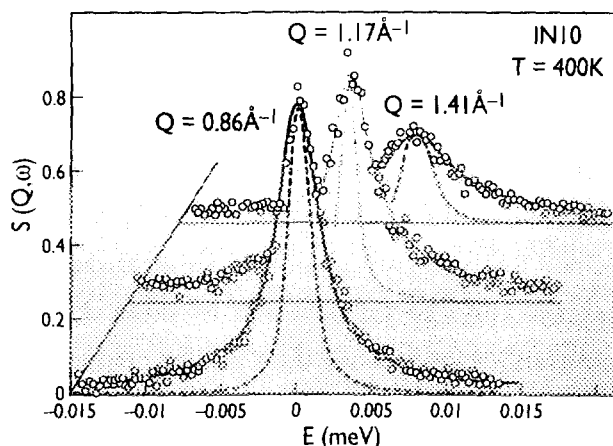


FIGURE 1: QENS spectra of PVME 65wt/dPS 35wt blend obtained at 400 K. The solid lines correspond to the simultaneous fitting according to the model proposed in this work.

The QENS spectra of this blend show a clear Q-dependent broadening (see Fig. 1). For pure PVME we had found previously [5] that the relaxation function, i.e. the intermediate scattering function $I(Q, t)$, follows a stretched exponential function for $350 \text{ K} < T < 400 \text{ K}$:

$$I(Q, t) \propto \exp \left[- \left(\frac{t}{\tau(Q)} \right)^{0.45} \right] \quad (2)$$

and the relaxation time shows a power law dependence on the momentum transfer Q:

$$\tau(Q) = C Q^{-1.7} \quad (3)$$

As a consequence of this power law one can rewrite eq. 1 as follows:

$$I(Q, t) = \int_{-\infty}^{\infty} \exp \left[- \frac{\log^2 \left(\frac{C}{C_m} \right)}{2 \sigma^2} \right] I_{\text{pure}}(Q, t) d \log C \quad (4)$$

Thus the Q-dependence drops out from the distribution function and only the intermediate scattering function I_{pure} depends on Q. Eq. 4 was used to analyse the blend data. Thereby $I_{\text{pure}}(Q, t)$ was taken from the pure PVME and the distribution width σ was fixed from DR and NMR measurements (see Fig. 2). Therefore, in addition to a flat background which accounts for the fast rotation of the PVME methyl group, C_m remains the only relevant fitting parameter. A simultaneous fitting of all Q spectra was performed at each temperature.

The fitting curves to the QENS spectra (see Fig. 1 for 400 K) show that the model can perfectly well describe the segmental dynamics of PVME in the blend. Converting results for C_m from the fits into relaxation times τ_m according to eq. 3, we can compare the QENS, dielectric and NMR results.

We find that not only the relaxation times obtained from QENS follow the T-dependence of the macroscopic relaxation times, but they also coincide around the same Q value which has previously been determined for pure PVME ($Q = 0.86 \text{ \AA}^{-1}$), see Fig. 2.

Thus a consistent description for the microscopic and macroscopic relaxation behaviour of miscible blends is found.

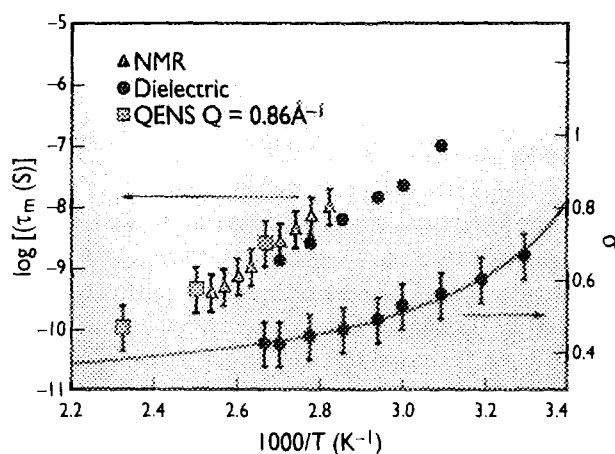


FIGURE 2: Temperature dependence of both α obtained from macroscopic measurements, and the characteristic relaxation times as obtained from macroscopic and microscopic measurements. The solid line was used for the evaluation of the values of σ for the fitting of the QENS spectra.

- J. A. ZETSCHKE, E.W. FISCHER, ACTA POLYMER 45 (1994) 168 ■ J. C.M. ROLAND, K.L. NGAI, MACROMOLECULES 25 (1992) 363
 ■ J. A. ALEGRIA, J. COLMENERO, K.L. NGAI, C.M. ROLAND, MACROMOLECULES 27 (1994) 4486 ■ J. A. ALEGRIA, I. CENDOYA,
 J. COLMENERO, J.M. ALBERDI, B. FRICK (TO BE PUBLISHED) ■ J. COLMENERO, A. ALEGRIA, J.M. ALBERDI, F. ALVAREZ, B. FRICK, PHYS.
 REV. B 44 (1991) 7321.

BUTTERFLY PATTERNS IN A SHEARED LAMELLAR-SYSTEM

■ P. LINDNER (ILL),
■ J. ZIPFEL AND W. RICHTER (UNIV. FREIBURG).

FR9704849

A TECHNOLOGICALLY IMPORTANT EXTENSION OF "CLASSICAL" SCATTERING TECHNIQUES IS TO INVESTIGATE SOFT-MATTER SYSTEMS UNDER NON-EQUILIBRIUM CONDITIONS. SHEAR FLOW IS KNOWN TO HAVE A PROFOUND INFLUENCE ON THE STRUCTURE AND ORIENTATION OF COMPLEX FLUIDS LIKE THERMOTROPIC OR LYOTROPIC LIQUID-CRYSTALS, COLLOIDAL AND POLYMERIC SOLUTIONS. THERE IS A FUNDAMENTAL INTEREST IN UNDERSTANDING THE MICROSCOPIC STRUCTURE AND DYNAMICS OF SUCH COMPLEX FLUIDS AS THE MACROSCOPIC MATERIAL PROPERTIES MIGHT CHANGE WITH THE APPLICATION OF AN EXTERNAL PERTURBATION LIKE SHEAR. THE FOLLOWING EXAMPLE ILLUSTRATES A RECENT STUDY OF THE INFLUENCE OF SHEAR ON THE STRUCTURE OF A LYOTROPIC LAMELLAR PHASE. RESULTS USING A CONE-AND-PLATE AND THE ILL COUETTE TYPE SHEAR-CELL WERE OBTAINED BY RHEO-SMALL-ANGLE LIGHT SCATTERING (RHEO-SALS) AND SMALL-ANGLE NEUTRON SCATTERING (SANS) AT D11. BECAUSE OF THE BROAD RANGE OF MOMENTUM TRANSFER Q AVAILABLE AT D11 A CHARACTERISTIC BUTTERFLY-PATTERN(*) WITH A SCATTERING PEAK REVEALING BOTH THE STRUCTURE AND THE SUPRAMOLECULAR STRUCTURE OF THE SYSTEM COULD BE DETECTED AT VERY LOW Q .

The influence of shear on the structure of lyotropic lamellar phases was studied with aqueous mixtures of the non-ionic surfactant C12E4 (tetraethyleneglycol dodecylether) with 33.6% C12E4 in D₂O by weight. At low shear-rates, a four lobe pattern was observed in depolarised rheo-SALS indicating the existence of vesicles on the length scale of a few micrometers [1]. SANS experiments at relatively high Q ($\geq 0.01 \text{ \AA}^{-1}$) using the ILL Couette type shear-cell with a 1 mm gap at the instrument D11 revealed a lamellar spacing of 80 \AA (d_l in Fig. 3). The scattering intensity was higher perpendicular to the flow direction as compared to along the flow direction. From these results we concluded that the vesicles are elongated under flow.

At high shear-rates, a characteristic butterfly pattern was found in rheo-SALS. The SANS measurements at high Q ($\geq 0.01 \text{ \AA}^{-1}$), however, revealed no obvious changes at high shear-rates. Thus the local structure was not significantly altered at higher shear-rates. Therefore additional SANS experiments at *very low* Q were performed, in order to investigate the structure under shear on a greater length-scale. With the D11 detector at 35.7 m ($0.0011 \leq Q [\text{ \AA}^{-1}] \leq 0.0063$) a butterfly pattern has been observed at shear-rates of about 1200 s^{-1} (see Fig. 1). It disappeared immediately after cessation of flow (Fig. 2). This butterfly pattern was accompanied by a scattering peak at 0.0048 \AA^{-1} perpendicular to the flow direction.

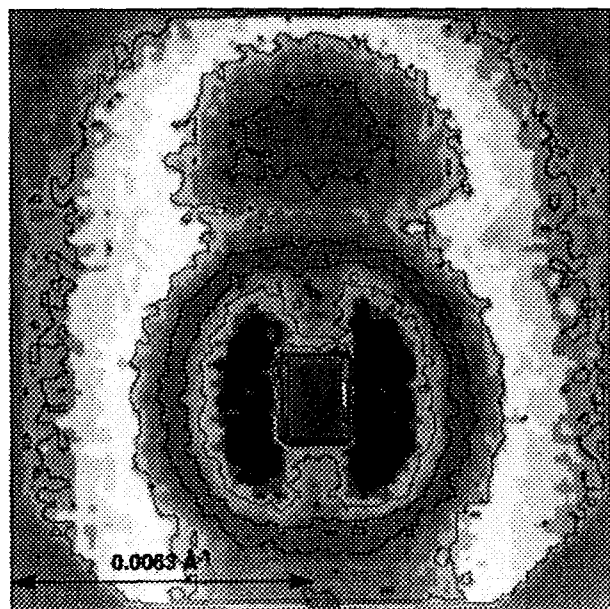


FIGURE 1: Butterfly pattern at a shear gradient of 1200 s^{-1} (sample-to-detector distance 35.7 m, wavelength $\lambda = 10 \text{ \AA}$).

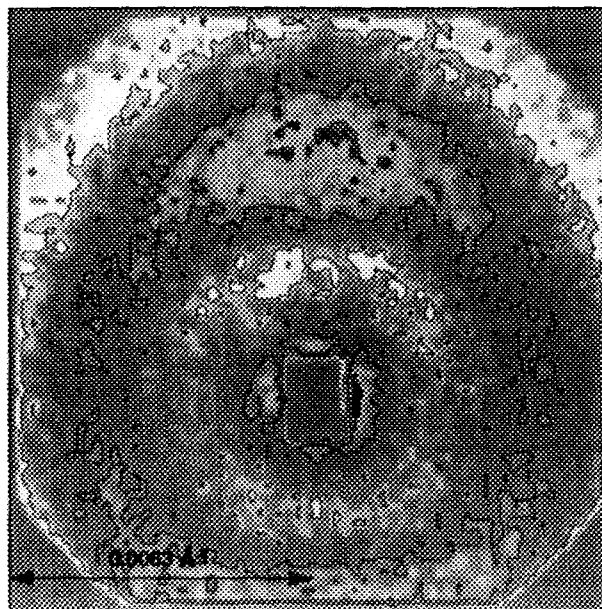


FIGURE 2: Pattern after cessation of flow.

(*) A "butterfly" describes a scattering pattern with enhanced scattering in the direction of flow.

After cessation of flow the diffraction pattern showed a ring at the same Q but with an intensity maximum still perpendicular to the direction of flow.

This corresponds to a structure with a preferential distance of approximately 1300 Å (d_2 in Fig. 3) between individual vesicles. Fig. 3 displays the angular dependence of the absolute scattering intensity for both higher and very low Q experiments combined.

The data are averaged over 30°-sectors parallel and perpendicular to the flow direction. Also shown in the figure is a model for the structure in real space in the quiescent state (left side) and under shear (right side).

At low Q one can see in Fig. 3 (a) the enhanced scattering intensity along the direction of flow, (b) the scattering peak perpendicular to the flow direction.

At high Q , the scattering peak due to the distance between surfactant double layers (d_1) can be observed both perpendicular and along the flow direction.

The butterfly pattern indicates the formation of flow-enhanced concentration fluctuations along the flow direction and is known from semi-dilute polymer solutions [2] and polymer networks [3]. The length scale of the concentration fluctuations along the flow direction is of the order of approximately 7000 Å. In the quiescent state the scattering ring (1300 Å) indicates that the vesicles have a random dense packing. Under shear the vesicles are elongated and the ordered structure is perturbed along the flow direction but prevails perpendicular to the flow direction where no enhancement of scattering was observed at small angles, thus explaining both the butterfly pattern and the diffraction peak. It is also possible to control the size of the relatively mono-

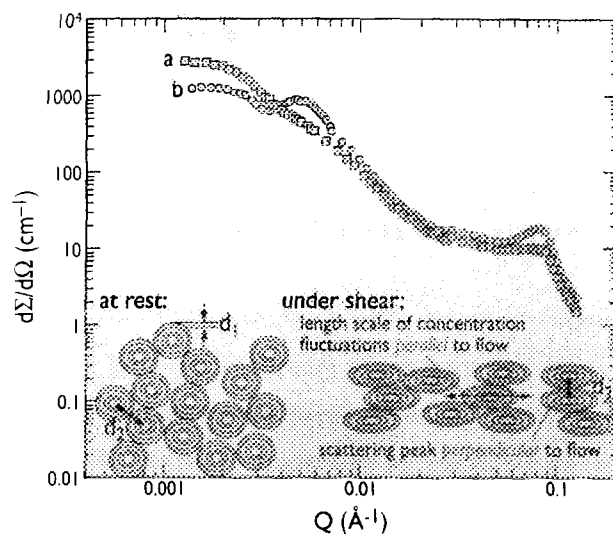


FIGURE 3: Absolute scattering intensity averaged over 30°-sectors along (a) and perpendicular (b) to flow direction. Model for the structure at rest (left side) and under shear (right side) in real space. d_1 corresponds to the distance of the double layers, d_2 to the preferential distance between individual vesicles.

disperse vesicles by means of the shear-rate. [4] For example, when the shear-rate was reduced to 80 s⁻¹, the butterfly pattern was still observed but at smaller momentum transfers Q . Again a ring was found after cessation of shear and the scattering peak was now at 0.0021 Å⁻¹ corresponding to a vesicle distance of 3000 Å.

This work describes a new structure of a lyotropic lamellar phase at high shear-rates, in addition to the previously reported aligned defect free lamellar phase [4] and the hexagonal assembly of vesicles [5].

- R. WEIGEL, J. LAUGER, W. RICHTER, P. LINDNER, J. PHYS. II FRANCE 6 (1996) 529 ■ F. BOUÉ, P. LINDNER, FLOW-INDUCED STRUCTURES IN POLYMERS, A. NAKATANI, M. DADMUN (EDS), ACS SYMPOSIUM SERIES 597, WASHINGTON 1995 ■ A. RAMZI, E. MENDES, F. ZIELINSKI, C. ROOF, A. HAKIKI, J. HERZ, R. OESER, F. BOUÉ, J. BASTIDE, J. PHYS. IV FRANCE 3 (1993) 91 ■ O. DIAT, D. ROUX, F. NALLET, J. PHYS. II FRANCE 3 (1993) 1427 ■ O. DIAT, D. ROUX, F. NALLET, PHYS. REV. E 51 (1995) 3296.

TIME-RESOLVED SMALL-ANGLE NEUTRON SCATTERING OF A MICELLE-TO-VESICLE TRANSITION

■ S. U. EGELHAAF (ILL),
■ P. SCHURTENBERGER (ETH ZURICH).

FR9704850

AMPHIPHILIC MOLECULES SPONTANEOUSLY SELF-ASSEMBLE IN SOLUTION TO FORM A VARIETY OF AGGREGATES. THE UNDERSTANDING OF THE EQUILIBRIUM PROPERTIES OF THESE AGGREGATES, SUCH AS THEIR SHAPE AND SIZE, HAS MADE SIGNIFICANT PROGRESS. HOWEVER, ONLY LIMITED INFORMATION IS AVAILABLE ON THE KINETICS OF THE STRUCTURAL TRANSITIONS AS WELL AS ON THE EXISTENCE OF NON-EQUILIBRIUM OR METASTABLE STATES. AQUEOUS MIXTURES OF LECITHIN AND BILE SALT ARE VERY INTERESTING BIOLOGICAL MODEL-SYSTEMS WHICH EXHIBIT A SPONTANEOUS TRANSITION FROM POLYMERLIKE MIXED MICELLES TO VESICLES UPON DILUTION. THE SMALL-ANGLE NEUTRON SCATTERING (SANS) INSTRUMENT D22, WITH ITS VERY HIGH NEUTRON FLUX AND THE BROAD RANGE OF SCATTERING VECTORS COVERED IN A SINGLE INSTRUMENTAL SETTING, ALLOWED US FOR THE FIRST TIME TO PERFORM TIME-RESOLVED SCATTERING EXPERIMENTS IN ORDER TO STUDY THE MICELLE-TO-VESICLE TRANSITION. THE TEMPORAL EVOLUTION OF THE AGGREGATE STRUCTURES WERE FOLLOWED AND DETAILED INFORMATION WAS OBTAINED EVEN ON MOLECULAR LENGTH-SCALES.

Surfactants in solution exhibit a complex aggregation behaviour as a result of a delicate balance of opposing forces. An important aspect of surfactant systems is the relation between the chemical composition and the shape of the aggregates (Fig. 1). The structures are described by theoretical concepts based either on packing considerations of the surfactants in the aggregates or on the spontaneous curvature, which the surfactant film tries to realize. SANS is a particularly powerful technique in order to experimentally verify these theoretical models and to improve our understanding of the structural aspects of surfactant systems since it allows for a characterization of structural properties on all length scales.

EQUILIBRIUM PROPERTIES

Aqueous mixtures of lecithin and bile salt are important examples of multicomponent systems. They not only serve as interesting model-systems, but are also of great relevance in biology, physiology, and in pharmaceutical applications.

Depending on the bile salt-to-lecithin-ratio and the total lipid concentration, they form various structures [4]. A detailed SANS study using D22 resulted in the following picture (Fig. 2): Upon dilution of a mixed micellar stock solution the shape of the micelles changes from small spherical to elongated, flexible and locally cylindrical polymerlike structures. This is caused by the decrease of the bile salt-to-lecithin-ratio in the aggregates upon dilution, which appears to lower the average spontaneous curvature of the mixed micelles. Endcaps are therefore avoided and the micelles are forced to grow. At even higher dilutions the formation of locally lamellar structures is favoured and a spontaneous micelle-to-vesicle transition is induced. Beyond the micellar phase-boundary vesicles coexist with cylindrical micelles. In this region the sizes of the vesicles and micelles remain approximately constant and only their relative amount changes. At still higher dilutions a single phase of relatively monodisperse vesicles, whose size decreases upon dilution, exists.

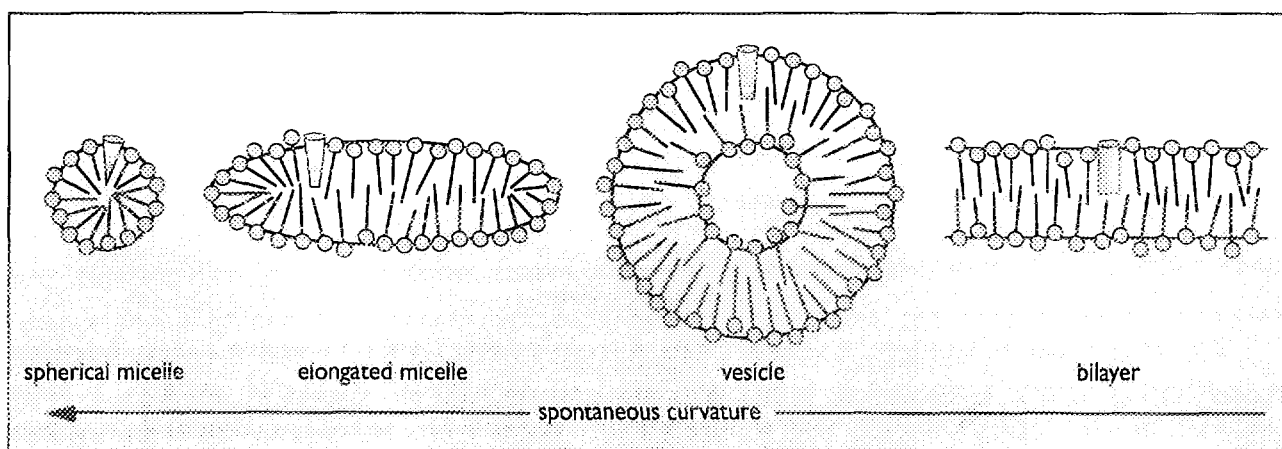


FIGURE 1: Shapes of surfactant aggregates as a function of the spontaneous curvature.

NON-EQUILIBRIUM EXPERIMENTS

While this transition has been observed in a number of surfactant systems, several aspects of it remain highly controversial. The exact sequence of the structural evolution and the existence of intermediate structures, such as connected networks or perforated bilayers, is still not conclusively determined. Not even the question of whether vesicles represent true equilibrium structures is unambiguously solved. Based on the well established phase behaviour, an investigation of the kinetic aspects of the micelle-to-vesicle transition using time-resolved light scattering (LS) and SANS was started. In these experiments the transition was induced by rapidly diluting an equilibrated micellar stock-solution to a concentration, where vesicles exist under equilibrium conditions (Fig. 2, blue lines).

LS measurements, which were performed on a dedicated multiangle instrument, indicate the presence of an initial and relatively rapid formation of an intermediary structure, followed by the formation of vesicles according to a first-order kinetics with a time-constant of typically 1.5 h.

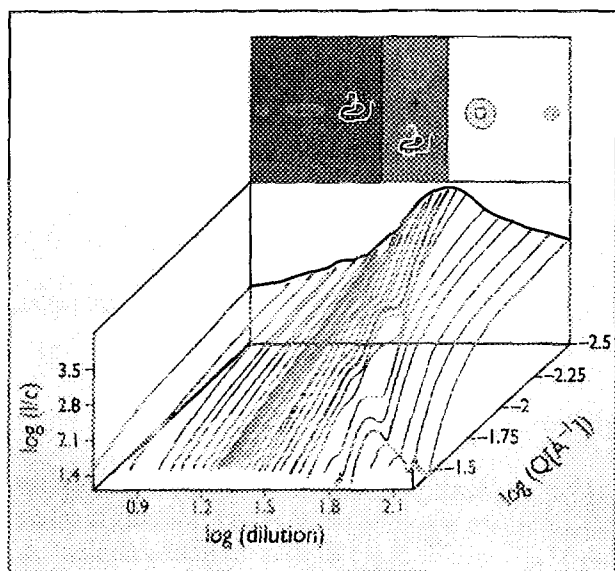


FIGURE 2: Normalised scattering intensity $I(Q)/c$ as a function of scattering vector Q for a dilution series of equilibrated aqueous mixtures of lecithin and bile salt as measured by SANS. The observed aggregates and phase boundaries are represented schematically. The blue lines correspond to the initial and final concentrations, respectively, of the dilution-induced micelle-to-vesicle-transition shown in Fig. 3.

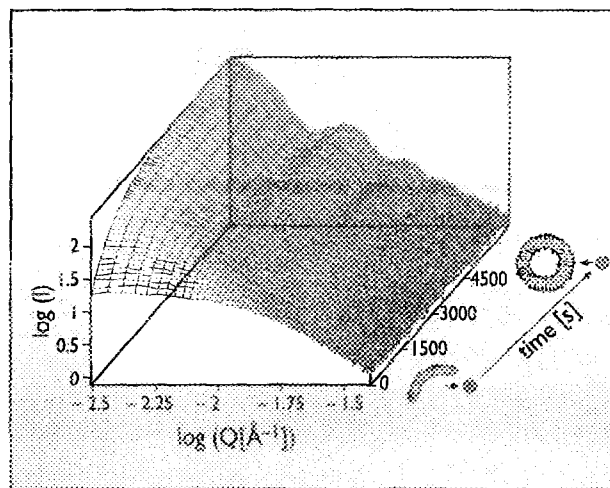


FIGURE 3: Temporal evolution of the scattering intensity $I(Q)$ as a function of scattering vector Q for a dilution-induced micelle-to-vesicle transition as observed by SANS.

From this intermediate structure the vesicles might form either directly or via a second, short-lived intermediate, which then very rapidly transforms into vesicles and is therefore not observable.

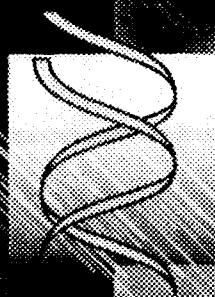
Due to the limited range of scattering vectors Q , LS allows for rather indirect conclusions on the structure of the aggregates only. This limitation can be overcome by SANS, which covers a Q -range that is ideal for such studies. Therefore SANS experiments were performed at D22, which offers the unique possibility for time-resolved studies of this transition due to its very high neutron flux and the large Q -range covered in a single instrumental setting. A measurement time of one minute already results in sufficiently good statistics, although the samples typically have surfactant concentrations c of only 1 mg/ml to avoid problems due to intermicellar interaction effects.

Fig. 3 provides an example of the temporal evolution of the Q -dependence of the scattered intensity $I(Q)$ during the course of a dilution-induced micelle-to-vesicle transition.

The SANS data not only confirm the conclusions drawn from LS, but furthermore provide us for the first time with information on molecular length-scales that have made possible a detailed analysis of the structural evolution during this important transition.



FR9704851



INSIGHT INTO THE ASSEMBLY OF CHAPERONES

by R. P. MAY (ILL),
 R. STEGMANN, E. MANAKOVA, M. ROSSLE, T. HERMANN AND H. HEUMANN (MPI MARTINSRIED),
 S. AXMANN AND A. PLÜCKTHUN (UNIV. ZÜRICH),
 A. WIEDENMANN (HMI BERLIN).

CHAPERONES ARE PROTEINS THAT HELP OTHER PROTEINS (SUBSTRATE PROTEINS) TO ACQUIRE A "GOOD" CONFORMATION. THE FOLDING IS A DYNAMIC PROCESS AND INVOLVES REPETITIVE BINDING AND RELEASE OF THE CHAPERONE COMPONENTS AND OF THE SUBSTRATE PROTEIN. SMALL-ANGLE NEUTRON SCATTERING CONTRIBUTES TO THE UNDERSTANDING OF THE STRUCTURAL CHANGES THAT APPEAR TO HAPPEN DURING THE FOLDING PROCESS.

INTRODUCTION

For quite some time it has been known that cells are able to recover from chemical and thermal stress that was expected to destroy cell components like proteins. In the eighties, it was found that a new class of proteins, chaperones, is involved in the protection of cells and in their recovery from external stress.

Chaperones [1] can be found in all cells. In the bacterium *Escherichia coli*, they consist of two major molecules, GroEL and GroES. GroEL can be described as a hollow cylinder formed by two heptameric rings ("double donut") with a molecular mass of altogether $14 \times 57000 = 798000$ g/mol. GroES forms a cap made of seven equal units (monomers) of 10 000 g/mol. The three-dimensional structures of GroEL and GroES are known at atomic resolution from X-ray crystallographic studies by the groups of Sigler and Deisenhofer, and their association/dissociation behaviour has been investigated by electron microscopy and by biochemical techniques. It appears that chaperones have no preference for certain cellular proteins, but they can differ between proteins which are correctly or incorrectly folded. It is suggested that the chaperone provides an environment for unfolded or badly folded proteins, favouring the correct folding which may require several rounds of binding to and release from the chaperone.

THE ROLE OF NEUTRON SCATTERING

In spite of the excellent quality of the studies mentioned above, the structural mechanisms that are necessary to ensure correct protein folding are far from being fully understood. This is partly due to the fact that the X-ray crystallographic results published so far concern the single components GroEL and GroES, and that some important parts of both molecules do not appear in the map due to molecular disorder.

On the other hand, the low resolution of electron micrographs can only indicate some of the structural transitions.

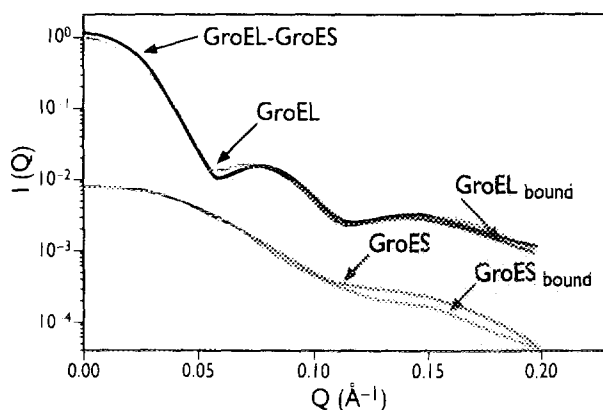


FIGURE 1: The scattering curves of the GroEL-GroES complex and those of GroEL and GroES, isolated and in the complex.

Small-angle neutron scattering studies published by an American group and also our own investigations contribute to filling in the missing information. Both data sets suggest that the missing protein parts in GroEL form a sort of plug in the centre that explains why the substrate protein cannot tunnel from one ring to the other.

We were now able to obtain GroEL and GroES in deuterated form by "overexpressing" them, i.e. by genetically modifying *E. coli* in such a way that they produce mainly those proteins, in heavy water (D_2O).

The neutron scattering curves of chaperones built from deuterated GroEL and GroES and from chaperones containing hydrogen in natural abundance were measured in varying amounts of D_2O in the solution. Data were obtained at D11 and D22 of the ILL and at the SANS facility of HMI Berlin. As a result, we were able to isolate the scattering contributions of GroEL and GroES when they are bound to each

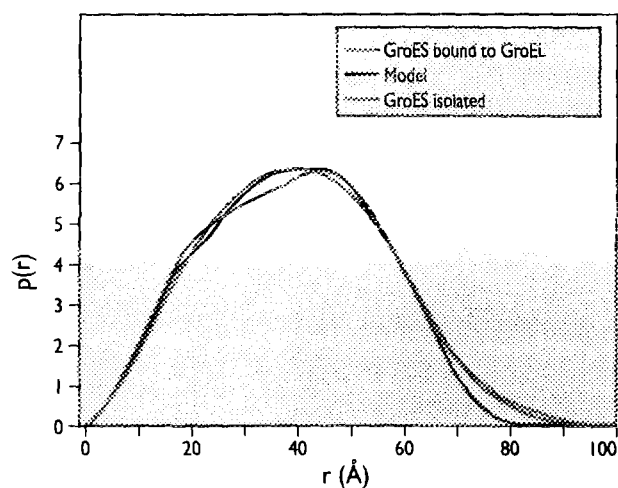


FIGURE 2: Pair distance distribution function of isolated GroES and of GroES bound in the complex with GroEL along with a curve corresponding to our model of bound GroES.

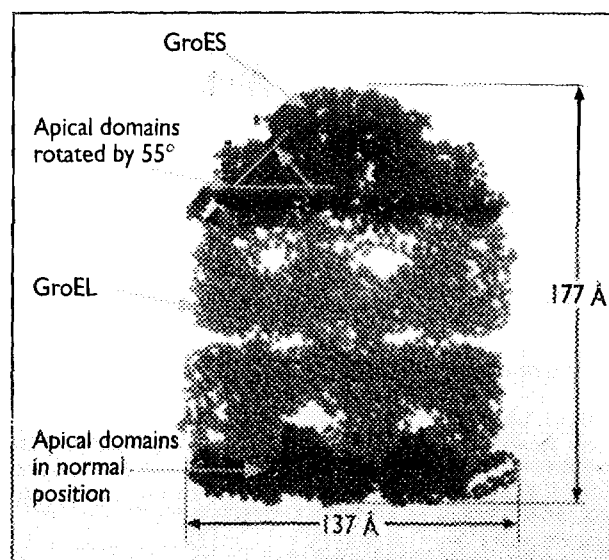


FIGURE 3: Model of the GroEL-GroES complex combining crystallographic data for the subunits and our small-angle neutron scattering results.

other and to compare them with the scattering from isolated GroEL and GroES. We found significant changes of the scattering curves of both GroEL and GroES upon binding. We can attribute these to structural changes in GroEL and GroES: In the complex with GroEL, the GroES dome structure is seen as becoming flatter than in the isolated state. The "apical domains", i.e. the part of the 14 GroEL monomers facing towards the ends of the GroEL hollow cylinder, assume two different conformations. At the end where they are in contact with GroES, they are turned by 55° outwards; at the other end, they keep the structure revealed by X-ray-crystallography. By combining the information from the different neutron scattering curves and the crystallographic data, we were able to suggest a model [2] for the association of GroEL and GroES (Fig. 3).

HIGH-RESOLUTION NEUTRON DIFFRACTION STUDIES OF BIOLOGICAL AND INDUSTRIAL FIBRES



FR9704852

P. LANGAN, S.A. MASON (ILL),
W. FULLER, V.T. FORSYTH, A. MAHENDRASINGAM, M. SHOTTON, L. SIMPSON (KEELE UNIV.),
H. GRIMM (FZ JÜLICH),
R. LEBERMAN (EMBL).

NEUTRON DIFFRACTION IS BECOMING AN IMPORTANT TOOL FOR STUDYING FIBRES DUE TO ITS COMPLEMENTARITY TO X-RAY DIFFRACTION. UNLIKE X-RAYS, SCATTERING OF NEUTRONS BY POLYMER ATOMS IS NOT A FUNCTION OF THEIR ATOMIC NUMBER. IN HIGH-RESOLUTION STUDIES (1.5-3 Å) ON D₁₉ DEUTERATION (REPLACING H BY D) IS BEING USED TO CHANGE THE RELATIVE SCATTERING POWER OF CHOSEN GROUPS MAKING THEM EASIER TO LOCATE. IN THIS CONTRIBUTION WE DESCRIBE RECENT STUDIES ON DNA AND CELLULOSE.

BIOLOGICAL FIBRES

Fibres provide an environment in which polymers and filamentous macromolecules which do not form single crystals can be ordered and studied using diffraction. The first detailed configurations for biological macromolecules came from X-ray fibre diffraction studies and pointed to a relationship between structure and function. Fibres are particularly well-suited to the investigation of this relationship because transitions between distinct conformations with different associated functions can be induced in them by varying their hydration. The relatively large scattering power of D₂O and the ability to replace H₂O in fibres by D₂O means that there are important advantages in using neutrons rather than X-rays in order to study hydration and the central role it plays in controlling biological structure.

One of the biological fibres being studied on D₁₉ is of DNA, a flexible polymer consisting of two polynucleotide chains in the form of a double helix which plays a central role in protein synthesis and is responsible for the transmission of our genetic code. X-ray studies have provided detailed models for the distinct forms of natural (A, B, C) and synthetic (D, S) DNA. Neutron studies have allowed detailed patterns of hydration to be imaged around the D and A forms. This year these studies have been extended to the B and S forms, with technological and methodological advances allowing new types of experiments. In addition to the isotopic substitution of water it is now possible to substitute H covalently bound to DNA. Specific deuteration is being used to highlight different components in a manner which is not possible with X-rays. Perdeuteration is being used to improve data quality by removing incoherent scattering from hydrogen. An efficient fibre precession geometry for data collection and an automatic humidity control-system have allowed the first high-resolution neutron fibre diffraction-study of a humidity-induced structural transition between two different forms of DNA. The gains in data quality resulting from deuteration are illustrated by studies on A-DNA hydration. Localised water is imaged as density in difference-Fourier maps; the diffe-

rences between amplitudes corresponding to DNA surrounded by D₂O and then H₂O are combined with phases calculated from X-ray models. The original hydrogenous A-DNA map has density corresponding to an ordered primary hydration shell. However the perdeuterated A-DNA map contains additional density lying across one of the DNA grooves, Fig. 1.

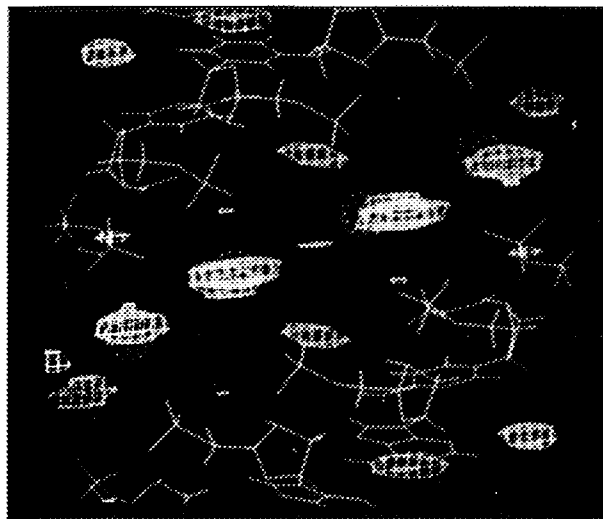


FIGURE 1: This figure illustrates how data quality has been improved by removing incoherent scattering from hydrogen. The neutron difference-density (blue) represents localised water around the A-form of perdeuterated DNA (yellow skeletal model) which did not appear in the density around hydrogenous DNA. This water is in the second hydration shell and co-ordinates with cations and water in the first shell.

This density represents water in a secondary hydration shell which appears to coordinate with the primary hydration shell and cation positions determined in X-ray studies. Ordered water in one helical groove of the A-form as a stabilising factor contrasts to a spine of hydration in the other groove of the D-form. These results suggested a mechanism for transition between the A-form, implicated in replication, and the B-form which is similar to the D-form and is the putative form of DNA when wrapped around the nucleosome.

INDUSTRIAL FIBRES

Fibres also have properties which make them important industrial materials. Whereas natural materials, such as cellulose our most abundant renewable material, consist of oriented crystallites, the synthesis of man-made polymers leads to unoriented materials. In both cases further processing is required to improve physical properties and X-ray fibre diffraction is used to relate these improvements to changes in orientation, crystallinity and molecular conformation. In a recent neutron experiment on D19 H/D substitution has been used to study the processing of cellulose. Natural cellulose, cellulose I, is used in industry after undergoing treatment with NaOH. This mercerisation process involves a structural conversion to cellulose II with associated improvements in strength, appearance and reception to dye. In this study data was collected from a sample treated with NaOH and then from another treated with NaOD. The corresponding difference synthesis indicates where hydrogen bonds have been disrupted and H exchanged for D during structural conversion (3), Fig. 2.

OUTLOOK

Although there will be further advances in methodology, particularly in sample preparation, as the trend for using this new technique attracts more projects, the most significant potential advance is in detector technology. High-resolution neutron fibre diffraction-studies are feasible only because of the availability of large position-sensitive detectors, PSD's, on high-flux diffractometers such as D19, which

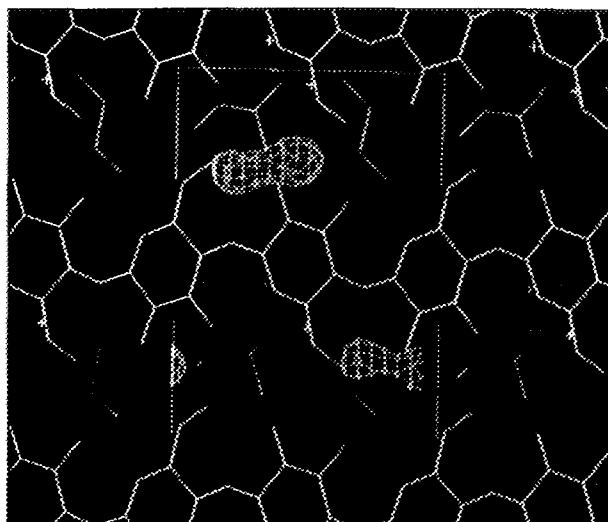


FIGURE 2: The Fourier-difference synthesis calculated using the differences between amplitudes corresponding to cellulose being treated with NaOH and NaOD combined with phases calculated from an X-ray model. The difference density indicates where hydrogen bonds have been broken and H exchanged by D during structural conversion from cellulose I to II.

allows the efficient coverage of large continuous volumes of reciprocal space. By increasing the size of the D19 PSD we can gain factors of 10 in data collection efficiency, allowing new types of experiments and smaller samples.

To this end, this year saw the first successful tests of a large image-plate detector on D19 and next year we plan to test a microstrip gas detector.

-
- V.T. FORSYTH, A. MAHENDRASINGAM, W.J. PIGRAM, R.J. GREENALL, K.A. BELLAMY, W. FULLER AND S.A. MASON, *INT. J. BIO. MACR.* 11 (1989) 236 ■ P. LANGAN, V.T. FORSYTH, A. MAHENDRASINGAM, W.J. PIGRAM, S.A. MASON AND W. FULLER, *J. BIOM. STR. DYN.* 10 (1992) 489 ■ V.T. FORSYTH, W. FULLER, P. LANGAN, A. MAHENDRASINGAM, M. WHALLEY, S.A. MASON AND C.C. WILSON, IN "NEUTRONS IN BIOLOGY", Eds SCHOENBORN, B. & KNOTT, R. (PLENUM) (IN PRESS) ■ P. LANGAN, R.C. DENNY, A. MAHENDRASINGAM, S.A. MASON AND A. JABER, *J. APP. CRYST.* 29 (1996) 383 ■ M. SHOTTON, J. ARCHER AND P. LANGAN (IN PREPARATION) ■ P. LANGAN, *PHYSICA B* (IN PRESS).

THE STUDY OF MEMBRANE-PROTEIN /DETERGENT INTERACTIONS BY NEUTRON CRYSTALLOGRAPHY

P.A. TIMMINS, S. PENEL (ILL),
E. PEBAY-PYROULA (IBS).



FR9704853

PROTEINS WHICH ARE FOUND EMBEDDED IN MEMBRANES CAN USUALLY ONLY BE PURIFIED AND STUDIED FROM THE POINT OF VIEW OF STRUCTURE BY DISSOLVING THEM IN DETERGENTS. THE STRUCTURE OF THE RESULTING MIXED PROTEIN-DETERGENT COMPLEXES ARE POORLY UNDERSTOOD. AN IMPORTANT METHOD FOR STUDYING THEM IS THROUGH NEUTRON DIFFRACTION OF THE CRYSTALLINE COMPLEXES. THIS ALLOWS US TO UNDERSTAND BETTER HOW THE PROTEINS BEHAVE IN THE NATURAL MEMBRANE AS WELL AS ALLOWING US TO VISUALISE AND HOPEFULLY IMPROVE THE CRYSTALLISATION PROCESS. STUDIES ON THE PORE-FORMING PROTEIN PORIN USING DATA COLLECTED ON THE DIFFRACTOMETER DB21 ARE DESCRIBED.

Many of the most important proteins controlling biological function are found embedded in cellular membranes. Their roles are many and various. Some act as signal transducers, transmitting signals from one side of the membrane to the other, others act as receptors, for example, for hormones, whilst others allow the passage of nutrients or other small molecules across the membrane.

The key to understanding of these functions lies in the determination of the structure of the proteins and their interaction with the membrane. Unlike intracellular or serum proteins, however, membrane proteins are usually insoluble in water and are therefore very difficult to study.

They may however, be removed from the membrane and solubilised in detergent solutions. It has in the last few years been possible to isolate and crystallise a few membrane proteins in this way and then to study their structures by X-ray crystallography. Such protein structures have provided a wealth of information enabling us to understand in more detail for example the photosynthetic process in photosynthetic bacteria and also the passage of small-size molecules through the outer membranes of Gram-negative bacteria via proteins known as porins.

The X-ray crystallographic results, however, have not been able to give any information concerning the detergent molecules which in the crystal interact with the protein molecules and play a role similar to phospholipid molecules in the real membrane.

Such information is important for two reasons : (1) knowledge of the protein detergent interaction will help us to understand the interactions between protein and lipid in the membranes and (2) it will also help us to understand better the process of membrane protein-crystallisation and perhaps allow us in future to design more rational approaches to membrane protein-crystallisation.

The reason why detergent molecules are not visible in X-ray crystallographic studies is that the detergent phase is fluid and for X-rays it is essentially indistinguishable from water.

This is not however the case for neutrons [1,2] where by varying the H_2O/D_2O ratio in the crystals (membrane protein crystals contain about 30-40% each of protein, water and detergent) it is possible to increase or decrease the contrast between the water and the detergent or the protein (Fig. 1).

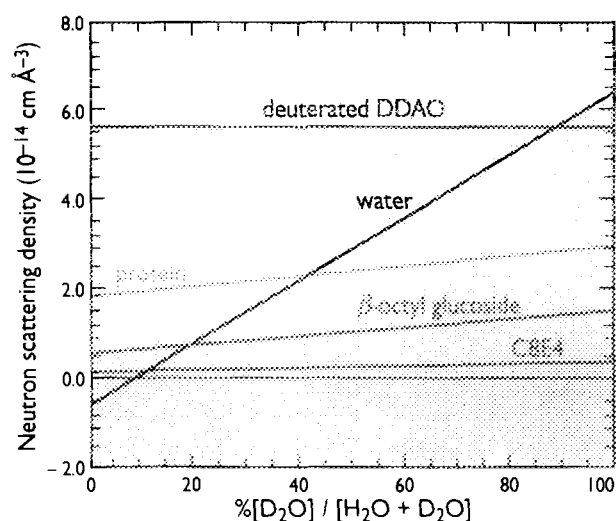


FIGURE 1: Scattering power of water, protein and various detergents as a function of the deuterium content of the solvent water. The scattering power of protein is seen to be the same as that of water in a solution containing 40% $D_2O/60\%$ H_2O whereas that of the detergents C8E4 and β -octyl glucoside are the same as 9.3% and 18.6% D_2O respectively. When the alkyl chain of the detergent is fully deuterated, as in DDAO, the match point is at 88.9% D_2O .

The membrane protein porin allows the passage of small molecules up to about 700 daltons molecular weight through the outer membrane of Gram-negative bacteria. The detergent binding in crystals of porin from two different bacteria, *E. Coli* and *Rhodobacter Capsulatus*, has been studied by neutron scattering.

In each case crystals of about 0.1 mm^3 in volume, containing detergent solubilised porin and water are soaked for about 3 weeks in H_2O/D_2O mixtures containing typically 0, 25, 70 and 100% D_2O .

Diffraction data are then measured from each crystal to a resolution of about 12 Å on the diffractometer DB21.

It is then possible to calculate a neutron-scattering density map for any of these crystals or by interpolation for a crystal containing any intermediate H₂O/D₂O ratio.

So, for example, a neutron density-map calculated for a D₂O content of 40% will render the protein invisible and reveal only the detergent.

Conversely at around 20% D₂O (depending on the exact chemical nature of the detergent) only the protein is visible.

In the case of the porin from *E. Coli* (also known as OmpF porin) crystals were produced containing either lauryl NN'-dimethyl amine oxide or partially deuterated decyl NN'-dimethyl amine oxide.

The neutron diffraction results show that the two detergents bind the protein in an identical way [1].

Fig. 2 is an illustration of a neutron-scattering density map (red) for a porin crystal containing a mixture of 40% D₂O/60% H₂O and where the observed density corresponds therefore to the detergent.

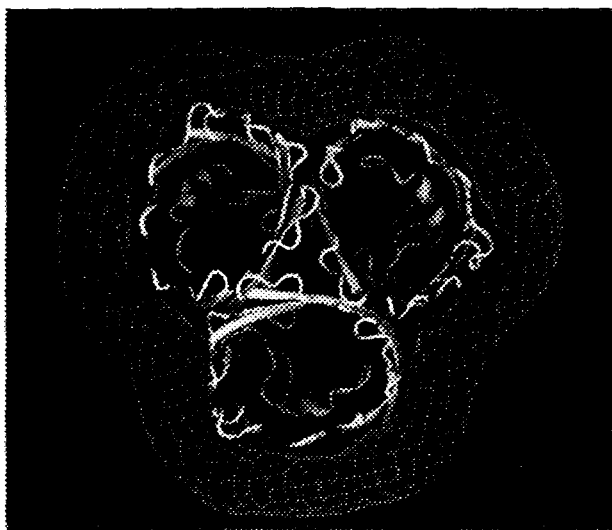


FIGURE 2: Structure of the detergent ring around a trimer of the OmpF porin from *E. Coli*. The red contours represent the detergent molecules which form a fluid belt around the protein molecule (yellow) which had previously been determined by X-ray crystallography.

The protein molecule, whose structure had previously been determined by X-ray crystallography is superimposed in yellow. It consists of a trimeric molecule of total molecular weight ~ 120 000. The figure shows how the detergent forms a well defined belt around the protein and detailed examination reveals that the borders of this belt are determined by specific interactions between hydrophobic aromatic amino acids in the side chains.

The packing of the protein/detergent complexes in the crystal is shown in Fig. 3. The protein molecules themselves form two interpenetrating lattices having no contacts between them. The cohesion of the crystal depends on the contacts between detergents belts (red contours) attached to protein molecules in the independent lattices.

ACKNOWLEDGEMENTS

The experiments on porin from *Rhodobacter Capsulatus* were carried out in collaboration with W. Welte, J. Hovers and Th. Wacker (Universities of Freiburg and Konstanz) and on OmpF porin with J. Rosenbusch, T. Schirmer and the late M. Zulauf (Biozentrum Basel) and R.M. Garavito (Michigan State University).

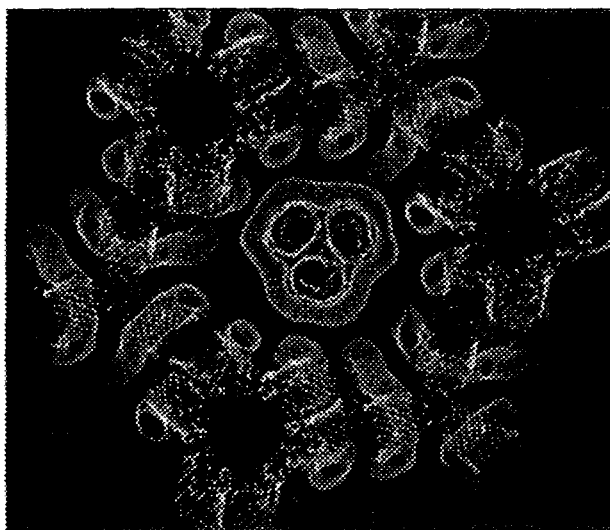
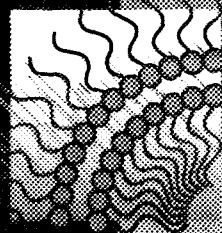


FIGURE 3: Crystal packing of a number of the protein detergent complexes as shown in Fig. 2. The picture shows the complex interactions present: protein-protein interactions within one network (yellow) but no protein-protein interactions between the central trimer and the surrounding network. Instead the contacts between the networks take place only through detergent-detergent (red) interactions. Even here the contacts are very tenuous.

.....
 ■ P.A. TIMMINS, E. PEBAY-PEYROULA, W. WELTE, BIOPHYS. CHEM. 53 (1-2) (1994) 27 ■ P.A. TIMMINS, NEUTRON NEWS 6 (1) (1995) 13 ■ E. PEBAY-PEYROULA, R.M. GARAVITO, J.P. ROSENBUSCH., M. ZULAUF, AND P.A. TIMMINS, STRUCTURE 3 (1995) 1051
 ■ P.A. TIMMINS, E. PEBAY-PEYROULA AND W. WELTE (1996) BROOKHAVEN SYMPOSIUM ON NEUTRONS IN BIOLOGY, (EDS. B. P. SCHOENBORN AND R. KNOTT), PLENUM PRESS, NEW YORK, BOSTON, LONDON.

SURFACES AND THIN FILMS



MAGNETIC STRUCTURE IN ULTRA-THIN Fe/Cr MULTILAYERS

V.V. LAUTER-PASSIOUX (UNIV. KONSTANZ),
H.J. LAUTER (ILL).

POLARISED NEUTRON REFLECTIVITY MEASUREMENTS ON D17 HAVE BEEN USED TO DETERMINE THE MAGNETIC MOMENTS IN PERIODIC ULTRA-THIN Fe/Cr MULTILAYERS.

Fe/Cr sandwiches and superlattices are known for the following effects: short and long-range exchange coupling oscillation as a function of the Cr spacing, non-Heisenberg biquadratic coupling, giant magneto-resistance, proximity magnetism and oscillations of magneto-resistance with thickness of Fe layers (see Ref. in 1,2).

Polarised neutron reflectometry (PNR) is an efficient tool in revealing details of the anti-ferromagnetic (AFM) coupling in these Fe/Cr multilayers [1,2]. Even though it is not yet clear what kind of interaction is responsible for the behaviour of the magnetisation. Also, the effects of imperfections play a crucial role in shaping the magnetic moments. Impurity and roughness effects are important.

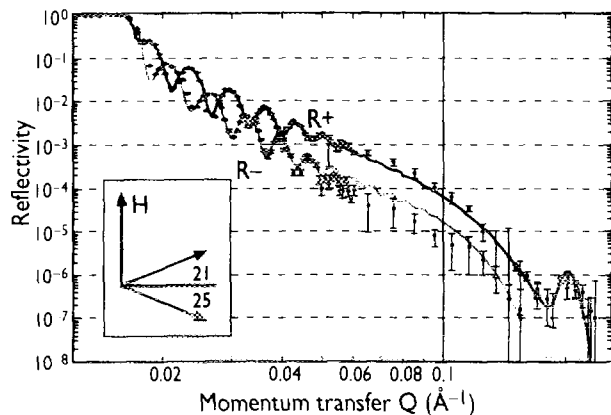


FIGURE 1: Spin-dependent reflectivities, R^+ and R^- , of a (Cr 6 Å / Fe 9 Å) $\times 50$ multilayer in an external magnetic field of 30 Oe, applied parallel to the sample surface. The fit to the data is represented by the solid lines. Insert shows the magnetisation directions in adjacent Fe-layers with respect to the external field.

Another interesting aspect of $^{57}\text{Fe}/\text{Cr}$ multilayers is their potential application in synchrotrons as switchable nuclear monochromators of μeV bandwidth.

Periodic Fe/Cr multilayers were prepared by molecular beam epitaxy. PNR measurements have shown an AFM coupling in these samples with certain peculiarities of the coupling and with a dependence on the details of preparation. The reflectivity curve from one of the samples is shown in Fig. 1. The quality of the samples was extremely good so we could measure the reflectivity profile with polarised neutrons down to 10^{-7} with a sample size of only $10 \times 10 \text{ mm}^2$. Off-specular scattering was about 3 orders of magnitude lower than the specular signal. The Bragg peak around 0.2 Å^{-1} is an AFM-peak arising from the doubling of the extremely small bi-layer period of $6 \text{ Å Cr} / 9 \text{ Å Fe}$.

The two reflectivities R^+ and R^- were obtained with the polarisation of the beam parallel or antiparallel to the external magnetic field of 30 Oe parallel to the sample surface. At this low external magnetic field the film shows magnetic domains. The oscillations at lower Q arise mainly from the total film thickness composed of 32 Å Fe on top of the Al_2O_3 substrate, 50 layers of $[6 \text{ Å Cr} / 9 \text{ Å Fe}]$ and a 58 Å thick covering Cr-layer. The components of the film magnetisation parallel to the magnetic field are obtained from the fit of the two reflectivity curves to the data.

This, together with the assumption of bulk magnetisation in the Fe-layers (which may not be very correct for a thickness of 9 Å) enables the configuration of the magnetisation to be constructed (see insert in Fig. 1).

The data analysis gave the AFM coupling between the Fe layers with a canted angle of 46 deg. At a low field of 30 Oe the antiferromagnetic domains have sublattice magnetisations pointing along one of the crystallographic directions that represent easy axes of magnetisation.

The slight difference in Q_c for R^+ and R^- (below Q_c is the region of total reflection) originates from the slight asymmetry of the magnetisation in the layers with respect to the perpendicular external field direction.

.....
 ■ A. SCHREYER, J.F. ANKNER, TH. ZEIDLER, H. ZABEL, M. SCHAFER, J.A. WOLF, P. GRUNBERG, C.F. MAJKRZAK, PHYS. REV. B 52 (1995) 16066 ■ S. ADENWALLA, G.P. FELCHER, E.E. FULLERTON, S.D. BADER, PHYS. REV. B 53 (1996) 2474 ■ V. LAUTER-PASSIOUK, H.J. LAUTER, D. NAGY, V.M. USTINOV, V.M. UZDIN, E. KORNILOV (TO BE PUBLISHED).

COMPOSITE THIN FILMS OF COPOLYMERS CONTAINING NANOPARTICLES OF $\gamma\text{-Fe}_2\text{O}_3$

V.V. LAUTER-PASSIOUK (UNIV. KONSTANZ),
 H.J. LAUTER (ILL).

STRUCTURAL INVESTIGATIONS HAVE BEEN MADE BY MEANS OF REFLECTIVITY MEASUREMENTS OF A NEW CLASS OF COMPOSITE MATERIALS. THESE ARE COPOLYMERS OF POLYSTYRENE-POLYBUTYLMETHACRYLATE CONTAINING NANOPARTICLES OF 40 OR 60 Å DIAMETER $\gamma\text{-Fe}_2\text{O}_3$. THE NANOPARTICLES ARE SHOWN TO BE CONCENTRATED NEAR THE CENTRES OF THE POLYSTYRENE LAMELLAE.

A new class of copolymers, composite materials, consisting of copolymers with incorporated nanoparticles, has been studied.

The key point is that the copolymer matrix is able to order nanoparticles in a macroscopic crystal with lattice parameters of several hundred Ångströms and that with a change of the copolymer characteristics the crystal structure can be varied (from lamellar to cubic). In addition, the size and material of the nanoparticles influence the macroscopic properties (optical, magnetic etc.) over a wide range.

The presence of nanoparticles induces an elastic distortion of the copolymer matrix, leading in the worst case to particle exclusion and in the best to self-organisation of the particles. Once the mixing is achieved, it is important to understand the interaction between the particles, the correlation between the adjacent layers and the influence of the particle presence on the properties of the medium. In a first step in the investigation of the magnetic behaviour of $\gamma\text{-Fe}_2\text{O}_3$ nanoparticles we report a structural study by reflectometry using D17, aimed at locating the nanoparticles within the polymer-film.

The first sample was symmetric polystyrene-polybutylmethacrylate (PSd-PBMA) diblock copolymer with the molecular weight $M_w = 170$ K. $\gamma\text{-Fe}_2\text{O}_3$ particles with the average diameter of 40 Å were incorporated in the deuterated PS with a concentration of a volume fraction of 20%.

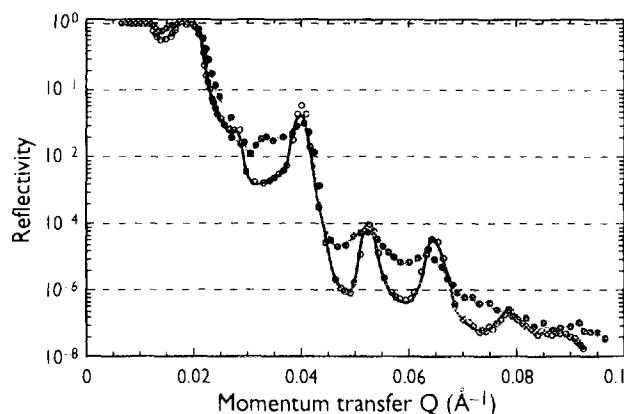


FIGURE 1: Reflectivity for a symmetric PS-PBMA film with 40 Å $\gamma\text{-Fe}_2\text{O}_3$ nanoparticles (•) and without (○) nanoparticles. Solid lines are fits.

The prepared copolymer including the $\gamma\text{-Fe}_2\text{O}_3$ particles was spincoated onto the Si-substrate.

Careful annealing yields a multilayer structure. Open circles in Fig. 1 correspond to the reflectivity profile from the PS-PBMA multilayer structure without nanoparticles. The five Bragg peaks arise from the lamellar structure of the film. Black circles correspond to the reflectivity from the same structure but with nanoparticles incorporated in the PS domains. An elastic distortion induced in the copolymer matrix by the presence of the particles results in the smoothing of the Bragg peaks.

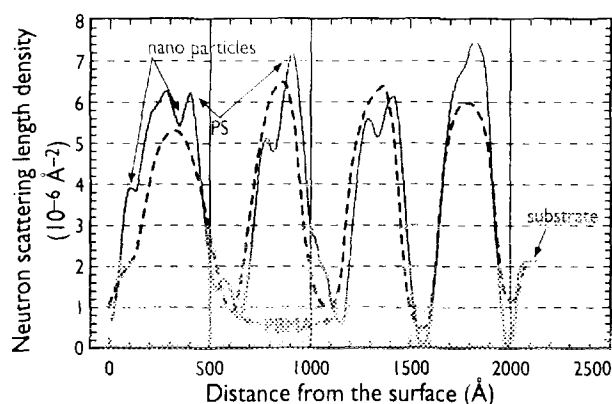


FIGURE 2: NSL-density profiles from the fit to the data (Fig. 2): dashed line shows pure PS-PBMA film structure, solid line shows film structure with 40 Å nanoparticles.

The fit to the data is shown by the solid lines in Fig. 1, it gives a very precisely modelled neutron scattering length (NSL) density profile as shown in Fig. 2. The nanoparticles are concentrated where small dips are visible.

The second sample was PSd-PBMA diblock copolymer with $M_w = 135$ K and 60 Å nanoparticles. The NSL-density profile resulting from the fit to the data shows in a more idealised presentation that the nanoparticles are 60 Å in size and very well concentrated in the centres of the PS lamellae (Fig. 3).

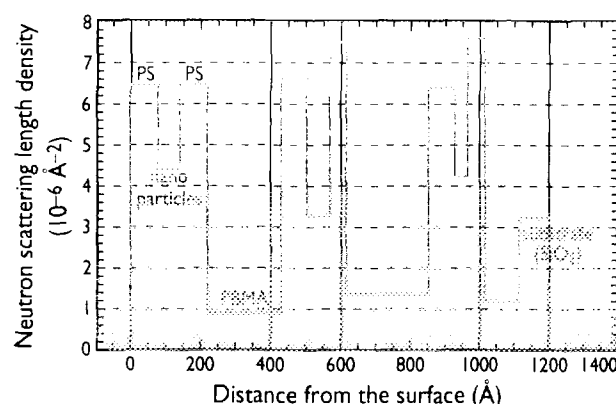
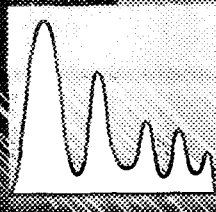


FIGURE 3: NSL-density profile for a symmetric PS-PBMA film with 60 Å nanoparticles.

MOLECULAR SPECTROSCOPY



FR9704854

NEUTRONS AND NUMERICAL METHODS - A NEW LOOK AT ROTATIONAL TUNNELLING

by M. R. JOHNSON AND G. J. KEARLEY (ILL).

MOLECULAR MODELLING TECHNIQUES ARE EASILY ADAPTED TO CALCULATE ROTATIONAL POTENTIALS IN CRYSTALS OF SIMPLE MOLECULAR COMPOUNDS. A COMPARISON WITH THE POTENTIALS OBTAINED FROM THE TUNNELLING SPECTRA PROVIDES A STRINGENT MEANS FOR VALIDATING CURRENT METHODS OF CALCULATING VAN DER WAALS, COULOMB AND COVALENT TERMS.

THE IMPORTANCE OF NEUTRON SCATTERING

There is currently a rapid expansion in the use of molecular-modelling techniques due to the availability of cheap powerful workstations. These techniques depend on the validity of the chosen atom-atom potentials, so how can we trust the results? It is here that inelastic neutron scattering (INS) has an important role to play. In this report we will restrict the discussion to quantum rotation of molecular groups, CH_3 and NH_3 , but the extension to other dynamics, such as molecular vibrations is straightforward. The strength of INS for quantum molecular-rotations stems from the almost exponential dependence of the tunnel-splitting (the separation between the first two rotational energy-levels) on the height of the rotational barrier. INS measures the tunnel splitting directly and thus provides a very sensitive probe of the rotational potential. If we know the crystal structure we can also calculate the rotational potential [1], but which, if any, of the methods, approximations and force-fields gives the right answers? We present the outline of a method which successfully correlates rotational potentials with crystal structures, and, as we will show, also provides a new insight into the rotational dynamics.

COMBINED *AB INITIO* AND EMPIRICAL METHODS

Although molecular-dynamics simulations are a principal use of atom/atom potentials, these simulations are more or less restricted to classical systems. To treat a system of

quantum rotors we make a time-independent analysis of the crystal-energy for different orientations of a molecular group (or groups) within the measured crystal-structure. The basic steps of this analysis are:

- 1) Obtain the liquid-helium temperature crystal-structure (neutron diffraction is ideal for locating H-positions).
- 2) For a molecule constrained to the crystallographically-determined geometry, rotate a symmetrised molecular

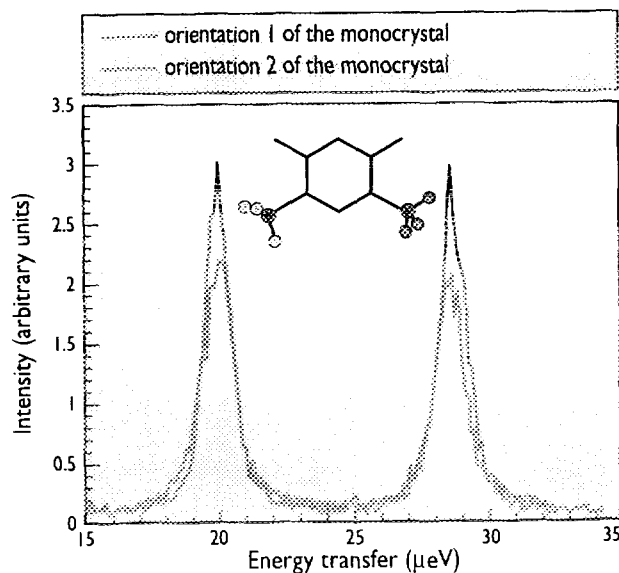


FIGURE 1: The spectrum due to rotational tunnelling of the two distinct methyl groups in dimethyl pyrazine at two different crystal-orientations.

group, and, for each orientation, calculate the ground electronic-state wavefunction and energy. This provides the intramolecular rotational potential and the partial charges.

3) Calculate the crystal-component of the rotational-potential from the dependence of the total intermolecular-potential on the orientation of the molecular group, using the partial charges from the *ab initio* calculations and suitable published (empirical) atom/atom potentials.

4) From the total rotational-potential (the sum of the inter- and intra-molecular contributions), construct the Hamiltonian, and compare its eigenvalues and eigenvectors with experiment.

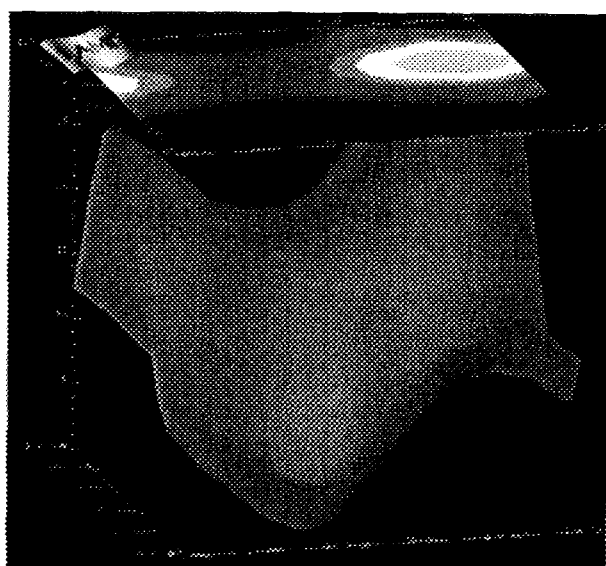
Is there a correlation between the rotational-barrier and crystal structure?

Fig. 1 shows INS spectra (IN10B) of CH_3 rotational tunnelling measured in a single crystal of dimethylpyrazine at two orientations. This enables the tunnel splitting of the

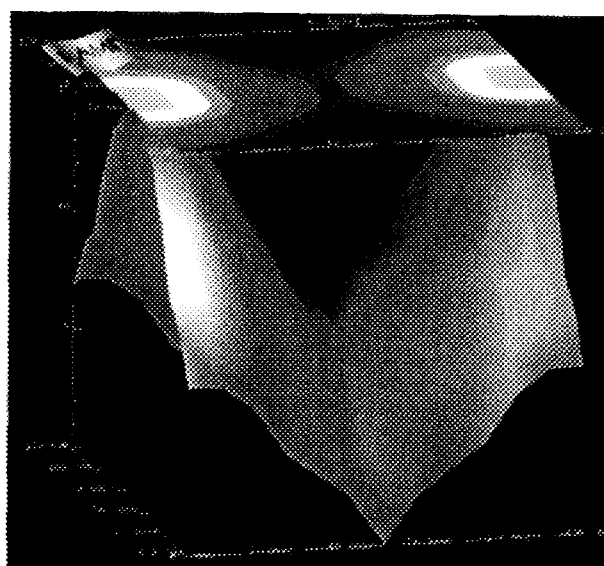
two crystallographically-distinct CH_3 groups to be distinguished. In the model, each of the two methyl groups was rotated according to the recipe above to obtain maps of the potential terms for all orientations of the two groups.

The orientation-dependence of the intra-molecular, van der Waals and Coulomb potentials for the two rotors is illustrated in Fig. 2. Whilst the minimum-energy orientation of the two CH_3 groups is anti-parallel for the isolated molecule, the orientations for the calculated total-potential are parallel, in agreement with the measured crystal structure. This is due to the dominating role of intermolecular van der Waals interactions between rotors (see Fig. 2).

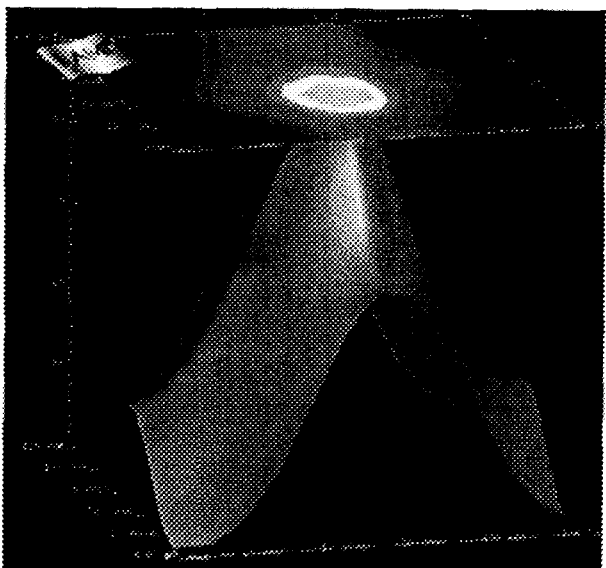
So far we have analysed 10 compounds in this way and the observed and calculated tunnel frequencies agree to within a factor of about 2, which, due to the exponential dependence described above, corresponds to a rather small error in the rotational barrier height. This correlation is shown in Fig. 3.



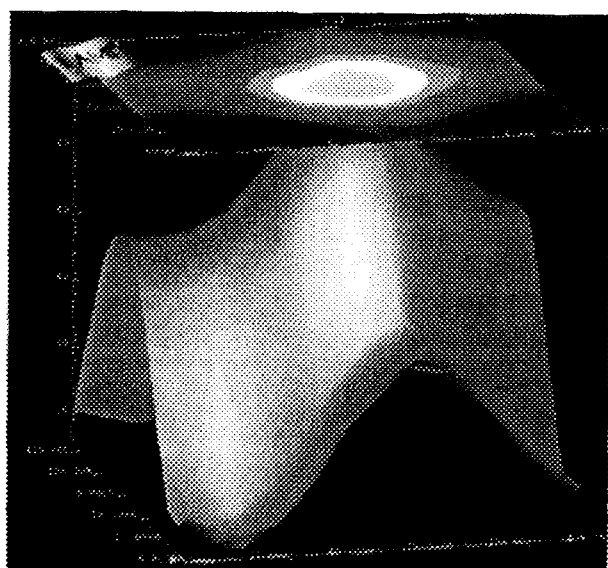
Coulomb



Torsion



van der Waals



Total

FIGURE 2: The potential energy surfaces as a function of the angular orientation of the two methyl groups in dimethylpyrazine. The x and y axes correspond to separate orientations of each group from 0° to $2\pi/3$ and the z axis corresponds to the potential energy.

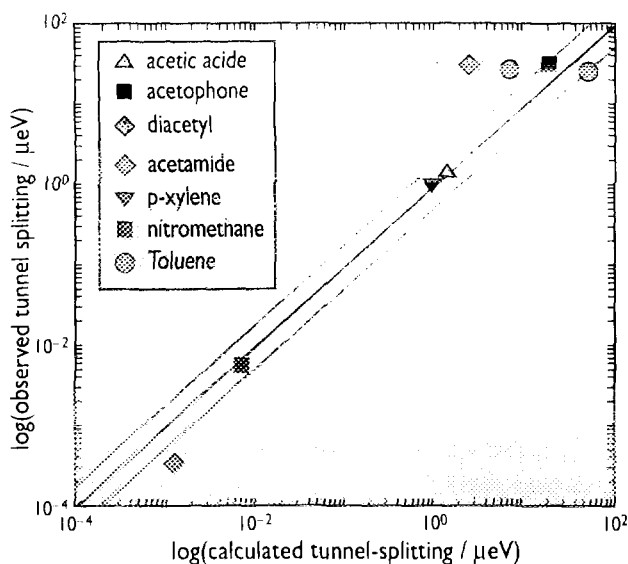


FIGURE 3: Comparison of measured and calculated tunnel-splittings for 7 methylated compounds over 6 orders of magnitude. The upper and lower diagonals correspond to agreement within a factor of 2.

PRECESSION OF ROTORS

Recently there has been some interest in a possible centre-of-mass movement during rotation of molecular groups (see ref. [2] and references therein). In one case, the Hofmann clathrate, the low-temperature crystal structure, INS rotational and vibrational spectra are all available, and we can therefore adjust some of the potential parameters on the basis of the extra data. For vibrations the analysis scheme (above) is modified by calculating the total energy as a function of small displacements of individual atoms, rather than rotation of groups. The distribution of H-atom density from a molecular-dynamics simulation using the derived potentials is shown in Figure 4, and clearly shows the precession of the N-atom during the NH_3 rotation.

NEW INSIGHTS

Calculation of the rotational barrier for the methyl group in acetic acid has been made for three comparatively high temperatures for which crystal-structure data is available [4]. Lattice expansion between 2 and 278 K results in a 40% decrease in the rotational-barrier height. This result demonstrates that the crystal structure must be known at the temperature of the tunnelling measurements (typically 2 K), or equivalently, a rotational potential derived from temperature-dependent data will be an average over that range.

In all of the systems studied, the rotational potential depends on the orientation of nearby methyl groups (see Fig. 2 for example). Often, the magnitude of the potential changes by about 30% for different orientations of neighbouring CH_3 groups, and yet in none of these samples has evidence of coupled dynamics been found experimentally. This supports a recent theory of coupled systems which predicts that as

the number of coupled rotors increases, so the INS spectrum tends towards that of a single rotor. Coupling is weakest when the rotors are coaxial, because in this arrangement the sum of the H-H distances between the two groups is only weakly modulated by the phase-angle between them. Ironically, this is just the arrangement which has been postulated for coupling in the past.

Coupling is often proposed to account for the presence of more than one peak in the tunnelling spectrum for samples containing only a single type of rotor. However, preliminary results for CH_3 rotation in metal acetates show that the rotational potentials calculated from the crystal structures, using the recipe described above, are much too high, but that these can be reduced in order to get agreement with the measured tunnelling spectrum by allowing an anisotropic centre-of-mass movement during rotation. Is centre-of-mass movement a common feature of quantum rotation?

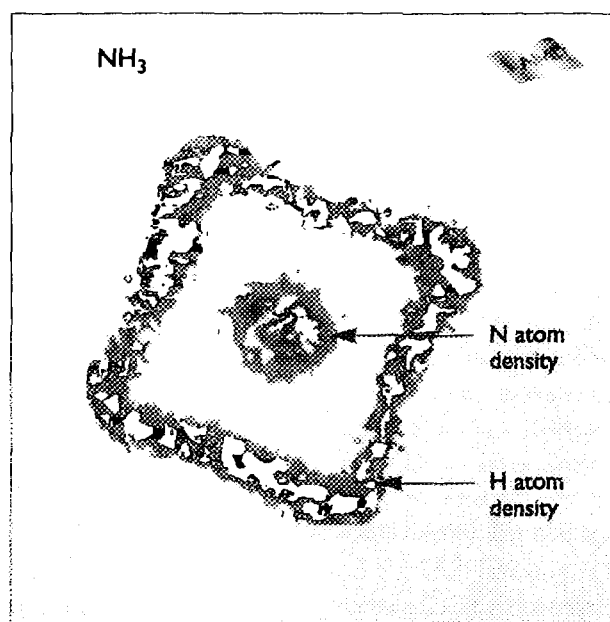


FIGURE 4: Atom-density of NH_3 group from a molecular-dynamics simulation showing the apparent "square" NH_3 group in the Hofmann clathrate.

APPLICATIONS

Direct applications of this type of work are considerable in number and importance. We have a sensitive probe of the functional form and parameters describing inter-molecular interactions for just those molecular groups which are of importance to biocides, drug-design, proteins, and polymers. Because these systems are somewhat complex and the classical motions are extensively mixed, it is impossible judge atom/atom potentials by comparing calculation and experiment. In contrast low-temperature quantum rotational-tunnelling in simple molecules occurs without dynamical response of the environment and we know exactly what is calculated and what is measured.

-
- M. R. JOHNSON, B. FRICK AND H. P. TROMMSDORFF, CHEM. PHYS. LETT. 258 (1996) 187 ■ M. KOLARSCHIK AND G. VOLL, PHYSICA B 222 (1996) 1 ■ M. NEUMANN AND G. J. KEARLEY, CHEM. PHYS. 215 (1997) 253 ■ M. R. JOHNSON, M. NEUMANN, B. NICOLA AND G. J. KEARLEY, CHEM. PHYS. (IN PRESS) ■ G. VOLL, PHYSICA B 202 (1994) 239.

PROTON TUNNELLING IN INTERMOLECULAR HYDROGEN BONDS

A.J. HORSEWILL (UNIV. NOTTINGHAM),
M.R. JOHNSON (ILL),
H.P. TROMMSDORFF (UNIV. GRENOBLE).



FR9704855

THE WAVEFUNCTIONS OF PARTICLES EXTEND BEYOND THE CLASSICALLY ACCESSIBLE REGIONS OF POTENTIAL ENERGY-SURFACES (PES). A MANIFESTATION OF THIS PARTIAL DELOCALISATION IS THE QUANTUM-MECHANICAL TUNNELLING EFFECT WHICH ENABLES A PARTICLE TO ESCAPE FROM A METASTABLE POTENTIAL-WELL. TUNNELLING IS MOST IMPORTANT FOR THE LIGHTEST ATOMS, SO THAT THE DETERMINATION OF ITS CONTRIBUTION TO PROTON TRANSFER, ONE OF THE MOST FUNDAMENTAL CHEMICAL REACTIONS, IS AN IMPORTANT ISSUE. WE HAVE EMPLOYED QENS AND NMR TECHNIQUES TO STUDY THE MOTION OF PROTONS IN THE HYDROGEN BOND OF BENZOIC-ACID CRYSTALS, A SYSTEM WHICH HAS EMERGED AS A PARTICULARLY SUITABLE MODEL SINCE PROTON TRANSFER OCCURS IN A NEAR SYMMETRIC DOUBLE-WELL POTENTIAL. THE INFLUENCE OF QUANTUM TUNNELLING WAS REVEALED AND INVESTIGATED IN THESE EXPERIMENTS. THIS WORK PROVIDES AN EXPERIMENTAL BENCHMARK FOR THEORETICAL DESCRIPTIONS OF TRANSLATIONAL PROTON-TUNNELLING.

Proton transfer reactions along hydrogen bonds are ubiquitous and of fundamental importance to many chemical and most biological systems, where proton transfer interconverts different possible tautomer structures of a molecule (e.g. nucleic acid-base pairs). The observation of large H/D isotope effects and of temperature-independent reaction rates at very low temperatures indicate that tunnelling contributes to these reactions. A proper quantitative description of these, of the relevant PES and, at higher temperatures, the issue of the contribution of tunnelling to the reaction rate remain subjects of intense current research. The principal difficulty lies in the fact that the proton displacement is accompanied by an electronic rearrangement, which results in minor readjustments of the equilibrium positions of the other atoms of the molecule and the environment. Because of this coupling, proton transfer must be described within a multidimensional PES.

While the force field of the molecule, as derived from vibrational spectroscopic data (IR, Raman, INS) gauges the PES near the equilibrium positions, tunnelling provides information about the barrier region separating potential minima. Tunnelling is quantitatively best characterised by the observation of a splitting of the otherwise degenerate levels localised in either well of a symmetric double-minimum potential ("coherent" tunnelling, Fig. 1a). This tunnelling splitting, Δ , depends exponentially on the mass, m_0 , of the tunnelling particle and the properties (width, d , height V_0) of the barrier separating potential minima as follows: $\log(\Delta) \approx -d(m_0 V_0)^{1/2}$. However, the coupling to the environment makes potential wells inequivalent (Fig. 1b), with the consequence that coherent tunnelling is suppressed and, in the limit of very low temperatures, the protons become localised in the more stable well. Inter-well relaxation can still be observed with a rate, which is determined by "incoherent" tunnelling and which scales with Δ^2 .

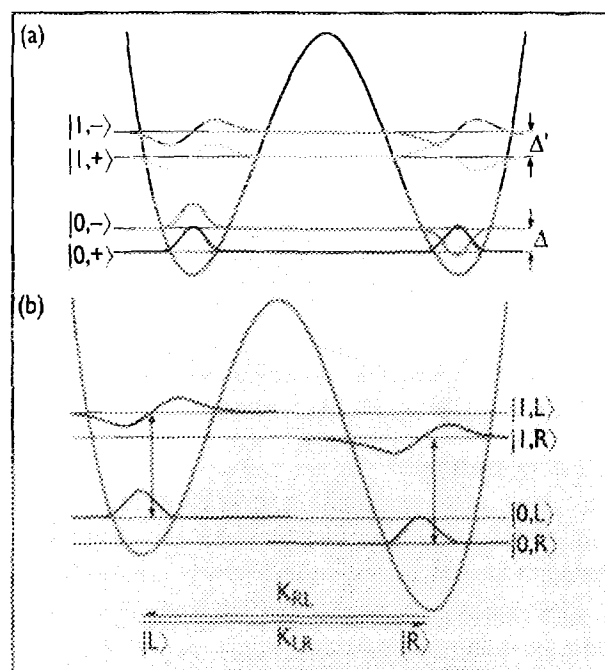


FIGURE 1: Manifestation of coherent and incoherent tunnelling in symmetric and asymmetric double-minimum potentials (DMP). For clarity only the four lowest energy-states are indicated.

a) Coherent tunnelling in a symmetric DMP is manifested by the $|1,+>$, $|1,->$ (tunnelling) splitting of the vibrational states, $|0>$, $|1>$, ...

b) In asymmetric DMP, vibrational states are localized in either well. Thermal equilibrium within each well is established by fast intrawell relaxation $|0> \leftrightarrow |1>$, while incoherent tunnelling is manifested by the slow interwell $|L> \leftrightarrow |R>$ relaxation.

Benzoic acid (Fig. 2) is the only compound in which both coherent and incoherent tunnelling of protons along a hydrogen bond has been measured in the limit of low temperatures by optical spectroscopic techniques. At higher temperatures, the proton correlation time, t_c , defined by $1/t_c = k_{LR} + k_{RL}$, was determined from NMR and QENS

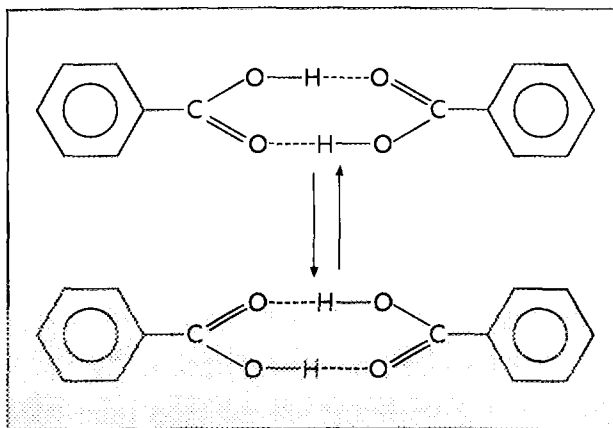


FIGURE 2: The interchange between the two tautomeric forms of benzoic acid is mediated by double proton-transfer in the hydrogen bonds. At low temperature these dynamics are dominated by translational quantum-tunnelling.

Of particular interest is the temperature region in which other thermally activated processes begin to contribute to the proton transfer and mark the onset of the transition from pure quantum mechanical to classical barrier crossing. This region was characterised by measurements of the proton correlation time using QENS on IN16. Because of the restricted energy transfer window of IN16 and because the intensity of the quasi-elastic line is a function of temperature, depending on the population of the higher energy potential well, hydrostatic pressure of 2 kbar was applied to the sample. Indeed, hydrostatic pressure decreases the energy asymmetry and leads to an enhanced overlap of the localised states and hence to a larger tunnelling matrix-element. Since $1/t_c$ scales with Δ^2 , the QE linewidth characterising the transition region can be brought within the energy transfer window of IN16.

In Fig. 3 the filled squares are the QENS measurements of $1/t_c$ as a function of temperature. These measurements enable us to calibrate NMR measurements of T_1 at the same pressure. The proton-transfer rates extracted from this analysis are shown as open circles. Figure 3 illustrates the quantum-to-classical transition for proton transfer in the double-

minimum potential associated with the hydrogen bond.

At low temperature the behaviour asymptotically approaches the quantum limit where the dynamics are governed by tunnelling in the ground state. At high temperature the classical limit (barrier hopping) is asymptotically approached. The dashed line is a fit to theory where simple interpolation between the two limiting cases is applied.

The deviation of this fit in the intermediate temperature region exposes the enhancement of tunnelling via the thermal excitation of vibrational levels involving modes which promote tunnelling.

The solid line in Fig. 3 represents a fit including only one excited vibrational state in which Δ is increased to Δ' . These measurements not only represent the first characterisation of proton transfer in hydrogen bonds in the quantum-to-classical transition region, but are also important in validating the analysis of conventional and novel NMR techniques which can be more generally applied to the study of these fundamental processes.

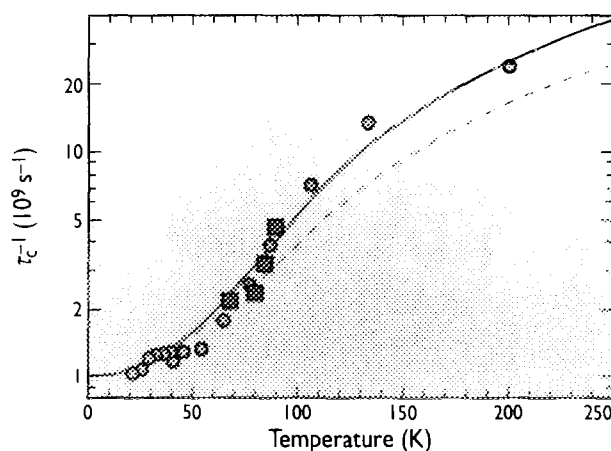


FIGURE 3: The proton transfer rate, τ_c^{-1} , in benzoic acid as a function of temperature at a pressure of 2 kbar. (QENS: squares, NMR: circles). The data asymptotically approach the incoherent quantum-tunnelling regime at low temperature and the classical barrier-hopping regime at high temperature. The lines are fits to theory; the solid line includes the contribution of tunnelling in both ground and first excited vibrational states.

- G.R. HOLTOM, R.M. HOCHSTRASSER, H.P. TROMMSDORFF, CHEM. PHYS. LETT. 131 (1986) 44 ■ CH. RAMBAUD, A. OPPENLANDER, M. PIERRE, H.P. TROMMSDORFF, J.C. VIAL, CHEM. PHYS. 136 (1989) 335 ■ OPPENLANDER, CH. RAMBAUD, H.P. TROMMSDORFF, J.C. VIAL, PHYS. REV. LETTERS 63 (1989) 1432 ■ A. STOCKLI, B.H. MEIER, R. KREIS, R. MEYER AND R.R. ERNST, J. CHEM. PHYS. 93 (1990) 1502 ■ A.J. HORSEWILL AND A. IKRAM, PHYSICA B. 226 (1996) 202 ■ A. STOCKLI, A. FURRER, CH. SCHONENBERGER, B.H. MEIER, R.R. ERNST AND I. ANDERSON, PHYSICA B 136 (1986) 161 ■ A.J. HORSEWILL, P.J. McDONALD AND D. VIJAYARAGHAVAN, J. CHEM. PHYS. 100 (1994) 1889.

WATCHING BUCKYBALLS JOIN TOGETHER

H. SCHÖBER (ILL),
B. RENKER (FZ KARLSRUHE).

SOME 10 YEARS AGO CLOSED ALL-CARBON MOLECULES (FULLERENES) WERE OBSERVED EXPERIMENTALLY FOR THE FIRST TIME, A DISCOVERY AWARDED THE NOBEL PRIZE FOR CHEMISTRY IN 1996. THE MOST SYMMETRIC OF THESE MOLECULES C_{60} HAS A SHAPE REMINISCENT OF A SOCCER BALL AND IS ALSO CALLED A BUCKYBALL. THE MOLECULES MAY UNDERGO SOLID-STATE CHEMICAL REACTIONS IF EXPOSED TO PARTICULAR CONDITIONS LIKE IRRADIATION WITH LIGHT, APPLICATION OF HIGH PRESSURE AT ELEVATED TEMPERATURES OR DOPING WITH AN APPROPRIATE AMOUNT OF ALKALI IONS (A_1C_{60} , $A = K, Rb, Cs$). IN THE DOPING SCENARIO THE FORMATION OF LONG POLYMER CHAINS (SEE FIG. 1) IS A THERMODYNAMICALLY REVERSIBLE PROCESS, MAKING A_1C_{60} A PARTICULARLY FAVOURABLE SYSTEM TO STUDY. WE HAVE USED THE HIGH-FLUX TIME-OF-FLIGHT SPECTROMETER IN6 TO FOLLOW THESE CHEMICAL REACTIONS IN REAL-TIME.

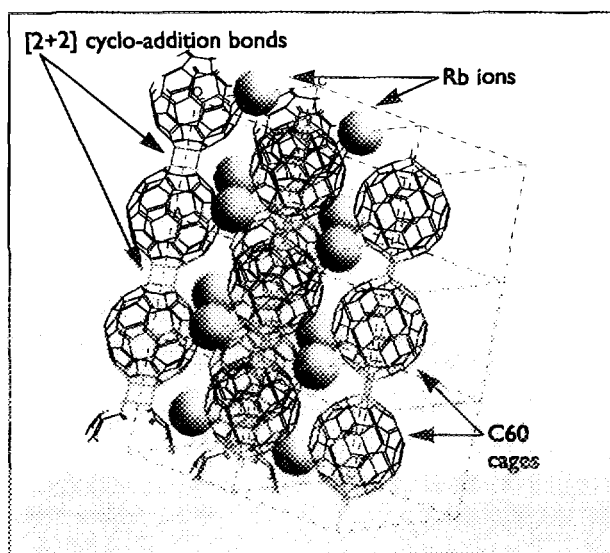


FIGURE 1: Schematic representation of the polymer phase of Rb_1C_{60} . The monomer cages are connected through [2+2] cyclo-addition bonds. The polymerisation, which is inaccessible to the pure C_{60} system, becomes possible due to a lowering of the energy barrier which is brought about by the extra electron donated from the alkali atoms.

In the spectra of the high-temperature phases of A_1C_{60} we observe the typical signatures of rotating monomers, i.e. strong quasi-elastic intensities and a well pronounced gap separating the external modes ($\hbar\omega < 8$ meV) from the internal on-ball vibrations ($\hbar\omega > 30$ meV) (see Fig. 3). The gap is a direct consequence of the two energy scales present in the system, i.e. weak van der Waals interactions between the balls opposed to strong covalent bonding among the atoms on the balls. This clear separation of scales breaks down upon polymerisation. Significant intensities are encountered in the former gap region both after dimerisation (produced by a fast quench from the rotator phase to liquid nitrogen temperatures) and polymerisation (slow cooling from the monomer phase or heating of the dimer phase) of the buckyballs. The highly specific differences in

the spectra can be understood by considering that while the $(C_{60})_2$ dimers dynamically behave like decoupled Einstein oscillators (leading to peaks in $G(\omega)$) the long polymeric chains possess strongly dispersive modes, thus producing a broad intensity distribution in the gap. Lattice dynamical models come up with a very satisfying description of the experimental data and, besides helping to characterise the spectra, yield important information on the chemical bonding. It turns out that the restoring forces linked to the dimer bond are only half as strong as the ones found for the polymer, indicating, as predicted by theoretical calculations, appreciable differences in the bonding itself.

The metastable dimer phase transforms irreversibly into the polymer phase with a strongly T-dependent conversion rate. Profiting from the strong fingerprints in the inelastic spectra we have followed this process at 260 K over 24 hours (see Fig. 2). The evolution of the spectra is rather complex. It is not possible to describe the data by a superposition of pure polymer and pure dimer response functions. This observation precludes any simple transformation via domain growth but, on the contrary, indicates the presence of a series of disordered intermediate stages which all may be quenched into a glassy phase.

The polymer phase of Rb_1C_{60} is thermodynamically stable up to 350 K. Above 410 K the polymers have dissociated completely and the C_{60} cages are performing fast rotational diffusion. The complexity of the transformation between the two stable phases goes beyond a simple hysteresis. Starting from the fully relaxed polymer sample at 350 K the inelastic spectra show a temperature evolution incompatible with a homogeneous harmonic system (Fig. 3).

However, in contrast to the dimer-to-polymer transition the susceptibilities in this intermediate region can now be expressed as a superposition of the ones obtained for the pure polymer and pure monomer.

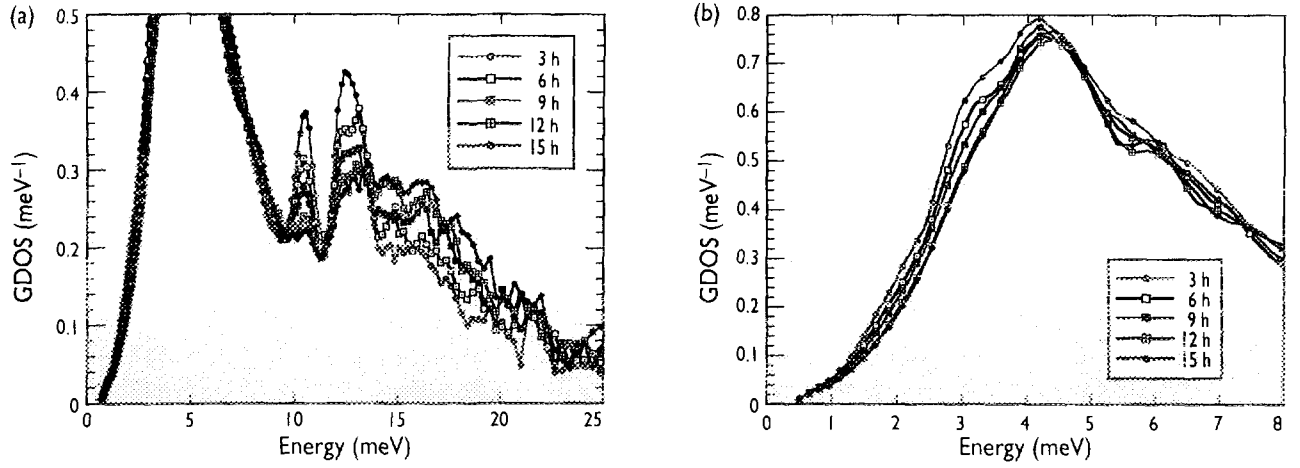


FIGURE 2: Evolution of the generalised phonon density-of-states (GDOS) for Rb_1C_{60} at 260 K starting from the metastable dimer phase obtained by quenching the sample from 430 K to liquid nitrogen temperatures. **a)** shows that the peaks around 10-12 meV typical for the decoupled dimer molecules diminish in intensity making way for a broader distribution in the polymer phase. **b)** shows the stiffening of the acoustic spectrum as expected when going from van der Waals bond dimers to polymer chains. The whole transformation process is rather complex precluding a simple growth mechanism.

We conjecture that this superposition property has its origin in the presence of monomer domains embedded in the polymer matrix. The amount of monomers increases exponentially with temperature. While up to 395 K the system is in thermal equilibrium (on the time scale of hours) the spectra change visibly with time above this temperature. For the cooling cycle the polymerisation induced phase

separation can (on IN6) readily be observed as a function of time for temperatures below 380 K. The amount of quasi-elastic signal from the monomers gradually diminishes, saturating after some time at a value superior to the one obtained at the same temperature upon heating the relaxed polymer. More details and further references can be found in Renker et al., Phys.Rev. B 53 (1996) R14701.

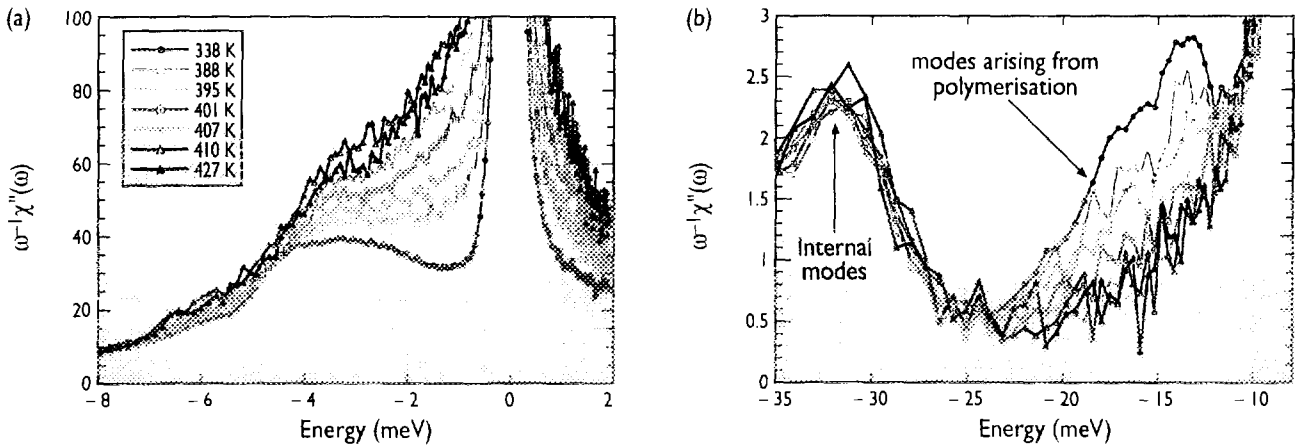


FIGURE 3: Temperature evolution of the generalised susceptibility $\omega^{-1}\chi''(\omega)$ for Rb_1C_{60} starting from the fully relaxed polymer sample. **a)** The increase in quasi-elastic signal is accompanied by a loss of intensity in the gap region **b)** indicating the presence of a growing number of monomers in the system (coexisting with the remaining polymers).

QUANTUM SYSTEMS

ROTON LIFETIMES IN LIQUID ^4He

K. H. ANDERSEN, J. BOSSY, J. C. COOK AND O. G. RANDL (ILL).

THE PHONON-ROTON DISPERSION CURVE OF THE ELEMENTARY EXCITATIONS IN SUPERFLUID ^4He (FIG. 1) HAS BEEN EXTENSIVELY MEASURED BY NEUTRON SCATTERING. WE HAVE REMEASURED THE EXCITATIONS IN THE ROTON REGION WITH THE HIGHEST ENERGY RESOLUTION TO DATE ($< 1 \mu\text{eV}$). OUR RESULTS SHOW THAT THE ROTON LIFETIME DOWN TO $T = 0.8 \text{ K}$ CONTINUES TO BE DETERMINED BY THE ESTABLISHED 4-QUASIPARTICLE DECAY PROCESS. THE SAME PROCESS ALSO PREDICTS THE EXPECTED TEMPERATURE VARIATION OF THE ROTON ENERGY. HOWEVER, OUR RESULTS ON THE ROTON ENERGY SHOW A MARKED DEPARTURE FROM THE EXPECTED TEMPERATURE DEPENDENCE. THE OBSERVED ROTON ENERGY CHANGES BY LESS THAN $0.2 \mu\text{eV}$ BELOW $T = 1.1 \text{ K}$, COMPARED TO AN EXPECTED CHANGE OF $1 \mu\text{eV}$, WHICH SHOULD BE EASILY OBSERVABLE WITH THE ENERGY RESOLUTION OF THE PRESENT MEASUREMENT.

At low temperature, the only kinematically allowed decay process for a roton is the 4-quasiparticle process [1]. The roton excited by the neutron combines with a thermally excited quasiparticle and then decays into two other quasiparticles as illustrated in Fig. 2. As the temperature is lowered, the number of thermally excited quasiparticles rapidly

decreases, giving rise to a rapid temperature variation of the roton lifetime and hence the energy linewidth of the roton. Until recently, the highest-resolution data available was obtained by the neutron spin-echo (NSE) technique. In a pioneering experiment [2], Mezei measured roton widths down to $T = 0.96 \text{ K}$.

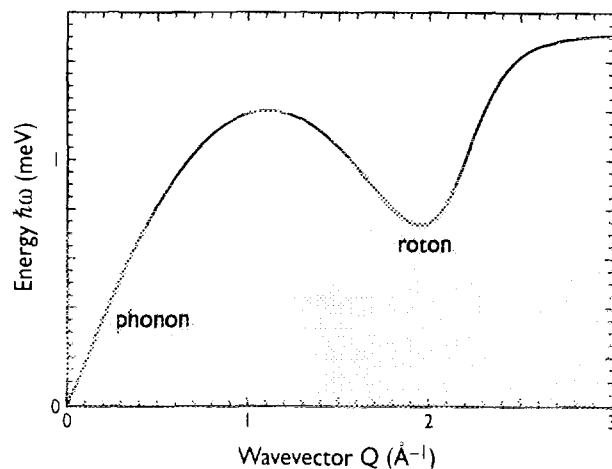


FIGURE 1: Measured phonon-roton dispersion curve of superfluid ^4He .

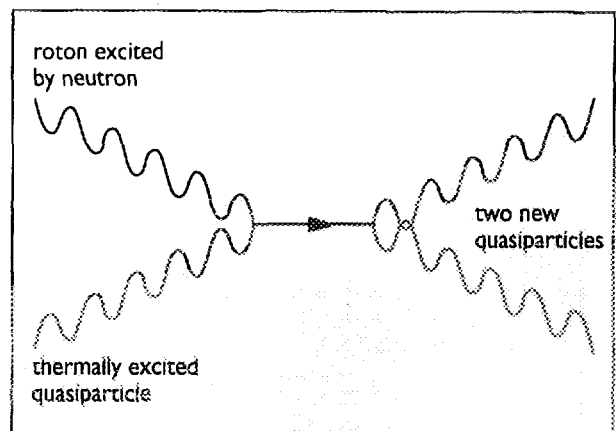


FIGURE 2: Illustration of the 4-quasiparticle decay process first proposed by Landau and Khalatnikov and refined by Bedell et al.

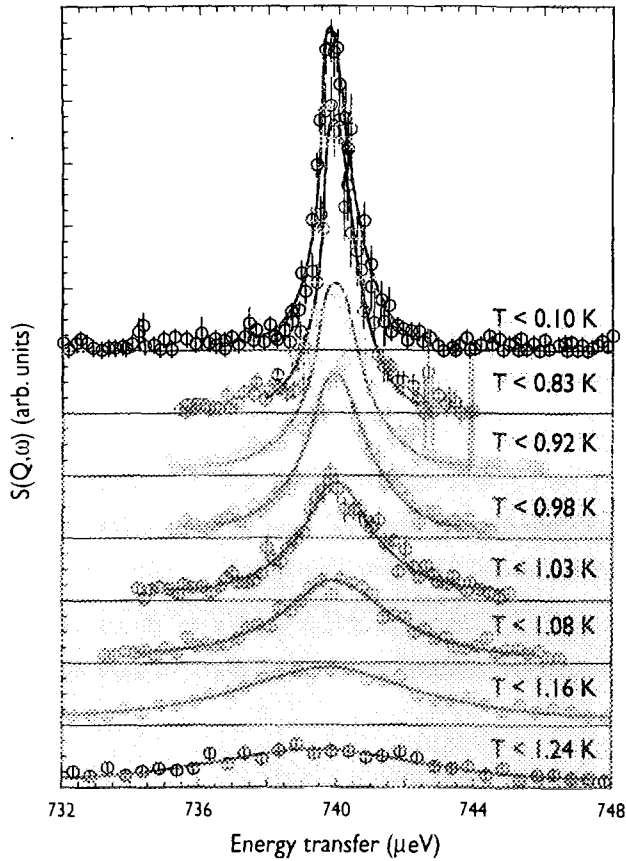


FIGURE 3: Roton peak measured on IN10B at different temperatures. The solid line is the best-fit lineshape. The shoulder on the high-energy side, which is most clearly seen at low temperature, is caused by the width of the instrumental Q -resolution.

The present experiment makes use of a recent development on the backscattering spectrometer IN10 (configuration IN10B).

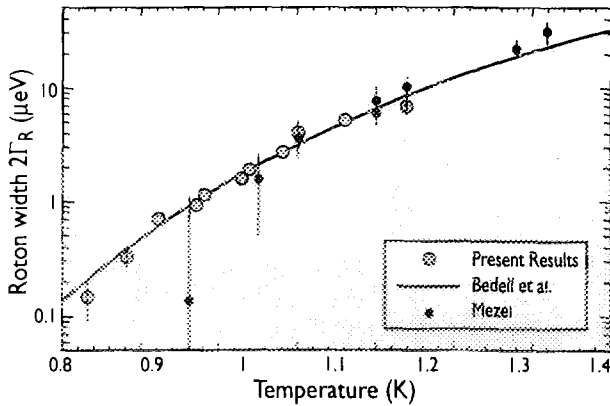


FIGURE 4: Best-fit roton width $2\Gamma_R$ from the present measurement, from the NSE data of Mezei and as predicted by the theory of Bedell et al. Agreement between experiment and theory is excellent.

Incident and scattered neutron energies are defined by Bragg scattering from NaF(111) and Si(111) crystals respectively, both oriented in backscattering configuration. Energy scans through the roton peak are performed by varying the temperature of the NaF monochromator and thereby its lattice parameter by thermal expansion. Examples of the measured raw spectra are shown in Fig. 3. An asymmetry in the peak shape can be seen when the intrinsic peak width is small compared to the energy resolution. This arises from the rough Q -resolution of the measurement, in which the scattering angle was selected using a Cd mask. The effect of the instrumental Q -resolution on the lineshape was calculated and the intrinsic lineshape was described by a Lorentzian. The extracted roton width and energies are shown in Figs. 4 and 5 as a function of temperature. The fitted roton widths are seen to be in excellent agreement with the theoretical predictions [7] and the NSE measurements [4]. It is clear from the magnitude of the error bars that the present measurement constitutes a significant improvement on NSE data, expanding the range of reliable measurement of the roton width by an order of magnitude. In contrast to the well-described roton lifetimes, the temperature dependence of the roton energy is clearly not in agreement with the calculations. The origin of this is not understood at present and will require further study. There may be temperature-dependent mechanisms that play a role in the roton energy but do not directly affect the temperature dependence of the roton lifetime, e.g. multiphonon effects [5]. Alternatively, the intrinsic roton lineshape may not be Lorentzian, but intrinsically asymmetric [6], which would shift the roton energy away from the centre of gravity of the peak. For more details, see ref. [7].

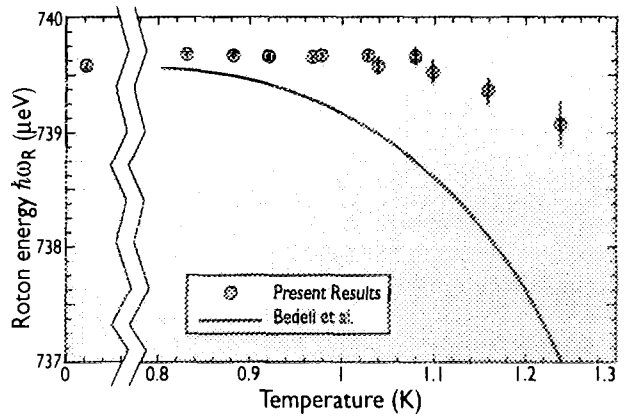


FIGURE 5: Best-fit roton energy $\hbar\omega_R$ from the present measurement. The temperature dependence is clearly less than expected from the theory of Bedell et al.

- L.D. LANDAU AND I.M. KHALATNIKOV, ZH. EKSP. TEOR. FIZ. 19 (1949) 637 ■ K. BEDELL, D. PINES AND A. ZAWADOWSKI, PHYS. REV. B29 (1984) 102 ■ F. MEZEI, PHYS. REV. LETT. 44 (1980) 1601 ■ J.C. COOK, W. PETRY, A. HEIDEMANN AND J.-F. BARTHELEMY, NUCL. INST. AND METHODS A (1992) 312 ■ B.E. CLEMENTS, E. KROTSCHKE AND J.A. SMITH, PHYS. REV. B 47 (1993) 5239 ■ P. NOZIERES, PRIVATE COMMUNICATION ■ K.H. ANDERSEN, J. BOSSY, J.C. COOK, O.G. RANDL AND J.-L. RAGAZZONI, PHYS. REV. LETT. 77 (1996) 4043.

EXCITATIONS IN LIQUID ^3He

B. FAK, N.H. VAN DIJK (CEA GRENoble),
K. GUCKELSBERGER (PTB BRAUNSCHWEIG),
H. GODFRIN (CNRS GRENoble),
R. SCHERM, H. SCHÖBER (ILL).

HELIUM IS THE ONLY ELEMENT IN NATURE THAT REMAINS LIQUID DOWN TO ABSOLUTE ZERO TEMPERATURE. THIS IS A CONSEQUENCE OF THE WEAK VAN DER WAALS INTERACTION BETWEEN THE ATOMS AND THE LARGE KINETIC ENERGY AT LOW TEMPERATURES. THE LATTER ARISES FROM THE ZERO-POINT MOTION, A PURELY QUANTUM-MECHANICAL EFFECT, THAT IS PARTICULARLY LARGE IN HELIUM DUE TO THE SMALL ATOMIC MASS. THERE ARE TWO STABLE ISOTOPES OF HELIUM: ^4He , WHICH FOLLOWS BOSE-EINSTEIN STATISTICS, AND ^3He WHICH FOLLOWS FERMI-DIRAC STATISTICS TO TWO PAIRED PROTONS. THE INFLUENCE OF THE STATISTICS OF THE HELIUM ATOMS BECOMES IMPORTANT AT TEMPERATURES SLIGHTLY BELOW THE BOILING POINT, WHICH IS ABOUT 4 K. SINCE THE INTERACTION BETWEEN TWO HELIUM ATOMS IS RELATIVELY SIMPLE, LIQUID HELIUM IS A SYSTEM WELL SUITED FOR STUDYING QUANTUM-MECHANICAL EFFECTS, BOTH THEORETICALLY AND EXPERIMENTALLY [1].

As the neutron has a spin of $1/2$, the neutron scattering cross-section for ^3He depends on the spin orientation of the ^3He nucleus with respect to the spin of the neutron. At high temperatures, there are no correlations between the nuclear spins, and the spin-dependent scattering cross-section goes

over into incoherent scattering, which probes single-particle properties. At low temperatures, however, the spins in liquid ^3He are correlated, as required by the Pauli exclusion principle. The Pauli principle states that two fermions (here ^3He atoms) cannot occupy the same quantum state, characterised by the k -vector and the spin. As a consequence, neutron scattering probes directly the nuclear-spin fluctuations in liquid ^3He . In addition, the spin-averaged neutron-nucleus interaction gives coherent scattering, which mea-

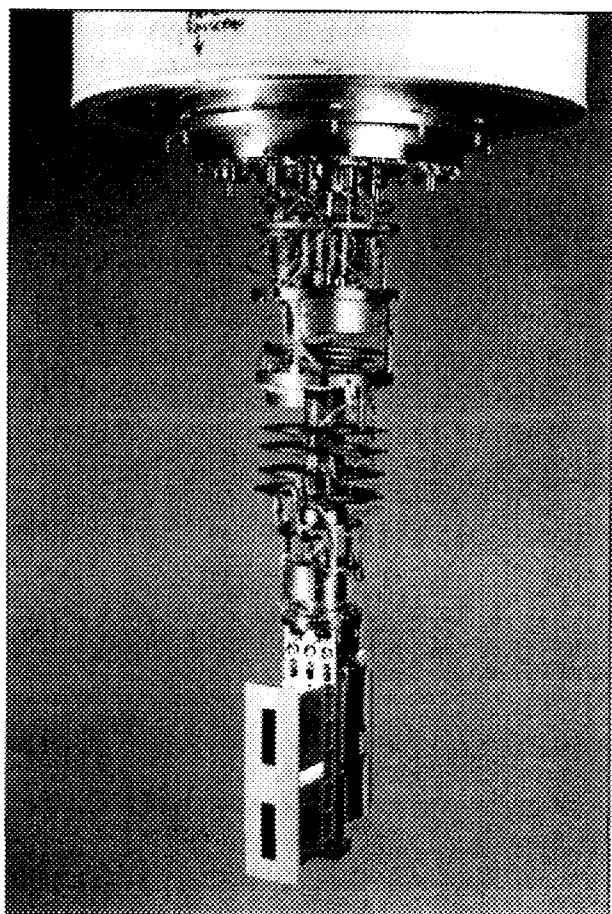


FIGURE 1: Transmission sample cell for ^3He experiments mounted on the dilution refrigerator. The upper window is used for the ^3He sample, and the lower for the vanadium calibration sample.

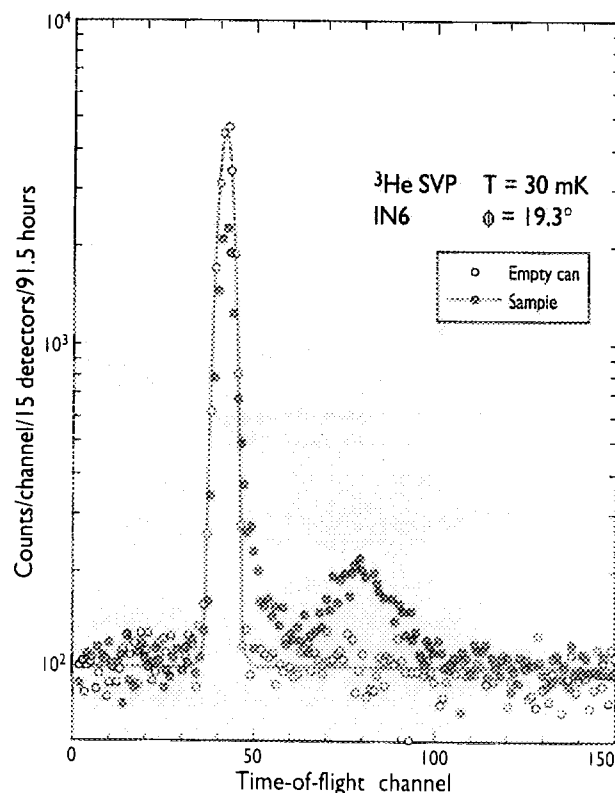


FIGURE 2: Typical time-of-flight spectrum from liquid ^3He and the empty can at $Q = 0.4 \text{ \AA}^{-1}$.

sures the density fluctuations in the system (sound modes or phonons).

The possibility to measure both spin and density fluctuations makes neutron scattering an ideal tool for the study of ^3He . Unfortunately, ^3He is also a very strong absorber for neutrons (a property used in most neutron detectors), which makes these experiments very difficult. For neutrons with a wavelength of 5 Å, the absorption cross-section is 15000 barn, while the scattering probability for a typical ^3He sample is 0.02% instead of the 10% typically used for standard powder samples. Therefore, one needs an instrument with high flux and low background in order to perform these experiments, like IN6, which was originally designed with this kind of experiments in mind. In order to optimise the signal-to-background ratio, the design of the sample cell is of the utmost importance. In all previous measurements, a reflection geometry was used, as the neutron penetration-depth in liquid ^3He is less than 0.1 mm.

In our most recent experiment, we used a cell in transmission, with a sample thickness of 32 μm . An elaborate design of the cadmium shielding of the cell reduced the background. Fig. 1 shows a photograph of the cell, mounted in the new very-low-temperature dilution refrigerator of the ILL. The beam heating due to neutron absorption by ^3He and gamma radiation increased the sample temperature from 18 mK to

30 mK as the beam was switched on. The use of a cell with particularly thin Al windows, but sufficiently sturdy that the deformation under 0.2 bar pressure was less than 2 μm , reduced the elastic signal by about a factor of 15, compared to our previous measurements (see Fig. 2).

Fig. 3 shows the measured intensity as function of wave vector Q and energy transfer. The excitation at low energies is due to nuclear-spin fluctuations, and can be described as a paramagnon resonance, i.e. an overdamped propagating mode inside the particle-hole band (or Stoner continuum). However, its energy is considerably lower, with a linear dispersion for wave vectors above 0.4 Å⁻¹ instead of the quadratic dispersion expected for a Fermi gas. The upper branch is due to collective phonon-like density excitations, the so-called zero-sound mode.

The good energy resolution in the present experiment in combination with the small elastic scattering from the sample cell allows us to compare the line shape of the observed excitations with theoretical calculations. It turns out that the existing theories cannot simultaneously describe both the density and the spin fluctuations in liquid ^3He . The problem appears to be related to the effective mass of the ^3He quasiparticles. Our measurements at higher temperatures ($T = 1.4$ K, see Fig. 4) are expected to shed more light onto this problem.

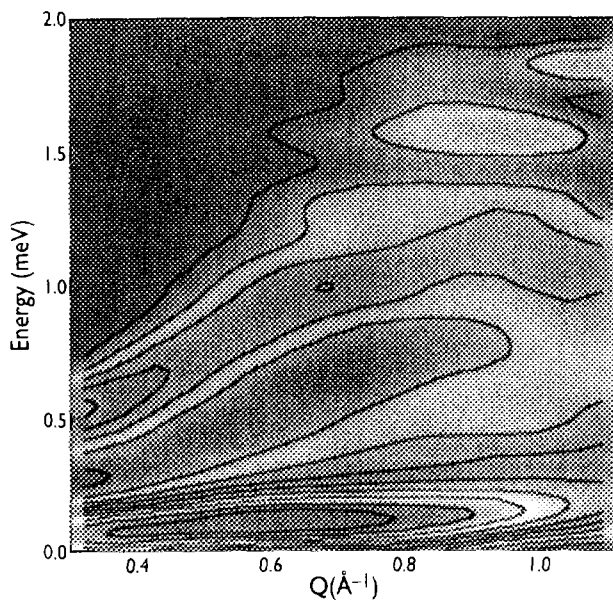


FIGURE 3: Dynamic susceptibility $\chi''(Q, E)$ of ^3He at $T = 0$ mK. The spin fluctuations at low energies are well separated from the density fluctuations at higher energies.

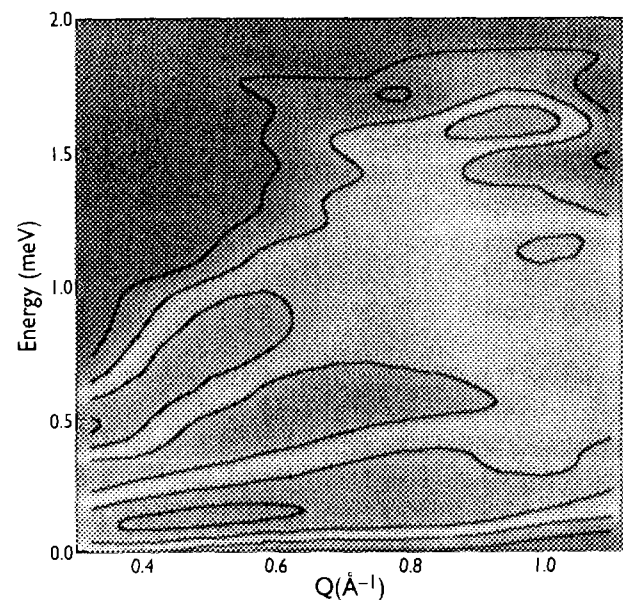


FIGURE 4: Dynamic susceptibility $\chi''(Q, E)$ of ^3He at $T = 1.4$ K. The spin fluctuations broaden more rapidly with temperature than the density fluctuations.



FR9704856



PARTICLE ELECTRIC DIPOLE-MOMENTS

■ J.M. PENDLEBURY (UNIV. SUSSEX).

THE INCENTIVE TO DETECT PARTICLE ELECTRIC DIPOLE-MOMENTS, AS A WINDOW ON TIME-REVERSAL VIOLATION, REMAINS UNDIMINISHED. EFFORTS TO IMPROVE THE MEASUREMENTS FOR THE NEUTRON, THE ELECTRON AND SOME NUCLEI ARE STILL MAKING RAPID PROGRESS AS MORE POWERFUL EXPERIMENTAL METHODS ARE BROUGHT TO BEAR. IN PARTICULAR, A NEW MEASUREMENT FOR THE NEUTRON AT ILL IS RUNNING WELL.

The world-wide programme aiming to detect particle electric dipole-moments (EDMs) continues. In the case of the neutron, the new project at the ILL has reached an uncertainty of $1 \cdot 10^{-25}$ e cm and should soon improve on the 1990 measurement [1,2]. In the meantime, EDM results for the electron have been pushed forward a factor of 20 in the last 8 years by E.D. Commins' Group at Berkeley [3]. They have been concentrating on the one unpaired electron of the thallium atoms using an atomic beam method. At this point they are slowed by severe problems of systematic errors, but the electron baton is being taken up by E.A. Hind's group at Sussex, concentrating on the unpaired electron in the diatomic molecule radical YbF [4]. Their method promises one or two more factors of ten improvement in the coming decade. The fourth notable runner in this race is the ^{199}Hg atom EDM measurement using optical pumping which has been improved by a factor of 30 since 1987 through the

work of N. Fortson's group in Seattle [5]. It gives competitive information on the electric dipole-moment distribution of the ^{199}Hg nucleus.

The directly measured atomic and molecular EDMs and the EDMs deduced from them are shown in the table below. The YbF molecule result comes from just a short test measurement, but it shows the impressive EDM amplification factor which is exploited in that case. The ^{199}Hg nucleus figure is very much an order of magnitude since the ratio between the measured EDM of the atom and that of its nucleus depends on which particular T violating process is responsible for the nuclear EDM.

It is not just a question of grasping at any atomic system which is susceptible to precision measurement. The complementary nature of the cases above enhances greatly the value of the results and that value lies in what they can convey about time-reversal symmetry (T) violation.

Species examined	Species EDM	Deduced EDM
Neutron	$< 1 \cdot 10^{-25}$ e cm	d(neutron) $< 1 \cdot 10^{-25}$ e cm
Thallium atom	$< 2 \cdot 10^{-24}$ e cm	d(electron) $< 4 \cdot 10^{-27}$ e cm
YbF molecule	$< 4 \cdot 10^{-19}$ e cm	d(electron) $< 4 \cdot 10^{-25}$ e cm
^{199}Hg atom	$< 9 \cdot 10^{-28}$ e cm	d(nucleus) $< 1 \cdot 10^{-24}$ e cm

TABLE 1: Upper limits from the measured species EDMs and the upper limits for the more interesting particle EDMs which can be deduced from them.

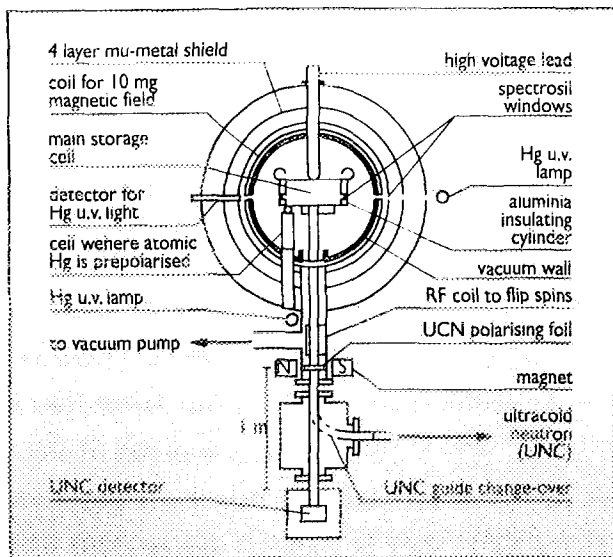


FIGURE 1: An outline of the instrument to measure the neutron electric dipole-moment at the ILL.

The latter, so far, has only two manifestations, the occurrence of K meson decay-modes which would otherwise be strictly forbidden and the excess of matter over anti-matter. In any case, as the Big Bang plasma began to come out of thermal equilibrium this excess of matter was only about $3 \cdot 10^{-9}$ fractional, a very small effect which suggests that the charge separation distances of EDMs are going to be similarly small fractions of the particle Compton wavelengths and thus, not far out of line with the EDM limits from the experiments given above.

It is known that parity violation is linked to the weak interaction, but not to the strong or the electromagnetic interactions. To which interaction, or interactions, T violation belongs is still an open question. If it stems from the gluon behaviour of the strong-force, an attractive hypothesis at the moment, then the neutron and the mercury nucleus EDMs may soon be detected by experiment while that of the electron is likely to be less by a factor of 10^7 . If, on the other hand, there are Higgs particles which generate T violation, an electron EDM may soon be detected as well as the other two.

The thrust of the new ILL measurements has been to reduce by a factor of 30 the magnetic-field drift noise and the systematic magnetic-field shift errors by making a simultaneous comparison between the precession frequency of the neutrons and the nuclei of ^{199}Hg atoms stored in the same measurement volume. Fig. 1 shows an outline of the instrument. The drift-prone plot in Fig. 2 is the precession frequency of the ^{199}Hg alone over a two-day period. The more level plot of Fig. 2 shows the ratio of the precession frequencies on a vertical scale which corresponds in sensitivity. An EDM would reveal itself as a small shift in the ratios synchronising with the reversal of the strong electric-field at once per hour.

Just now, hard carbon-films produced by the CVD process are being investigated to see whether they would make a better alternative to the present use of teflon as the neutron storage vessel surface coating. The higher scattering-length density of hard carbon would trap more neutrons and improve the statistics. For the longer term in the neutron case, further factors of ten improvement may be achievable by working at very low temperature.

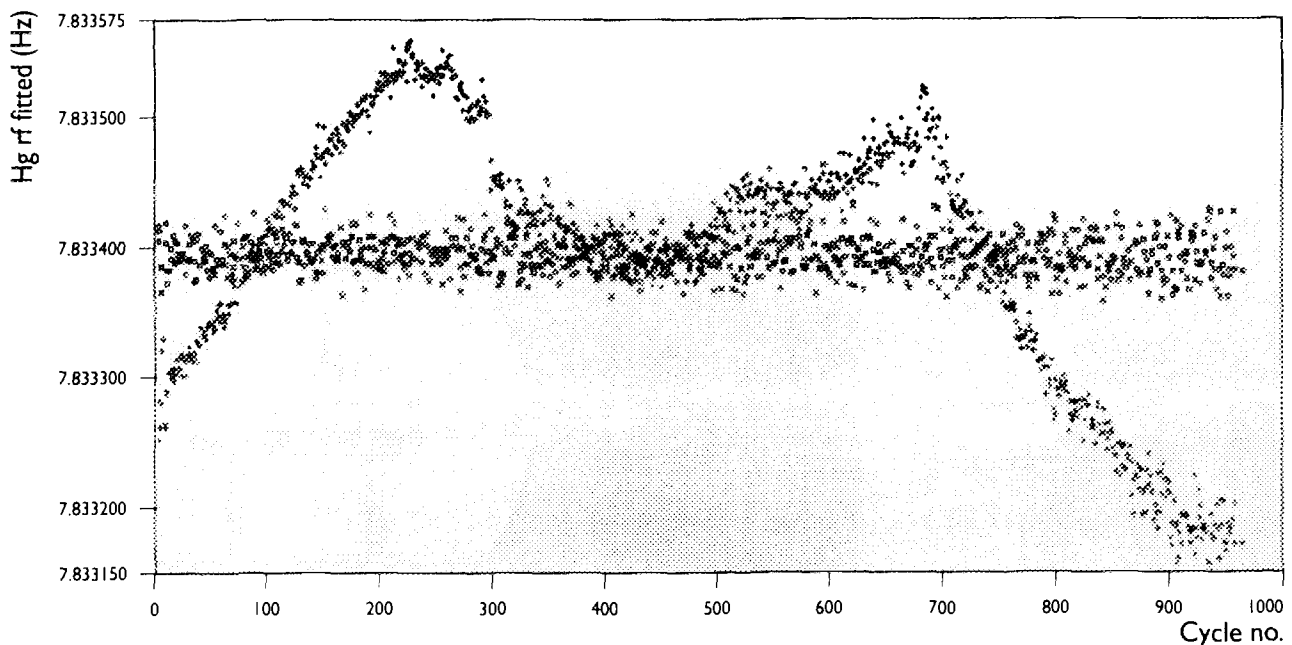


FIGURE 2: The drift-prone plot (+) shows the ^{199}Hg nuclear precession frequency measured over a period of two days. The more level plot (□) shows the ratio of the neutron and ^{199}Hg nuclear precession frequencies on a vertical scale with similar sensitivity.

- K.F. SMITH, N. CRAMPIN, J.M. PENDLEBURY ET AL., PHYS. LETT. B 234 (1990) 191 ■ I.S. ALTAREV, YU.V. BORISOV, N.V. BORIKOVA ET AL., PHYS. LETT. B 276 (1992) 242 ■ E.D. COHHINS, B.S. ROSS, D. DEMILLE AND B.C. REGAN, PHYS. REV. A 50 (1994) 2960 ■ B.E. SAUER, S.K. PECK, G. REDGRAVE AND E.A. HINDS, ICAP 15, AMSTERDAM (1996) ■ J.P. JACOBS, W.M. KLIPSTEIN, S.K. LAMOREAUX ET AL., PHYS. REV. A 52 (1995) 3521 ■ R. GOLUB AND S.K. LAMOREAUX, PHYSICS REPORTS 237 (1994) 2 ■ H. YOSHIK, BARYON INSTABILITY WORKSHOP, OAK RIDGE (1996).

LOOKING FOR SPECTRAL CHANGES OCCURRING DURING STORAGE OF ULTRA-COLD NEUTRONS



FR9704857

■ A. STEYERL, S.S. MALIK (UNIV. RHODE ISLAND),
■ P. GELTENBORT (ILL).

THE EXPERIMENT DESCRIBED HERE CAN ONLY BE PLANNED AND PERFORMED BY A TOTAL IGNORAMUS (THIS QUALIFICATION, OF COURSE, REFERS ONLY TO THE FIRST AUTHOR, AND TO NONE OF THE OTHER COLLABORATORS, EITHER: S. NEUMAIER, V.V. NESVIZHEVSKY, M. UTSURO AND Y. KAWABATA). AFTER ALL, WHO IN HIS/HER RIGHT MIND DOES NOT KNOW THAT A BUNCH OF ULTRA-COLD NEUTRONS (UCN) TRAPPED IN A "NEUTRON BOTTLE" WITH RIGID, FIXED WALLS PRESERVES ITS SPECTRUM DURING STORAGE? SIMPLY BECAUSE THE UCN DENSITY IS SO LOW AS TO RULE OUT ANY MEASURABLE NEUTRON-NEUTRON INTERACTION AND THE TOTAL REFLECTIONS SUFFERED AT THE WALLS MUST BE PERFECTLY ELASTIC. ONE CAN THINK OF THERMAL INELASTIC SCATTERING IN THE THIN LAYER OF WALL MATERIAL THAT THE UCN "SEE" DURING REFLECTION AS A POSSIBLE SOURCE OF SPECTRAL HEATING, BUT ANY SUCH INELASTIC EVENT WILL TRANSFER SO MUCH ENERGY TO THE UCN THAT IT IS KICKED OUT OF THE BOTTLE, LEAVING THE SPECTRUM OF REMAINING UCN UNCHANGED. WALL VIBRATIONS COULD IMPART SMALL SPECTRAL CHANGES, BUT THEY CAN BE SUPPRESSED TO A NEGLIGIBLE LEVEL. NEVERTHELESS, IT SEEMS THAT THE SPECTRUM DOES CHANGE. OUR DATA INDICATE WITH 5σ RELIABILITY, THAT A SMALL HEATING BY ABOUT $2 \cdot 10^{-10}$ eV (≈ 2 MM OF RISE HEIGHT AGAINST THE EARTH'S GRAVITY) OCCURRED DURING THE INITIAL $\approx 10^3$ WALL REFLECTIONS, AND NO CHANGE THEREAFTER.

A UCN spectrum with a narrow bandwidth of < 1 neV was defined in the large monochromator shown on the left of Fig. 1, using gravity, a "fence" and a rotating polyethylene roof to cut the spectrum from below and above.

This spectrum was then stored for times up to 800 s, either directly in the annular chamber 2 of the monochromator or, in a second independent set of experiments, in a separate flat storage vessel in "system 2" (shown on the right of Fig. 1)

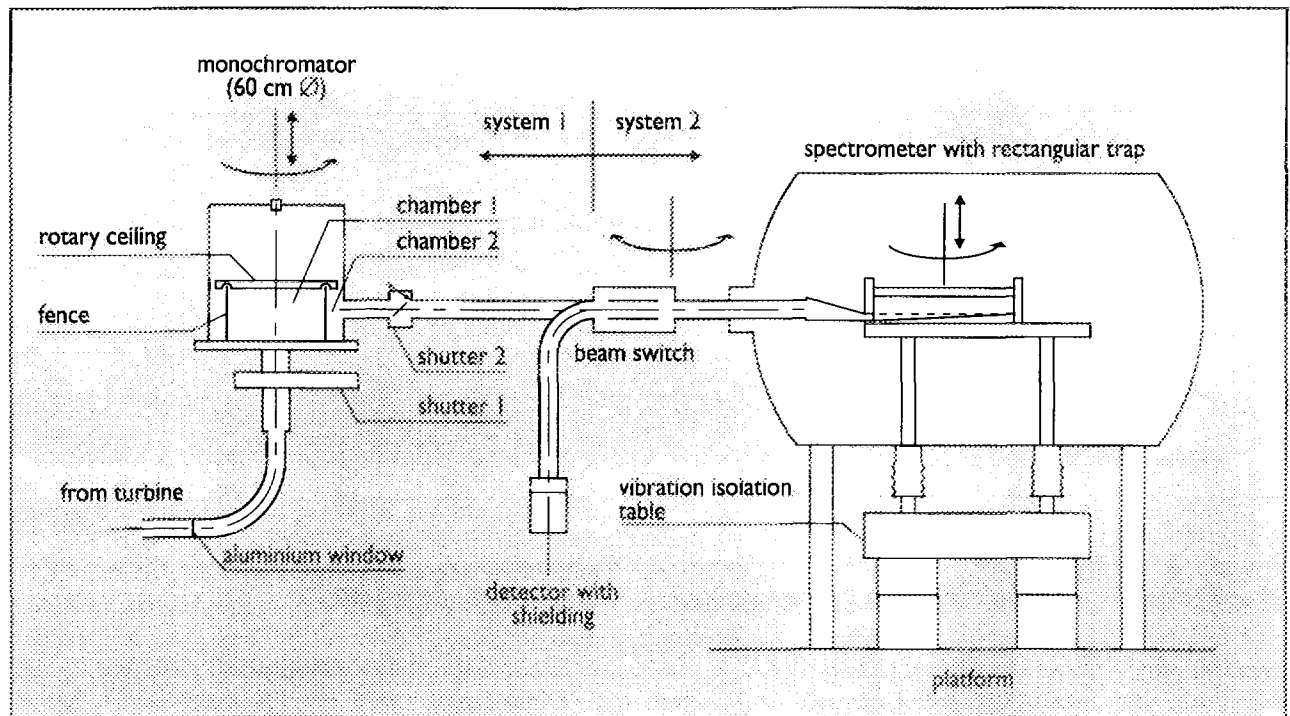


FIGURE 1: Experimental set-up used to measure slight spectral changes for UCN stored, either in the annular region (chamber 2) of the monochromator when only system 1 was used, or by the flat rectangular vessel in system 2. In either case, mono-energetic UCN were produced in the monochromator, using gravity to establish both a lower and an upper spectral cut-off. For scanning of the spectrum after various storage times the rotating absorber lid is positioned at the desired maximum jump height h for the neutron gas, left there sufficiently long for "scooping off" UCN with energies exceeding h , and then the surviving UCN are counted.

which was filled with the UCN from the monochromator. The storage cells were coated with Fomblin, using mainly the grease to ensure isotropy of the UCN spectrum as a result of the diffuse reflections on the rough grease surfaces. (Specular reflectivity would make data interpretation much more difficult.) In system 2, wall vibrations were strongly suppressed by an air-cushioned, massive vibration isolation table.

While the storage properties of system 1 were complicated by a "leak" due to the possibility of jumping back over the fence, losses in system 2 were only due to β -decay and wall losses. Long storage lifetimes up to 630 s were reached. The UCN spectrum was scanned after different storage times by lowering the absorber roof to a desired height h , leaving it there for ≈ 100 s to remove UCN whose maximum jump heights exceed h , and then counting the remaining UCN. Fig. 2 shows the results after 100, 200, 300, 400 and 800 s for one of two measurement series with system 2 (five more were taken with system 1, varying parameters such as minimum storage time and initial spectral width).

A quick calculation of mean spectral height for the data of Fig. 2 shows that the ramp apparently moved upward by about 0.5 mm between 100 and 200 s and also between 200 and 400 s (with $\approx 1\sigma$ error margins).

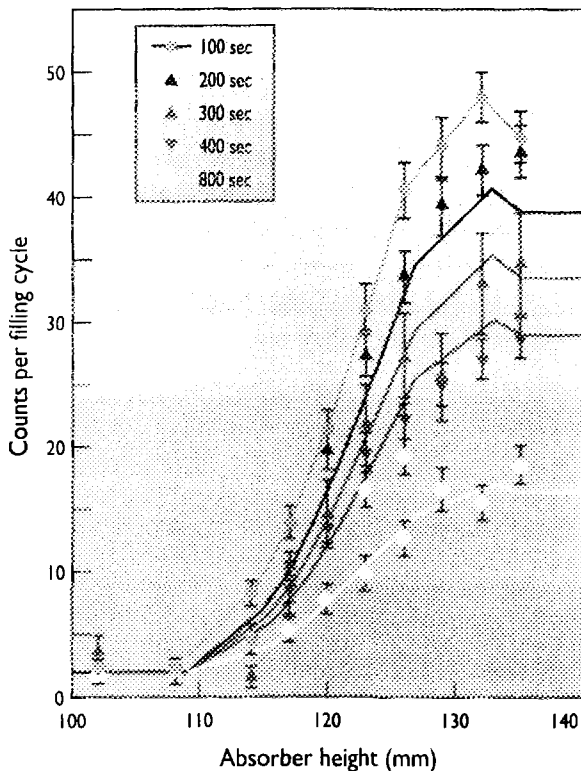


FIGURE 2: One of the UCN spectra measured in system 2 as a function of absorber height h after various storage times. h is measured from the trap bottom level. The curves represent best fits.

After a check of consistency of spectral development for the 7 data sets, all the data were jointly fitted using a model of spectral evolution involving wall losses, vibrational broadening (and the associated shifts, which are negligible), "back-jumping" losses (for system 1 only), and possible spectral shifts due to unknown reasons. It turned out that inclusion of these shifts significantly reduced the overall χ^2 . Fig. 3 shows the results in the form of shifts per 1000 wall reflections in the traps, plotted vs. the number of preceding wall reflections. The width of the yellow regions indicates plus/minus one standard deviation. The red exponential curve is a guide to the eye, showing the total shift of about 2 mm (the area under the red curve) and the decay constant of about 900 wall collisions.

So far, we have not found any systematic effect which might simulate the shift, nor is a simple explanation of initial micro-heating of UCN stored in a trap with fixed walls known to us. However, it appears worth mentioning that the data of Fig. 3 agree well with the prediction of a total initial shift by about 2 mm derived from the ideas described in [1,2]. The observed speed of initial shift (about 1 mm/1000 reflections) is also consistent with the estimate given in [1]. However, a discrepancy exists in the sign of the effect. While slight cooling was expected, we observed heating. A possible explanation of this difference and a full description of the experiment are given in [4].

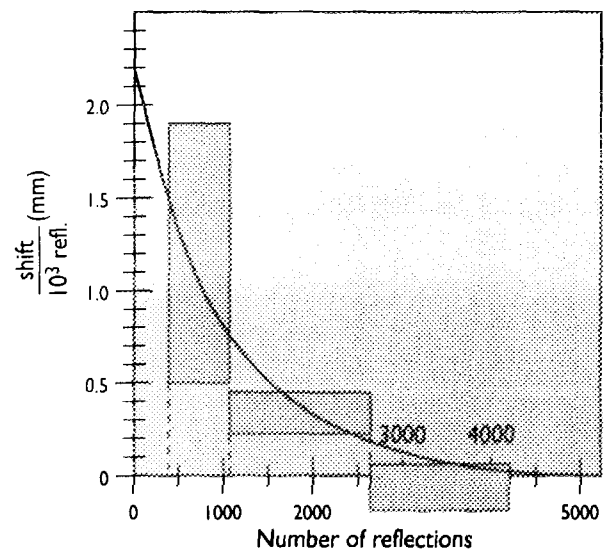


FIGURE 3: Temporal evolution of UCN spectra, shown as shifts per 1000 wall reflections in the traps and plotted vs. the number of preceding wall reflections. The width of the yellow regions indicates plus/minus one standard deviation. The red exponential curve is a guide to the eye, showing the total shift of about 2 mm (the area under the red curve) and the $1/e$ decay constant of about 900 wall collisions for the shift/reflection.

DETERMINATION OF THE FINE-STRUCTURE CONSTANT α BY MEASURING THE QUOTIENT OF THE PLANCK CONSTANT AND THE NEUTRON MASS

E. KRUGER, W. NISTLER, W. WEIRAUCH (PTB BRAUNSCHWEIG).



FR9704858

USING A SPECIAL HIGH-PRECISION APPARATUS AT ILL THE QUOTIENT h/m_n (h PLANCK CONSTANT, m_n NEUTRON MASS) HAS BEEN MEASURED WITH A RELATIVE UNCERTAINTY OF $7.7 \cdot 10^{-8}$. THE VALUE MEASURED FOR h/m_n LEADS TO $\alpha^{-1} = 137.03601082(524)$ (RELATIVE UNCERTAINTY: $3.9 \cdot 10^{-8}$). IT WAS THE FIRST TIME THAT THIS FUNDAMENTAL CONSTANT HAS BEEN DETERMINED BY MEANS OF NEUTRONS. THE EXPERIMENT, WHICH HAD BEEN RUNNING SINCE 1981 IN A PRELIMINARY VERSION AND SINCE 1987 IN THE FINAL VERSION, WAS FINISHED IN DECEMBER 1996.

On the basis of the atomic model created by Bohr it had been possible for the first time to understand the energy levels of the hydrogen atom. Their fine structure was explained by Sommerfeld's theory which expanded Bohr's model. After the introduction of quantum mechanics, Sommerfeld's theory was replaced by the theory of Dirac which also took into account the spin of the hydrogen atom. The fine-structure constant α here is of central importance.

Nowadays it is interpreted as the coupling constant of the electromagnetic interaction. Its exact value is of great importance for the system of fundamental constants. Several methods are used to measure α with high precision:

1. Measurement of the magnetic moment of the electron. This method needs a high degree of quantum electrodynamical calculations, but is the most precise method today.
2. Measurement of the von Klitzing constant R_K , i.e. the height of the resistance steps in the quantum Hall effect. The theory of this effect furnishes a relation between α and R_K .

To achieve high accuracy, the SI unit "ohm" must be determined by means of a calculable capacitor.

3. Measurement of the gyromagnetic ratio of the proton. The Larmor precession of the proton spin inside the magnetic field of a precise coil is measured. Additional constants needed for the evaluation of α from the measured data are very precisely known.

4. Measurement of the muonium hyperfine structure. The splitting of the ground level leads to a value of α by means of quantum electrodynamical calculations.

5. Measurement of the quotient of Planck constant and neutron mass. The velocity and the wavelength of thermal neutrons are determined and according to de Broglie this gives h/m_n . In order to measure the velocity, the polarisation vector of polarised neutrons is modulated in a special time-of-flight method by a high-frequency magnetic field. The wavelength of the neutrons is determined by back-reflection in a nearly perfect silicon crystal. Details of the measuring arrangement can be found in [1].

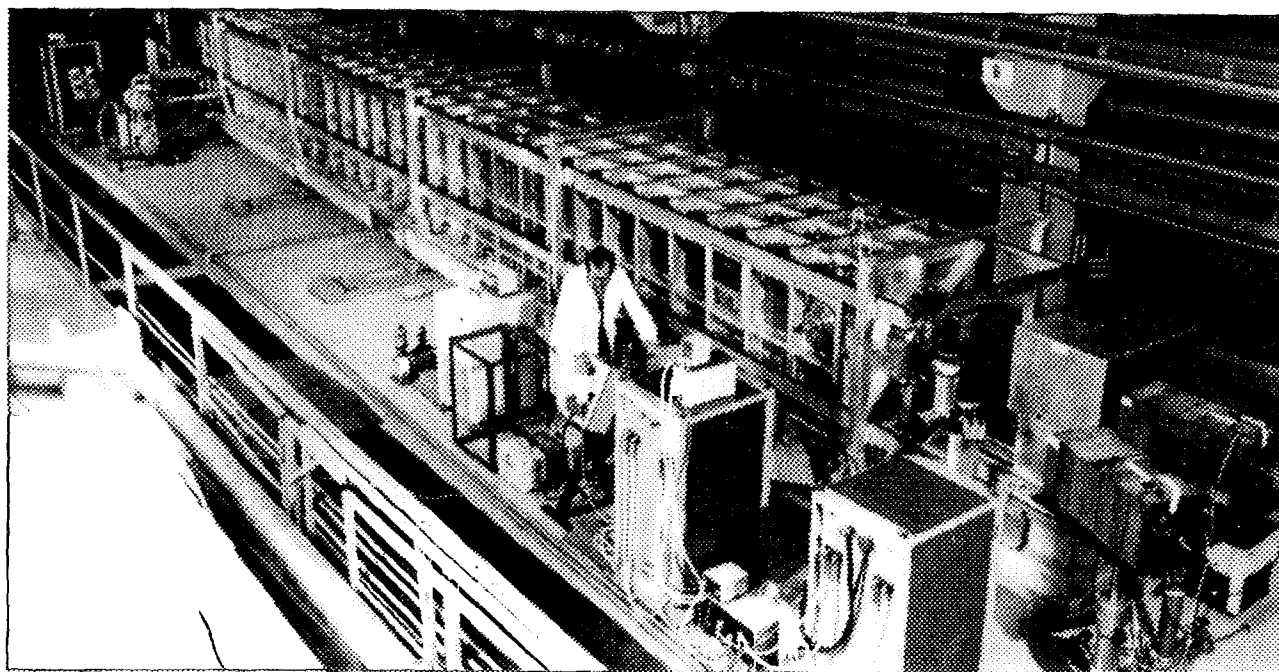


FIGURE 1: Apparatus for measuring h/m_n , installed in the neutron guide hall of the ILL.

The relation between α and h/m_n is as follows:
 $\alpha = [(2R_\infty/c)(M_n/M_e)(h/m_n)]^{1/2}$.
 (R_∞ Rydberg constant, c speed of light in vacuum, M_n , M_e relative atomic masses of neutron and electron.) The quantities needed in addition to h/m_n are very precisely known. The method for measuring h/m_n was proposed by one of the authors in 1977. Preliminary investigations were carried out at the reactor of the Physikalisch-Technische Bundesanstalt (PTB) in Braunschweig. They were followed by detailed test measurements at the ILL in 1981. Finally, the high-precision experiment was installed in 1987 (see Fig. 1). Measurements were done until the reactor shutdown in 1991. After its restart in 1995 they were continued until the end of 1996.

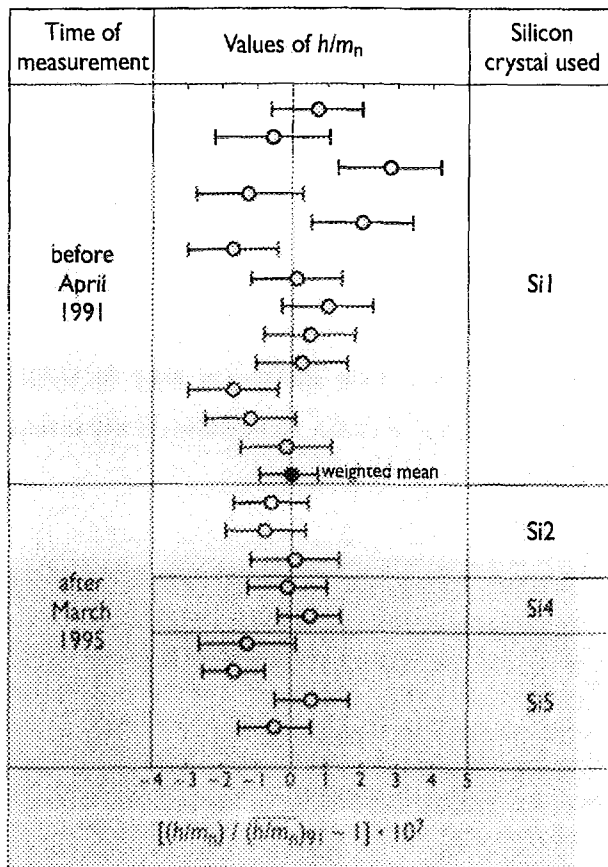


FIGURE 2: Values of h/m_n . Empty circles: measured values, in chronological order from top to bottom; solid circle: weighted mean of the values measured before April 1991. The latter, denoted in this figure by $(h/m_n)_{91}$ is used as a reference value.

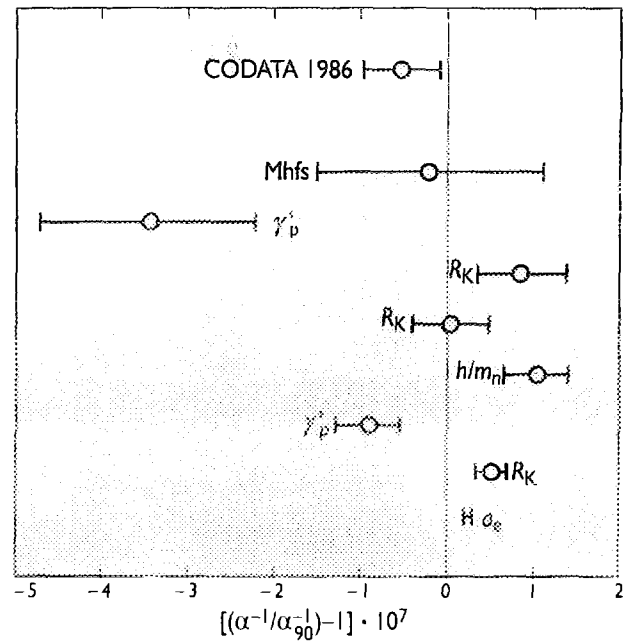


FIGURE 3: Values of the reciprocal fine-structure constant α^{-1} . Methods: CODATA 1986: least-squares adjustment of the fundamental constants in 1986; Mhfs: measurement of the muonium hyperfine structure; γ_p' : measurement of the gyromagnetic ratio of the proton; R_K : measurement of the von-Klitzing constant by means of the quantum Hall effect; a_e : measurement of the magnetic moment of the electron; h/m_n : this experiment. The reference value α_{90}^{-1} is calculated from the defined value $R_{K,90}$ of the von-Klitzing constant.

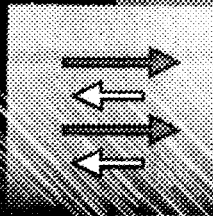
Many measurements were carried out with various alterations of the measuring parameters. Fig. 2 shows the results. Four crystals from two silicon bars were used in the measurements. They have different lattice parameters as the content of carbon impurities differs. So far, only the lattice parameter of Si1 has been measured at the PTB by means of X-rays. It is intended to measure the other crystals during the final evaluation of the h/m_n measurement. In Fig. 2 it is assumed for the moment that Si4 and Si5 are perfect crystals and the lattice parameter of Si2 equals that of Si1.

The evaluation of the values measured before 1991 resulted in $h/m_n = 3.956\,033\,320\,(302) \cdot 10^{-7} \text{ m}^2\text{s}^{-1}$ with a relative uncertainty of $7.7 \cdot 10^{-8}$. It follows that $\alpha^{-1} = 137.036\,010\,82\,(5\,24)$ the relative uncertainty being $3.9 \cdot 10^{-8}$. The present situation for α^{-1} is shown in Fig. 3. The differences between the measured values are greater than expected in view of their uncertainties. The discrepancies could not be clarified so far. Nevertheless, the value of CODATA tabulated in 1986 seems to be too low.

STRONGLY CORRELATED ELECTRON SYSTEMS



FR9704859



NEUTRON-DIFFRACTION INVESTIGATIONS OF FLUX-LINES IN SUPERCONDUCTORS

- E.M. FORGAN (UNIV. BIRMINGHAM),
- * S.L. LEE (UNIV. ST. ANDREWS),
- * D. MCK. PAUL (UNIV. WARWICK),
- H.A. MOOK (OAK RIDGE),
- R. CUBITT (ILL).

SANS HAS PROVED AN EXTREMELY USEFUL TOOL FOR INVESTIGATING FLUX-LINE STRUCTURES WITHIN THE BULK OF SUPERCONDUCTORS. WITH HIGH- T_c MATERIALS, THE SCATTERED INTENSITIES ARE WEAK, BUT CAREFUL MEASUREMENTS ARE GIVING IMPORTANT NEW INFORMATION ABOUT FLUX LATTICES, FLUX PINNING AND FLUX-LATTICE MELTING.

More than a quarter-century ago, small-angle neutron diffraction confirmed that magnetic fields pass through type-II superconductors in the form of flux lines, each carrying a quantum of flux $h/2e$ [1]. With the advent of high- T_c superconductors, a huge injection of new interest came to this subject. The first observation, by neutron diffraction, of flux lines in high- T_c materials was carried out on Yttrium Barium Copper oxide (YBCO) using D11 at the ILL [2]. Later, the lattice of flux lines in Bismuth Strontium Calcium Copper oxide (BSCCO) was observed to melt [3] at temperatures well below T_c , providing direct confirmation of the conclusions of a μ SR study [4] by some members of the same collaboration. The process of flux-lattice melting has a large influence on flux-line dynamics, since a flux line liquid is likely to be free to move through a superconductor, whereas a flux-line solid can be pinned in position. This, in turn, has practical importance, since the motion of flux lines under the influence of a current will give rise to dissipation, even though the superconducting state is not destroyed.

A beautiful example of diffraction by a hexagonal flux-lattice is seen in Fig. 1. Such observations are often taken as part of the initial lineup. Some as yet unpublished measurements of temperature and field-dependence of the scattered intensity from BSCCO are shown in Fig. 2.

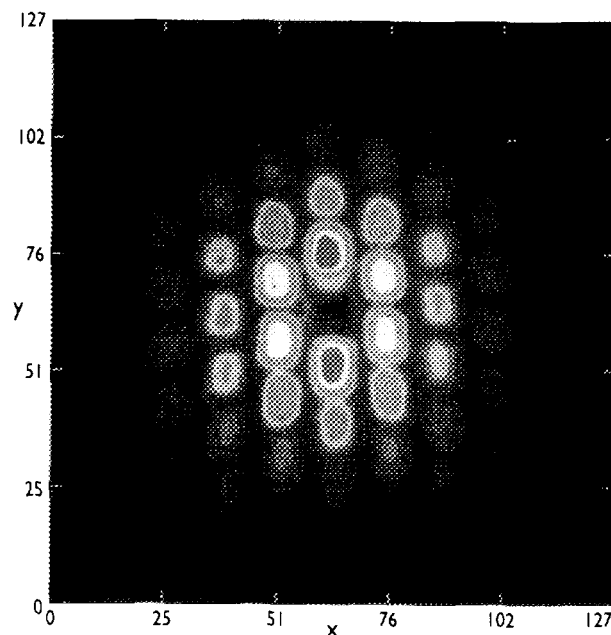


FIGURE 1: Diffraction pattern from the flux lattice in the low T_c material Nb, observed on D22. The sample and magnet orientation have been adjusted until the average flux-line direction is parallel with the incident neutron-beam. Slight divergencies in both neutron beam and flux-line directions allow the observation of many orders of diffraction. The attentive reader will note that differences between the top and bottom of this picture show the combined effects of gravity and neutron wavelength spread.

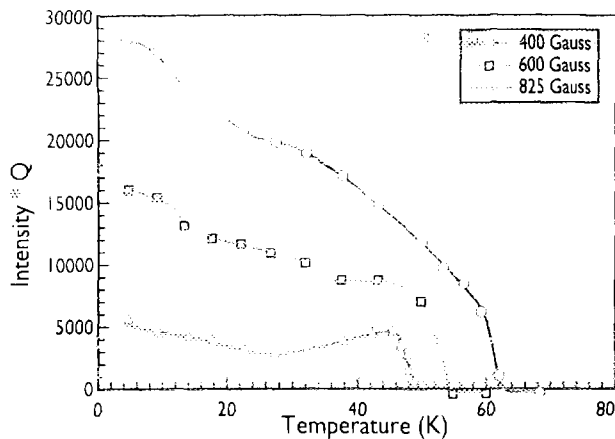


FIGURE 2: Temperature dependence of the diffracted intensity from flux lines in BSCCO for various values of trapped field. Note the non-monotonic temperature-dependence at high fields, explained in the text.

Simple considerations of the temperature dependence of the magnetic penetration-depth and the Debye-Waller factor suggest that the flux lattice diffracted intensity would fall monotonically with increasing temperature, finally disappearing at the melting temperature.

This is indeed observed at low fields, but at higher fields the intensity is already suppressed at low temperatures and recovers as the temperature is increased. This is believed to be due to pinning-induced distortions of the flux lattice, which are larger at high field, and which can be relieved by thermal depinning [10]. Neutron-diffraction measurements on the flux lattice in YBCO, performed on D17 in much higher fields (which are still much less than H_{c2}) are shown in Fig. 3 [11]. The linear dependence indicates that in this twinned sample the melting transition is second order (whereas there is some evidence for a first-order transition in

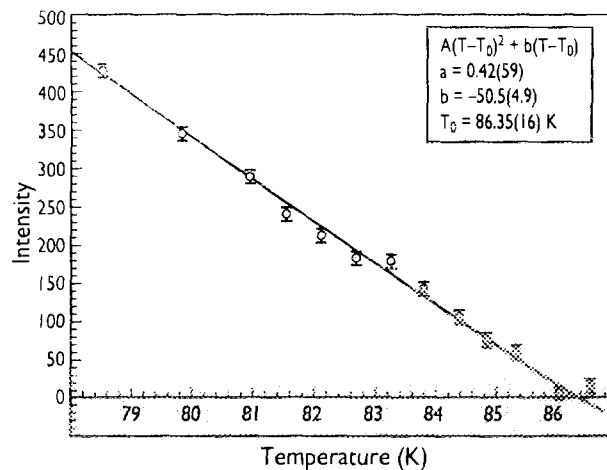


FIGURE 3: Diffracted intensity from the flux lattice in YBCO, measured at 4 T with the field at 51 deg to the c -axis: this data shows a flux-lattice melting transition at approximately 86.4 K.

BSCCO at low fields). Further measurements on a large detwinned crystal will take place shortly.

The zero intensity in the flux liquid in both YBCO and BSCCO indicates that the flux lines are not straight in this phase. There is no space here to do more than mention further and continuing work in other areas: detection of the motion of flux lines using NSE techniques on IN11 [17]; observation of the flux-line structures in BSCCO induced by columnar defect pinning; detailed measurements of the temperature dependence of flux lattice signals [18]; measurements of unusual pinning in CeRu_2 [9] and square flux-lattices in borocarbide superconductors [19]. As new samples become available - for instance organic superconductors - we may expect many further advances, making use of the uniquely high intensity and/or resolution which is available on ILL instruments.

-
- D. CRIBIER, B. JACROT, L. MADHAV RAO AND B. FARNOUX, *PHYS. LETT.* 9 (1964) 106 ■ E.M. FORGAN, D. MCK. PAUL, H.A. MOOK, P.A. TIMMINS, H. KELLER, S. SUTTON AND J.S. AKELL, *NATURE* 343 (1990) 735 ■ R. CUBITT, E.M. FORGAN, G. YANG, S.L. LEE, D. MCK. PAUL, H.A. MOOK, M. YETHIRAJ, P.H. KES, T.W. LI, A.A. MENOVSKY, Z. TARNAWSKI AND K. MORTENSEN, *NATURE* 365 (1993) 407 ■ S.L. LEE, P. ZIMMERMAN, H. KELLER, M. WARDEN, I.M. SAVIC, R. SCHAUWECKER, D. ZECH, R. CUBITT, E.M. FORGAN, P.H. KES, T.W. LI, A.A. MENOVSKY AND Z. TARNAWSKI, *PHYS. REV. LETT.* 71 (1993) 3862 ■ E.M. FORGAN, M.T. WYLIE, S. LLOYD, S.L. LEE AND R. CUBITT, *PROC. LT21: CZECH. J. PHYS.* 46, S3 (1996) 1571 ■ M.T. WYLIE, E.M. FORGAN, S. LLOYD, S.L. LEE, R. CUBITT, M. YETHIRAJ AND H.A. MOOK, *PROC. LT21: CZECH. J. PHYS.* 46, S3 (1996) 1569 ■ E.M. FORGAN, S.L. LEE AND CH. SIMON, *ILL EXPERIMENTAL REPORT* 4-03-811 (1995) ■ T. CHATTOPADHYAY, G. BRANDSTAETTER, H.W. WEBER, R. CUBITT, H. FISCHER AND A. WIEDENMANN, *ILL EXPERIMENTAL REPORT* 5-32-534 (1996) ■ A. HUXLEY, R. CUBITT, D. MCK. PAUL, E.M. FORGAN, M. NUTLEY, H. MOOK, M. YETHIRAJ, P. LEJAY AND J.M. PENISSON, *PHYS. CA B* 224 (1996) 169 ■ M. YETHIRAJ, ET AL., *PHYS. REV. LETT.* (SUBMITTED).

THE NOVEL HEAVY-FERMION SYSTEM $\text{Nd}_{2-x}\text{Ce}_x\text{CuO}_4$

N. PYKA (ILL),
M. LOEWENHAUPT (TU DRESDEN),
A. METZ (FZ JÜLICH).



FR9704860

INELASTIC NEUTRON SCATTERING EXPERIMENTS ARE REPORTED IN THE HEAVY FERMION STATE OF $\text{Nd}_{2-x}\text{Ce}_x\text{CuO}_4$. A COMPLEX MAGNETIC RESPONSE HAS BEEN OBSERVED IN ZERO FIELD THAT CAN BE DEVIDED INTO CONTRIBUTIONS FROM CORRELATED Nd SPINS (INELASTIC, q -DEPENDENT; REMINISCENT OF THE SPINWAVES IN Nd_2CuO_4) AND FROM INDEPENDENT, SLOWLY RELAXING Nd SPINS (QUASI-ELASTIC, q -INDEPENDENT). AN APPLIED MAGNETIC FIELD OF $H > 3$ TESLA GIVES RISE TO DIFFERENT CORRELATIONS IN $Q - \omega$ SPACE THAN IN ZERO FIELD. FIELD DEPENDENT SPECIFIC HEAT AND μSR EXPERIMENTS CAN BE BETTER UNDERSTOOD IN THE LIGHT OF THESE INS RESULTS. THE EXPERIMENTS WERE PERFORMED ON A SINGLE CRYSTAL AT $T \leq 0.1$ K WITH APPLIED MAGNETIC FIELDS OF $H = 0 - 6$ TESLA AT THE IN14 SPECTROMETER.

Heavy-fermion behaviour has recently been discovered in $\text{Nd}_{2-x}\text{Ce}_x\text{CuO}_4$ (NCCO) and is reflected by a large linear specific-heat coefficient and a large Pauli-like magnetic susceptibility [1]. This was a surprising observation since the conduction electrons of NCCO in the Cu-O planes are highly correlated which would render this compound a novel heavy-fermion (HF) system [2]. Standard HF compounds can be described within a microscopic model which assumes a lattice of f-electrons embedded in a sea of conduction electrons with no mutual interactions but a weak hybridisation between f- and conduction electrons. Doping Nd_2CuO_4 with non-magnetic Ce^{4+} essentially dilutes the magnetic sublattices of Cu and Nd by the conversion of magnetic into non-magnetic ions. With the reduction of the Cu staggered field the Nd magnons that are present in the undoped compound are renormalised to lower energies. In the extreme limit of the heavy fermion regime of doping at $x = 0.20$ they become fully quasi-elastic [3].

INS measurements on a single crystal at IN14 have now gained deeper insight into the complex magnetic dynamics of the HF state of NCCO. Spin waves do not exist anymore in the $x = 0.15$ doped compound. Instead, magnetic correlations and local modes have been observed [4]. In Fig. 1 an energy scan at $Q = (001.8)$ shows a broad inelastic signal. On the other hand a measurement at $Q = (.900)$ exhibits pure quasi-elastic scattering (dashed line). The distribution of magnetic intensity in Q -space, taken at an energy transfer of 0.2 meV see Fig. 2, shows in fact two contributions to the dynamic magnetic susceptibility: Q -independent quasi-elastic scattering and on top of this along $[001]$ a pronounced correlation peak centered at $Q = (002)$. Hence, the genuine correlation, Fig. 1b, can be extracted by subtracting the quasi-elastic signal from Fig. 1a. The magnetic Nd-Nd correlation deduced in this way is of dynamical nature with energy \approx width ≈ 0.15 meV. The fact that the width of the quasi-elastic scattering is smaller than the experimental resolution can be interpreted in terms of slowly fluctuating uncorrelated Nd spins. A slowly fluctuating Cu exchange

field with some Cu ions being occasionally non-magnetic, causes the perturbation of neighbouring Nd spins which thus fluctuate in an uncorrelated manner. μSR measurements are in perfect agreement with this finding: A time scale of 10^{-9} sec has been determined for the Nd dynamics [5].

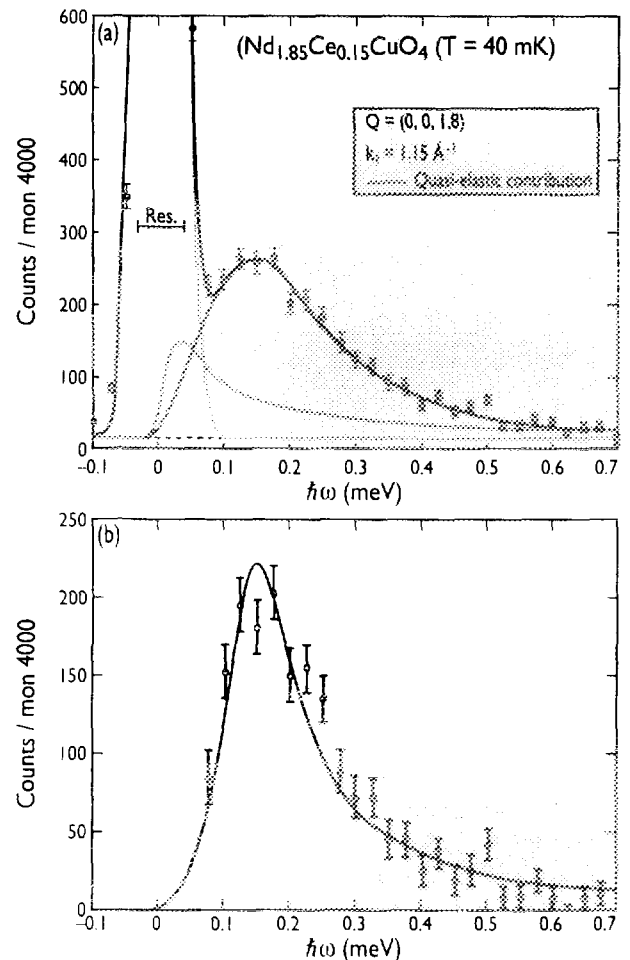


FIGURE 1: **a)** Energy scan at $Q = (001.8)$ representing a superposition of quasi-elastic, as e.g. measured at $Q = (.900)$, and inelastic scattering. A harmonic oscillator function describes the combined signal. **b)** Same energy scan as top but the quasi-elastic contribution and the resolution-limited elastic line have been subtracted point by point. The outcome is of Lorentzian line-shape.

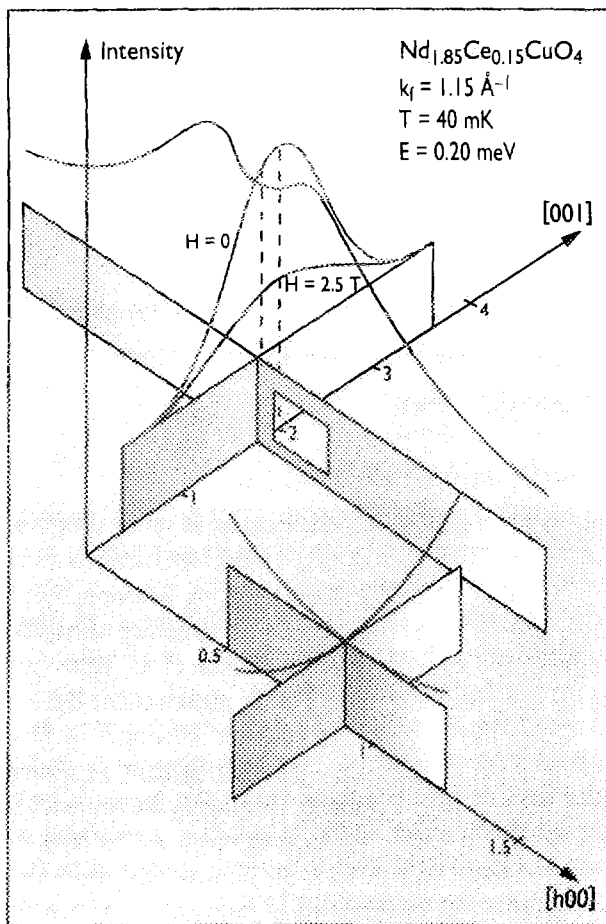


FIGURE 2: *Q*-scans in the *a*-*c* scattering plane at an energy transfer of 0.2 meV in zero field. The dashed area represents the *Q*-independent quasi-elastic contribution (instrumental background is subtracted). One scan at *H* = 2.5 Tesla is included for comparison.

The peaked structure at $Q = (002)$ represents a stacking of planes of Nd magnetic moments which are correlated via the Cu site in the *c*-direction. The correlation lengths extracted from the *Q*-scans of Fig. 2 are only about one lattice constant in the respective directions. At first sight the short correlation length along *c* is surprising because the Nd-Nd exchange interaction in this direction is strong in the undoped compound. Keeping in mind that planes of Nd spins are separated by Cu spins along *c* the situation becomes more clear: The additional itinerant electrons cause non-magnetic Cu ions which destroy locally the Nd-Nd correlation along *c*. Another conspicuous feature of Fig. 2 is the double-peak structure, which cannot be reproduced by two simple Gaussians.

The interpretation of these incommensurate peaks is not evident at the present state of investigation. It is probable that they represent a dynamic precursor effect which might lead to a superstructure at a certain doping. Unfortunately at present no diffraction data of the magnetic structure as a function of doping are available.

A first INS experiment with applied magnetic-fields up to 6 Tesla revealed important changes in the dynamic magnetic properties. The quasi-elastic line turns into a broad inelastic distribution, Fig. 3, and strongly increases its energy and changing its line shape with increasing external field.

The correlation peak increases its energy marginally and seems to vanish at about $H \approx 3$ Tesla. At higher fields a new pronounced inelastic peak appears, increasing its energy considerably with increasing field. It seems that at $H \approx 3$ Tesla the Nd-Nd correlations existing in lower fields become suppressed, the scan at $H = 2.5$ Tesla, Fig. 2, suggests this. For $H > 3$ Tesla the applied magnetic field is stronger than internal fields and reorients the magnetic moments. Hence new magnetic correlations appear, which might involve also the Cu moments. This microscopic behaviour is reflected in the specific heat with the reappearance of the Schottky anomaly at $H > 2$ Tesla which indicates the shift of the correlations to higher energies [1].

More INS and neutron diffraction measurements have to be performed to get a complete picture of this complex novel heavy-fermion system.

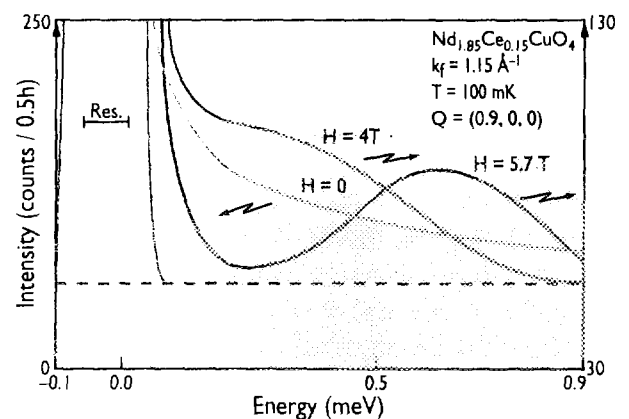


FIGURE 3: Magnetic-field dependence of the quasi-elastic scattering, $H//[010]$. At $H = 0$ the scattering is a resolution limited Lorentzian distribution. For $H > 3$ Tesla it becomes inelastic, non-Lorentzian and very broad ($\approx 6 \times$ resolution). Note the different scales for $H = 0$ and $H > 0$.

- T. BRUGGER, T. SCHREINER, G. ROTH, P. ADELMANN, G. CZJZEK, PHYS. REV. LETT. 71 (1993) 2481 ■ P. FULDE, V. ZEVIN, G. ZWICKNAGL, Z. PHYS. B 92 (1993) 133 ■ M. LOEWENHAUPT, A. METZ, N.M. PYKA, D. MCK. PAUL, J. MARTIN, J.J.M. FRANSE, H. MUTKA, W. SCHMIDT, ANN. PHYSIK 5 (1996) 197 ■ N.M. PYKA, M. LOEWENHAUPT, A. METZ, N.T. HIEN, PHYSICA B (IN PRESS)
- M. HILLBERG, M.A.C. DE MELO, H.H. KLAUB, W. WAGNER, F.J. LITTERST, P. ADELMANN, G. CZJZEK, PHYSICA B (IN PRESS)
- G. CZJZEK ET AL. (TO BE PUBLISHED).

THEORETICAL STUDIES OF STRONGLY CORRELATED FERMIONS

D. LOGAN (ILL).



FR9704861

AN UNDERSTANDING OF STRONGLY CORRELATED FERMIONS UNDERPINS A DIVERSE RANGE OF PHENOMENA SUCH AS METAL-INSULATOR TRANSITIONS, HIGH-TEMPERATURE SUPERCONDUCTIVITY, MAGNETIC IMPURITY PROBLEMS AND THE PROPERTIES OF HEAVY-FERMION SYSTEMS, IN ALL OF WHICH LOCAL MOMENTS PLAY AN IMPORTANT ROLE.

From a theoretical viewpoint the many-body problem is notorious, and theorists have naturally focused on models which, with minimal complexity, are believed to capture the essential underlying physics. One such is the Hubbard model. This is the canonical model for interacting fermions on a lattice but, while notionally the 'simplest' to describe competition between electron localisation and itinerancy, its many facets remain a major challenge to theorists after more than thirty years of study.

Traditionally, much attention has been given to the Hubbard model in low spatial dimensions, d , but in the late '80s Metzner and Vollhardt pointed to the importance of the opposite extreme, $d \rightarrow \infty$. Here, the many-body problem simplifies significantly, to a dynamical single-site mean-field problem -- in effect to a self-consistent version of an Anderson-model, itself a paradigm for single impurity magnetism. While clearly 'special', the large- d limit retains at least some important vestiges of finite- d behaviour and this, combined with its accessibility, has stimulated intense worldwide study of the large- d Hubbard model.

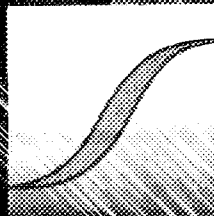
At the ILL, together with M. Tusch and M. Eastwood at Oxford, we have been developing an explicit 'local moment' approach to the large- d Hubbard, and related, models. While physically intuitive, the notion of local moments is more difficult to render theoretically tangible, and the simplest level at which they arise -- a static mean-field approximation -- is inherently incapable of capturing either Fermi liquid behaviour in a metallic phase or the correct strong coupling (large interaction strength) properties of a Mott insulator. Nevertheless, as long stressed by Mott, local moments are an essential ingredient in the description of Mott insulators, whether magnetically ordered or not. To include them in some way is both desirable and necessary, and one also needs to understand their importance for the strongly correlated metallic phase accessed at the point of the Mott insulator-metal transition.

In developing this approach, we have focused on the identification of low-energy scales for spin-flip excitations, and their subsequent coupling to single-particle dynamics.

For the true ground state of the half-filled Hubbard model -- an antiferromagnetic (AF) insulator -- the resultant description of single-particle spectra appears sound for all

interaction strengths: it becomes exact in strong coupling, where the asymptotics of the t - J model are correctly recovered; shows essentially strong coupling behaviour over a wide range of interaction strengths (in agreement with QMC studies), and correctly predicts the loss of AF order only in the non-interacting limit. For the paramagnetic phase -- obtained either by neglecting magnetic ordering or by 'frustrating' it out of existence -- the Mott-Hubbard insulating state has also been examined. Here again the approach is asymptotically exact, and local moments are found to be well developed right down to the finite critical interaction strength for the insulator-metal transition, at which the single-particle band gap is found to close continuously and the Mott insulator collapses. The resultant description of the transition is significantly different from that originally proposed by Hubbard, and is in apparent agreement with inferences that can be drawn from numerical work.

But can the metallic regime be handled by an explicit local moment approach? Apparently so. The first, natural problem to examine here is the single impurity Anderson-model itself, which is known to be a Fermi liquid for all interaction strengths. The local moment approach to the single-particle spectra produces correctly Fermi liquid behaviour, indicative of moment quenching on timescales in excess of the spin-flip timescale. It yields in a surprisingly simple way the exponential strong coupling asymptotics associated with the Kondo regime, and also captures correctly the strong coupling behaviour of the high-energy satellite (or 'Hubbard') bands in the spectrum. Thus far, only the (particle-hole) symmetric Anderson-model has been examined in detail, but in contrast to more conventional approaches does not seem to be a 'special case', and it is hoped to extend this approach to the asymmetric case too. Finally, the paramagnetic phase of the half-filled large- d Hubbard model is in effect a self-consistent version of the symmetric Anderson-model. An important remaining problem is thus to examine the metallic phase of the Hubbard model, and in particular the metal-insulator transition as it is approached from the metallic side, in an attempt to shed light on the claim that the critical interaction strength for collapse of the metallic solution differs significantly from that for the destruction of the insulating solution. Preliminary results suggest that this is unlikely to be the case.



FR9704862

HIGH-RESOLUTION NEUTRON POWDER-DIFFRACTION IN CMR MANGANATES

E. SUARD AND P.G. RADAELLI (ILL).

MANGANESE-OXIDE MATERIALS HAVE RECENTLY BEEN THE SUBJECT OF RENEWED ATTENTION, DUE TO THE "COLOSSAL" MAGNETORESISTANCE (CMR) DISPLAYED NEAR THE SPIN-ORDERING TEMPERATURE T_C BY SOME OF THESE COMPOUNDS. CMR HAS BEEN EVIDENCED IN AT LEAST THREE FAMILIES OF MANGANESE OXIDES: THE PEROVSKITES (WITH GENERAL FORMULA $A_{1-x}A'_xMnO_3$, $A = La, Pr, Y...$; $A' = Ca, Sr, Ba...$) THE RUDDLESDEN-POPPER (RP) PHASES (WITH GENERAL FORMULA $(A_{1-x}A'_x)_{n+1}Mn_nO_{3n+1}$) AND THE $Ti_2Mn_2O_7$ PYROCHLORE. IN MOST CASES, THE CMR COMPOUNDS BEHAVE AS PARAMAGNETIC SEMICONDUCTORS AT HIGH TEMPERATURES, AND AS FERROMAGNETIC METALS BELOW T_C . THE STUDY OF THIS METALLISATION PROCESS HAS LEAD SOME THEORISTS TO CHALLENGE ITS TRADITIONAL INTERPRETATION IN TERMS OF THE SO-CALLED DOUBLE-EXCHANGE MECHANISM, AND TO PROPOSE ALTERNATIVE SCENARIOS IN WHICH THE COUPLING OF THE CHARGE CARRIERS WITH THE LATTICE PLAYS A PARAMOUNT ROLE. FOR THIS REASON, CRYSTALLOGRAPHIC METHODS IN GENERAL AND POWDER DIFFRACTION IN PARTICULAR ARE AT THE FOREFRONT OF CMR RESEARCH.

Neutron diffraction has demonstrated an unquestioned superiority over X-ray crystallographic techniques in the precise determination of atomic positions, especially in the presence of mixtures of light and heavy atoms. Neutron-powder diffraction (NPD) patterns like the one shown in Fig. 1 allow a reproducible determination of atomic bond lengths in a distorted perovskite structure with a maximum uncertainty of $6 \cdot 10^{-4} \text{ \AA}$ (0.03%). At this level of accuracy, the atoms themselves become extremely sensitive probes of the most subtle electronic effects occurring in the material. These remarkable results can be obtained by combining:

- a) very high resolution (HR) at high Q (up to $\Delta Q/Q = 4 \cdot 10^{-4}$ at $2\theta = 120^\circ$: see Fig. 2),
- b) a wide Q -range (0.1 to 15 \AA^{-1}),
- c) optimal peak profiles, which allow a minimisation of the weighted profile factors R_{wp} (3-4%).

However, the information content of an HR-NPD pattern goes well beyond the determination of atomic positions with

the Rietveld method. For instance, structural and magnetic phase-transitions may be accompanied by the appearance of extra Bragg peaks, as well as by a splitting of the main reflections due to the metric distortion of the lattice.

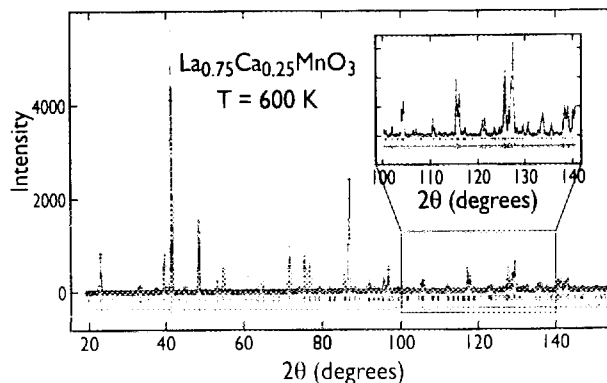


FIGURE 1: Rietveld refinement plot of the neutron-diffraction data for $La_{0.75}Ca_{0.25}MnO_3$ measured on D2B with the highest-resolution configuration.

Likewise, phase separation phenomena are signalled by an asymmetric broadening or splitting of the Bragg peaks. Very often, the detection of these effects is not the primary goal of the experiment, but an on-line data analysis reveals that something is “wrong”, and that more resolution is needed. In other cases, a preliminary indication obtained with another technique is followed up with an HR-NPD experiment to obtain more complete information.

In this context, D2B is a powerful tool for these studies. We have implemented the concept of flexible resolution, whereby several instrumental configurations and 5 different wavelengths (from 1.05 Å to 2.4 Å) can be chosen at the push of a button (Fig. 2). This flexibility allows the user to “focus” the high-resolution Q-range to match the region of interest of the powder pattern.

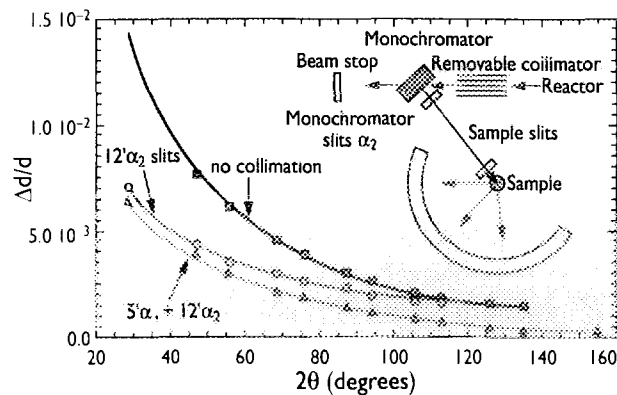


FIGURE 2: D2B resolution functions for three configurations. The inset shows a schematic view of the instrument.

This concept is illustrated in Fig. 3 by examples taken from some of the numerous CMR experiments performed on D2B. For $\text{Pr}_{0.6}\text{Sr}_{0.4}\text{MnO}_3$ (Fig. 3a), a preliminary D1B experiment had revealed an unusual peak broadening below 120 K. A 5-hour data collection on D2B ($\lambda=2.400$ Å, $20'\alpha_2$ slit) was sufficient to show an incomplete phase-transition to another monoclinic phase (I2/a), with part of the sample (~10%) still remaining in the high-temperature orthorhombic phase (P4/mmm).

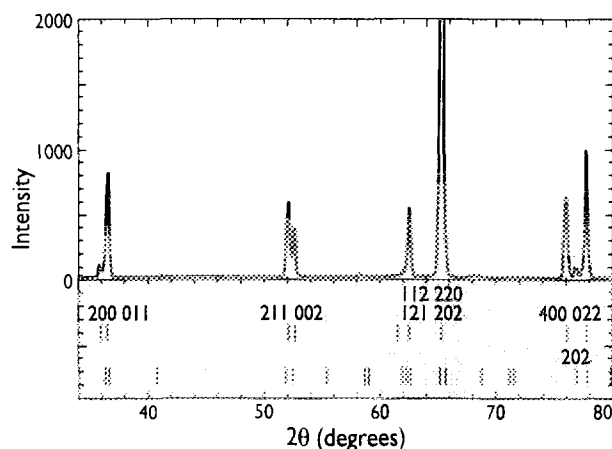


FIGURE 3a: Rietveld refinement plot of the neutron-diffraction data for $\text{Pr}_{0.6}\text{Sr}_{0.4}\text{MnO}_3$ measured on D2B at $\lambda=2.4$ Å with a $20'\alpha_2$ slit. The tick marks below the spectrum indicate the calculated position of the Bragg reflections. The upper row corresponds to a phase with $a \approx c = 5.39$ Å and $b = 7.77$ Å, whereas the lower one corresponds to the high temperature $Pnma$ phase with $a = 5.46$ Å, $b = 7.66$ Å, and $c = 5.42$ Å.

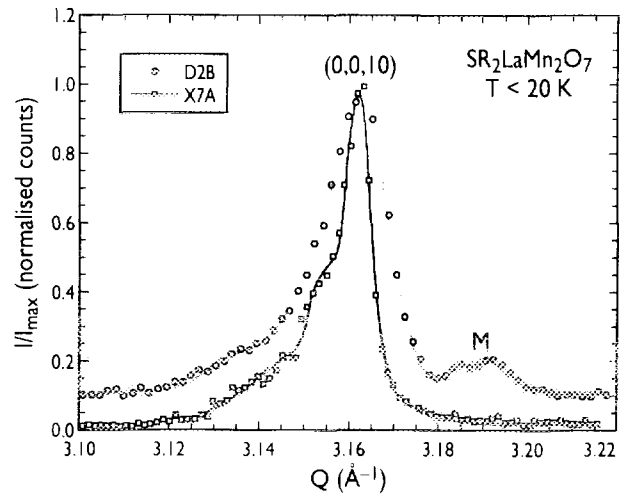
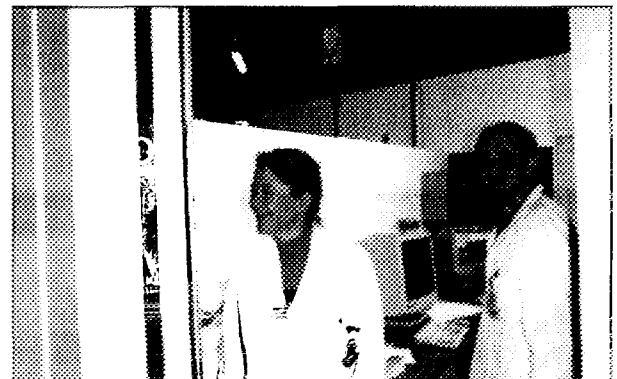


FIGURE 3b: Comparison of the same region of diffraction pattern for neutron data measured on D2B and synchrotron data measured on X7A (NSLS, Brookhaven) for the sample $\text{Sr}_2\text{LaMn}_2\text{O}_7$. (M magnetic peak only visible on neutron pattern).

For the $\text{Sr}_2\text{LaMn}_2\text{O}_7$ RP phase (Fig. 3 b), synchrotron X-ray data had indicated that the sample was 2-phase at low temperatures. A simultaneous refinement of $\lambda = 2.400$ Å and $\lambda = 1.594$ Å D2B data allowed the structural parameters of the two quasi-isomorphous phases (one ferromagnetic, the other antiferromagnetic) to be refined independently [2].

For $\text{Nd}_{0.7}\text{Ca}_{0.3}\text{MnO}_3$ (Fig. 3c), a preliminary attempt to fit the 1.7 K NPD pattern ($\lambda=1.59$ Å) revealed unexpected discrepancies. The use of a longer wavelength ($\lambda = 2.400$ Å) and of the $20'\alpha_2$ slit, with a factor of 3 resolution increase, revealed a splitting of the 202 reflection, due to a phase transition to a previously unknown monoclinic phase ($P2_1/m$) [2]. This high-resolution neutron-diffraction study has revealed the existence of two different sites for the manganese (Mn(1) and Mn(2)), which are characterised by an average Mn-O distance of 1.95 Å and 1.98 Å, respectively. Taking into consideration the ionic radii of Mn^{3+} and Mn^{4+} ions, it can be assumed that the Mn(2) sites are occupied by Mn^{3+} ions, whereas Mn(1) sites are occupied randomly by 40% Mn^{3+} and 60% Mn^{4+} . Consequently, the structure can be described as built up by two types of rows of MnO_6 octaedra running along b; these rows are occupied by Mn^{3+} and $\text{Mn}^{3+}/\text{Mn}^{4+}$ respectively (Fig. 3c). Such a charge ordering has not been observed in $\text{Pr}_{0.7}\text{Ca}_{0.3}\text{MnO}_3$. Below 60K, $\text{Nd}_{0.7}\text{Ca}_{0.3}\text{MnO}_3$ shows a ferromagnetic transition with



Happy days on D2B; from left: Emmanuelle Suard and Peter Cross.

manganese moments oriented along the b and/or c axis, which can be explained by double exchange of electrons between Mn^{3+} and Mn^{4+} . Moreover, the evidence of charge ordering at low temperature could explain why $\text{Nd}_{0.7}\text{Ca}_{0.3}\text{MnO}_3$ remains insulating since the charge carriers are localised in a charge-ordered state.

The reason why $\text{Nd}_{0.7}\text{Ca}_{0.3}\text{MnO}_3$ is charge-ordered at low temperature, whereas, for example $\text{Nd}_{0.7}\text{Sr}_{0.3}\text{MnO}_3$ is not, can be explained by the very small average size of the inter-

polated cation ($\text{Nd}_{0.7}\text{Ca}_{0.3}$), which results in a very large deviation of the Mn-O-Mn bond angle from 180° .

These powder examples show that very accurate information can be obtained by using high resolution in neutron diffraction.

It is still possible to improve the instruments, but we have also to be very careful in the preparation of the samples, as the instrumental resolution is now good enough to be limited by the sample itself.

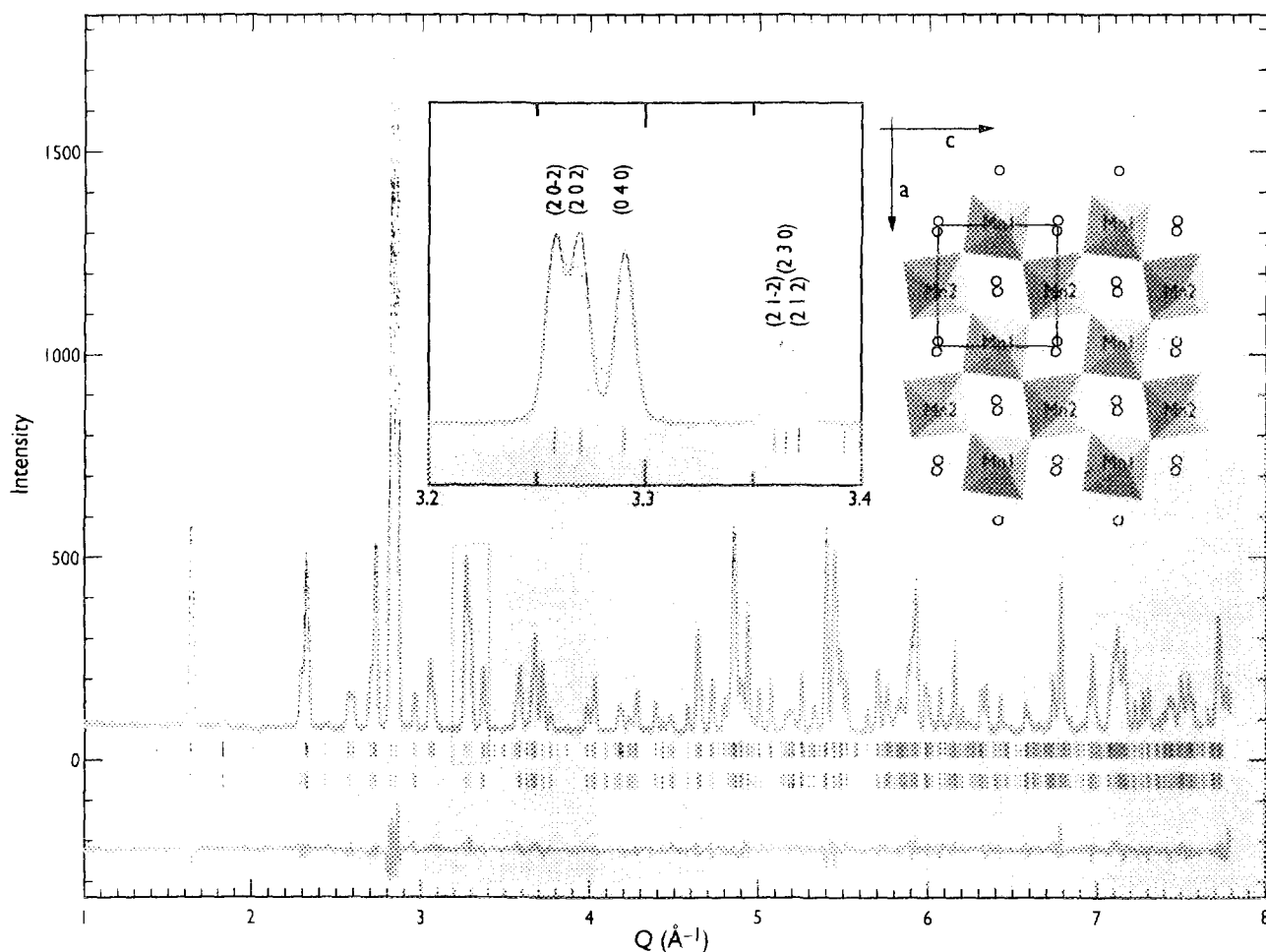


FIGURE 3c: Rietveld refinement plot of the neutron diffraction data for $\text{Nd}_{0.7}\text{Ca}_{0.3}\text{MnO}_3$ measured on D2B at 1.7 K. The inset shows the monoclinic distortion evidenced with the D2B high-resolution configuration at $\lambda=2.4 \text{ \AA}$.

- C. RITTER, P.G. RADAELLI, M.R. LEES, J. BARRAT, G. BALAKRISHNAN AND D.M. PAUL, J. SOL. ST. CHEM. (IN PRESS.)
- P.D. BATTLE, M.A. GREEN, N.S. LASKEY, J.E. MILLBURN, P.G. RADAELLI, M.J. ROSSE-NSKY, S.P. SULLIVAN AND J.F. VENTE, PHYS. REV. B (IN PRESS)
- F. MILLANGE, V. CAIGNAERT, G. MATHER, E. SUARD, B. RAVEAU, J. SOL. ST. CHEM. 127 (1997) 131
- V. CAIGNAERT, F. MILLANGE, M. HERVIEU, G. MATHER, B. RAVEAU, E. SUARD, P. LAFFEZ, G. VAN TANDELOO, PHYS. REV. B (IN PRESS).

ATOMIC AND MAGNETIC CORRELATIONS IN A COPPER - 5% MANGANESE ALLOY

A.P. MURANI, O. SCHARPF, K. ANDERSEN (ILL),
R. RAPHEL (CNRS, GRENOBLE).



FR9704863

INTEREST IN MAGNETISM OF Cu-Mn ALLOYS HAS BEEN REVIVED AND SUSTAINED BY A NUMBER OF VERY INTERESTING NEUTRON INVESTIGATIONS ON SINGLE-CRYSTAL SAMPLES WHICH SHOW 'SPIN-DENSITY WAVE' (SDW) PEAKS AT INCOMMENSURATE WAVE-VECTORS. RECENTLY SUCH PEAKS HAVE BEEN OBSERVED EVEN IN VERY DILUTE SAMPLES WITH Mn CONCENTRATION AS LOW AS ~ 0.5 AT.%. THE PROPOSED INTERPRETATION BY THE AUTHORS THAT THESE PEAKS REPRESENT INCOMMENSURATE ANTIFERROMAGNETIC ORDERING, THEREFORE, QUESTIONS THE WIDELY-HELD VIEW THAT AT LOW ENOUGH TEMPERATURES THE SOLUTE SPINS IN THIS AND SIMILAR ALLOYS FREEZE WITH RANDOM OR QUASI-RANDOM ORIENTATIONS, FORMING A SPIN-GLASS STATE. WE HAVE MAPPED OUT THE ATOMIC AND MAGNETIC CORRELATIONS IN A SINGLE CRYSTAL OF Cu-5 AT.% Mn WITHIN THE FIRST BRILLOUIN ZONE USING POLARISED NEUTRONS AND MAKING USE OF THE MULTI-ANGLE THREE-DIMENSIONAL POLARISATION ANALYSIS CAPABILITY OF THE D7 SPECTROMETER AS A FIRST STEP IN OUR AIM TO SHED FURTHER LIGHT ON THE PHENOMENON.

Dilute solid solutions of Mn atoms in the noble metals, including Cu, have been investigated for well over four decades. Amongst the early investigations of the magnetic properties of such alloys were the measurements of the magnetisation in a constant field of around 1 kOe by Owen et al. [1] which showed broad maxima as a function of temperature. These results were interpreted by Overhauser [2] as representing spin-density wave antiferromagnetic ordering. Neutron diffraction measurements on polycrystalline Cu-Mn alloys by Meneghetti and Sidhu [3] reported around the same period as ref. 1, however, did not show any long-range magnetic order except in concentrated alloys with Mn concentration above ~ 70 at.%. The latter measurements did,

nevertheless, reveal broad magnetic short-range order humps situated between (1, 0, 0) and (1, 1, 0), identified by later workers as (1, 1/2, 0) and equivalent positions which are also the centroids of the atomic short-range order which is more extended in Q-space than the magnetic short-range order. Absence of any signs of a phase transition in the specific heat and transport properties of these alloys and the 'sluggish' magnetic behaviour around the susceptibility maximum has led to a still widely-held view that at low enough temperatures, spins in such alloys freeze randomly or quasi-randomly into a spin-glass state.

Neutron investigations on single crystals which followed showed that the magnetic short-range order also contained

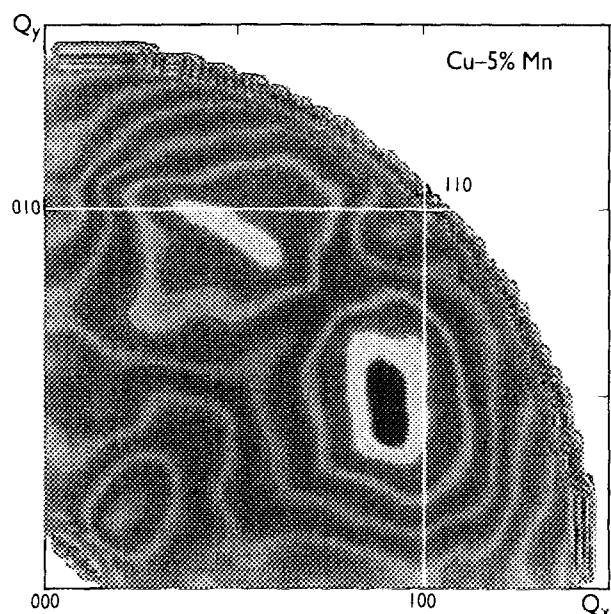


FIGURE 1: Two-dimensional map of atomic correlations in a Cu-5 at.% Mn single crystal sample showing the broad short-range order humps close to the (1, 1/2, 0) and (1/2, 1, 0) positions.

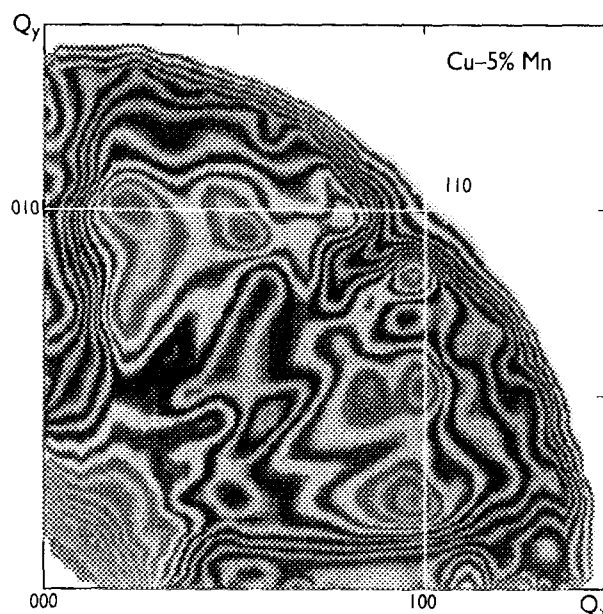


FIGURE 2: Magnetic correlations in a Cu-5 at.% Mn alloy, showing the strong forward peak (at low q 's), the magnetic short-range correlations centred on the (1, 1/2, 0) and equivalent positions and the relatively sharp SDW-like peaks centered on (1, 1/2 $\pm \delta$, 0)-type positions.

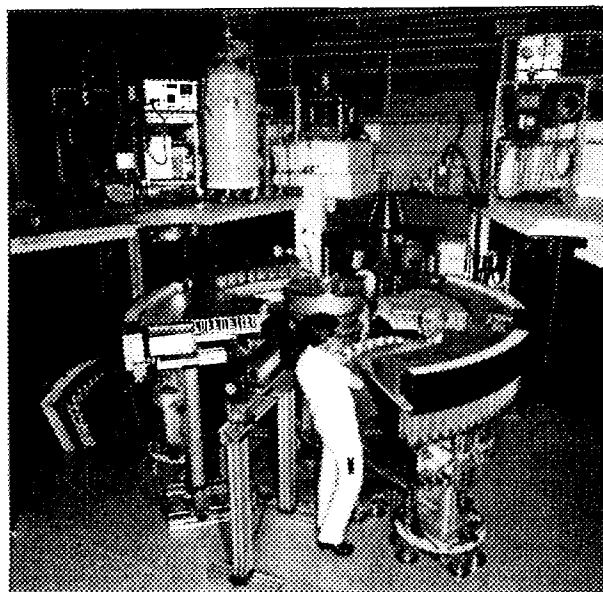
relatively sharp peaks situated on either side of the short-range order hump at Q-vectors $(1, 1/2 \pm \delta, 0)$. The latest studies on very dilute alloys show that the positions δ of these peaks vary almost linearly with concentration extrapolating, for zero concentration, to a Q-vector which correlates well with the Fermi wave-vector $2k_F$ of Cu. On the basis of these observations the authors suggest that Cu-Mn alloys are SDW antiferromagnets, with the magnetic order driven by the intrinsic instability on the Fermi surface of Cu.

We have performed three-dimensional polarisation analysis on a single crystal of Cu-5 at.% Mn alloy to map out the atomic and magnetic correlations. Figs. 1 and 2 show the results of our measurements at 1.5 K, well below the 'freezing' or 'ordering' temperature of ~ 25 K. The sample was rotated in 5° steps about the [100] axis to cover the full circle (360°) in the scattering plane containing the [110] and [100] axes and full xyz polarisation analysis was performed at each orientation. The data were then folded into a single quadrant, to increase the statistical accuracy and to average over any dependence on the sample orientation.

Cu-Mn alloys show an inherent tendency towards atomic short-range order whereby a Mn atom is preferentially surrounded by Cu atoms, particularly in the surrounding near-neighbour shell. The amount of short-range order is known to decrease with decreasing Mn concentration but is still non-negligible in the present alloy containing only 5 at. % Mn. The two-dimensional contour map in Fig. 1 shows broad atomic short-range order situated close to positions $(1, 1/2, 0)$ and $(1/2, 1, 0)$. These data confirm and supplement similar two-dimensional maps for single crystals of Cu containing 25 at. % Mn¹ and 17 at. % Mn², while most other studies on more dilute samples have been limited to one-dimensional scans along the $[1, k, 0]$ and equivalent directions. A similar contour plot for magnetic correlations is shown in Fig. 2. It reveals several interesting features: i) strong forward scattering at low Q's, showing small peaks at well defined low Q-values along the principal directions ii) an elongated but relatively narrow magnetic peak, compared with the atomic short-range order humps, centred around $(1, 1/2, 0)$

and $(1/2, 1, 0)$ and iii) the 'SDW-like' peaks also elongated in the reciprocal space but centered on $(1, 1/2 \pm \delta, 0)$ and equivalent positions, with the peak at $(1/2 + \delta)$ not having the same intensity or form as the one at $(1/2 - \delta)$.

The spin correlations evidenced from the present data are rather complex. It is interesting that while the widths of the SDW-like peaks indicate a relatively long correlation length of ~ 10 -30 Å, as found previously, the cross-section represented by the peaks is fairly small. In fact, the overall cross-section of all the sharp structures taken together (including that related to the atomic short-ranger order represents only a fraction of the total cross-section, a significant part of which forms a constant uniform background in reciprocal space, associated with spins which are frozen into random orientations. From previous measurements on single crystals it would appear that the fraction of spins of the latter kind increases with decreasing Mn concentration. We aim, therefore, to extend our investigation of magnetic correlations to lower concentration alloys in order to study this evolution in more detail.



The spectrometer D7 which was used for the measurements reported; René Rebescio (left) and Otto Schürpf are dismantling the guide field.

-
- J. OWEN, M. BROWNE, V. ARP AND A. F. K. P., J. PHYS. CHEM. SOLIDS 2 (1957) 85 ■ A.W. OVERHAUSER, J. PHYS. CHEM. SOLIDS 13 (1960) 71 ■ D. MENEGHEIT AND S. S. CHU, PHYS. REV. 105 (1957) 130 ■ J.W. CABLE, S. A. WERNER, G. P. FELCHER AND N. WAKABAYASHI, PHYS. REV. LETT. 49 (1982) 829 ■ F.J. LAMELAS, S. A. WERNER, S. M. SHAPRO AND J. A. MYDOUSH, PHYS. REV. B 51 (1995) 621 ■ M. RIEGER, B. SCHÖNFELD, G. KOSTORZ, W. BÜHRER, J. L. ROBERTSON, P. ZSCHACK AND G.E. ILIE, SCRIPTA MATER. A 34 (1996) 1393. ■

ANTIFERROMAGNETIC CORRELATIONS IN ICOSAHERAL R-Mg-Zn QUASICRYSTALS (R = RARE EARTH)

B. CHARRIER, D. SCHMITT (CNRS GRENOBLE),
B. OULADDIAF (ILL).



POWDER NEUTRON-DIFFRACTION EXPERIMENTS PERFORMED ON R-Mg-Zn QUASICRYSTALS HAVE SHOWN FOR THE FIRST TIME THE EXISTENCE OF MAGNETIC ORDERING OF THE RARE EARTH IN THESE SYSTEMS AT LOW TEMPERATURE ($T_C \leq 6.5$ K DEPENDING ON THE RARE EARTH). BOTH NARROW AND BROAD MAGNETIC DIFFRACTION PEAKS HAVE BEEN OBSERVED SHOWING THE PRESENCE OF TWO DIFFERENT SCALES OF MAGNETIC CORRELATIONS.

$R_8Mg_{42}Zn_{50}$ (R = rare earth and Y) are the only known rare-earth-based icosahedral quasicrystals. These phases are stable and present a highly ordered structure [1]. One of the most important points in studying their magnetic properties is to get insight into the structure of the quasicrystals and particularly the local environment of the rare-earth ions through their magnetic response. Moreover, investigating the propagation of the exchange interactions in such a symmetry is also of great interest. Recent susceptibility and specific-heat measurements suggested either a spin-glass-like behaviour or random anisotropy antiferromagnetism [2]. Indeed, these measurements show a broad anomaly at low temperature, with irreversible effects similar to those observed in spin-glass systems. The susceptibility follows a Curie-Weiss law at higher temperature with a slight deviation just above the critical temperature. This latter varies from $T_C = 6.5$ K for Tb to 2 K for Ho compounds.

Here, we show the results of neutron-diffraction experiments performed on the $i-R_8Mg_{42}Zn_{50}$ rare-earth quasicrystals, using the multidetector diffractometer D1B with a neutron wavelength $\lambda = 2.524$ Å. The samples were prepared with a conventional solidification technique at the Louis Néel Laboratory (CNRS, Grenoble). In this diffraction experiment the temperature dependence of the magnetic correlations in powder $i-R_8Mg_{42}Zn_{50}$ compounds have been investigated. The high-temperature paramagnetic spectra for all compounds show mainly the nuclear peaks similar to that of the Y-compound. These peaks can be indexed according to the (N,M) scheme proposed by Cahn et al. [3]: for each peak, the modulus of the corresponding scattering vector Q can be expressed in terms of two integer indices (N,M) by $Q^2 \propto (N + \tau M)$, where $\tau = (1+\sqrt{5})/2$ is the golden mean. It turns out that the intensity of the neutron-diffraction peaks roughly follows that of the corresponding X-ray diffraction lines [1,2]. In particular the most intense two lines are the same in each case, namely (18,29) and (20,32) as shown in Fig. 1a. Within the series, the intensity of these nuclear peaks changes slightly. In addition, the patterns show a few small extra peaks which correspond to a few percents of impurity phase of probable composition Mg_7Zn_3 , already observed by X-ray diffraction.

The spectra obtained at low temperature exhibit numerous additional lines of magnetic origin, which cover a wide range of Bragg angles. This is clearly shown in the difference between low and high temperature spectra (see Fig. 1b for $Ho_8Mg_{42}Zn_{50}$). The main spectacular feature of this magnetic diffraction is the coexistence of wide and narrow diffraction peaks, indicating the coexistence of two different scales of the magnetic correlations, i.e. short-range-like and long-range-like order. These two magnetic contributions show a similar thermal dependence and vanish at the same temperature. The present result is rather unexpected considering the spin-glass-like behaviour observed in other respects by magnetostatic measurements.

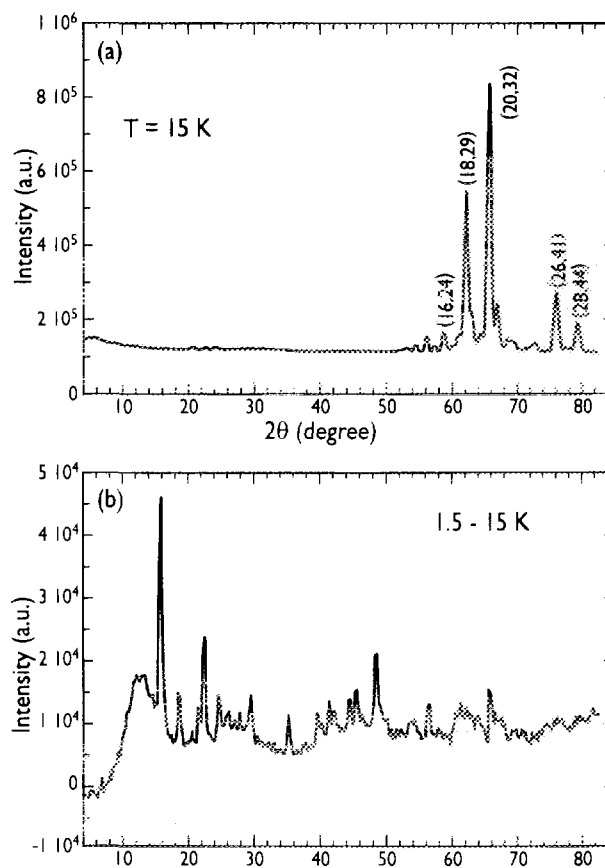


FIGURE 1 a) Powder-diffraction pattern of $Ho_8Mg_{42}Zn_{50}$ at $T = 15$ K; b) difference pattern (1.5 K - 15 K) for $Ho_8Mg_{42}Zn_{50}$.

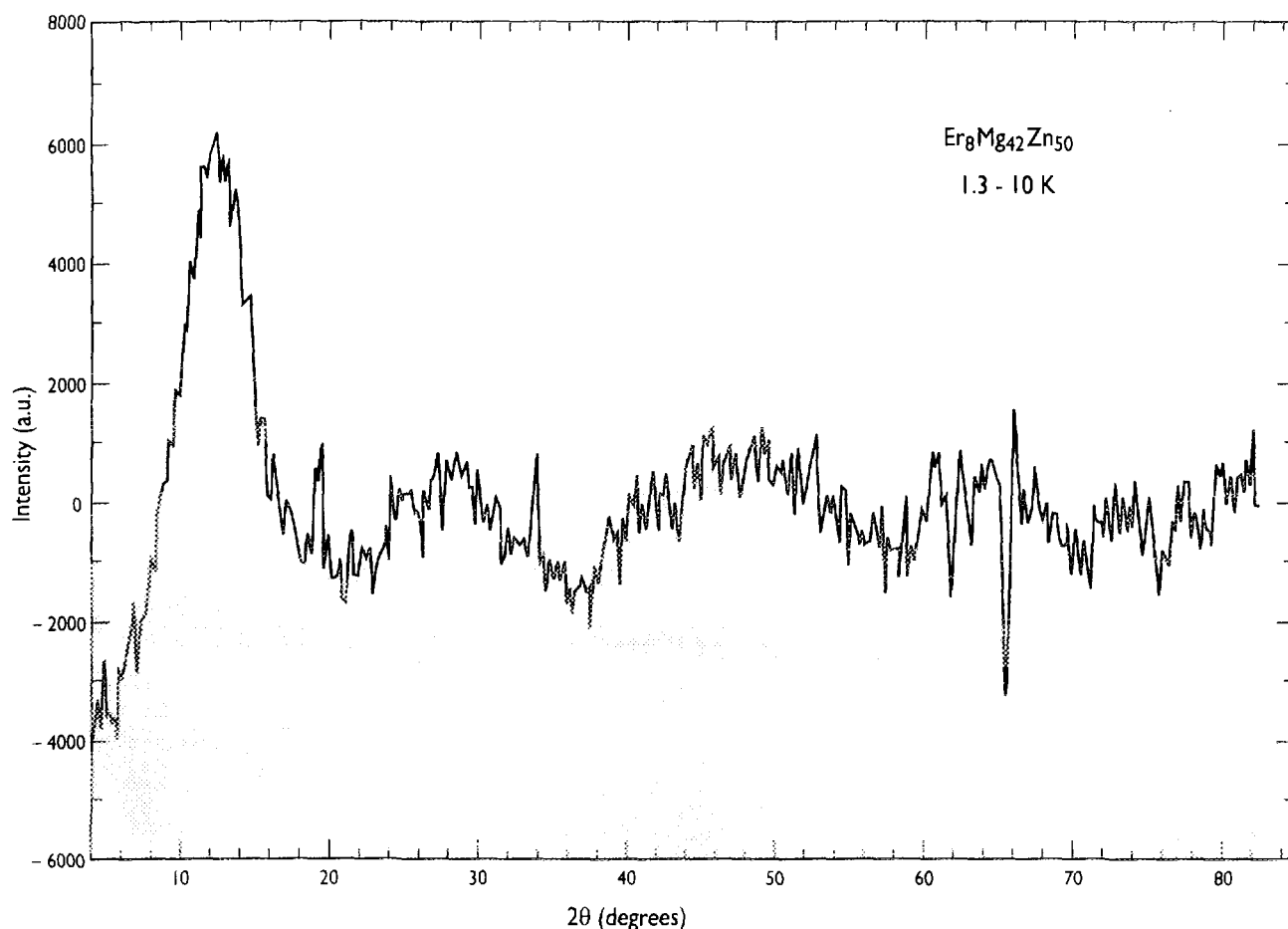
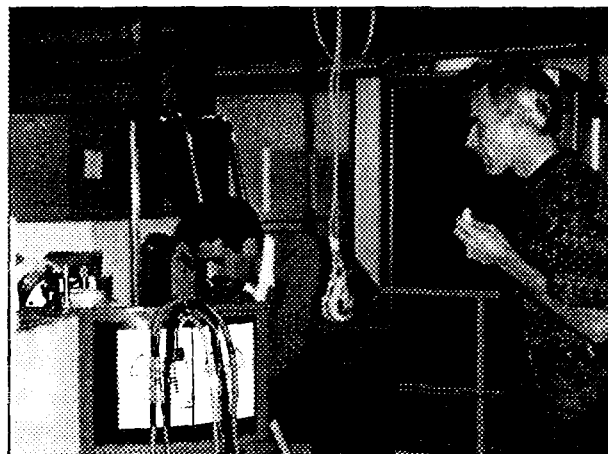


FIGURE 2: Difference pattern (1.3 K – 10 K) for $\text{Er}_8\text{Mg}_{42}\text{Zn}_{50}$.

Furthermore, a preliminary analysis shows that, some magnetic lines exhibit scaling properties (inflation), i.e. the difference of the modulus of the corresponding scattering vectors $|Q|$ of the peaks taken in pairs is proportional to $N + \tau M$ (N, M integer) similar to the icosahedral nuclear peaks. This is direct evidence of the quasiperiodic character of the magnetic peaks. Similar overall behaviour is also observed for the other rare-earth compounds as, for example, for the Er-compound (Fig. 2) but this compound shows mainly only the broad magnetic components.

The detailed analysis of these magnetic spectra is under way. The first step is to find a coherent set of indices for all the magnetic peaks. Then a model will have to be proposed to explain their intensity as well as the different correlation lengths observed.

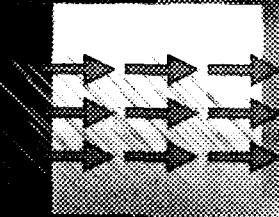


The instrument responsible set up D1B; from left: Bachir Ouladdiaf and Clemens Ritter.

-
- A. P. TSAI, A. NIJKURA, A. INOUE, T. MASUMOTO, Y. NISHIDA, K. TSUDA AND M. TANAKA, *PHIL. MAG. LETT.* 70 (1994) 169
 - B. CHARRIER AND D. SCHMITT (TO BE PUBLISHED) ■ J. W. CAHN, D. SCHECHTMAN AND D. GRATIAS, *J. MATER. RES.* 1 (1986) 13.



FR9704865



EXCITATIONS IN THE ITINERANT MAGNET UFe_2

- L. PAOLASINI (LLB SACLAY),
- G.H. LANDER (EITU),
- R. CACIUFFO (UNIV. ANCONA),
- B. ROESSLI (ILL).

NEUTRON INELASTIC-SCATTERING EXPERIMENTS HAVE BEEN USED TO STUDY A SINGLE CRYSTAL OF THE ITINERANT FERROMAGNETIC UFe_2 . THE MOST SURPRISING ASPECT OF THIS MATERIAL IS THE ENHANCED Fe-Fe EXCHANGE COMPARED TO THE ISO-STRUCTURAL LAVES PHASES WITH RARE EARTHS. TRIPLE-AXIS SPECTROSCOPY, BOTH COLD WITH POLARISATION ANALYSIS AND THERMAL, HAS GIVEN NEW INSIGHTS INTO THE INTERACTIONS BETWEEN THE URANIUM 5f AND IRON 3d ELECTRONS.

Compounds containing rare-earth elements (RE) and Fe (or Co) are important for a large number of technical applications, ranging from permanent magnets, to magneto-optical storage media, to transducers. To provide useful magnets the Curie temperature (T_C) must be high and a large coercivity is obtained by a combination of shape and intrinsic anisotropy. Loosely speaking, it is the Fe that provides the high T_C , and the rare-earth that provides the intrinsic anisotropy. A good example is $\text{Nd}_2\text{Fe}_{14}\text{B}$. In the early 1970's the cubic Laves phase materials REFe_2 ($T_C \sim 650$ K) became of interest for transducers, and the basic understanding of their properties was enhanced by a series of neutron inelastic-scattering experiments. The results [1] showed that the dominant microscopic exchange interaction is that between the Fe moments $\mathcal{J}_{\text{Fe-Fe}}$, and the pure Fe sublattice spin-wave mode was observed to be very similar to that for pure Fe. In these materials the direct interaction between the RE 4f and Fe 3d electrons is small.

A different situation is present in the itinerant ferromagnets CeFe_2 and UFe_2 . In these compounds there is a direct hybridisation between the Ce or U f and Fe 3d electrons, the anisotropy associated with localised f electrons is not found, and the properties are best described in terms of band states:

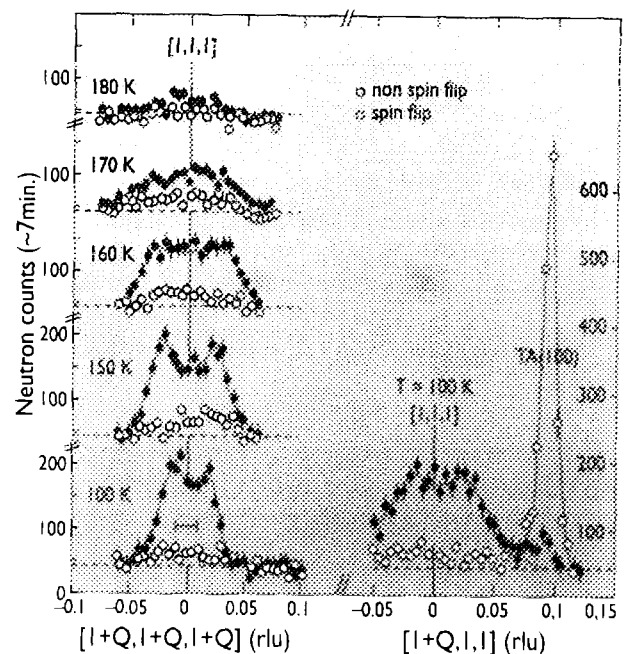


FIGURE 1: Data taken with polarisation analysis on UFe_2 . The solid points have the neutron spin flipped, and thus represent a magnetic signal. Left-hand side: The temperature dependence shows that the scattering changes character at T_C (165 K). The right-hand side shows the transverse acoustic phonon, and shows the lack of any interaction between the two modes at low energy. (Taken from Ref. 3).

i.e. the compounds are itinerant magnets. The most obvious result of this hybridisation is a reduction in T_C . In the heavy rare-earth Fe_2 compounds $T_C \sim 650$ K, whereas it is 220 K and 165 K in CeFe_2 and UFe_2 , respectively. In the latter compound the uranium has the interesting property that the spin and orbital moments are $\sim 0.25 \mu_B$, but they are oppositely directed so the total moment is essentially zero. Neutron inelastic-scattering experiments have been performed on a single crystal of UFe_2 to determine the microscopic exchange interactions. Early experiments were performed at Risø, Silø and Brookhaven reactors while ILL was down. An experiment using polarisation analysis was performed in 1995 at IN14 to measure the low-energy part of the spin dynamics, and, in particular, to test whether there is a gap in the excitation spectrum of the Fe spin-wave mode. The results are shown in Fig. 1. Constant-Q scans established that the spin-wave gap of this excitation is 0.4 meV. This mode, the only one observed so far, has been identified as arising from the precession of the Fe spins. In addition, we expect to find the magnetic acoustic mode involving precession of both moments, but this is apparently broadened and spread diffusely over the Brillouin zone. We show in Fig. 2 the energy of the Fe mode plotted as a function of Q squared. The slope of the straight line gives a value for the spin-wave stiffness D , which is also related to $\tilde{J}_{\text{Fe-Fe}}$. As expected, D is slightly less for ErFe_2 as compared to that of pure Fe. For UFe_2 there are two surprising features of the spin-wave relationship.

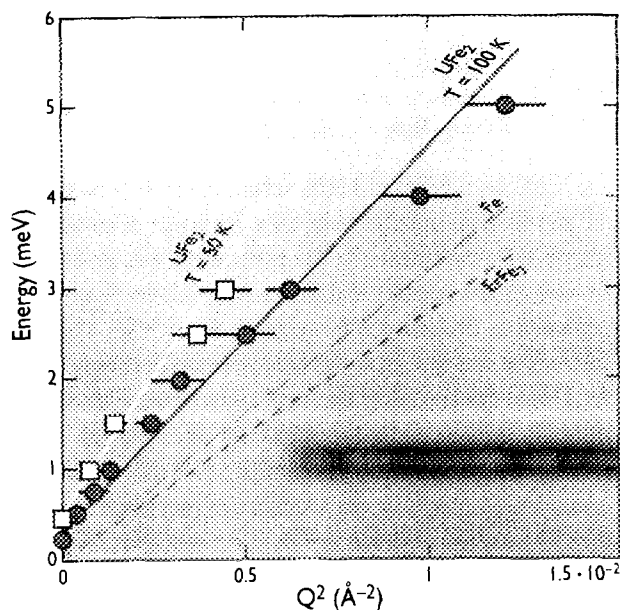


FIGURE 2: Analysis of the low- Q region for various materials. Dashed line is the best fit to the data for pure Fe with a slope of $D = 325 \text{ meV } \text{\AA}^2$. Dotted curve gives the data for ErFe_2 from Ref. 1 with a 8 meV gap suppressed, and $D = 280 \text{ meV } \text{\AA}^2$. The two solid lines are fits to the data shown for UFe_2 and clearly have a larger value of D than Fe. (Taken from Ref. 3).

The first is that D is actually larger than in pure Fe. We believe this is a consequence of the hybridisation between the U 5f and Fe 3d electrons. The rise in $\tilde{J}_{\text{Fe-Fe}}$ has some potentially interesting applications, but, at least in UFe_2 , there is also a reduction in the Fe spin (S_{Fe}), and it is the product ($\tilde{J}_{\text{Fe-Fe}} \cdot S_{\text{Fe}}$) that determines T_C . The second feature of Fig. 2 is that $D(\text{UFe}_2)$ is dependent on temperature. For most materials D is only weakly dependent on T up to about $0.75 T_C$, above which a strong renormalisation of the spin waves usually occurs, but in UFe_2 the effect is evident even by $0.5 T_C$. The above was the situation at the completion of the thesis work of L. Paolasini (Univ. of Grenoble), presented in early 1996, and published [4]. In September 1996 the experiments were continued and the dispersion curve of the Fe mode is given in Fig. 3. The intensity of IN8 has allowed the Fe mode to be followed up to ~ 20 meV. Above ~ 10 meV there is a strong interaction with another mode. We believe this interaction occurs with the Λ_3 phonon, which is optic and involves a motion of the Fe sublattice. Over the energy region 14 -16 meV the excitation is weak and broad; both below and above this energy it is well-defined. The next stage is therefore to study the phonons. Interestingly, there is no comparable effect reported in the REFe_2 compounds, but almost no phonons of these materials have been studied.

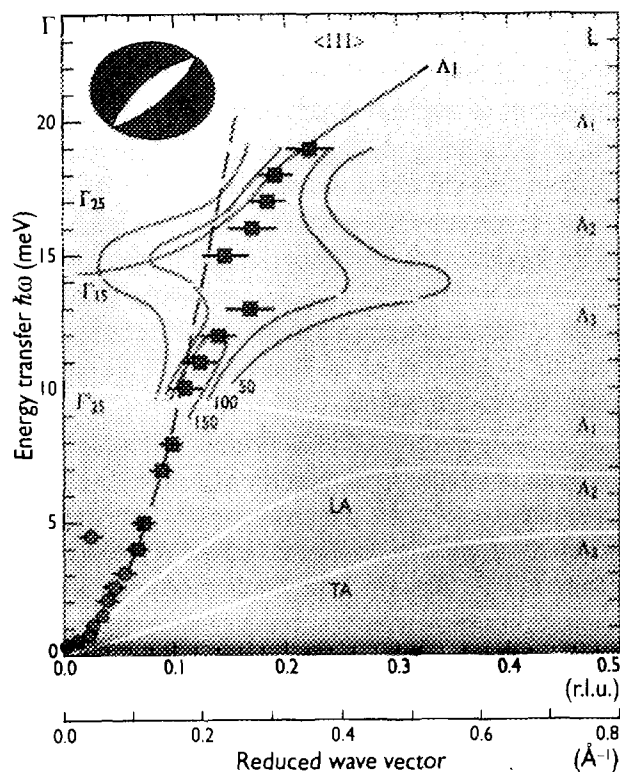


FIGURE 3: The dispersion curve deduced at 100 K in a recent experiment on IN8. The quadratic relationship at low Q (consistent with the lines in Fig. 2 and shown as a broken line) holds up to 8 meV, but deviates considerably above that energy. The strong interaction of the Fe spin-wave mode around 14 meV is shown by contours of equal intensity. The resolution function is shown in the upper left-hand corner. The phonon energies are shown as thin solid lines.

MINUTE SPLITTING OF MAGNETIC EXCITATIONS IN CsFeCl_3 DUE TO DIPOLAR INTERACTION OBSERVED BY POLARISED NEUTRONS

■ B. DÖRNER (ILL),
■ M. BAEHR (HMI BERLIN),
■ D. PETITGRAND (LLB SACLAY).

FR9704866

USING INELASTIC NEUTRON SCATTERING WITH POLARISATION ANALYSIS IT WAS POSSIBLE, FOR THE FIRST TIME, TO OBSERVE SIMULTANEOUSLY THE TWO MAGNETIC MODES SPLIT DUE TO DIPOLAR INTERACTION. THIS WOULD NOT HAVE BEEN POSSIBLE WITH ENERGY RESOLUTION ONLY. AN ANALYSIS OF EIGENVECTORS WAS ALSO PERFORMED.

Dipolar interactions in magnetic materials are created by the magnetic field around one or more oriented elementary magnetic moments. They are most often weak compared to exchange interactions which arise from an overlap of the wavefunctions of magnetic electrons. Contrary to exchange interactions, dipolar forces are of long range. This is the reason why they may become important near magnetic phase transitions. Here we present an experimental study on CsFeCl_3 [1], where the use of polarised neutrons made it possible to observe the minute splitting, caused by dipolar interaction, of originally doubly degenerate states.

Due to this splitting the dispersion curves of the magnetic excitations are changed so that minima in energy, originally located at commensurate positions in reciprocal space, such as the K-points, $(1/3, 1/3, 0)$ and $(2/3, 2/3, 0)$, are moved to incommensurate positions. In the "soft mode" picture of phase transitions the minima in the excitation energy correspond to positions where Bragg peaks of the ordered magnetic structure appear.

For this study we chose CsFeCl_3 which is isostructural with the quasi one-dimensional magnetic system RbFeCl_3 . The latter orders below 2.5 K into an incommensurate structure which is explained by dipolar interactions [2] between the chains of Fe^{2+} ions which are ferromagnetically aligned along the hexagonal (z) axis with an antiferromagnetic interaction between neighbouring chains. CsFeCl_3 does not order magnetically down to the lowest temperature so that the dipolar interactions can be studied without being disturbed by temperature dependent excitation energies (soft modes). The lowest excitation energies appear for the dispersion curve perpendicular to the chain direction and the main features of the dispersion correspond to the antiferromagnetic exchange interaction between the chains. The influence of dipolar forces is strongest on these low frequency modes, see Fig. 1.

The experiment with polarised neutrons was performed on the three-axis spectrometer IN14, with a sample of volume 0.5 cm^3 . The experimental set-up was such that magnetic fluctuations of S^x type (see Fig. 3) show up in the non-spin-flip (NSF) channel, while S^y fluctuations are detected in the spin-flip (SF) channel.

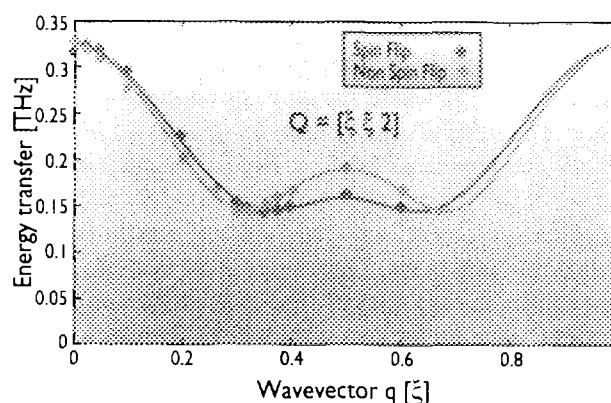


FIGURE 1: Dispersion of the magnetic excitations in the y-direction $[\xi\xi0]$, perpendicular to the chain direction, which are split due to dipolar interaction. NSF (blue) and SF (red) correspond respectively to S^x and S^y fluctuations (see Fig. 3). The curves represent a least squares fit of a dispersion relation containing exchange interaction between neighbouring chains and dipolar forces.

Fig. 2 shows a series of scans, where the shift between the SF and the NSF signals can be seen. Each pair of curves was measured simultaneously: the instrument was positioned for one energy transfer and then a polarisation flipper was activated or deactivated to measure SF or NSF. Then the instrument was moved to the next position in energy transfer. Due to this procedure the small shifts between the signals are only influenced by the statistical uncertainties of the measured data but not by positioning inconsistencies of the spectrometer. Anyway, the sequence of measured frequencies, like a chain of pearls in Fig. 1, confirms the reliability of the experimental technique.

One part of the results consists in the first observation of the splitting of the modes (degenerate in the absence of dipolar interaction) and in the shift of the minima of the dispersion curves away from the commensurate K-points, see Fig. 1, thus indicating the possibility for an incommensurate magnetic order. In fact such an incommensurate magnetic structure appears not only in RbFeCl_3 but also in CsFeCl_3 , if an external magnetic field is applied parallel to the chain direction. The other part of the results is connected to the correlation between SF/NSF and S^y/S^x fluctuations. This correlation makes it possible to derive eigenvectors of the observed modes.

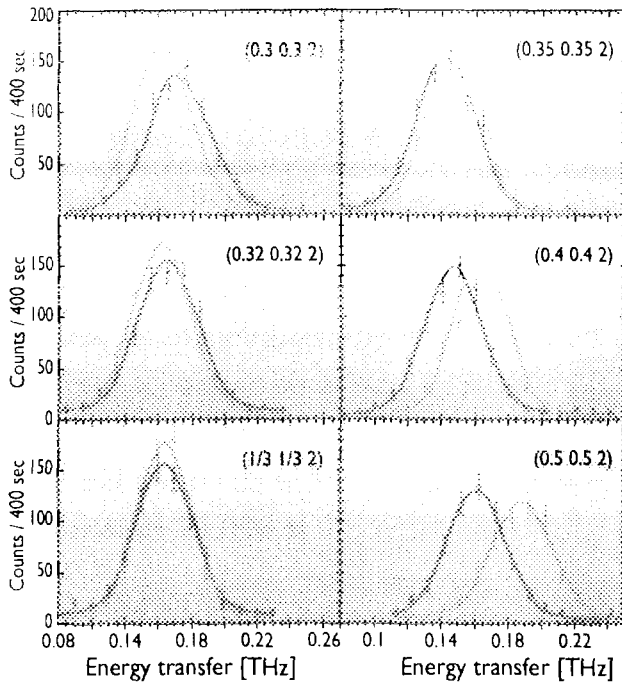


FIGURE 2: A series of constant- Q scans at different positions along the y -direction, $Q = [\xi \xi 2]$. Blue and red symbols correspond to NSF and SF, respectively.

Fig. 3a shows the eigenvectors at small wavevector $q = 2\pi/\lambda$ (wavelength $\lambda \gg a$, where a is the lattice parameter in the hexagonal plane). It is obvious that the S^y -mode has to have the higher frequency because here the dipolar interaction is "stretched" contrary to the case for the S^x -mode. Fig. 3b gives the eigenvectors of the degenerate modes at the K-point ($\lambda = 3a/2$) and Fig. 3c displays the eigenvectors at the M-point ($1/2, 1/2, 0$) ($\lambda = a$). Here the S^y mode has the lower frequency.

It is remarkable that this S^y eigenvector is equal to the static order in the isostructural substance CsNiF_3 , where the dipolar interactions dominate over the exchange between the chains.

This experiment demonstrates in a convincing way the possibilities of polarised neutrons: For the first time the two modes, split due to dipolar interaction, were measured simultaneously. This would not be possible with energy resolution only. Polarisation analysis also made it possible to extract the eigenvectors of the modes. These eigenvectors confirm the qualitative predictions [1] of the incommensurate magnetic structure in RbFeCl_3 near the K-point and the commensurate structure of CsNiF_3 at the M-point.

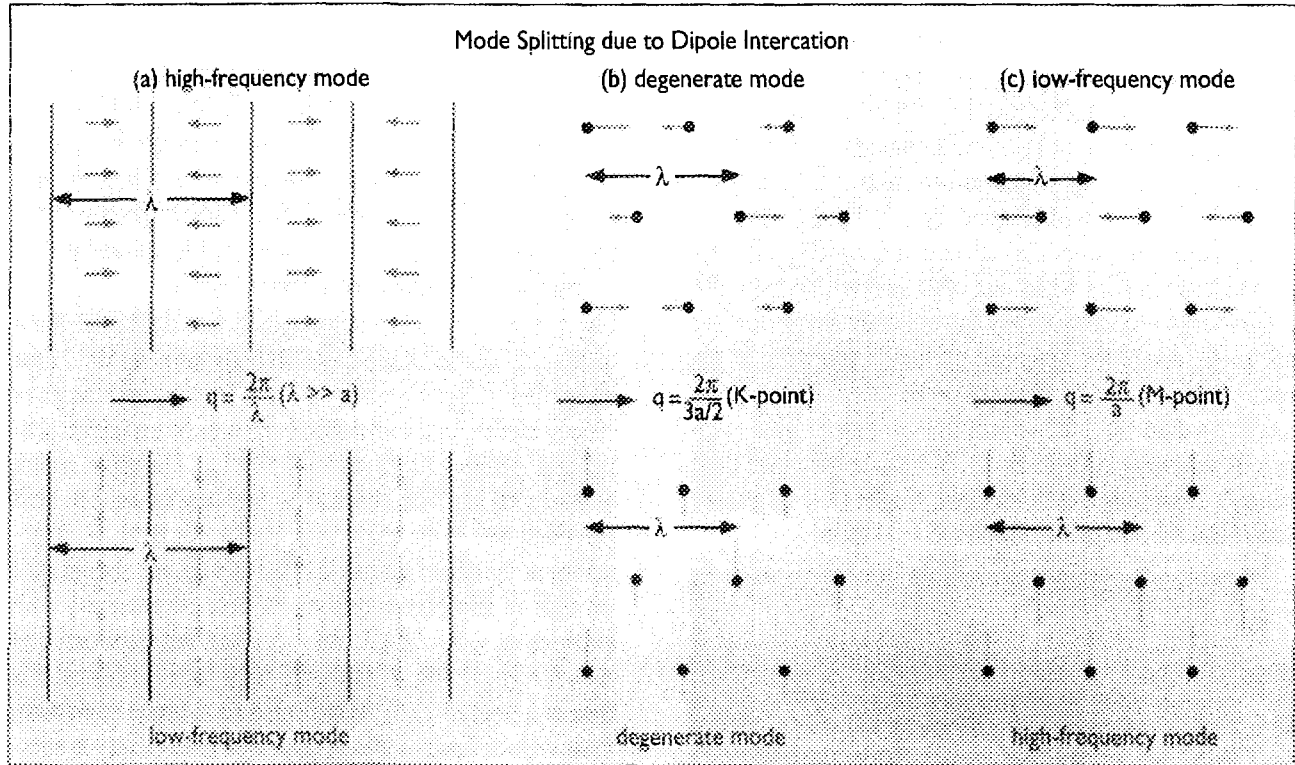


FIGURE 3: Eigenvectors of the magnetic fluctuations at different wavevectors q : a) at small q , b) at $q = 4\pi/3a$ (K-point), c) at $q = 2\pi/a$ (M-point). The red and blue arrows indicate S^y and S^x fluctuations, respectively.

- [1] B. DORNER, B. TOPFERG, M. BAEHR AND D. PETITGRAND, PROCEEDINGS OF ECNS'96, INTERLAKEN, PHYSICA B (IN PRESS)
- H. SHIBA, SOL. ST. COMM. 41 (1982) 511 ■ K. KNOP, M. STEINER AND P. DAY, J. MAGN. MAGN. MAT. 31-34 (1983) 1033
- M. STEINER, SOL. ST. COMM. 11 (1973) 73.

■ L. P. REGNAULT (CEA GRENOBLE).



FR9704867

THE ONE-DIMENSIONAL SPIN-1/2 HEISENBERG ANTIFERROMAGNETIC SYSTEM COUPLED TO A THREE-DIMENSIONAL PHONON FIELD UNDERGOES A STRUCTURAL DISTORTION BELOW A FINITE TEMPERATURE T_{SP} (SPIN-PEIERLS TRANSITION) WHICH INDUCES THE FORMATION OF A NON-MAGNETIC SINGLET GROUND-STATE AND THE OPENING OF A GAP IN THE EXCITATION SPECTRUM AT THE ANTIFERROMAGNETIC POINT. THE RECENT DISCOVERY OF THE GERMANATE CuGeO_3 AS A SPIN-PEIERLS SYSTEM HAS CONSIDERABLY RENEWED THE INTEREST IN THIS FASCINATING PHENOMENON. INELASTIC NEUTRON SCATTERING AND NEUTRON DIFFRACTION HAVE BROUGHT VERY QUANTITATIVE PIECES OF INFORMATION WHICH CAN BE DIRECTLY COMPARED TO THE PREDICTIONS OF THE STANDARD MODEL.

In its simplest version, a "spin-Peierls" (SP) system is a spin system which undergoes a structural distortion driven by quantum magnetic fluctuations. Such a nontrivial behaviour was predicted to exist in the one-dimensional (1D) spin-1/2 Heisenberg antiferromagnetic system (well known to develop large spin fluctuations as $T \rightarrow 0$) coupled to a 3D phonon field [1,2]. Below some finite temperature T_{SP} (called the spin-Peierls transition temperature) a structural instability occurs (characterized by a commensurate structural propagation vector k_{SP} corresponding to out-of-phase atomic displacements), which transforms the uniform chain system into a system of coupled dimers. The existence of such a lattice distortion has several consequences on the magnetic properties which are well understood from the progressive appearance below T_{SP} of intrachain alternating exchange. As for the magnetic excitation spectrum of the spin-1/2 alternating antiferromagnetic chain, the standard model predicts for a SP system the opening of a spin gap at a finite energy Δ (with $D \approx 1.76 \text{ kT}_{\text{SP}}$ in the mean field theory), separating a non magnetic singlet ($S = 0$) ground state from the first excited triplet ($S = 1$) states.

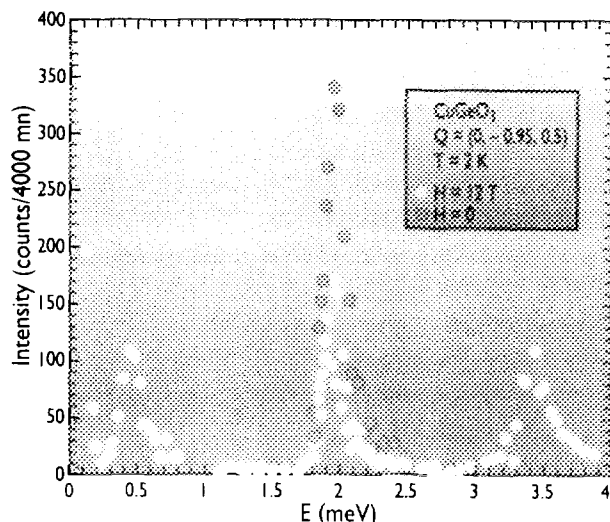


FIGURE 1: Energy scan near " $q = \pi$ " in zero field and at a field of 12 T showing the splitting of the excited triplet.

With the discovery of the inorganic material CuGeO_3 (for which crystals of centimetre size could be easily synthesised), many predictions have been clarified and new results acquired. Very comprehensive studies have been undertaken by various techniques (including neutron scattering) which have confirmed the occurrence of a spin-Peierls transition in this compound at $T_{\text{SP}} \approx 14.2 \text{ K}$ and with $k_{\text{SP}} = (1/2, 0, 1/2)$. Neutron scattering has played a crucial role in the understanding of the mechanism of this transition, which results from the interplay between the magnetic and structural fluctuations. The existence of both the singlet ground-state and the gap in the excitation spectrum have been unambiguously observed from quasi-elastic and inelastic-neutron-scattering experiments [3,4].

Fig. 1 shows a typical energy scan in zero field carried out on the cold neutron three-axis CRG spectrometer IN12 near the antiferromagnetic point (" $q \approx \pi$ "). This typical scan gives clear evidence for a well defined and narrow excitation peaked at an energy of $1.95 \text{ meV} \approx 1.59 \text{ kT}_{\text{SP}}$. The triplet nature of this mode has been checked by applying a magnetic field perpendicular to the chain axis. Under this field, the degeneracy of the excited states is lifted and the gap should split (in case of triplets) into three distinct components with energies $\Delta_1 \approx \Delta - g\mu_B H$, $\Delta_2 \approx \Delta$ (field independent) and $\Delta_3 \approx \Delta + g\mu_B H$. Fig. 1 shows the same scan performed this time at a field of 12 T. As expected for a triplet excitation, three well-defined modes are detected respectively at energies 0.45, 1.95 and 3.45 meV. Fig. 2 gives the field dependencies of gaps between 0 and 12 T, which are quantitatively understood from the linear relations taking $g = 2.18$. Following the standard model, the SP system undergoes a first order field-induced phase transition at a characteristic field $H_C \approx 0.84 \Delta / g\mu_B$, which is associated with the emergence of a new incommensurate lattice-distortion [5,6]. Schematically, this phase can be described as a stacking of non-magnetic dimerised segments regularly spaced by "normal" segments carrying magnetisation (soliton lattice structure). Among other consequence, one predicts that the com-

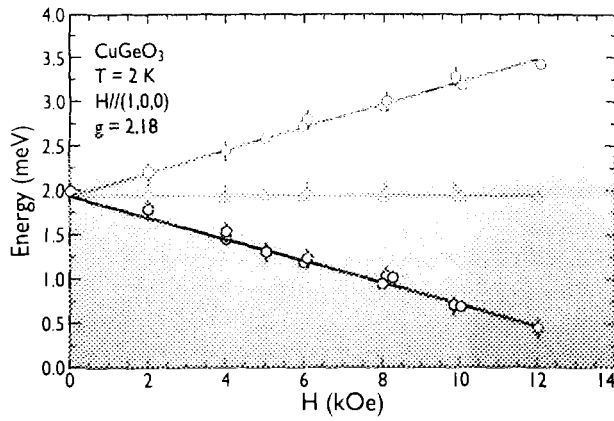


FIGURE 2: Field dependencies of gaps in field perpendicular to the chain axis.

ponent along the chain of the propagation vector will take incommensurate values, with a shift to commensurability directly related to the intersoliton distance $L/2$ and the magnetisation M by the simple relation:

$$\delta k_{\text{SP}}(H) = k_{\text{SP}}(H) - k_{\text{SP}}(0) \approx 2\pi / L \propto M.$$

Neutron-diffraction experiments have recently been successfully performed on a weakly Si-doped compound. Si-doping has been shown to reduce very rapidly both T_{SP} and H_C , in such a manner that the substitution of only 0.3% of germanium by silicon was sufficient to decrease H_C below 12 T, the highest field available to date.

From accurate neutron-diffraction experiments performed on the spectrometer IN8, it has been possible to confirm the existence of a high-field incommensurate phase in $\text{CuGe}_{0.997}\text{Si}_{0.003}\text{O}_3$. Fig. 3 demonstrates clearly the emergence of a two-peak structure between 11.5 T and 12 T in increasing field ($H_C \approx 11.7$ T), associated with an incommensurate component $\delta k_{\text{SP}} \approx 0.0075 = \text{reciprocal lattice units (r.l.u.)}$.

All the data collected are consistent with the soliton lattice picture and confirm the X-ray-scattering results [6]. In addition, it has been possible for the first time to detect directly the intrasoliton magnetic component, a result that only neutron diffraction could obtain.

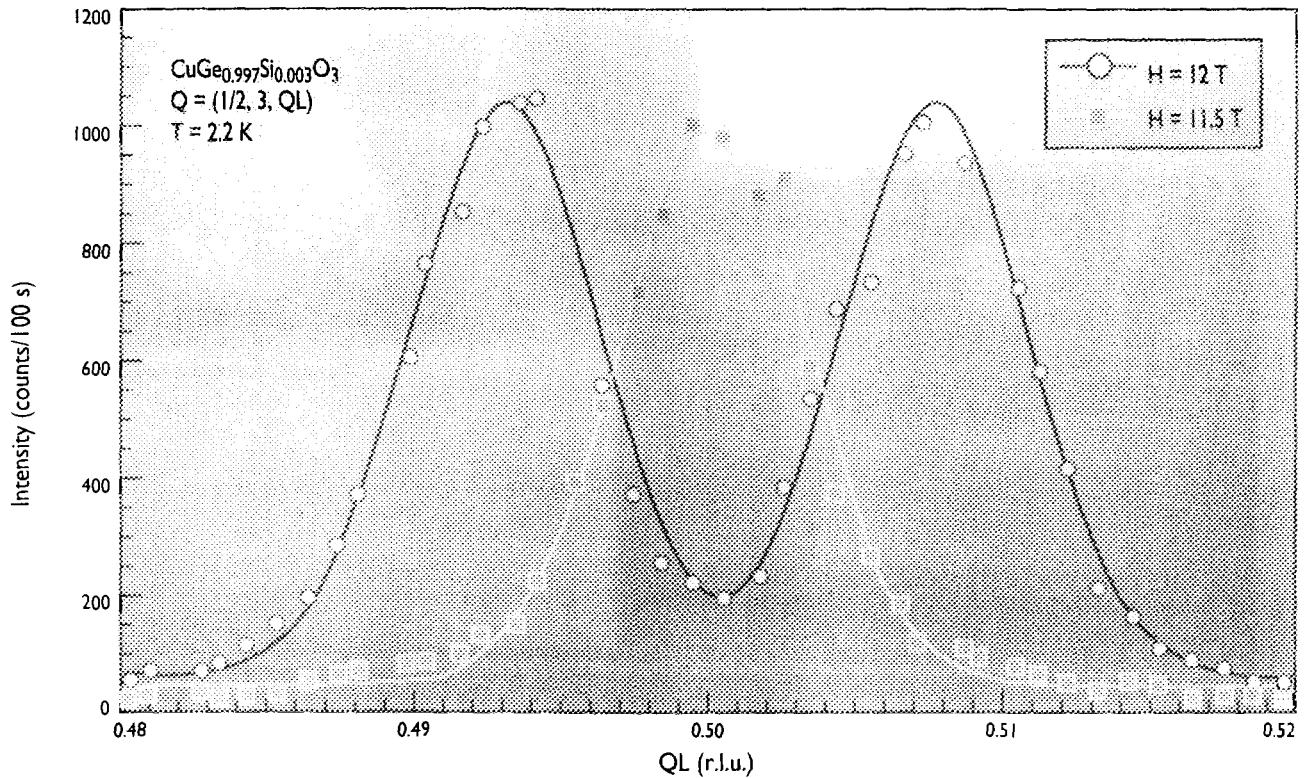
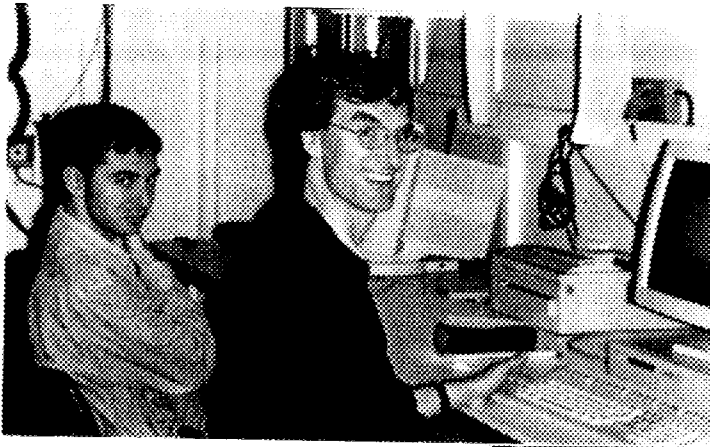
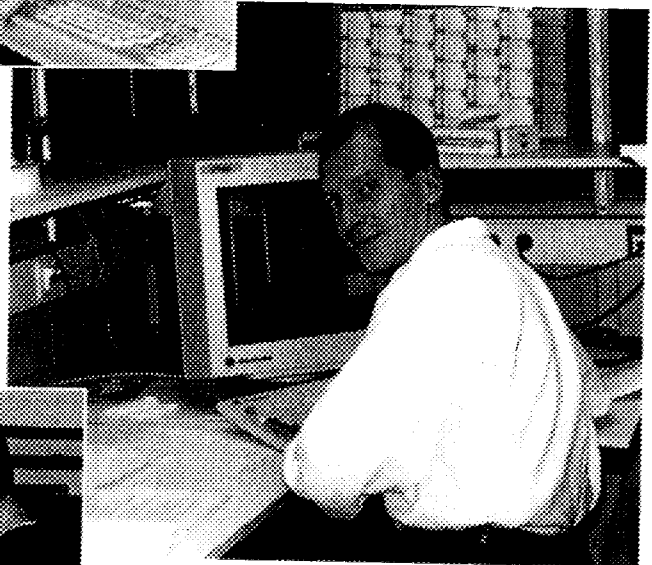


FIGURE 3: Elastic scan across the $(1/2,3,1/2)$ superlattice peak at 11.5 T and 12 T showing the emergence of an incommensurate phase above a critical field $H_C \approx 11.7$ T.

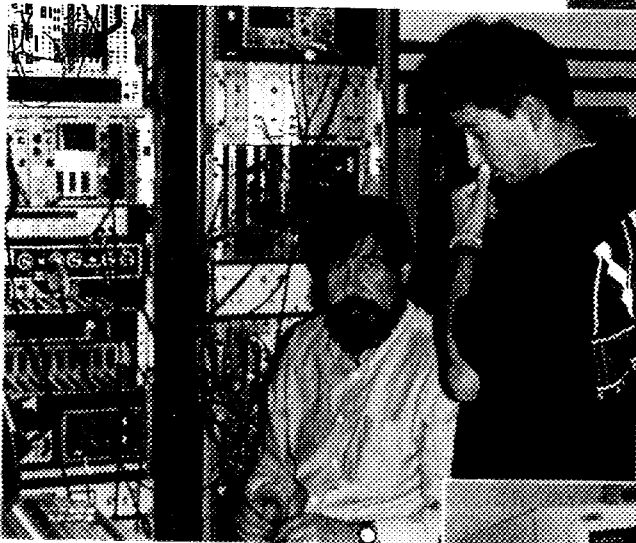
- E. PYTTE, PHYS. REV. B10 (1974) 2309 ■ M.C. CROSS AND D.S. FISHER, PHYS. REV. B19 (1979) 402 ■ M. NISHI, O. FUJITA AND J. AKIMITSU, PHYS. REV. B50 (1994) 6508 ■ L.P. REGNAULT, M. A.N. B. HENNION, G. DHALLENNE AND A. REVCOLEVSKI, PHYS. REV. B53 (1996) 5579 ■ A.I. BUZDIN, M.L. KULIC AND V.V. TUGUSHEV, SOLID STATE COMMUN. 48 (1983) 483 ■ V. KIRYUKIN, B. KEIMER, J.P. HILL AND A. VIGLIANTE, PHYS. REV. LETT. 76 (1996) 4608.



*Happy IN8 users? From right:
Stephen Hayden and Robert Double.*



Alexander Krimmel is running D10.



*Nicolas Stritt (right) is sceptical about
Hans Börner's explanation.*



*Alan Hewat (behind T. Ohta) explains DIA to Richard Dronskowski, Tomoko Ohta
and Michael Scholten (from left).*

WORKSHOPS

2

THESE ARE WORKSHOPS WHERE ILL PLAYED A MAJOR ROLE IN THE ORGANISATION.

NEW OPPORTUNITIES FOR BETTER USER GROUP SOFTWARE (NOBUGS)	ILL	10-12 JAN. 96
SCIENTIFIC PROSPECTS FOR NEUTRON SCATTERING WITH PRESENT AND FUTURE SOURCES	AUTRANS	11-13 JAN. 96
JOURNÉES DES POLYMERS ET DES COLLOÏDES	ILL	13-14 FEB. 96
SCATTERING METHODS APPLIED TO SOFT-CONDENSED MATTER	BOMBANNES	2-8 JAN. 96
INELASTIC AND QUASIELASTIC NEUTRON SCATTERING IN BIOLOGY	ILL	14-15 OCT. 96

WORKSHOPS

ILL/ESRF COMPUTING WORKSHOP: NOBUGS, 10-12 JANUARY 1996, ILL

The joint ILL/ESRF workshop "New Opportunities for Better User Group Software" (NOBUGS) brought together over 60 computing representatives from virtually all of the major neutron and synchrotron sources. There were about 50 formal presentations which covered software for data-analysis, modelling, instrument design and control. Recurrent themes were: tools for modernising old but well tested software, and the difficult choice between developing applications in-house or using commercially available packages and modules.

By pooling ILL and ESRF resources it was possible to provide a broad range of computing platforms for general use. This was especially useful for hands-on practical sessions where almost all participants demonstrated and discussed their latest software projects. These sessions were highly successful and it was agreed that NOBUGS-2 (in about 2

years time) should devote even more time to practical sessions. Information and abstracts from this workshop can be found on <http://www.ill.fr/Computing/computing.html>.



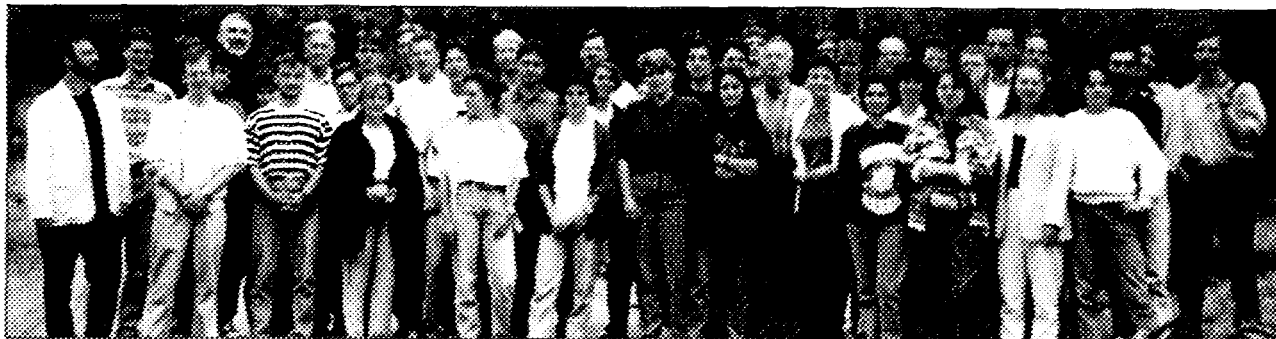
Look - no hands! Romuald Jouffrey demonstrates the ILL data-base browser "touch-base" to Ray Osborn.

THIRD EUROPEAN SUMMER SCHOOL ON "SCATTERING METHODS APPLIED TO SOFT CONDENSED MATTER", 2-8 JUNE 1996, BOMBANNES

The third summer school on "Scattering Methods Applied to Soft Condensed Matter", held from 2 June to 8 June 1996 in Bombannes, Gironde, France, proposed advanced training for young European researchers at post-graduate and post-doctoral level (typically aged between 25 to 35 years) and was based on the positive experience with two events already held in the past (1990 and 1992). It was organised by P. Lindner, ILL, Th. Zemb CEA Saclay, P. Schurtenberger, ETH Zürich, J.S. Pedersen, Risø National Laboratory, O. Glatter, University of Graz.

This series of schools is devoted to a practical approach to neutron, X-ray and light-scattering experiments and aimed to young colloid and polymer scientists using scattering methods in their home laboratory and/or at large scale facilities. The primary objective is to explain the current methodology of static and dynamic techniques and to provide a forum for exchanging experience on complementary methods. A particularly successful feature of the Bombannes schools is the combination of general lectures given by the teachers (morning and late afternoon sessions, 1 - 2 hours each) with the compulsory short oral contributions by students on their own field of activity and discussions in the

evening sessions. Accommodation of all participants on a closed site as well as the possibility of a common sporting activity during the afternoon reduce barriers between teachers and students and help to establish rapidly an open discussion atmosphere. In total about 90 candidates applied for the school. The organising committee run a selection procedure after the deadline for application, according to information given by the applicants (age, academic education, subject of research work, nationality etc.). The aim was to fill the available places for students with an optimal composition with respect to age, scientific subjects and experimental method as well as to encourage participation of students from less favoured regions, women researchers and researchers from industry. Finally, 13 female and 23 male students (of which 31 were PhD-thesis students, 2 beginners of a thesis, 1 research scientist and two post-docs) from 11 different countries attended the school. Lectures were given by 15 recognized European experts in the field of soft-condensed matter research. The financial contributions of the sponsoring institutions (PSI Villigen, Risø National Laboratory, IFF Jülich, CEA Saclay and ILL Grenoble) created the basis necessary for the organisation of the school.



**WORKSHOP IN COLLABORATION
WITH THE EUROPEAN NEUTRON
SCATTERING ASSOCIATION, ENSA,
ON "SCIENTIFIC PROSPECTS FOR NEUTRON
SCATTERING WITH PRESENT AND FUTURE SOURCES",
11-13 JANUARY 1996, AUTRANS**

On January 11-13, 1996, the European Science Foundation (ESF) organised a workshop in Autrans, France, on "Scientific prospects for neutron scattering with present and future sources" with financial support from the EU/TMR programme and assisted by the ILL. About 80 scientists, mainly non-neutron professionals, met to discuss the future of neutron scattering in Europe. The following subjects were covered by the ten working groups: particles and nuclei, magnetism and superconductivity, amorphous materials and liquids, polymers and soft matter, biology, atomic and molecular aspects of new materials, chemical reactions, catalysis and electrochemistry, earth sciences, materials sciences, engineering. The workshop concluded with the reports of the individual group leaders followed by a panel discussion, chaired by H. Curien, former French minister for research and a past ESF president, stimulating a lively discussion. The report of this meeting has been published by the ESF

and is available on the web : on the ESF homepage: <http://www.esf.org>. It contains the individual reports of the ten working groups with an introductory summary.



During the panel discussion, from left: Hubert Curien, Gerry Lander, Reinhard Scherm.

**WORKSHOP ON
"INELASTIC AND QUASIELASTIC
NEUTRON SCATTERING IN BIOLOGY",
14-15 OCTOBER 1996, ILL**

The workshop, financed jointly by the ILL, EMBL and IBS, took place at the ILL on 14-15 October 1996. The organisers were H. Büttner (ILL), S. Cusack (EMBL), M. Ferrand (ILL), P. Langan (ILL) and P. Timmins (ILL). The workshop was attended by 80 people, giving invited talks, short oral contributions and posters within the following topics:

- Presentation of the neutron spectroscopy technique. Other techniques used to probe dynamics of biomolecules: optical spectroscopies, NMR, X-ray diffuse scattering, Mössbauer.



Discussion amongst workshop participants. From left: Ahmed Aamouche, Jozef Ulicny, John Tomkinson.

- Molecular dynamics of small molecules of biological interest, using INS, QENS and/or MD simulations.
- Lipid bilayer dynamics studied by QENS and NMR.
- Water dynamics in hydrogels, polysaccharide gels and on protein surfaces (QENS).
- Contribution of INS, QENS and MD to the understanding of protein dynamics: theoretical aspects and experimental studies.

During this conference the emphasis was placed both on the potentialities of inelastic and quasielastic neutron scattering and on the complementary and competing aspects of other techniques. Hot topics were: the description of protein activity in terms of dynamical features, the use of coherent neutron scattering to sample protein inter-domain motions, the accuracy of data analysis (multiple scattering effects), the increasing role of molecular modelling and molecular dynamics simulations to give a quantitative description of dynamics of biomolecules.

The proceedings will be published in the "Journal of Biomolecular Structure and Dynamics" (Adenine Press).

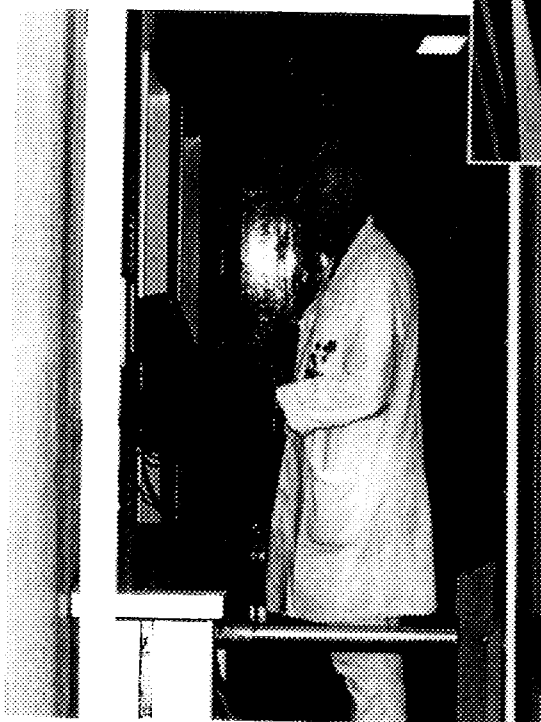
*Michel Ferrand (left) starts up his user
Jean-Marc Zanotti on IN5.*



Pierre Palleau explains his instrument.



*Demonstration of the radioprotection control-system
by Jacques Mari.*



An on-floor discussion of IN22: Louis-Pierre Regnault. IN22 is a new CRG instrument under construction.



NEW DEVELOPMENTS

3

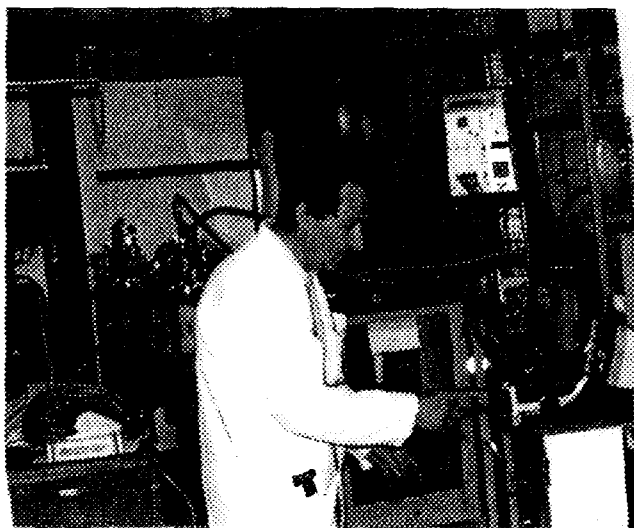
A CONTINUING PROGRAMME OF INSTRUMENT DEVELOPMENT AND TECHNICAL INNOVATION IS AN ESSENTIAL PART OF ILL'S ACTIVITIES AND OF GREAT IMPORTANCE FOR ITS FUTURE HEALTH. THIS DEVELOPMENT PROGRAMME IS WIDE RANGING IN CHARACTER AND IN THIS SECTION WE PRESENT NEWS AND SELECTED HIGHLIGHTS FROM 1996. UP-TO-DATE INFORMATION WILL ALSO BE GIVEN IN THE ILL NEWSLETTER WHICH WILL HENCEFORTH BE PUBLISHED TWICE A YEAR IN DECEMBER AND JUNE.



NEW DEVELOPMENTS

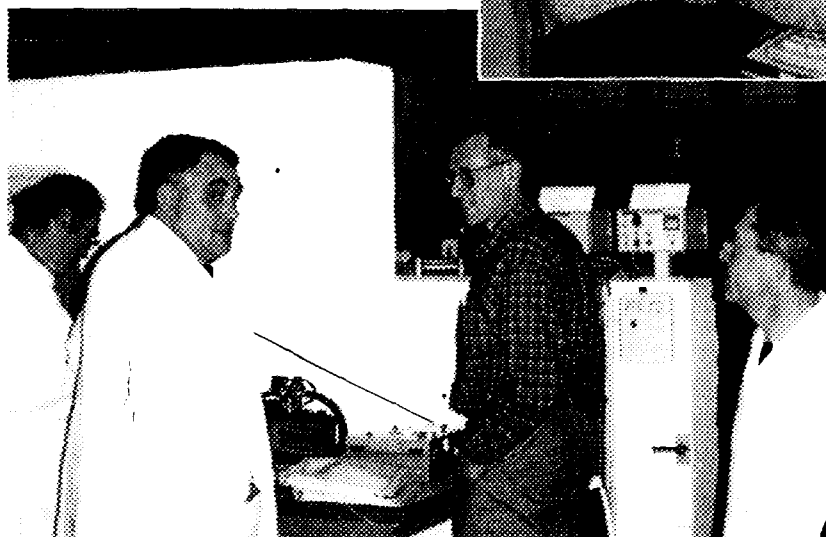
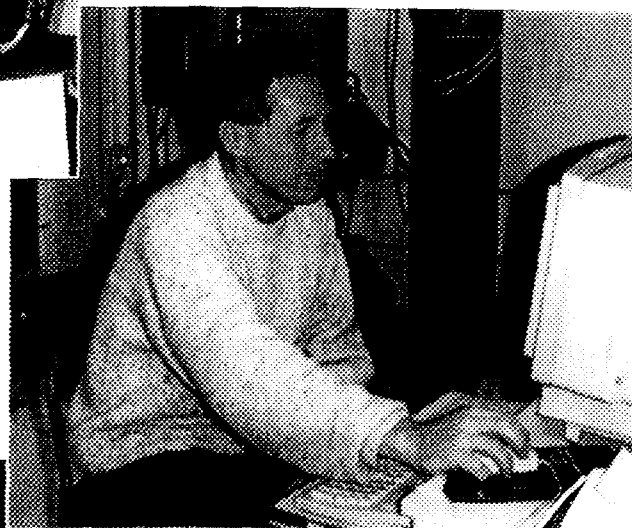
TECHNICAL DEVELOPMENTS

AT THE ILL THERE ARE PERMANENT DEVELOPMENT PROGRAMMES IN A NUMBER OF UNDERLYING TECHNICAL AREAS RELEVANT TO MOST INSTRUMENTS, NAMELY MONITORING, NEUTRON OPTICS, SAMPLE ENVIRONMENT, ELECTRONICS AND DETECTORS. THESE AREAS ARE OF FUNDAMENTAL IMPORTANCE TO ALL NEUTRON APPLICATIONS BECAUSE THEY PROVIDE THE MOST CONSIDERABLE MEANS OF IMPROVING THE PERFORMANCE OF EXISTING TYPES OF INSTRUMENTS, AND ACHIEVING NEW TYPES. EXAMPLES OF PROGRESS AND ACHIEVEMENT FROM THE LAST YEAR ARE GIVEN BELOW.



André Rambaud cures a detector problem.

Jean-Louis Ragazzoni sets up a dilution-fridge experiment.



TASSE starts; from left: Michel Berneron, Pierre Flores, Claude Zeyen, Ariel Brun.



FR9704868

PROPER PHASING IS AN ESSENTIAL CHARACTERISTIC OF THE CHOPPER SYSTEMS USED AT ILL. A WIDE VARIETY OF CHOPPERS AND SELECTORS DIFFERING IN WEIGHT, SPEED AND BEARING TYPES ARE CONTROLLED BY A UNIQUE ELECTRONIC CARD PERFORMING DIGITAL ADAPTATIVE FILTERING.

By the strict application of basic concepts such as synchronous filtering, it has been shown that for each device, it is possible to damp phase oscillations down to the theoretical limits arising from the chopper mechanical characteristics: i.e. between a thousandth and a hundredth of a degree.

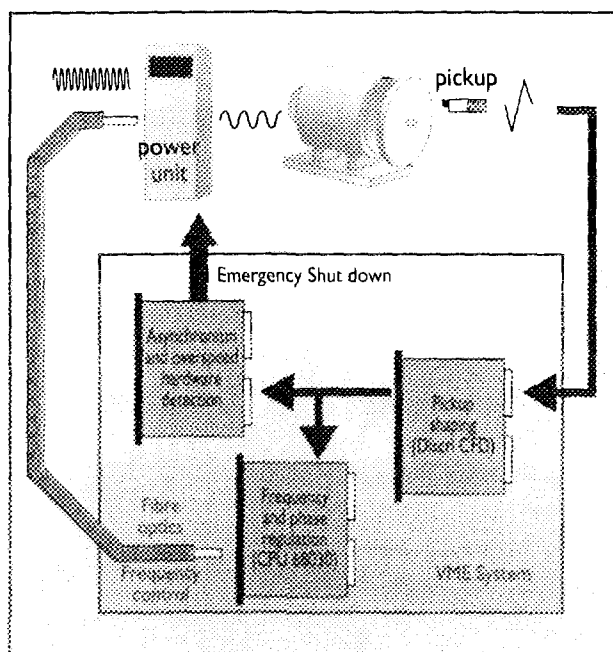


FIGURE 1: The whole chopper control system is composed of a power unit (REFU 317) and controlled by a 68030 processor fitted with frequency and phase meters. The control frequency is sent to the power unit through fiber optics.

Fig. 1 shows the main parts of the regulation system. A magnetic pickup fixed on the motor gives a bipolar signal used for phase and speed control. This signal is shaped through a constant fraction discriminator and passed to a VME CPU board which does the frequency and phase regulation. Before the phasing, the program measures the oscillation period of the rotor and builds the ideal awaited signal. During the phasing, the filter performs the correlation between observed and ideal sinewave. A fine damping of the chopper oscillation is obtained, suppressing the perturbations arising from electronics or oscillation due to the yaw in the magnetic bearings. (Fig. 2). The former figure comes from the tests performed on IN5. The yaw from the magnetic bearing sets the real chopper stability.

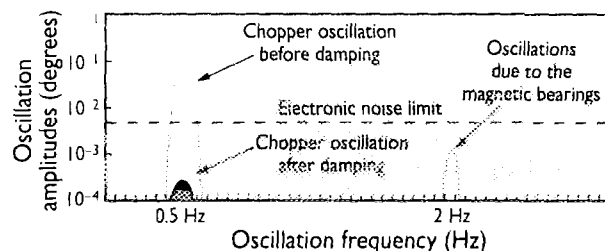


FIGURE 2: The period of the oscillations of the IN5 choppers are around half a Hertz. The damping filters electronic noise and other oscillations due to the magnetic bearings.

Figure 2 shows real-time measurements on the phase of IN5 (magnetic bearings) and IN16 (ball bearings).

The irregular phase distribution of IN5 is due to its magnetic bearings whereas ball bearings flatten the distribution and make it Gaussian (Fig. 3).

Presently, the chopper regulation system has been installed on three instruments (D11, IN5, IN16). It should equip most instruments using choppers and selectors by mid 1997. The boards have been also installed on the MIBEMOL instrument at the Laboratoire Léon Brillouin at Saclay. But the most outstanding application will be the control of the new IN4C experiment, using heavy choppers with speed reaching 30 000 revolutions per minute.

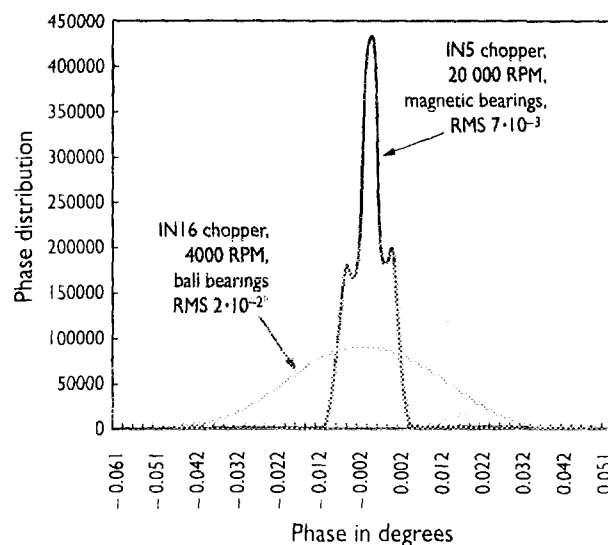


FIGURE 3: The chopper phase is permanently monitored by the VME Board. The curves are those of choppers on IN5 and IN16. They have different shapes depending on the mechanical stability and the bearing type.

SYNTHETIC MOSAIC COPPER MONOCHROMATORS

B. HAMELIN (ILL).



FR9704869

RECENT ADVANCES IN THE PRODUCTION OF MONOCHROMATOR CRYSTALS WITH ANISOTROPIC MOSAICS ARE DESCRIBED.

Neutron beams have to be optimised to deliver a maximum beam-intensity for given resolution conditions. For this reason, mosaic crystal monochromators are normally used in preference to perfect crystals in order to match the incident beam divergence in the scattering plane and obtain adequate integrated intensities. In the plane perpendicular to the scattering plane, however, the crystal mosaic should be small in order to permit efficient focusing of the beam onto the sample being studied. Thus, the creation, in a controlled and reproducible manner, of an anisotropic mosaic in crystals is extremely important for the production of an ideal neutron monochromator. Experience in the production of

mosaic and anisotropic neutron monochromators by the classical method (compressive stress) shows that the process is inefficient in both time and material: a large proportion of the crystals are unusable at the end of the production stage and a significant amount of time is dedicated to testing and characterisation. The idea of building a composite monochromator from thin wafer stacks was originally put forward by Maier-Leibnitz (1967). Essentially there are two approaches which may be followed (Fig. 1). In the first approach the stack is built up from crystalline wafers, each of which has a mosaic close to the global value required for the whole stack.

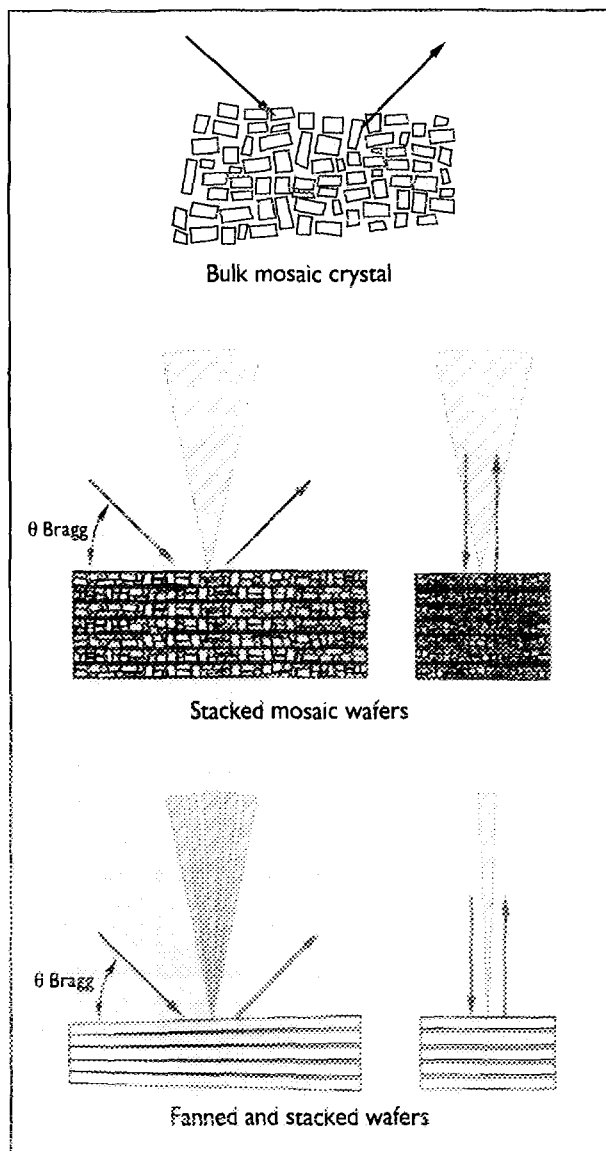


FIGURE 1: Schematic showing the production of a mosaic crystal using wafers. The figures indicate the resulting mosaic parallel and perpendicular to the diffracting plane.

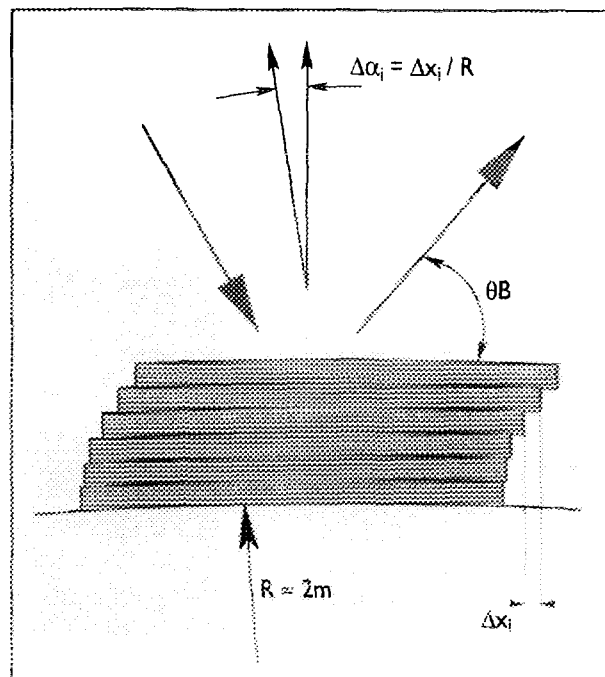


FIGURE 2: The « onion-peel method ».

This method has been developed in several laboratories, in particular for Ge crystals, and involves a plastic deformation process (alternate bending) on each wafer to produce the required mosaic. The new Ge (335) monochromator for D2B was made using this technique (ILL Annual Report 1995). The second method to use is "fanned and stacked wafers" – in which a highly anisotropic mosaic crystal is obtained by stacking nearly perfect crystalline wafers with a controlled misorientation. In a fanned stack monochromator, the global reflectivity distribution is obtained from the contributions of several thin crystalline wafers each with a rather narrow mosaic compared to the composite value but slightly misoriented with respect to the other wafers in the stack.

The shape of the reflectivity curve can be predetermined and moreover, because the initial mosaicity required is small, it is not necessary to use mosaic wafers and hence for each wafer to undergo a long and tedious plastic deformation process. Regardless of the very attractive properties of fanned wafer monochromators, the problem was how to determine, produce and control the required individual misorientation. This problem has been solved by the use of a very simple method, only possible nowadays thanks to modern machining techniques: the "onion-peel" method developed at the ILL. It is based on the following principle (illustrated in Fig. 2): wafers are machined into a given cylindrical (or a spherical) shape. (spark-erosion machine for metallic crystals or lapping in the case of non-conducting crystals). The crystallographic planes are not bent and are not affected by this machining if it is performed correctly. When all the wafers are stacked, the individual misorientation of the wafers is obtained by sliding each one with respect to its neighbour by a distance of a few mm (depending on the cutting radius and the required misorientation). This method works equally well in reflection or transmission geometry. However in order to obtain high performance anisotropic monochromators, a number of parameters (e.g. wafer thickness, intrinsic mosaic, misorientation, etc.) have to be determined both by experiment and numerical simulation. In particular, the asymmetric profile of peak reflectivity due to the absorption process, can be compensated by a well-adapted distribution of individual misorientations.

A copper monochromator prototype has been constructed and tested. The monochromator consisted of an assembly of 5 thin monocrystalline Cu wafers (thickness 1.5 mm) cut to a radius of 2200 mm. The wafers were oriented following a predetermined sequence and then soldered together. Results of measurements on this prototype (in both reflection and transmission geometry) are shown in Fig. 3. Fig. 3a (reflection in Bragg geometry for the horizontal plane as illustrated in Fig. 2) compares the experimental results with the theoretical calculation of diffracted intensity for a wafer assembly and for a bulk Gaussian mosaic crystal (same mosaicity). Fig. 3b shows the measurement of minimum mosaicity also in reflection but in the vertical plane. Comparison of Figs. 3a and b shows that the mosaicity is highly anisotropic with a factor of 3 between the FWHM of the rocking curves measured in the horizontal (scattering plane) and vertical directions.

Fig. 3c shows the maximum mosaicity of the same prototype in a transmission measurement (Laue geometry). Clearly the "onion-peel" technique is very promising for

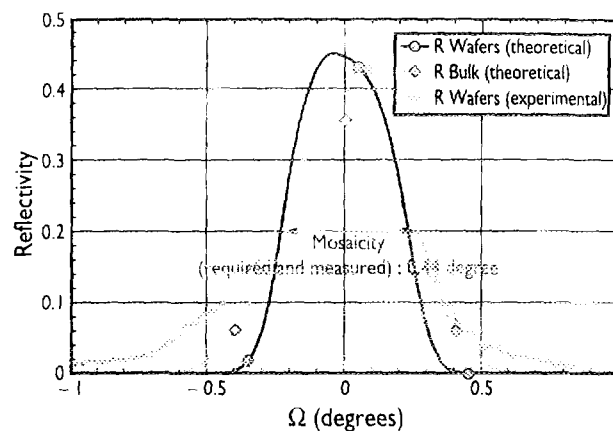


FIGURE 3a: Comparison of experimental results (horizontal plane) with the theoretical calculation for a wafer assembly and for a bulk Gaussian mosaic crystal (same mosaicity).

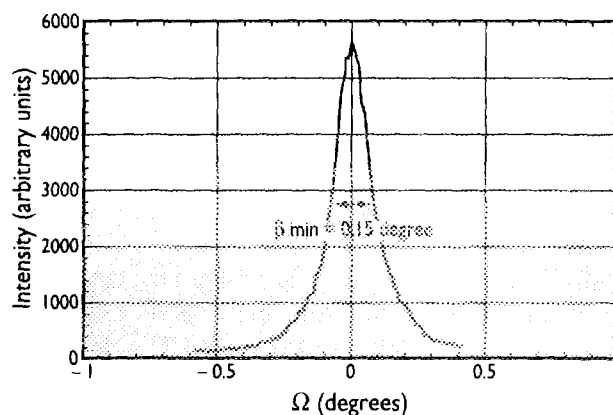


FIGURE 3b: Experimental results (vertical plane).

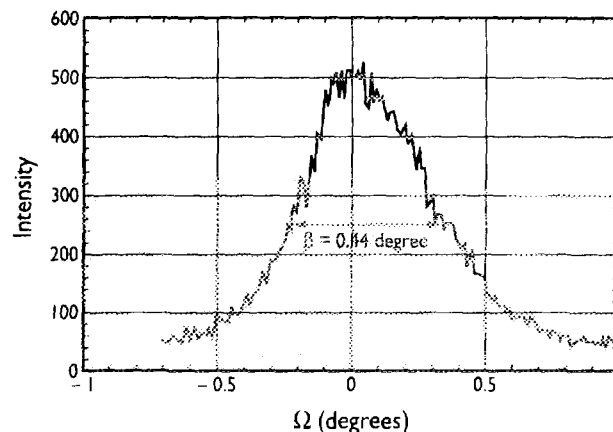


FIGURE 3c: Measurement of maximum mosaicity in transmission (Laue geometry) of the same prototype.

the fabrication of high-performance anisotropic monochromators in which the anisotropy can be tailored to the beam optics.

A HARD X-RAY LABORATORY FOR MONOCHROMATOR CHARACTERISATION

B. HAMÉLIN (ILL).



FR9704870

SINCE THEIR INSTALLATION AT ILL DURING THE 1970'S THE ILL γ -RAY DIFFRACTOMETERS HAVE BEEN INTENSIVELY USED IN THE DEVELOPMENT OF NEUTRON MONOCHROMATORS. HOWEVER, THE AGEING OF THE SOURCES AND NEW DEVELOPMENTS IN HARD X-RAY DIFFRACTOMETRY LEAD TO A DECISION AT THE END OF 1995 TO REPLACE THE EXISTING γ -RAY LABORATORY WITH A HARD X-RAY LABORATORY, BASED ON A 420 KEV GENERATOR, MAKING AVAILABLE IN THE LONG TERM SEVERAL BEAM-LINES FOR RAPID CHARACTERISATION OF MONOCHROMATOR CRYSTALS. THE FACILITY IS NOW INSTALLED AND ITS CHARACTERISTICS AND ADVANTAGES ARE OUTLINED BELOW.

Gamma-ray diffractometry, using the monochromatic radiation ($\Delta\lambda/\lambda \sim 10^{-6}$) from radioactive sources was developed in the 1970's as a means of volume characterisation of single crystals. The method has the advantage that it is only sensitive to the intrinsic mosaic of the crystal and allows volume measurements on samples a few centimetres thick with a resolution of a few seconds of arc. Since their installation at ILL during the 1970's the gamma-ray diffractometers (based on two sources ^{198}Au , $E = 412 \text{ keV}$, $\lambda = 0.03 \text{ \AA}$ and ^{137}Cs , $E = 662 \text{ keV}$, $\lambda = 0.02 \text{ \AA}$) have been well used, however, they do have certain inconveniences related to the weak source flux and the limited beam-dimensions. Typically, collimations of a few seconds of arc are employed leading to a small (or the order of a few mm^2) sample-volume analysed. Thus, analysis of a large crystal requires a series of measurements to be made (in practice a series of rocking curves) each of which can be quite lengthy in time. Furthermore only one set of diffracting planes can be measured at a time. Recently an alternative method was proposed based on a high-energy X-ray generator associated with a commercially available high-resolution two-dimensional detector, which permits the study of the bulk properties of large single crystals with the thickness of several centimetres essentially in real time. The principle of this hard X-ray diffractometer is illustrated in Fig. 1a.

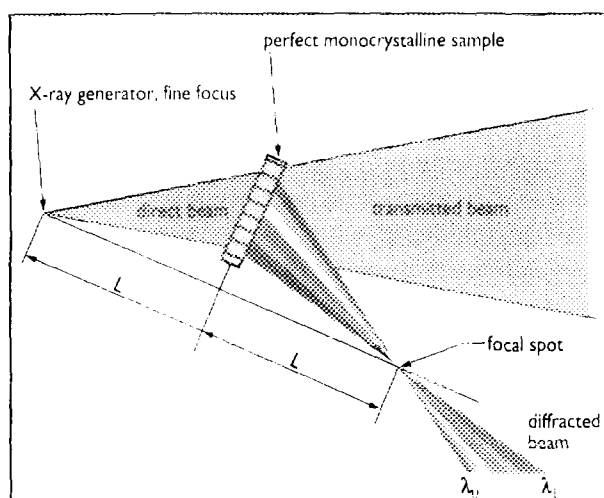


FIGURE 1a: Schematic of white-beam focalisation principle.

A crystalline sample is illuminated by a white, divergent X-ray beam emitted from a point source. The beam does not need to be collimated and can cover several cm^2 of the sample.

A family of lattice planes will select from the beam a band of wavelengths which satisfy the Bragg condition and the resulting diffracted beams are redirected to a focus which is symmetric to the source with respect to the normal to the diffracting planes. This focusing only occurs in one direction so in reality one obtains a focal line normal to the plane of Fig. 1a.

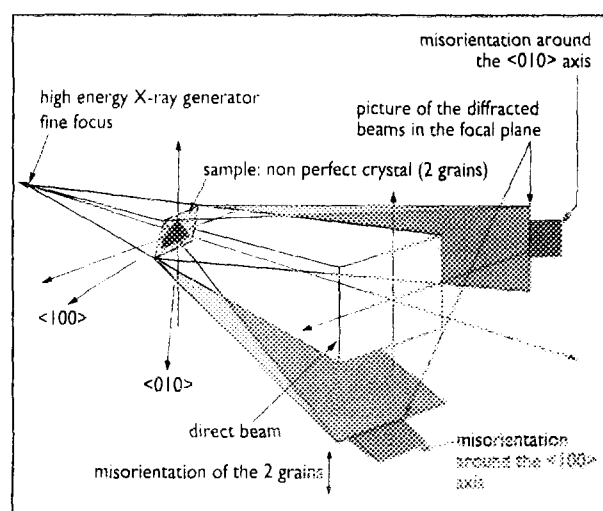


FIGURE 1b: Two-dimensional focalisation of hard X-rays with detection of parasitic subgrain.

In general, due to the extended wavelength range in the incident bremsstrahlung radiation a number of reflections come into play simultaneously as illustrated schematically in Fig. 1b. Furthermore, due to the high incident-energy used, the Bragg angles are small so that the different reflection lines are located close to the transmitted beam in a focal plane which is essentially normal to the beam direction. Thus various reflection lines can be measured simultaneously in a two-dimensional detector placed at this focal plane.

The analysis of these reflection lines reveals a great deal of information concerning the sample crystal. For an infinitely thin perfect crystal the width of the lines is determined by the dimension of the source (or the detector resolution if it is worse). A broadening of the diffraction lines is then directly related to the mosaic of the crystal which can be measured with a resolution of a few arc seconds for source – detector distances of several metres. Furthermore, precise localisation of the diffraction lines in the focal plane can be used to determine the orientation of the crystal and parasitic grains if they exist.

In summary this elegant method allows a complete structural analysis of a large crystal sample in a “one shot” measurement that requires only a few seconds of beam time! The first beam-line in the new hard X-ray laboratory has been equipped with a 250 mm diameter X-ray image intensifier (Thomson) coupled to a cooled CCD camera. The excellent spatial resolution of the camera, ≈ 0.2 mm, associated with long sample-detector distances (up to 3.7 m), allows angular resolutions of the order of 10 seconds of arc or less to be obtained.

A diffraction image obtained from a 5 second exposure of a 4 cm thick nearly perfect silicon crystal is shown in Fig. 2. The maximum intensity in the focal line is 34200 counts compared to 250 in the background indicating the high sensitivity of the instrument. Furthermore, the orientation of the crystal can be determined directly as can the perfection (the inset shows the intensity variation across a focal line which is a direct measurement of the crystal mosaic). A similar bulk measurement for one reflection only using a γ -ray diffractometer would have required more than 4 hours! The hard X-ray diffractometer is a unique tool for the rapid and precise characterisation of single crystals where it has

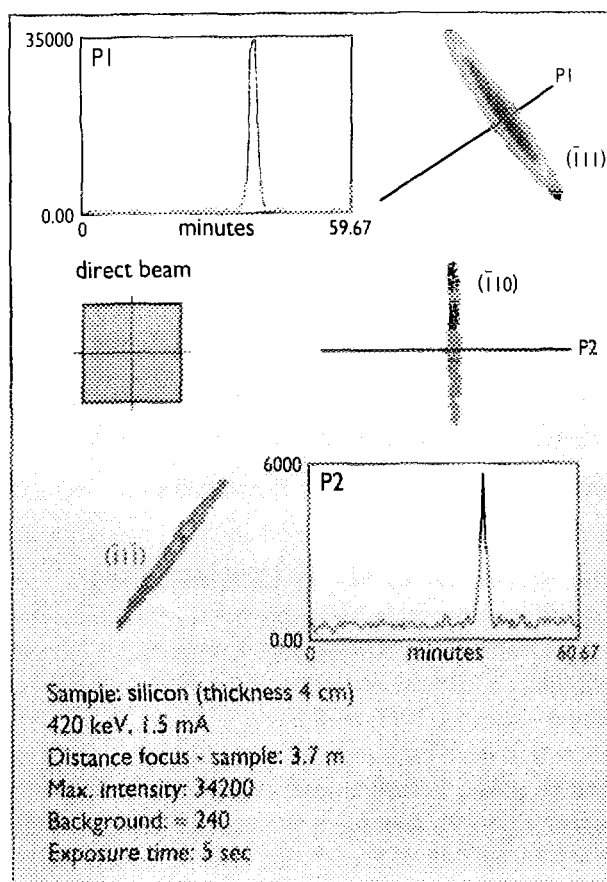


FIGURE 2: First hard X-ray analysis with nearly perfect silicon crystal sample

proved itself to be superior to the existing γ -ray diffractometers. It will be an essential element in the production of new composite monochromators based on thin wafers where rapid characterisation is a necessity.

Further applications of the technique to topography, texture analysis etc. are in progress.



FR9704871

IT IS NOW 20 YEARS SINCE SUPERMIRRORS WERE FIRST USED AS A NEUTRON OPTICAL ELEMENT. SINCE THEN THE FIELD OF MULTILAYER NEUTRON-OPTICS HAS MATURED WITH MULTILAYERS FINDING THEIR WAY TO APPLICATION IN MANY NEUTRON SCATTERING INSTRUMENTS. HOWEVER, THERE IS STILL ROOM FOR PROGRESS IN TERMS OF MULTILAYER QUALITY, PERFORMANCE AND APPLICATION. ALONG WITH WORK ON MULTILAYERS FOR NEUTRON POLARISATION WE HAVE OPTIMISED Ni/Ti SUPERMIRRORS. WE PRESENT THE STATE-OF-THE-ART Ni/Ti SUPERMIRROR PERFORMANCE AND THE RESULTS OBTAINED IN TWO NEUTRON-OPTICS APPLICATIONS OF Ni/Ti MULTILAYERS.

OPTIMISATION OF Ni/Ti SUPERMIRRORS

Significant progress in Ni/Ti supermirror manufacturing has been obtained by moving from the evaporation process originally used towards sputter deposition techniques. Sputter deposited Ni/Ti multilayers with $m = \theta_c / \theta_c^{Ni} = 2$, where θ_c is the critical angle of reflection, are now used in neutron guides in several institutes. However, for Ni/Ti supermirrors with more layers as required in order to obtain $m = 3$ the build-up of stress in the layers is detrimental to the reflectivity. By adding N_2 to the Ar gas used for sputtering this problem can be overcome. Fig. 1 shows the neutron reflectivity curve for a supermirror deposited with this method on a Si substrate. The reflectivity is above 90% at $m = 2$ and above 85% at $m = 3$. A roughness of 8 Å for all Ni/Ti interfaces was used together with the bulk scattering-length densities of Ni and Ti in the simulation shown in Fig. 1. Furthermore, magnetometer measurements show this type of supermirror to be non-magnetic, which is an advantage in some applications with polarised neutrons.

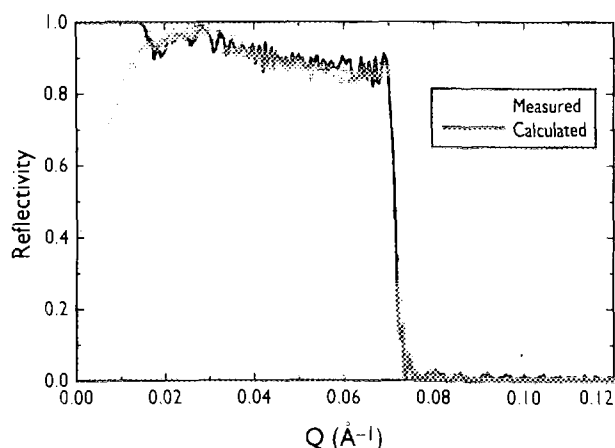


FIGURE 1: Measured and calculated neutron reflectivity as a function of momentum transfer Q for a $m = 3$ supermirror with 400 Ni/Ti layers deposited on a Si substrate. The measurement was carried out at the Riso TAS8 reflectometer using a wavelength of 4.75 Å. The calculation was performed using the design structure of the supermirror.

A DOUBLE REFLECTION MONOCHROMATOR WITH LARGE BAND-WIDTH

In collaboration with the Research Reactor Institute, Kyoto University, and the Faculty of Integrated Arts and Sciences

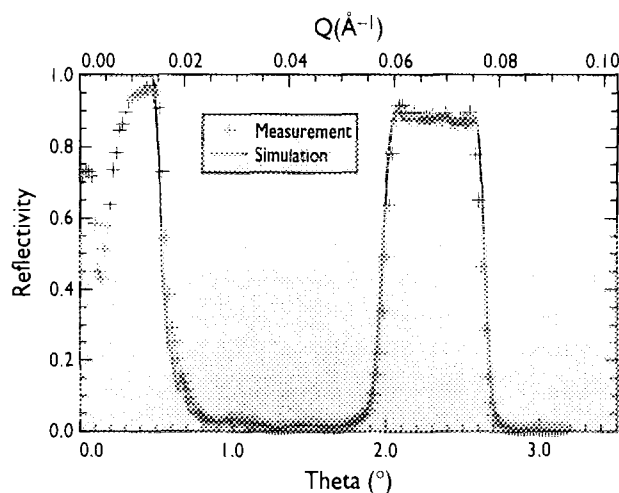


FIGURE 2: Reflectivity profile measured from a large wavelength band monochromator consisting of 438 layers of Ni and Ti.

at Hiroshima University a double-reflection multilayer monochromator was developed for the neutron spin-echo instrument at Jaeri. Such a monochromator has the interesting property that both the wavelength resolution and the outgoing beam collimation are determined by the $\Delta d/d$ of the multilayer sequence

$$2\Delta\lambda/\lambda = 2\Delta\theta/\theta = \Delta d/d$$

The monochromator was designed to reflect a $\Delta\lambda/\lambda$ of 15% after two reflections at 5.9 Å which implies a $\Delta d/d$ for the multilayer of 30%. This design specification was achieved using 438 layers of Ni and Ti sputtered onto polished silicon substrates. Fig. 2 shows the reflectivity curve measured from one of the 12 elements of the monochromator showing a reflectivity of 90% over a band width of 30%. Flux test on the instrument after installation of the monochromator revealed a four-fold increase in flux at the sample position compared to the previous configuration.

A LONG WAVELENGTH CUT-OFF FILTER FOR PF1

In some experiments the presence of long-wavelength neutrons is undesired. That is the case for an experiment with polarised neutrons currently being carried out at the PF1 instrument, where the polarisation of the neutrons with

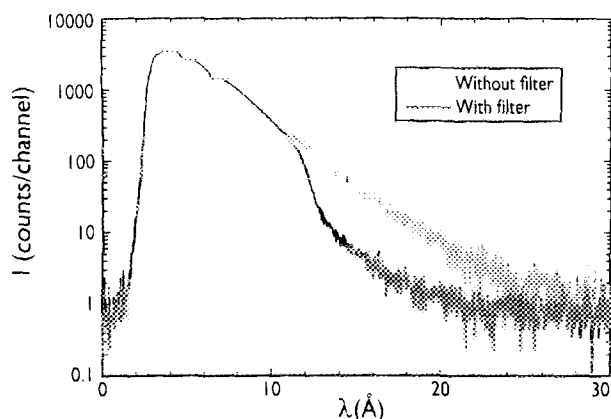


FIGURE 3: Time-of-flight spectrum of the PFI direct beam and the same beam with a stacked supermirror filter described in the text. Background is not subtracted.

$\lambda \geq 13 \text{ \AA}$ was difficult to establish. The neutron beam cross-section is $55 \text{ (W)} \times 45 \text{ (H)} \text{ mm}^2$. A supermirror can be used to separate neutrons with $\lambda \geq 13 \text{ \AA}$ from the main beam, but if one would use a single $m = 3$ supermirror it would have to be approximately 750 mm long, which is rather impractical to manufacture and to use. Instead we deposited $m = 3$ supermirrors on 118 Si wafers with dimensions $0.525 \times 8 \times 48 \text{ mm}^3$ and stacked the mirrors on top of each other giving a device just 8 mm long.

In the resulting filter each mirror intercepts just the part of the beam corresponding to the thickness of one Si wafer. All transmitted neutrons pass through 8 mm of Si and the $m = 3$ Ni/Ti supermirror.

Fig. 3 shows a TOF spectrum of the PFI beam with and without the filter in place. The intensity of neutrons with

$\lambda \geq 13 \text{ \AA}$ is reduced a factor of 10, while the intensity loss from absorption is about 10%. The filter was also turned to intercept the beam at a larger angle with a resulting cut-off at wavelengths smaller than 13 Å.

CONCLUSION

Problems of stress in Ni/Ti supermirrors can be overcome by using reactive sputtering. $m = 3$ aperiodic multilayers and supermirrors of high quality can be produced and applied in numerous neutron-beam defining devices, such as broadband monochromators and long wavelength cut-off filters. Several ILL projects for 1997 should profit from the results shown here.



Discussion amongst some members of the multilayer team; from left: Christine Chevalier, Peter Hoghoj and Werner Graf.

TWO-DIMENSIONAL MICROSTRIP DETECTOR FOR NEUTRONS

A. OED (ILL).



FR9704872

BECAUSE OF THEIR ROBUST DESIGN, GAS MICROSTRIP DETECTORS, WHICH WERE DEVELOPED AT ILL, CAN BE ASSEMBLED RELATIVELY QUICKLY, PROVIDED THE PREFABRICATED COMPONENTS ARE AVAILABLE. AT THE BEGINNING OF 1996, ORDERS WERE RECEIVED FOR THE CONSTRUCTION OF THREE TWO-DIMENSIONAL NEUTRON DETECTORS. BASED ON THE PREPARATORY WORK OF TWO THESIS STUDENTS, J. ASSAF AND N. VELLETTAZ, IT WAS POSSIBLE TO COMMISSION TWO OF THESE DETECTORS IN NOVEMBER. THE REMAINING ONE IS DUE TO BE DELIVERED IN JANUARY 1997. ONE OF THESE DETECTORS WILL THEN BE AVAILABLE TO ANYONE INTERESTED IN USING IT TO CARRY OUT TEST MEASUREMENTS ON HIS OR HER INSTRUMENT.

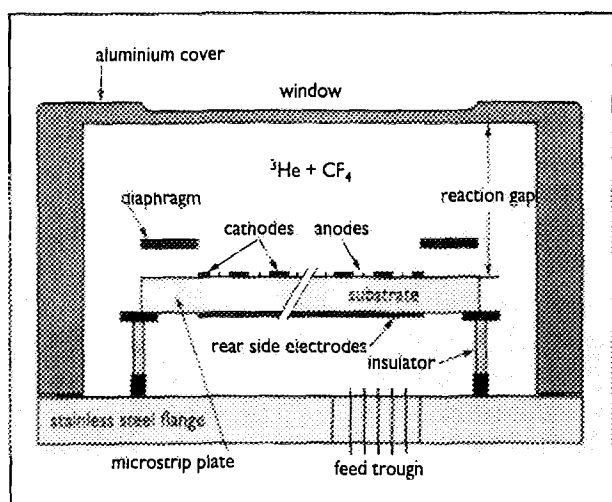


FIGURE 1: Schematic arrangement of the two-dimensional microstrip gas chamber. Reaction gap: 10 to 80 mm; max. pressure: 10 bar.

A schematic diagram of the mechanical construction of this detector is given in Fig. 1. This arrangement corresponds to an axial ionisation chamber with the electric field parallel to the direction of the incident radiation. The anode, which in the ionisation chamber is just a simple metal plate, is replaced by a semiconducting glass-plate (SCHOTT type S 8900) on which very thin metallic strips are engraved by means of the photolithographic technique.

A schematic design of this structure is shown in Fig. 2. This microstrip (MS) plate amplifier works in the following way: the potential of the thin strips is positive relative to the adjacent strips. An electron produced anywhere in the gas volume which reaches the electric field between the strips of the MS plate, will drift along the field lines towards the positive conductor strip, where it will experience an avalanche amplification at sufficiently high field strength.

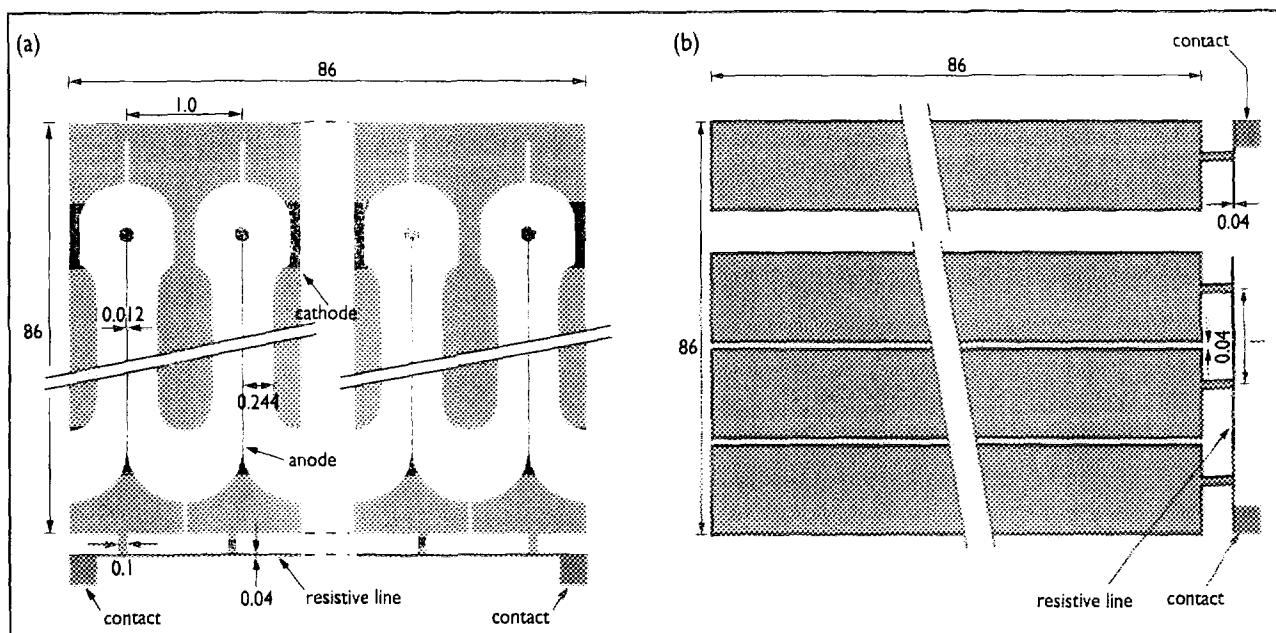


FIGURE 2: Schematic design of the microstrip a) front side and b) rear side structure made on the substrate SCHOTT S8900 with chromium layers 1500 Å in thickness. The anodes and also the rear side electrodes are interconnected with a 0.04 mm strip in order to determine the position by charge division of the signals. The anodes have a width of 0.012 mm, the cathodes 0.5 mm and the pitch of the front and the rear structures is 1 mm. Indicated dimensions are in mm.

This signal determines one coordinate of the position. Across the uncovered surface of the substrate, the ions of the avalanche also induce a signal on the rear layer of the plate. If this rear coating is divided into strips which are perpendicular to the conductor strips of the front side, the second coordinate can be determined.

On the MS plates of these detectors, all anode strips and all rear-side electrodes are interconnected by each other with a small resistive strip in order to achieve localisation by charge division of the signals. This technique was chosen because, on the one hand, it is well-suited to the relatively slow rise time of neutron signals and, on the other hand, only five amplifiers are needed to determine the coordinates of the neutron reaction, which considerably reduces the cost of the detector. This type of read-out does, nevertheless, produce a small image distortion of about 2% at the edges. The complete data-acquisition system comprises 5 ADCs and a multiparameter card from FAST, which plugs into a PC.

The data acquisition can be controlled directly by the instrument's electronics or the data system delivers a signal to the instrument at the end of each measurement operation.

The neutron images appear live on the PC screen.

Fig. 3 shows a diffraction image of a stainless steel rod with a diameter of 2 mm recorded with monochromatic neutrons of 2.6 Å. The diffraction pattern shows the partial recrystallisation within the material.

The spatial resolution of the detector (FWHM) is 1.4 mm in both directions. The size of the sensitive area is 86 mm × 86 mm. The housing is designed to withstand a maximum pressure of 10 bar. The depth of the detection gap can be set to between 10 mm and 80 mm. At a ^3He pressure of 3 bar, the minimum detection probability for thermal neutrons (1.8 Å) is therefore 33% and the maximum probability 96%.

A smaller detection gap depth is applied for measurements for which the parallax error must be as small as possible.

At present, the detector's counting capacity of more than 100 kHz cannot be fully exploited.

It is limited to approximately 30 kHz due to the data transmission line and to the position calculation. Efforts have already begun to eliminate this bottleneck.

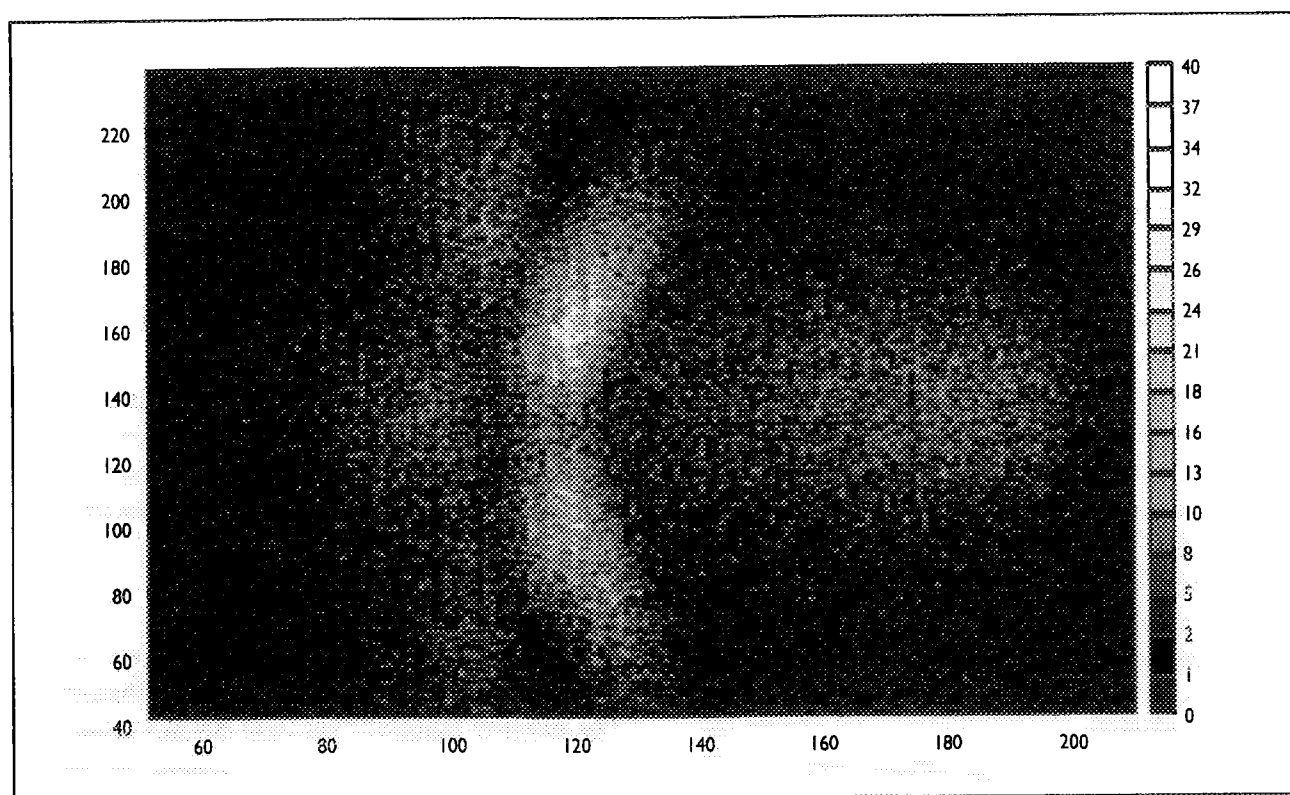


FIGURE 3: Powder-diffraction image of a stainless steel rod of 2 mm in diameter; measured with a two-dimensional microstrip gas chamber. Exposure time: 215 s; sensitive area: 86 mm × 86 mm; spatial resolution (FWHM): 1.4 mm in both directions.

NEW EXPERIMENTAL TECHNIQUES

HERE WE ARE CONCERNED WITH NOVEL TECHNIQUES WHICH MAY EVOLVE INTO NEW INSTRUMENTS OR GIVE SIGNIFICANT UPGRADES TO EXISTING INSTRUMENTS. THERE ARE CURRENTLY THREE SUCH DEVELOPMENT PROJECTS: QUASI-LAUE DIFFRACTION FOR PROTEIN CRYSTALS USING AN IMAGE PLATE DETECTOR (LADI: SEE 1995 ANNUAL REPORT AND ILL NEWSLETTER DECEMBER 1996), THE ^3He NEUTRON-SPIN FILTER FOR WIDE-BAND NEUTRON POLARISATION, AND THERMAL NEUTRON SPIN-AXIS SPINECHO-SPECTROSCOPY. BRIEF REPORTS ON PROGRESS ON THE LAST TWO ITEMS ARE GIVEN BELOW. IN ADDITION, THE TECHNIQUE OF SPHERICAL NEUTRON POLARIMETRY HAS BEEN FURTHER DEVELOPED WITH THE SUCCESSFUL COMMISSIONING OF CRYOPAD II ON IN20 (SEE ILL NEWSLETTER DECEMBER 1996). IT IS NOW POSSIBLE TO MEASURE THE THREE COMPONENTS OF THE SCATTERED POLARISATION VECTOR FOR ANY PARTICULAR INCIDENT POLARISATION WITH NO SPECIAL DIFFICULTY AT A RESOLUTION OF 3° .



FR9704873

THE ^3He NEUTRON-SPIN FILTER AT ILL

F. TASSET, W. HEIL, H. HUMBLLOT, E. LELIÈVRE-BERNA AND T. ROBERTS (ILL).

NEUTRON-SPIN FILTERS (NSF) USING GASEOUS POLARISED ^3He HAVE LONG BEEN RECOGNISED AS OF ENORMOUS POTENTIAL VALUE IN MANY POLARISED NEUTRON-SCATTERING APPLICATIONS AND, ACCORDINGLY, ILL STARTED A DEVELOPMENT PROGRAMME SOME YEARS AGO. THIS REPORT GIVES AN ACCOUNT OF THE PRESENT STATUS OF THE PROJECT.

Let us first briefly recall the reasons why the ^3He NSF is desirable as a generic polarisation tool:

- being a pure transmission device, NSF naturally decouples the neutron spin selection from other optical functions. Designing polarised instruments will be simplified by removing geometrical constraints due to Bragg optics or beam deviation in the polariser. Angular acceptance and energy band pass are much widened, making polarisation handling much more compatible with focusing geometry and time-of-flight techniques.

- gaseous NSF naturally achieves well defined transmission functions. Quantitative interpretation of intensity measurements in polarisation-analysis mode will be much easier. Very homogeneous polarisation will be achieved for large beam areas, a feature which is particularly attractive for precision measurements.

- fully polarised ^3He is an ideally effective NSF with 50% transmission of the incident unpolarised beam. Already with half ^3He polarisation it seems that NSF can improve some existing instruments when polarising crystals or supermirrors are not good reflectors. To understand this point, it is important to define and calculate a relevant quality factor in order to properly handle the tradeoff in between neutron polarisation and neutron flux. As an example, we have been able to show that the inverse standard deviation in the measurement of small magnetic structure-factors is proportional to P/T , P being the neutron-beam polarisation and T the filter transmission.

At optimum gas-pressure this quantity turns out to be linearly proportional to the ^3He polarisation in such a way that we can say that present NSFs are only a factor 2 away from the ideal. Improving the ^3He polarisation remains most important for polarisation analysis work where this quality factor is generally squared.

Finally, practical aspects like portability, refilling period and ease of use are very important issues which should be properly addressed at this stage of the development. It is the object of this paper to summarise the present situation.

^3He NSF: A SHORT REVIEW OF PREVIOUS WORK

Only those neutrons with spins antiparallel to the ^3He spin may be absorbed via the resonance reaction $^3\text{He}(n,p)t$ [2]. The attractive features of polarised ^3He as a broad band polariser for thermal and epithermal neutrons was recognised long ago [3]. Following an initial pulsed-beam demonstration at Los Alamos [4], we used the same simple technique (spin transfer from a thick vapour of optically pumped Rb into a dense buffer of ^3He gas) to produce a first target of polarised ^3He at ILL. On the D3 polarised neutron facility, we could clearly see the different transmission for the two possible neutron spin-states but the ^3He polarisation remained low, less than 10% [5].

This somewhat modest result forced us to envisage [6] a more sophisticated polarisation technique based on direct optical pumping of a metastable excited state of ^3He [7].

The excited state being obtained in a discharge at low gas-pressure, a subsequent compression process is necessary.

Rapid progress was made in that direction at Mainz University in the group of E. Otten and W. Heil who managed to obtain 50% polarisation in a dense ^3He gas target installed on a polarised electron beam. A so-called Toepler mercury compressor was used, not desirable on a neutron beam-tube. Since then it has been replaced by a fully non-magnetic mechanical compressor made of titanium and glass. Also, it was realised that metallic coating could improve drastically the ^3He relaxation rates in the high-pressure target. All this made possible the production of long-life detachable neutron-spin filters inflated at several atmospheres which were successfully tested on the Mainz Triga reactor.

THE ILL ^3He -COW AND DETACHABLE NSF

With the help of the EC-HCM programme, ILL embarked 3 years ago on a collaboration with Mainz University and the ENS Paris in order to duplicate the ^3He polarisation and compression system being developed in Mainz. In 2.5 years, H. Humblot completed a new system (^3He -COW) which was commissioned in July 1996 at Mainz with performance meeting expectations, that is 50% ^3He polarisation at 3.5 bars with a potential production of 1/2 mole per day. The system was transported safely to Grenoble where it is now installed in a dedicated laboratory.

A remote type of operation based on relaxation times longer than 100 hours has been demonstrated at Mainz and we envisage the same at ILL.

In order to keep the ^3He polarisation close to 50% on the average, we plan to refill the NSF with fresh gas every day. Knowing that the optimum NSF transmission requires an amount of gas per unit surface of the neutron beam of the order of $10^{-3}/\lambda$ [mole $\text{\AA}^{-1} \text{cm}^{-2}$] it appears that the ^3He -COW can potentially supply several instruments and developments are being made along this line. This seems ideally suited for a large installation hosting many instruments.

H4 BEAM ARRANGEMENT

The first tests of polarised cells produced by the ^3He -COW were made in November 96. In view of planned polarisation-analysis measurements at 0.33 \AA of parity and time violation in the vicinity of the π -wave resonance of ^{139}La , (a collaboration with A. Serebrov and A. Petukhov from Gatchina, Russia), these tests were made on the D3 polarised neutron-diffractometer down to 0.25 \AA wavelength. The experimental beam-arrangement used is shown in Fig. 1. The incident neutron beam H4 coming from the hot source of the ILL-HFR has a 0.5° horizontal divergence, it is monochromatised and deflected using the 200 polarising reflection of a CoFe monochromator crystal (0.5° mosaic spread). A special Soller collimator (0.5° divergence) is inserted on the monochromatic beam. The beam is filtered for $\lambda/2$ com-

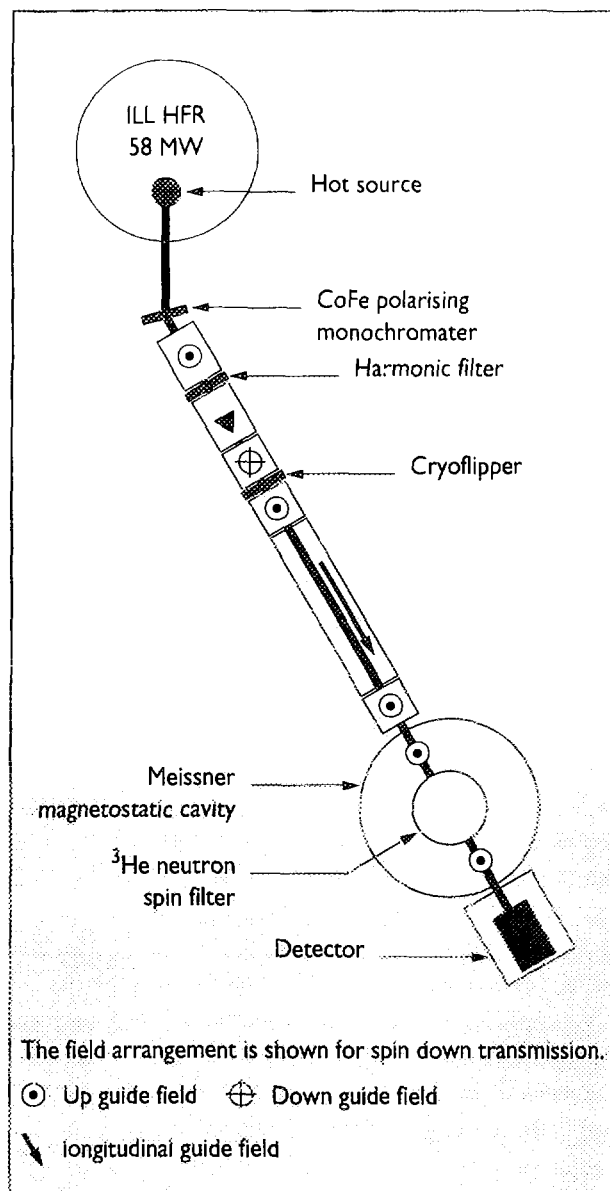


FIGURE 1: The ILL-H4 D3/Cryopad polarised neutron beam arrangement for the ^3He -NSF polarisation measurement.

ponent using resonant filters available on D3. The regular Cryoflipper is used to reverse at will the neutron-beam polarisation relative to the guide-field. A 1.4 meter long gap is provided at the sample axis in order to host the Gatchina polarimeter during the ^{139}La measurement. During this test, it is simply bridged with a 100 G longitudinal guide field from a solenoid. Finally the neutron beam enters the Cryopad-II nutator which rotates the polarisation into the vertical direction before it crosses the ^3He cell installed in the sample chamber. A 10 G vertical field has been trapped inside the cylindrical Cryopad's Meissner shields as a guide for the ^3He and the neutron polarisation. Depending on the Cryoflipper state, essentially pure "up" or "down" neutrons are crossing the ^3He cell. Downstream to Cryopad, the usual D3 detector is used which is connected to appropriate scalars and records the transmitted intensity as a function of the incident neutron spin state. The complete arrangement can rotate around the primary monochromator axis in order to adjust the neutron wavelength.

³He NSF : INITIAL POLARISATION AND LIFE-TIME MEASUREMENT

The ³He cell used for the tests was a 9 cm inner diameter spherical cell of 382 cm³ equipped with a radial refilling appendage comprising a valve and a connection flange. Made of uncoated "Iron Free Supremax glass", it had shown a relaxation time of 40 hours at the ³He -COW filling-station prior to the measurement. Connected to the high-pressure end of the running compressor, the cell was inflated with polarised ³He gas up to 2.5 bars in approximately 3 hours. Optical measurement indicated a 52% ³He polarisation. Then it was detached and moved into a specially built transportation Helmholtz-coil powered by a small battery. The transportation coil was able to maintain a small homogeneous magnetic guide-field on the cell during the time it was carried from the ³He -COW laboratory up to the D3 instrument in the ILL reactor hall. A total time of 12 minutes was needed to transfer the cell at the end of which the Helmholtz-coils were swiftly presented at the bottom of Cryopad II and the ³He cell raised in the sample chamber up to the beam axis.

A beam of polarised neutrons at 0.84 Å wavelength was transmitted through the sphere at the equator, the filling appendage being at the pole, out of the way. The counting rate was high and remained compatible with the detector dead-time calibration only after reduction of the diameter of the beam down to 1 cm. The magnetic state of the D3 cryoflipper being reversed every second, we could evaluate immediately the flipping ratio by looking at the detector ratemeter. It was low, due to a coil being accidentally reversed in the 1.4 m gap solenoid producing a large depolarisation. As a consequence, data are missing during the first six hours of the run. Later, having realised and corrected this trivial mistake, we recovered a good neutron-beam polarisation and could collect valuable flipping ratios every 1/2 hour for more than a day. Then, we depolarised the cell by exposition to a small permanent magnet and recorded the unpolarised cell-transmission and later the empty-cell transmission (94%).

Using the measured absorption coefficient T_0 for the unpolarised ³He gas buffer and assuming the incident neutron-beam polarisation to be $P_n = 98.4\%$ (value from a prior calibration with a CoFe test crystal), we can use the experimental flipping ratio in order to extract the ³He polarisation:

$$P_{3He} = \frac{\log(1 + P_n - R + P_n R) - \log(-1 + P_n + R + P_n R)}{2 \log T_0}$$

The values are shown in Fig. 2 with crosses, they are very precise due to the high counts of highly polarised neutrons. The polarisation decay obtained during the first 10 hours (23/11/96, 2:00-12:00) fits extremely well with an exponential curve $P = P_0 \exp(-t/\tau)$ indicating $\tau = 15.49 \pm 0.01$ h. In the course of the relaxation measurement, we found it useful to estimate the losses due to the loading process and experimented at the three special points marked by arrows

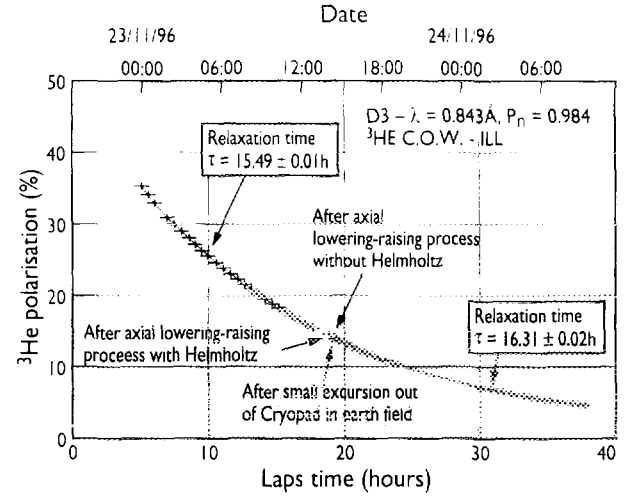


FIGURE 2: The ³He polarisation measurements as deduced from the polarised neutron experimental flipping-ratios. The wavelength used is 0.843 Å. The statistical error is too small for being visible but it does not take into account the uncertainty in the incident beam polarisation coming from prior calibration. The two exponential decay curves are obtained from least square fitting of the corresponding data taken with slightly different magnetic configurations.

and comments on the curve. The cell was moved back and forth from the Cryopad sample chamber to the Helmholtz coil in conditions comparable to the initial load. The losses were judged undetectable. After moving out in the earth-field for 5 or 6 seconds and back into Cryopad, we measured the remaining part of the relaxation curve. Such a drastic manipulation results in only 3% loss of polarisation. A large ferromagnetic stand placed at the bottom of Cryopad, gave little change in the relaxation rate. Qualitatively, we find our system quite insensitive to the details of the magnetic environment outside Cryopad and not critically sensitive to the loading process.

DEPENDENCE OF FLIPPING RATIO ON WAVELENGTH

At the early stage of our relaxation measurement, (after solving the magnetic guide-field problem), we measured the wavelength dependence of the flipping ratio down to 0.33 Å to check the $1/\nu$ dependence of the absorption cross-section. The measurements are shown in Fig. 3 together with values calculated using the following formula:

$$R = \frac{1 - P_{n,\lambda} \tanh(P_{3He} A(\lambda))}{1 + P_{n,\lambda} \tanh(P_{3He} A(\lambda))}$$

$$A(\lambda) = \frac{\lambda}{\lambda_0} \log T_0$$

$$P_{3He} = P_{3He} \exp(-t/\tau)$$

The neutron beam polarisation $P_{n,\lambda}$ being taken from our previous CoFe calibration, τ from the relaxation measurement and T_0 from the absorption measurement done at $\lambda_0 = 0.843$ Å we obtain the best fit when the ³He initial polarisation is taken as 49%.

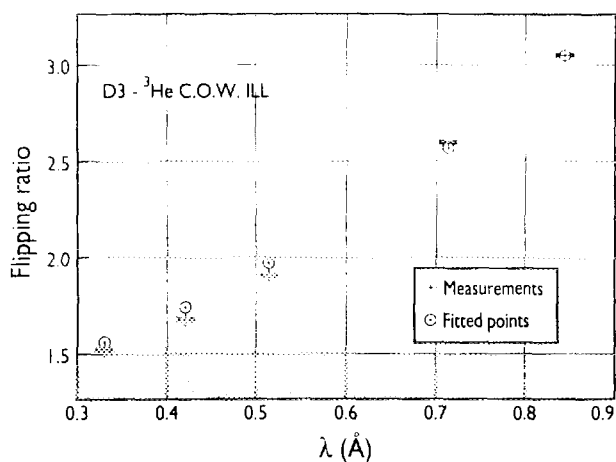


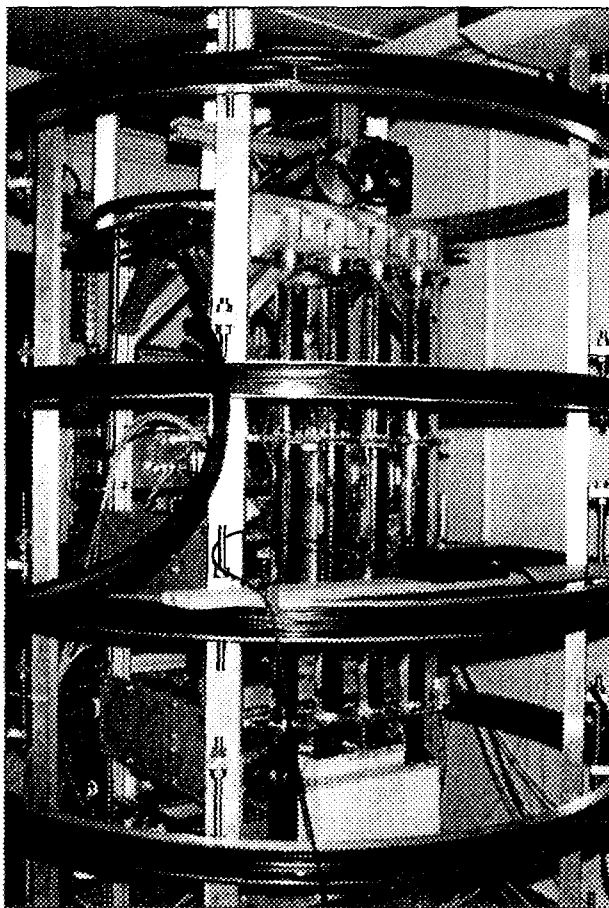
FIGURE 3: The short wavelength experimental flipping-ratios (including errors) are compared with the calculated values using a $1/v$ dependence of the ^3He absorption cross-section and prior calibration of the neutron-beam polarisation.

CONCLUSIONS

Important practical progress has been made during the last few years at Mainz University concerning the production of polarised ^3He gas through optical pumping at room temperature. Large quantities at 50% polarisation can now be compressed up to several bars and stored in removable glass-containers with good lifetimes and such a system is now installed at ILL. By inserting such pre-polarised closed containers on a beam, passive, room temperature gaseous neutron-spin filtering can readily be accomplished, although further development of optimised magnetostatic cavities for mounting the filters on the instruments is required.

The ^3He -NSF performance will increase greatly if 70% nuclear-spin polarisation of the ^3He gas in the required pressure range can be achieved (this was the declared aim from the early stages of this project). In the meantime it turns out that the step from 50% to 70% will be the result of many

small, but in their entirety, important improvements of the existing set-up. This includes a better adaptation of the light source (laser) to the Doppler-broadened resonance line, a reduction of the still moderate polarisation losses during compression and, concerning the storage of the polarised ^3He -gas, glass containers which show long wall-relaxation times in a more reliable and reproducible way.



The ^3He COW set-up.

-
- F. TASSET AND E. RESSOUCHE, NIM A 359 (1995) 537 ■ L. PASSEL AND R.J. SCHERMER, P-HYS. REV. 150 (1966) 146
 - H. POSTMA, POLARISED NEUTRONS ON POLARISED TARGETS, IN 3RD INT. SYMP. ON POL. PHENOMENA IN NUCLEAR REACTIONS, MADISON (1970) ■ K.P. COULTER ET AL., NUCL. INST. METH. A 288 (1990) 463 ■ F. TASSET ET AL., PHYSICA B 180 & 181 (1992) 896 ■ F. TASSET, PHYSICA B 213 & 214 (1995) 935 ■ F.D. COLEGROVE ET AL., PHYS. REV. 132(6) (1963) 2561
 - P.J. NACHER ET AL., J. PHYS. LETTRES 43 (1982) L525 ■ G. ECKERT ET AL., NUCL. INST. METH. A320 (1992) 53
 - M. MEYERHOF ET AL., PHYSICS LETTERS B 327 (1994) 201 ■ W. HEIL ET AL., PHYSICS LETTERS A 201(4) (1995) 337
 - J. BECKER ET AL., JOURNAL OF NEUTRON RESEARCH 5(2) (1996) 1 ■ R. SURKAU ET AL., NIM A (IN PRESS).

THREE-AXIS SPIN-ECHO SPECTROSCOPY (TASSE)

■ C. M. E. ZEYEN AND T. MAY (ILL).



FR9704874

THE FIRST TEST OF THE SPIN-ECHO OPTION FOR THREE-AXIS SPECTROSCOPY BASED ON SUPERCONDUCTING PRECESSION COILS WAS SUCCESSFULLY COMPLETED IN NOVEMBER.

The Three-Axis Spectrometer Spin-Echo (TASSE) option based on superconducting precession coils was tested on IN20 in November. The superconducting Optimised Field Shape (OFS) [1] coils were designed with the following, to some extent contradictory aims:

1) Provide sufficient field-strength to yield very significantly improved energy resolution for thermal neutrons ($\int |B| d\ell$ magnetic induction line integral of 1,5 Tesla-meter).

2) Very homogeneous line integrals for significantly divergent beams (better neutron economy).

3) Extremely low stray-field patterns to allow for extensive variation of scattering angles without retuning of the echo. An analytical optimisation of the field homogeneity had led us to the concept of OFS [1]. Excellent results with this optimisation principle had previously been obtained on both SANS spin-echo spectrometers [2] and thermal neutron three-axis-spectrometers with spin-echo (TASSE) [3,4].

During November the TASSE option was successfully tested with 15 meV neutrons and the IN20 Heusler polariser/analyser systems. IN20 TASSE could be used for a real experiment during the last 4 days of the allocated time, namely for the study of the very slow dynamics of the strain-mediated phase-transition in KDCO_3 .

The same system was first studied using the PONTA TASSE in Japan. The present IN20 TASSE experiment confirmed the PONTA [5] results but with a Fourier time extended by an order of magnitude (from 0.15 to 1.6 nanosec).

In conclusion and after the first neutron beam time, the IN20 TASSE option improved the energy resolution by several orders of magnitude. One problem was caused by the relatively strong vertical guide-fields used around the monochromator and analyser housings. These fields interfered with the cylinder symmetry OFS fields leading to significant depolarisation. Because the spiral correction coils can only correct for cylinder symmetry inhomogeneities, those resulting from the IN20 guide fields could not be corrected.

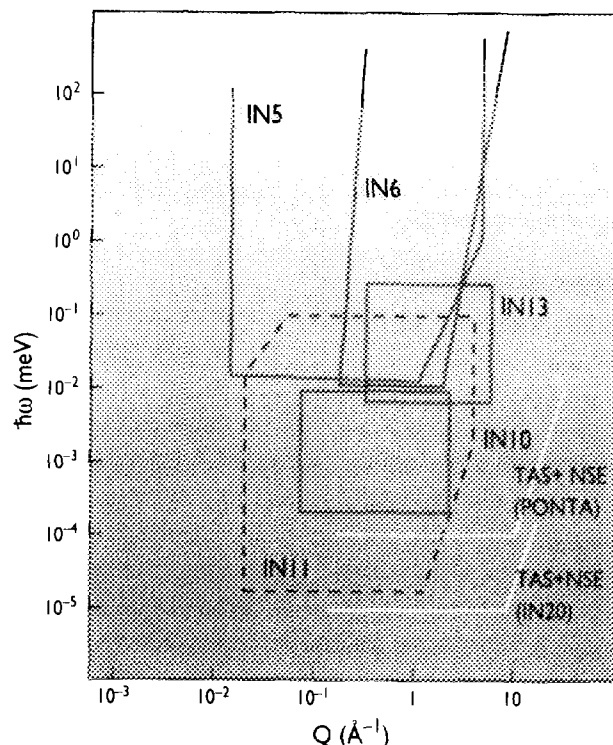


FIGURE 1: Comparison of the energy-range as a function of momentum transfer Q , for various spectrometers: time-of-flight (IN5, IN6), backscattering (IN10, IN13), and neutron spin-echo (IN11 and TASSE).

As a result the resolution performance had to be limited to 40% of the nominal performance (Fourier time ≈ 1.6 nanoseconds instead of the 4 nanoseconds achievable with 2.4 \AA neutrons. At 20 \AA this would correspond to a Fourier time of 4 microseconds). For comparison to other spectrometers, see Fig. 1.

We are in the process, in collaboration with the IN20 physicists, to modify the guide fields to a spin-echo compatible geometry.

In parallel, gradient coils which will allow to use TASSE for high-resolution phonon spectroscopy, including focusing to dispersive branches, are under construction and will be tested during 1997 both in Japan and at the ILL.

-
- C.M.E. ZEYEN AND P.C. REM. MEAS. SCIEN. & TECHN. 7, NR. 5 (1996) 782 ■ T. TAKEDA, S. KOMURA, S. SETO, M. NAGAI, H. KOBAYASHI, E. YOKOI, T. EBISAWA, S. TASAKI, C.M.E. ZEYEN, Y. ITO, H. YOSHIZAWA, NUCL. INST. & METH. IN PHYS. RES. A364 (1995) 186 ■ C.M.E. ZEYEN, K. KAKURAI, J. NEUTRON RESEARCH 4 (1996) 241 ■ C.M.E. ZEYEN, K. KAKURAI, M. NISHI, K. NAKAJIMA, T. SAKAGUCHI, Y. KAWAMURA, S. WATANABE, M. BERNERON, K. SASAKI, Y. ENDOH, NEUTRON NEWS (IN PRESS) ■ K. KAKURAI, T. SAKAGUCHI, M. NISHI, C.M.E. ZEYEN, S. KASHIDA, Y. YAMADA, PHYSICAL REVIEW B53 (1996) R5974

INSTRUMENT UPGRADES

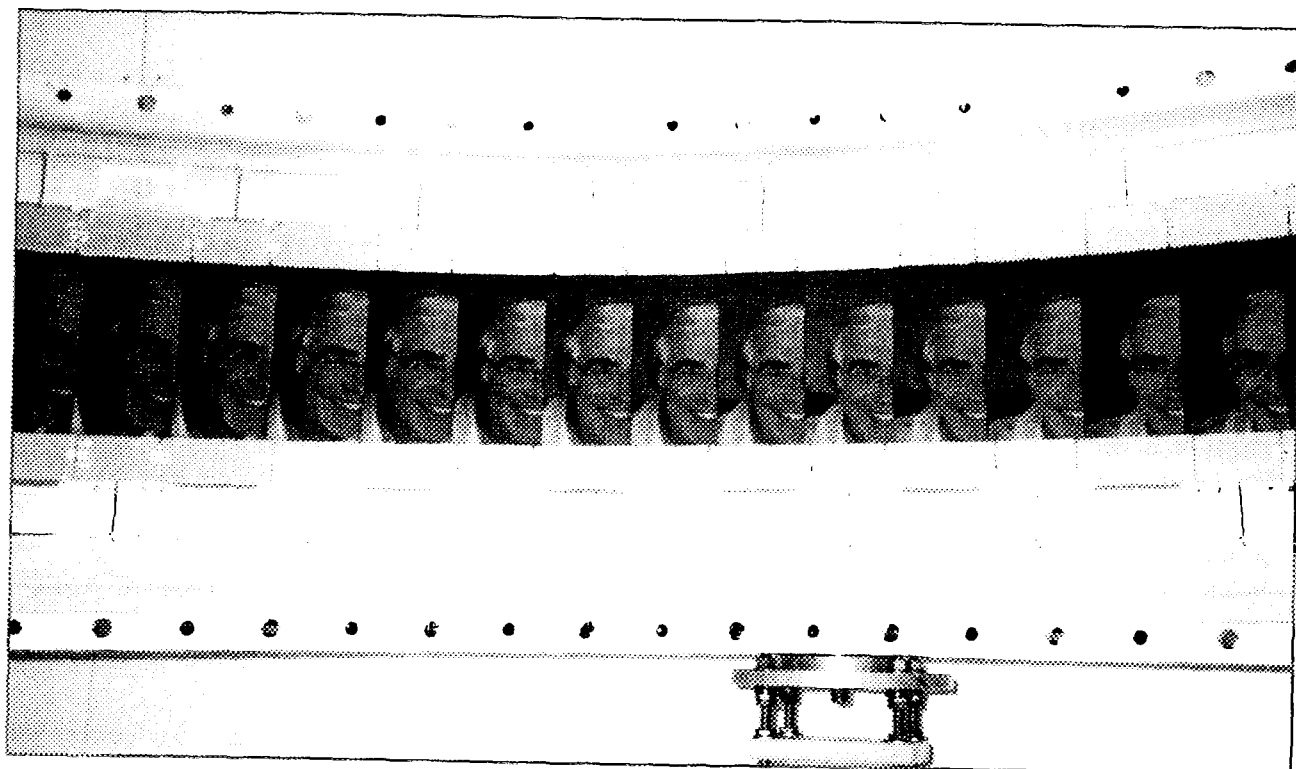
PROGRESSIVE MINOR IMPROVEMENTS ARE A CONTINUING PROCESS ON NEARLY ALL INSTRUMENTS BUT IT IS ESSENTIAL, WHERE IT IS TECHNICALLY AND FINANCIALLY FEASIBLE, TO SEEK SIGNIFICANT UPGRADES IN INSTRUMENT PERFORMANCE BY MORE MAJOR MODIFICATIONS WHICH MAY OFTEN BE BASED ON THE RESULTS OF TECHNICAL DEVELOPMENTS (E.G. IN DETECTORS OR TUBES OR OPTICS) OF THE TYPES MENTIONED EARLIER. A NUMBER OF PROJECTS ARE IN PROGRESS, SOME JUST BEGINNING AND SOME NEARING COMPLETION.

Two projects are nearing completion: the high-resolution double-crystal γ -spectrometer GAMS5 and the high-intensity powder-diffractometer D20. The construction of GAMS 5 is finished and commissioning is in progress.

It is planned that GAMS5 will be available for users in the second half of 1997 when it will complement GAMS4 on the PN3 instrument and replace GAMS2/3 which will then be taken out of service. With these two high-quality spectrometers, PN3 will be well placed to continue the development of high-resolution γ -ray spectroscopy and the new

technique of γ -ray induced Doppler broadening (GRID: see 1995 Annual Report).

The D20 diffractometer is ready and waiting for its 160°, 1600 cell banana detector based on microstrip technology. The construction of the detector is now complete and it will have its first neutron tests early in 1997. First user experiments are expected in the third cycle of 1997 and in anticipation of the operation of D20, D1B will become a CRG instrument in 1997 (see also ILL Newsletter, December 1996).



Pierre Chieux poses for the D20 detector.

NEW INSTRUMENT UPGRADE PROGRAMME

At the end of 1995 a programme of instrument upgrades was approved by the Steering Committee, which began in 1996 and is scheduled for completion by the year 2000. The instruments D17, D16, IN5, D4 and IN8 will all be upgraded to give major improvements in performance - up to about an order of magnitude in each case.

In the first place the highly curved neutron guides H17 (currently having D17 on the end position) and H18 (not used) will be straightened so as to transmit a wider spectrum of neutrons at shorter wavelengths. D17 will be relocated onto H18 and D16, which currently shares the guide H16 with IN5, will move to the end position on H17. This leaves IN5 to view the whole of H16 instead of 1/3 as at present. The work of rebuilding the guides has begun. It will take place in the two winter shutdowns 96/97 and 97/98, the first devoted to rebuilding the shielding and the second to installation of the guides.

The instrument D17 will then be rebuilt in 1998 as a dedicated reflectometer with a much more suitable neutron spectrum from the straightened guide and it will utilise a focusing

guide to enhance the flux on the specimen. The low Q diffractometer D16 will have a new focusing monochromator and later a new detector. IN5 will have a new and improved chopper system and a focusing guide to take advantage of the availability of the whole 30 cm height of the guide. For these three instruments 1996 has been devoted mainly to design work.

The D4 diffractometer will have a new detector based on microstrip technology with ten times the solid angle of the current instrument; construction of a prototype detector has started. The triple-axis spectrometer IN8 will be reconfigured to reduce distances, it will have a monochromator with horizontal as well as vertical focusing and eventually a new beam tube to take full advantage of the horizontal focusing possibilities. Design work was started in 1996. Overall, this is a very cost-effective programme which will provide major improvements to ILL's instrument profile at a total capital investment cost of less than 30 MF, but its completion within the planned time-scale will depend on the actual availability of funds.

REFLECTOMETRY ON D17

R. CUBITT (ILL).



FR9704875

AS PART OF THE PACKAGE OF INSTRUMENT UPGRADES PLANNED OVER THE NEXT FEW YEARS (SEE ABOVE), D17 WILL BE RESITED ON A STRAIGHTENED COLD NEUTRON-GUIDE AND CONVERTED INTO A DEDICATED AND VERSATILE REFLECTOMETER. IN THE MEANTIME, IN ORDER FOR ILL TO BECOME AS FULLY INVOLVED AS POSSIBLE IN THIS GROWING AREA OF ACTIVITY, THE CURRENT D17 HAS BEEN OPTIMISED FOR REFLECTOMETRY.

D17 has been used primarily for reflectometry since the third cycle of 1996 except for a few high-field small-angle scattering experiments which cannot be done elsewhere. This situation will continue until December 1997 when the rebuilding will start, with the new instrument scheduled to be ready for testing about a year later. The changes made to D17 and its current performance as a reflectometer are outlined below. The modifications to the old SANS instrument have been fairly modest but already render D17 a world class reflectometer. A precision goniometer and translation drive have been added to the sample position, which coupled with scanning software in MAD allow for easy sample alignment. Collimation is achieved by two vertical-axis rotating slit devices separated by 2.5 m which can position to a precision of 10 microns. Wavelength resolution is still defined by either the 5 or 10% $d\lambda/\lambda$ velocity selectors.

The addition of a 2 m collimating guide between the two slits resulted in considerable gains in intensity over the old vacuum-tube. Only the horizontal guide faces reflect neutrons so the angular resolution in the horizontal reflection plane remains unaffected. The full beam-height at the sample position is 80 mm. Polarised neutrons are also available with spin-flipping. A polarisation analyser for the reflected beam will be installed by February 1997.

The most efficient method of obtaining a reflectivity profile is to keep the relative angular resolution constant i.e. open both collimating slits in proportion to the reflection angle. Thus both Q-resolution and sample illumination are constant with the added bonus of the incoming intensity rising as Q^2 . The incoming flux for the set of slit positions is calibrated using plastic attenuators to avoid detector

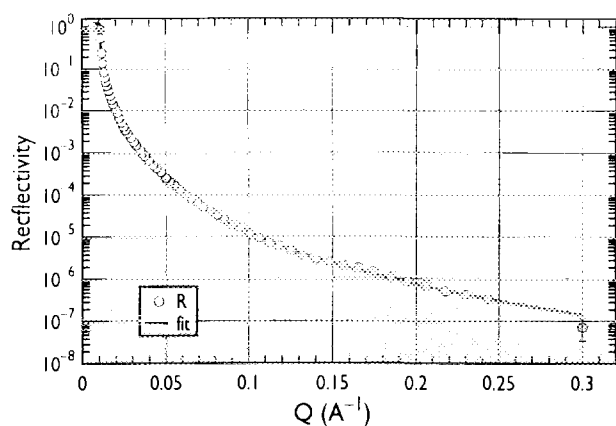


FIGURE 1: Reflectivity profile from a silicon air boundary. The fit is for a pure silicon substrate, a 50 Å oxide layer with a 30 Å interface region and an oxide surface roughness of 3 Å.

saturation. This can be done in half an hour and used for all reflectivity profiles with the same illumination and resolution conditions.

The data in Fig. 1 show a reflectivity profile from a large, polished silicon disc. An area of 80 × 60 mm was illuminated throughout the entire scan with a relative Q-resolution of 11%. The 10% velocity selector was employed with

11 Å neutrons. The scan was completed in only two and a half hours, including the calibration run. In this case the point separation was double the theoretical Q-resolution. The data demonstrate that for this counting period a practical lower limit of measurable reflectivity is just above 10^{-7} . This was mainly limited by background from the sample holder which is presently being re-designed.

A more practical example is shown in Fig. 2. Neutron reflectivity was used to study the swelling and solvent content of an electroactive metallopolymer spin coated onto a gold electrode in a D_2O/H_2O mix [R. Hillman and R. Wilson (Leicester and ILL)]. Despite the strong background scattering from the liquid, the reflectivity was measured down to 10^{-6} and the entire profile was recorded in under 2.5 hours. The new instrument will have a guide height four times greater than at present but will have focusing sections such that the beam height at the sample position will remain at 80 mm. The guide will also be straightened enabling transmission of peak flux neutrons from the cold source. These two additions will result in approximately 7.5 times more flux than at present, when working in the monochromating mode at the same resolution.

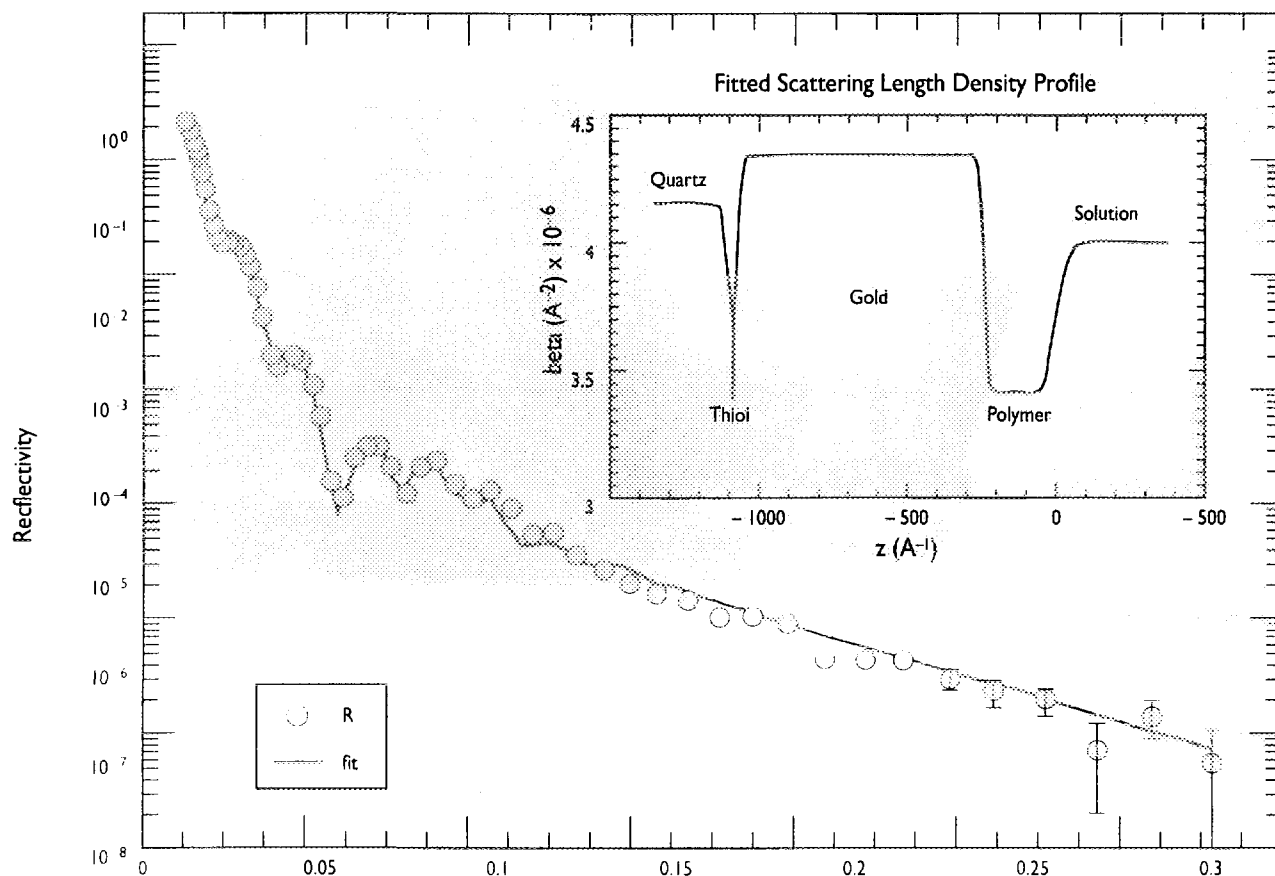
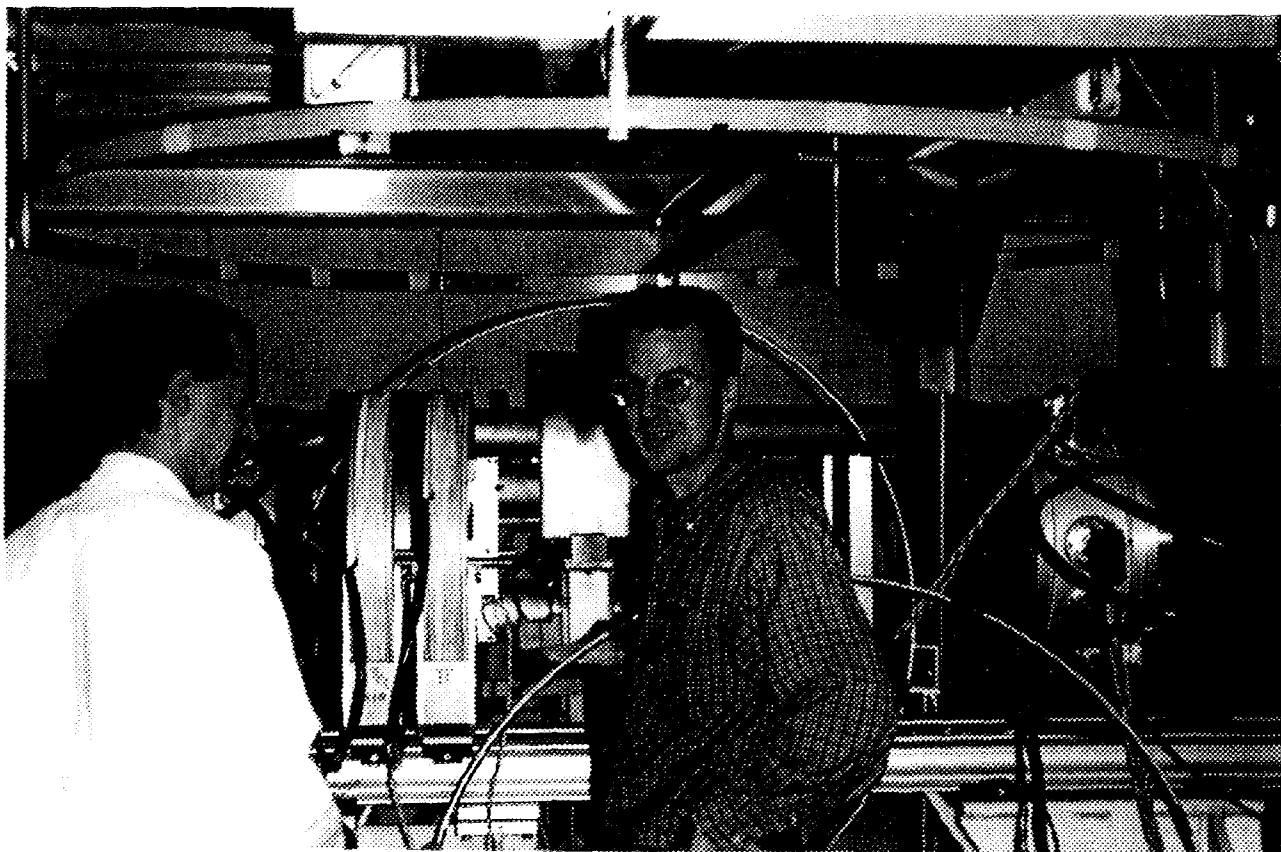


FIGURE 2: Neutron reflectivity profile of $[Os(bipy)_2PVP_{10}Cl]^+$ on an Au electrode in quartz contrast matched water. The thiol polymer is simply an adhesive between the quartz block and the evaporated gold layer. The inset shows corresponding scattering-length density profile calculated using SLAB fitting software. The fit clearly shows the polymer layer situated upon the metallic electrode and suggests the ingress of solvent into the film at the solution interface.

NEW INSTRUMENTS

TWO NEW INSTRUMENTS ARE EXPECTED TO BECOME AVAILABLE FOR USERS IN 1997: IN15 (SEE BELOW) AND IN4, THE TIME-OF-FLIGHT SPECTROMETER WHOSE CONSTRUCTION IS NEARING COMPLETION. THIS SPECTROMETER, BUILT WITH CONTRIBUTIONS FROM CNR ITALY, IS DESIGNED FOR THE STUDY OF EXCITATIONS IN CONDENSED MATTER AT ENERGIES OF UP TO ABOUT 100 MEV. COMMISSIONING WILL START EARLY IN 1997 WITH SOME TEST EXPERIMENTS INVOLVING DEUTERON BEAMS. EXPECTED DATA IN 1997: A REPORT WILL BE GIVEN NEXT YEAR.



Setting up IN15, from left: Patrick Giraud and Paul Schleger.

IN15 ULTRA-HIGH-RESOLUTION SPIN-ECHO PROJECT: FIRST EXPERIMENT

P. SCHLEGER, C. HAYES (ILL),
A. KOLLMAR (FZ JÜLICH).



FR9704876

THE IN15 PROJECT IS A COLLABORATION BETWEEN THE ILL, HMI (BERLIN), AND FZ (JÜLICH) TO CONSTRUCT A SPIN-ECHO SPECTROMETER WITH A FOURIER TIME-RANGE SURPASSING HALF A MICROSECOND. THREE DIFFERENT OPERATIONAL MODES ARE POSSIBLE: NORMAL, WITH NEUTRON FOCUSING, AND TIME-OF-FLIGHT.

The extended time-range obtainable with IN15 will allow one to investigate relaxation processes that were previously not measurable using existing spectrometers. Systems which exhibit interesting slow relaxation are for example, polymers, membranes, biological systems, and nanostructured materials; not to forget the more "traditional" critical phenomena. Since slow dynamics inevitably occurs when collective motion on long length-scales is involved, a particular design emphasis was on providing a good small-angle scattering capability.

IN15 is situated on an excellent cold-source providing a workable range between $\lambda = 8$ and 25 \AA . Longer wavelengths not only result in a better Q -resolution, but drastically increase the accessible Fourier time-window (the maximum time increases with λ^3). The inevitable loss of intensity at long wavelengths is compensated by two components: a $32 \text{ cm} \times 32 \text{ cm}$ position-sensitive detector (PSD), and a 4 m long toroidal neutron-focusing mirror. This year saw the installation of the polarisation analyser mirror-assembly from HMI covering the entire PSD area. The focusing mirror had already been installed late in 1995 [1], providing very high Q -resolution (Q_{\min} about $3.5 \cdot 10^{-3} \text{ \AA}^{-1}$) above 17 \AA without using collimators.

Going to long wavelengths is only one ingredient needed to access long Fourier times. Spin echo relies on a coherent refocusing of the neutron spin, for all possible neutron flight-paths within the spin-precession region. Any magnetic-field inhomogeneities degrade the echo. With good magnets, by far the largest de-phasing contribution comes from the radial field profile of the main precession magnets, which must be compensated by so-called Fresnel spiral-coils placed strategically in the flight path. At present, the maximum reachable Fourier time on IN15 is about 200 nsec . In order to increase this range, new Fresnels will be developed in the coming year. But in the meantime, one can already do some interesting experiments: The first ever spin-echo experiment out to $t = 180 \text{ nsec}$ was conducted late in 1996. The measurements were done on a 32000 molecular weight copolymer at $Q = 0.155$ and 0.077 \AA^{-1} (see Fig. 1).

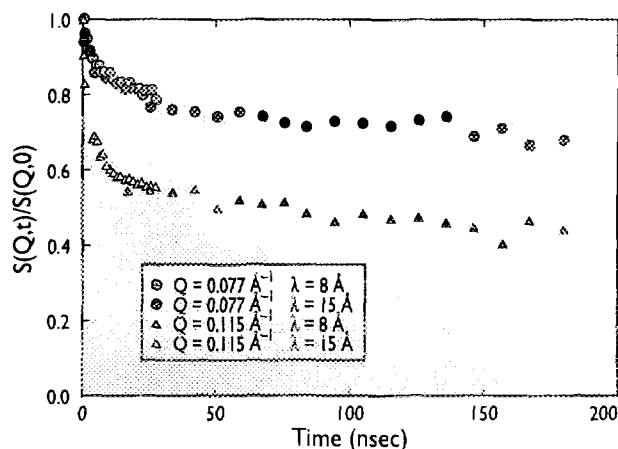
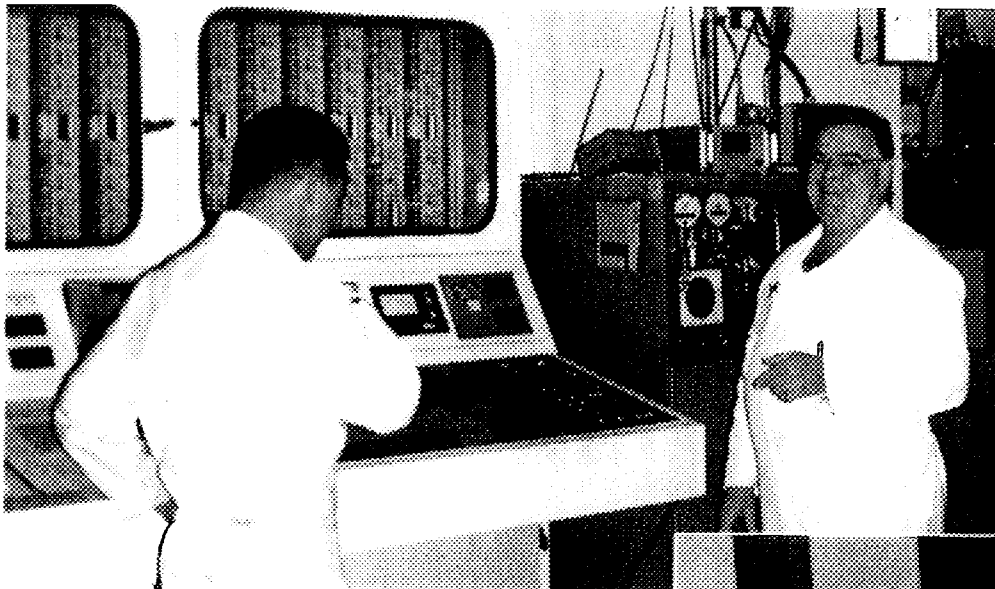


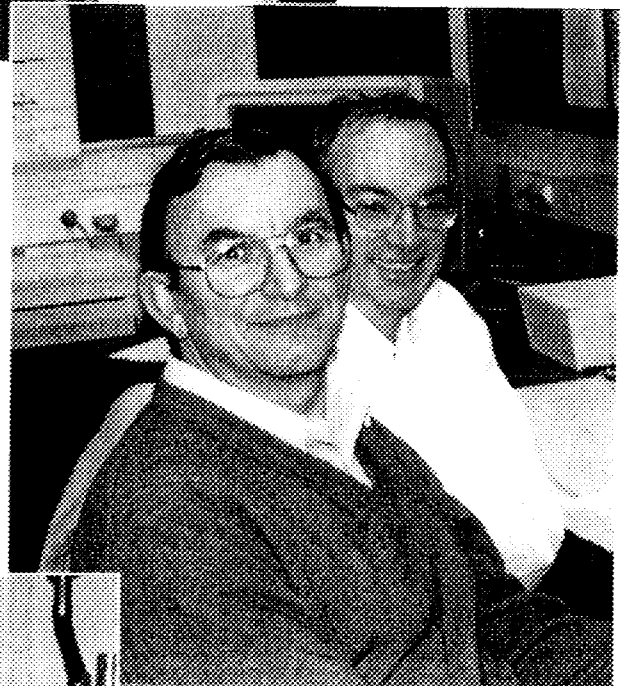
FIGURE 1: Intermediate scattering function of singly protonated $M_n = 32000$ polyethylene-1 butene copolymer (PEB-2) at 509 K .

The dynamics of such a large molecular-weight sample is expected to be dominated by topological constraints confining individual chain-motion. The famous reptation-model [2] pictures this as a localised tube defined by the entanglements in which the polymer chain is constrained. A characteristic signal of this is the existence of a plateau in $S(Q,t)$ after an initial short-time decay. Previous spin-echo measurements on IN11 [3], restricted to 40 nsec , had seen the onset of a plateau. However, it was somewhat uncertain whether it continued appreciably, or if $S(Q,t)$ would monotonically decay to zero. The IN15 experiment to 180 nsec clearly shows that the plateau in $S(Q,t)$ persists out to very long times (see Fig. 1). A closer look at Fig. 1, however reveals a small slope, indicating that the situation is more complicated and that other very slow relaxational modes exist.

In summary, IN15 is finally well on its way to seeing most of its goals reached. Working on a new Fresnel design this year should push the time range out even further, hopefully beyond half a microsecond. Together with the focusing mirror, a whole new dynamical window becomes available for exploration, and a true overlap with other spectroscopic techniques is in sight.



Wayne Clancy (left) and Louis Morganti from the reactor change PN3's target.



IN16 is working well for Marc Bée (left) and Hervé Jobic.



Deblocking the cold valve: Maurice de Palma.

EXPERIMENTAL PROGRAMME

4

INSTRUMENTS

REACTOR OPERATION

BEAM-TIME ALLOCATION

INSTRUMENT PERFORMANCE

EXPERIMENTAL
PROGRAMME

LIST OF INSTRUMENTS

ILL INSTRUMENTS

D1A (1/2)	powder diffractometer	operational
D1B	powder diffractometer	operational
D2B	powder diffractometer	operational
D3	single-crystal diffractometer	operational
D4 (1/2 with IN1)	liquids diffractometer	operational
D7	diffuse-scattering spectrometer	operational
D9	single-crystal diffractometer	operational
D10	single-crystal diffractometer	operational
D11	small-angle scattering diffractometer	operational
D16	small momentum-transfer diffractometer	operational
D17	reflectometer/small-angle scattering diffractometer	operational
D19	single-crystal diffractometer	operational
D20	powder diffractometer	commissioning
D22	small-angle scattering diffractometer	operational
IN1 (1/2 with D4)	three-axis spectrometer	operational
IN4	time-of-flight spectrometer	under construction
IN5	time-of-flight spectrometer	operational
IN6	time-of-flight spectrometer	operational
IN8	three-axis spectrometer	operational
IN10	backscattering spectrometer	operational
IN11	spin-echo spectrometer	operational
IN14	three-axis spectrometer	operational
IN16	backscattering spectrometer	operational
IN20	three-axis spectrometer	operational
PF1	neutron beam for fundamental physics	operational
PF2	ultracold neutron source for fundamental physics	operational
PN1	fission product mass-spectrometer	operational
PN3	gamma-ray spectrometer	operational

JOINTLY FUNDED INSTRUMENTS

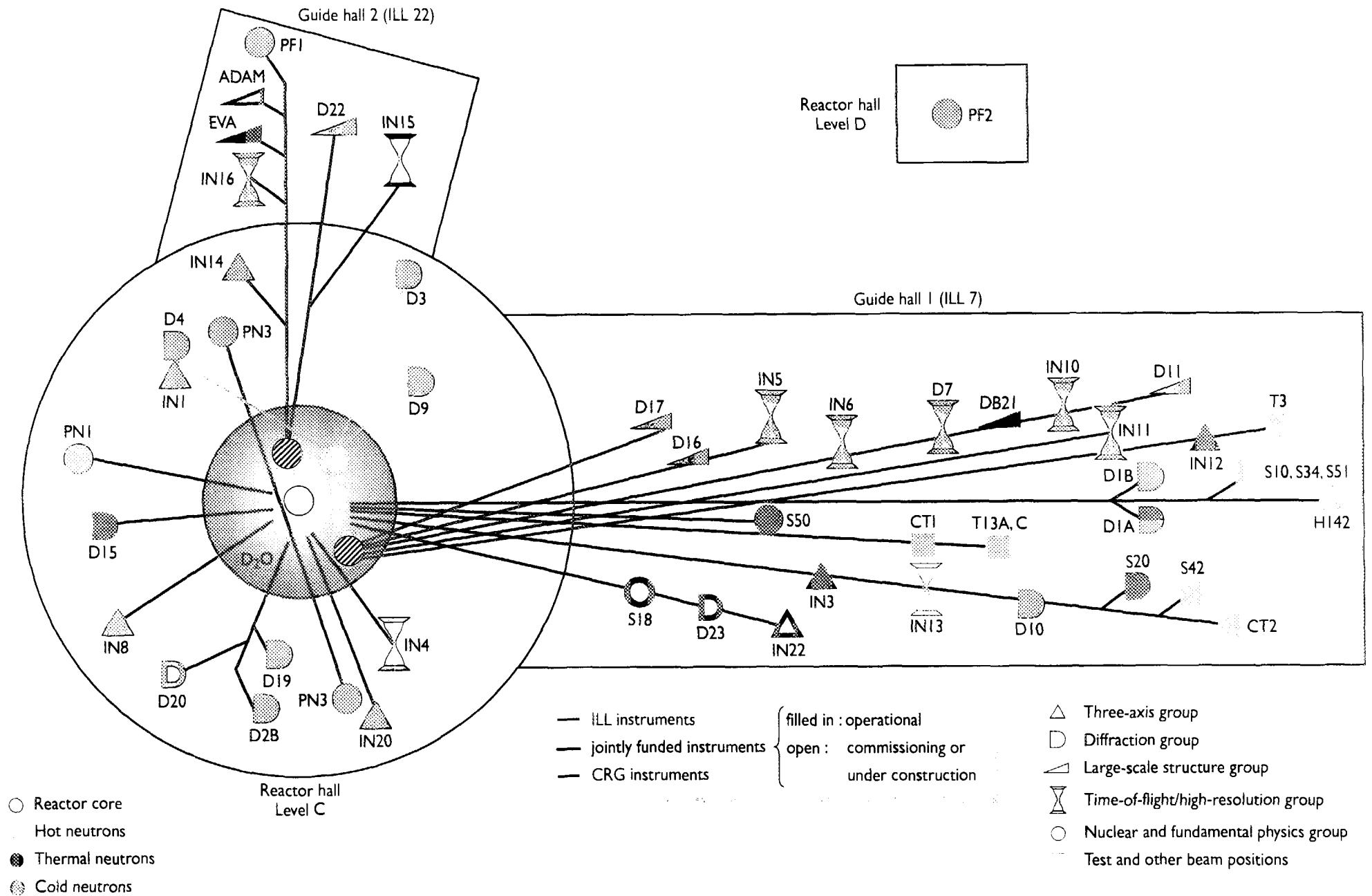
DB21	single-crystal diffractometer	operational, with EMBL
IN15	spin-echo spectrometer	commissioning, with KFA Jülich and HMI Berlin

CRG INSTRUMENTS

ADAM	reflectometer	CRG-B commissioning
D1A (1/2)	powder diffractometer	CRG-A operational
D15	single-crystal diffractometer	CRG-B operational
D23	single-crystal diffractometer	CRG-B under construction
EVA	reflectometer	CRG-B operational
IN3	three-axis spectrometer	CRG-A operational
IN12	three-axis spectrometer	CRG-B operational
IN13	backscattering spectrometer	potential CRG (currently unused)
IN22	three-axis spectrometer	CRG-B under construction
S18	interferometer	CRG-C commissioning
S20	topography	CRG-B operational
S50	h/m measurements	CRG-C operational

TEST BEAMS

CT1, CT2	detector test-facility
S42	Laue crystal alignment facility
T3	neutron optic test-facility
T13A,C	monochromator test-facility
H142 test	cold neutron-beam test-facility currently used mainly for development of LADI, image-plate detector for Laue diffraction
S10, S34, S51	uninstrumented beam-positions



REACTOR OPERATION

Since the refurbishment of the reactor and the removal of some of the internal structures of the reactor block (beta beam-tube, etc.), we now have a certain margin of flexibility regarding the length of the reactor cycle and at the beginning of 1996 our request to extend the cycle from 47 to 50 days was accepted by the safety authorities.

This has allowed us to devise a new system for scheduling the cycles over the course of the year. The major shutdown which is necessary to carry out lengthy maintenance work will now take place at the end of the year, as the cost of electricity is higher in December and January.

While maintaining inter-cycle shutdowns of about 2 to 3 weeks, the annual operating schedule is now set at 225 days spread over 4.5 cycles.

The major advantage of this new schedule is that it can be carried over from one year to the next and that it allows us to save half a fuel element per year while at the same time minimising electricity consumption.

In 1996 there were no unscheduled shutdowns. Several cycles began with the taking of flux measurements in the neutron guide beam-lines. These measurements involve the irradiation of gold foils and make it possible to assess the quality of the guides and their alignment.

The table below sets out the operating and shutdown periods in 1996.

This year the ILL had to prepare the replacement of some of the reactor's peripheral installations. Although not part of the reactor block itself, the peripheral installations are vital for the reactor's operation. Some of these installations date back to the reactor's construction and are becoming more and more difficult to maintain. A number of pieces of equipment were replaced this year, including converter sets for power supplies and neutron-flux chambers forming part of the reactor-control mechanism.

The internal parts of the reactor block must be replaced at regular intervals. They are purpose-built and represent a significant share of the budget. In order to keep tight control of the budget, the procurement of such material is spread out over several years, e.g. in 1996 a through beam-tube was purchased.

Most of the new projects are the result of a tightening up of regulations governing the monitoring of discharges of gaseous effluents and waste and rainwater. In 1996, two facilities were built for making radiological measurements of effluents and a station for monitoring waste and rainwater is currently under construction.

cycle n°	start date	finish date	number of days scheduled	number of days operation	number of unscheduled shutdowns	observations
cycle 104	25/1/96	15/3/96	50	50	0	flux measurement on 24/1/96
cycle 105	2/4/96	22/5/96	50	50	0	
cycle 106	13/6/96	2/8/96	50	50	0	flux measurement on 12/6/96
cycle 107	27/8/96	16/10/96	50	50	0	flux measurement on 26/8/96
cycle 108/1*	5/11/96	30/11/96	25	25	0	flux measurement on 4/11/96

* The fuel element used for cycle 108/1 will be used for the first cycle of 1997.

INSTRUMENTS

The instrumental facilities at the ILL are shown in the schematic diagram on page 101. Besides the ILL instruments there are CRG-instruments, which are operated by external Collaborating Research Groups. There are currently three different categories of CRG instruments: CRG-A in which the external group leases an instrument owned by ILL. They have 50% of the beam time at their disposal and for the other 50% they support ILL's scientific user programme.

The CRG-B category owns their instrument and have 70% of the beam time, supporting the ILL programme for the other 30%. Finally, CRG-C instruments are used full time for specific research programmes by the external group who has exclusive use of the beam.

DB21 and IN15 have a special status, since they are a joint venture of ILL with other laboratories: in the case of DB21 with EMBL and for IN15 with FZ Jülich and HMI Berlin. The list of instruments by type as at Dec. 1996 is summarised below (CRG instruments are marked with an asterisk *)

- powder diffractometers: D1A* (note that D1A is only half a CRG instrument), D1B, D2B, (D20 in commissioning)
- liquids diffractometer: D4
- single-crystal diffractometers: D3, D9, D10, D15*, D19, DB21, (D23* under construction)
- small-angle scattering: D11, D22, (D17 only for special SANS experiments, priority is given to reflectivity experiments)

- small momentum-transfer diffractometer: D16
- reflectometers: D17, EVA*, (ADAM* in commissioning)
- diffuse-scattering spectrometer: D7
- three-axis spectrometers: IN1, IN3*, IN8, IN12*, IN14, IN20 (spin-echo option in commissioning), (IN22* under construction)
- time-of-flight spectrometers: IN5, IN6, (IN4 under construction)
- backscattering and spin-echo spectrometers: IN10, IN11, IN16, (IN15 in commissioning)

- topography: S20*
 - nuclear-physics instruments: PN1, PN3, (option GAMS5 on PN3 in commissioning)
 - fundamental-physics instruments: PF1, PF2
- Details of the instruments can be found on the web under <http://www.ill.fr>. S50*, precise determination of h/m , and S18*, interferometer, are so-called CRG-C instruments and they are not available as 'user' instruments. S50 finished its contract with the end of 1996.

BEAM-TIME ALLOCATION

Overall the subcommittees of the scientific council scrutinised over 1000 proposals, out of which over 700 proposals received beam time, allocating some 4000 instrument days of beam time on the different instruments. Almost 800 experiments were carried out. Table 1 shows the request and allocation of beam time per instrument.

instrument	beam-time requested (in days)	beam-time available (in days)	number of experiments
D1A*	127	125	47
D1B	346	197	80
D2B	373	175	62
D3	203	176	21
D4	202	79	20
D7	325	155	17
D9	232	195	28
D10	335	177	22
D11	372	154	75
D15*	94	50	12
D16	299	173	21
D17	227	132	35
D19	259	177	16
DB21	173	185	5
D22	163	82	40
EVA*	38	59	4
IN1	246	87	18
IN3*	66	89	13
IN5	398	163	37
IN6	485	171	45
IN8	363	183	21
IN10	262	152	24
IN11	377	152	17
IN12*	50	56	9
IN14	442	150	21
IN16	251	123	19
IN20	153	123	20
PF1	321	142	5
PF2	417	216	11
PN1	200	167	11
PN3	441	194	15

TABLE 1: Beam-time requested and allocated by instrument.

* CRG instruments are marked with an asterisk.

Note that D4 and IN1 share a beam and that the CRG instruments offer a reduced number of days for ILL users. Although S20 the CRG topography instrument had beam time available, it is not listed because there were no requests for beam time by users. The low allocation-rate on the small-angle instrument D22 is due to its detector breakdown in 1995; repair was successfully completed in May 1996, but experiments were only possible in the second half of the year. For PF2 several experiments share the beam taking neutrons alternatively, so the table contains the beam-days allocated but gives the total number of experiments running simultaneously. In addition, the scientific council endorsed a test of zero-field spin-echo on the test beam-position H142; this experiment will have some further test time in 1997. Table 2 shows the distribution of beam-time request and allocation amongst the member and scientific-member countries: Beam-time request and allocation for 1996, i.e. SC Oct. 95 and SC Apr. 96.

country	requested days	requested in %	allocated days	allocated in %
AUT	131.1	1.6%	90.9	2.1%
CH	433.2	5.3%	255.5	5.8%
D	2708.7	33.0%	1423.3	32.6%
E	271.8	3.3%	149.5	3.4%
F	2206.8	26.9%	1272.5	29.1%
GB	2367.6	28.8%	1136.5	26.0%
I	90.3	1.1%	44.0	1.0%
total	8209.6	100.0%	4372.3	100.0%

TABLE 2: Beam-time requested and allocated by country.

In 1996 the member and scientific-member countries were France, Germany, UK, Spain, Switzerland, and Austria. Italy received beam time due to specific instrument contracts (from 1997 it will be a scientific member). The attribution is based on the location of the laboratory of the proposers, not their individual nationality. For a proposal involving laboratories from more than one member country, the total number of days is divided equally among the collaborating countries. When a proposal involves a collaboration with a non-member country, the allocated time is attributed entirely to the collaborating member country (or countries).

When ILL scientists are proposers or co-proposers, the allocated "ILL time" is attributed among the member countries according to their financial contributions to ILL. Local contacts are not counted as proposers.

In 1996, three quarters of ILL's annual 1500 visitors came from the member countries including 408 from France, 331 from Germany and 306 from the UK and many of them were welcomed more than once. There were thus over 2000 visits carrying out some 800 experiments. The distribution

of beam time for these experiments amongst the different 'colleges' was as follows: 19% of the days were allocated to nuclear and fundamental physics (college 3), 16% to structural and magnetic excitations (college 4), 31% to crystal and magnetic structures (college 5), 8% to structure and dynamics of liquids and glasses (college 6), 7% to materials science, surfaces and spectroscopy (college 7), 11% to biology (college 8) and 8% to structure and dynamics of soft-condensed matter (college 9).

INSTRUMENT PERFORMANCE

Table 3 below gives a summary of instrument performance for 1996. For each cycle a record is kept of any time lost from the total available beam-time, and the reasons for the

lost time are analysed for all the instruments. The table gives a global summary for the year:

instrument	days lost	% lost	sched. days	days used	instrument
D1A	11.0	6.8%	149.0	148.5	D1A
D1B	4.5	2.0%	195.0	198.0	D1B
D2B	2.0	0.9%	173.0	193.0	D2B
D3	7.0	3.1%	139.0	132.0	D3
D4	12.2	11.3%	79.0	82.3	D4
D7	4.5	2.0%	163.0	174.0	D7
D9	35.5	15.8%	192.0	179.5	D9
D10	18.6	8.3%	190.0	196.3	D10
D11	17.9	8.0%	156.0	146.0	D11
D16	2.5	1.1%	178.0	180.0	D16
D17	23.3	10.4%	156.0	159.0	D17
D19	6.0	2.7%	186.0	189.0	D19
DB21	13.5	6.0%	184.0	196.0	DB21
D22	74.1	32.9%	85.0	85.5	D22
IN1	6.5	5.2%	90.0	96.0	IN1
IN5	4.9	2.2%	170.0	208.3	IN5
IN6	13.5	6.0%	195.0	198.0	IN6
IN8	4.0	1.8%	176.0	182.0	IN8
IN10	15.3	6.8%	164.0	172.0	IN10
IN11	23.0	10.2%	160.0	159.0	IN11
IN14	14.3	6.3%	178.0	186.0	IN14
IN16	8.5	3.8%	127.0	147.6	IN16
IN20	11.0	4.9%	184.0	194.0	IN20
PF1	18.0	8.0%	218.0	206.0	PF1
PF2	1.2	0.5%	*	*	PF2
PN1	43.2	19.2%	210.0	177.5	PN1
PN3	19.7	8.8%	199.0	203.3	PN3
total	415.6		4296.0	4388.8	total

TABLE 3: Instrument performance for all the ILL scheduled instruments.

* PF2 consists of several long-term experiments so comparison of days scheduled and used is not meaningful.

Overall about 400 days of the total available beam-time was lost due to various malfunctions. However, most of this time was not lost to users because time for minor breakdowns, tests, calibrations and scheduling difficulties is allowed for by initially scheduling about 80% of the total available beam-time. Thus the total number of days delivered to users was higher than the number of days originally scheduled: 4388 compared with 4296 originally scheduled.

Detailed comments on the larger beam-time losses are as follows:

- D22's detector problems have already been discussed.
- PN1 experienced some time loss due to breakdowns in high-tension equipment.
- D9 lost time because of users who were not able to provide their crystals in time for the scheduled experiment and alternative scheduling was not possible.

FACTS AND FIGURES FOR 96

5



FACTS
AND FIGURES FOR 96

FACTS AND FIGURES FOR 1996

NAME: Institut Max von Laue - Paul Langevin (ILL)

FOUNDED: 1967

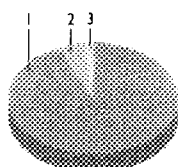
ASSOCIATES: France: Commissariat à l'Energie Atomique (CEA)
Centre National de la Recherche Scientifique (CNRS)
Federal Republic of Germany: Forschungszentrum Jülich
United Kingdom: Engineering and Physical Sciences Research Council (EPSRC)

COUNTRIES WITH SCIENTIFIC MEMBERSHIP:

Spain: Comisión Interministerial de Ciencia y Tecnología (CICT)
Switzerland: Schweizer Bundesamt für Bildung und Wissenschaft (SBBW)
Austria: Österreichische Akademie der Wissenschaften
Russia: Russian Ministry of Atomic Energy - Minatom (from 14 November 1996)
[Italy: Istituto Nazionale per la Fisica della Materia (INFN) from 1 January 1997]

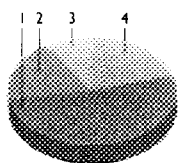
STAFF: 398 people including 49 experimentalists in the scientific sector
248 French, 64 German, 54 British, 32 others

BUDGET: 347.275 MF



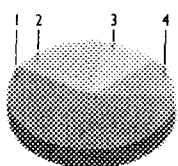
INCOME IN MF (EXCLUDING TAXES, EXCLUDING INCOME FROM CRGs)

- 1) 322.589 - 92.89% from associates, (divided: F, 37.87%; D, 37.13%; UK, 25.00%)
- 2) 18.978 - 5.46% from scientific members,
- 3) 5.708 - 1.64% own income



EXPENDITURE IN MF (EXCLUDING TAXES AND EXCLUDING EXPENDITURE ON CRGs)

- 1) 180.880 - 52.09% personnel
- 2) 63.598 - 18.31% operation
- 3) 32.361 - 9.32% investments
- 4) 70.436 - 20.28% fuel cycle



PURCHASES IN MF (OVER 50kF):

- 1) 20.7 - 59% France
- 2) 6.7 - 19% Germany
- 3) 3.9 - 11% UK
- 4) 4.0 - 11% others

BODIES: Steering Committee, meeting twice a year
Scientific Council with 8 Subcommittees, meeting twice a year
Management Board, meeting weekly

REACTOR: 58 MW, running 4.5 reactor cycles per year (with cycles of 50 days)

EXPERIMENTAL PROGRAMME:

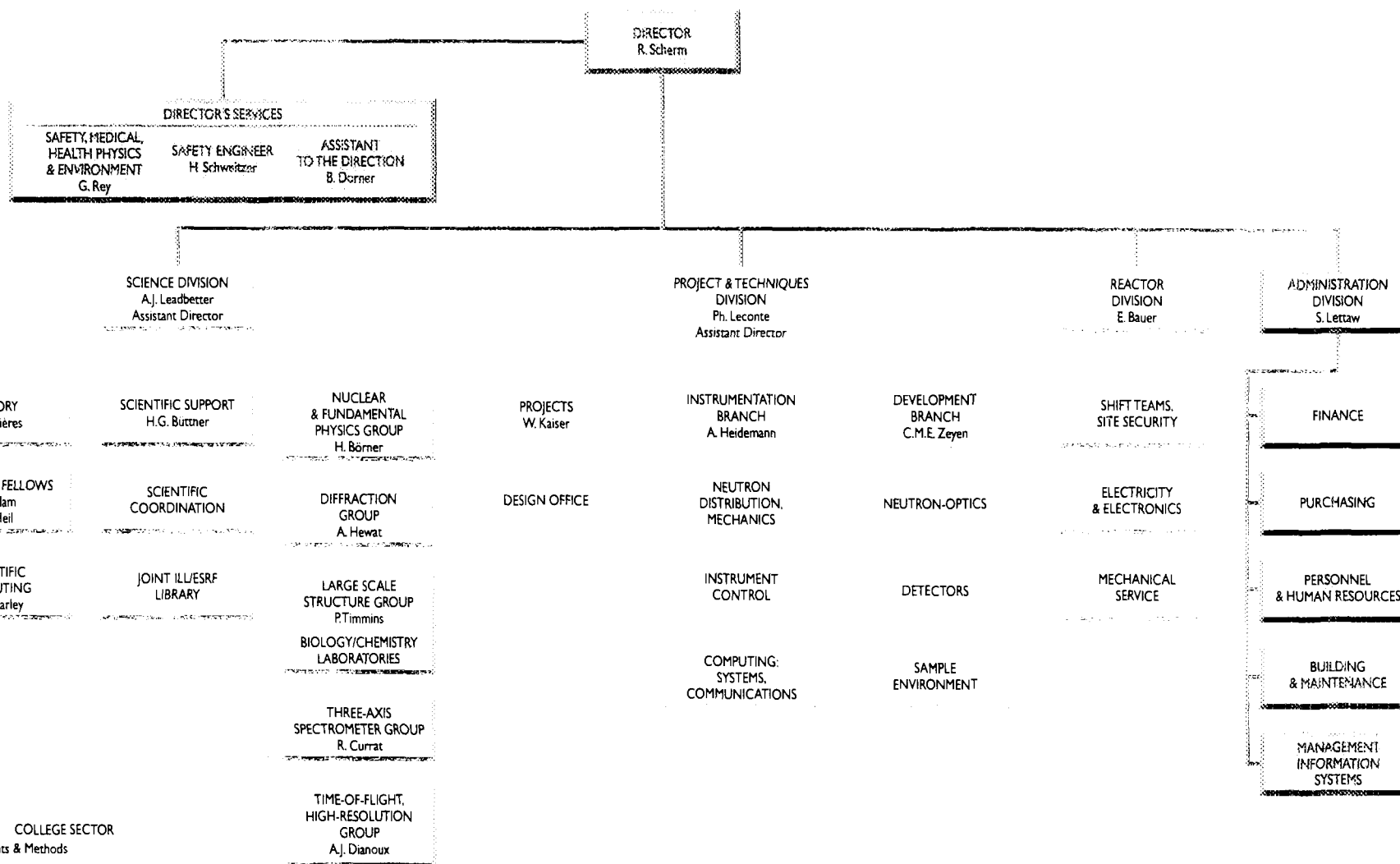
about 800 experiments (allocated by subcommittees) on 25 ILL-funded and 6 CRG instruments
about 1500 visitors coming from 31 countries
about 1000 proposals submitted and 700 accepted

EXPERIMENT SELECTION BY THE SCIENTIFIC COUNCIL VIA ITS 8 SUBCOMMITTEES:

nuclear and fundamental physics (college 3)
structural and magnetic excitations (college 4)
crystallographic structures (college 5a)
magnetic structures (college 5b)
structure and dynamics of liquids and glasses (college 6)
materials science, surfaces and spectroscopy (college 7)
biology (college 8)
structure and dynamics of soft-condensed matter (college 9)

SCIENTIFIC LIFE: based on 10 colleges

8 of which map on to the subcommittees plus two others:
instruments and methods (college 1); theory (college 2)



PUBLICATIONS

6

IN 1996 THE ILL RECEIVED NOTICE OF 414 PUBLICATIONS BY ILL STAFF AND USERS. THE DISTRIBUTION BY SUBJECT IS AS FOLLOWS: 44 IN INSTRUMENTS AND METHODS, 16 IN THEORY, 20 IN FUNDAMENTAL AND NUCLEAR PHYSICS, 56 IN STRUCTURAL AND MAGNETIC EXCITATIONS, 58 IN CRYSTALLOGRAPHIC STRUCTURES, 41 IN MAGNETIC STRUCTURES, 63 IN STRUCTURE AND DYNAMICS OF LIQUIDS AND GLASSES, 71 IN MATERIALS SCIENCE, SURFACES AND SPECTROSCOPY, 13 IN BIOLOGY, 32 IN STRUCTURE AND DYNAMICS OF SOFT-CONDENSED MATTER. IN ADDITION A SURVEY PERFORMED IN JULY, AIMED AT UPDATING OUR PUBLICATION LIST, REVEALED AN ADDITIONAL 330 PUBLICATIONS RELATED TO EARLIER MEASUREMENTS WHICH WERE NOT ALREADY IN OUR RECORDS.

PUBLICATIONS

This list gives publications received during 1996 resulting from research carried out at the ILL.
It was generated from the library database LORIS-DORIS and can be consulted on the Web at <http://www.ill.fr>.

PAPERS PUBLISHED IN SCIENTIFIC PERIODICALS, BOOKS AND CONFERENCE PROCEEDINGS

- ABOLFATHI E., MODLEN G.F., WEBSTER P.J., MILLS G. The effect of the manufacturing test load on the fatigue of hoist chains.
Proceedings of the Institution of Mechanical Engineers **290**, 133-139 (1995)
- ACHIBATT., DUVAL E., DUPUY-PHILON J., JAL J.F., PREVEL B., ZORKANI I. Low-energy excitations in glass-forming aqueous lithium-chloride.
Journal of Chemical Physics **102**, 8114-8117 (1995)
- ADAM M., LAIREZ D., RASPAUD E., FARAGO B. Dynamic properties of semidilute solutions at the theta point.
Physical Review Letters **77**, 3673-3676 (1996)
- ADROJA D.T., RAINFORD B.D., NEVILLE A.J. Crystal field study of the Kondo compound CePtGa.
Physica B **223-224**, 279-282 (1996)
- AEPPLI G. Neutrons for technology and science.
In "Neutron Beams and Synchrotron Radiation Sources" (OCDE, 1994) pp. 19-36
- AEPPLI G., BROHOLM C. Magnetic correlations in heavy-fermion systems: neutron scattering from single crystals.
Handbook on the Physics and Chemistry of Rare Earths **19**, 123-175 (1994)
- AEPPLI G., LITTLEWOOD P., CHEONG S.W., MOOK H.A., MASON T.E., CLAUSEN K.N., HAYDEN S.M., TAYLOR A.D., PERRING T.G., FISK Z. Neutron scattering and magnetic dynamics in insulators, metals and superconductors.
In "Perspectives in Many-Particle Physics. Proceedings of the International School of Physics Enrico Fermi", BROGLIA R.A.M. et al. Eds. (Societa Italiana di Fisica, 1994) pp. 205-230
- ALEKSEEV P.A., BÜHRER W., LAZUKOV V.N., NEFEODOVA E.V., SADIKOV I.P., CHISTYAKOV O.D., ZOLLIKER M. Low-temperature effects in magnetic spectral response of CeAl₃-based systems.
Physica B **217**, 241-251 (1996)
- ALEKSEEV P.A., KCHLOPKIN M.N., LAZUKOV V.N., ORLOV V.G., SADIKOV I.P., SUCK J.B., SCHMIDT H. Magnetic excitation spectra and thermodynamics of amorphous PrNi₅.
Physical Review B **54**, 3884-3894 (1996)
- ALEXANDROVICH A.Y., GAGARSKII A.M., KRASNOSCHEKOVA I.A., PETROV G.A., PETROVA V.I., PETUKHOV A.K., PLEVA Y.S., GELTENBORT P.G., LAST J., SCHRECKENBACH K. New observation of space-parity violation in neutron-induced fission of ²²⁹Th, ²⁴¹Pu and ²⁴¹Am.
Nuclear Physics A **567**, 541-552 (1994)
- ALFIMENKOV V.P., VAL'SKII G.V., GAGARSKII A.M., GELTENBORG B., GUSEVA I.S., LAST J., PETROV G.A., PETUKHOV A.K., PIKEL'NER L.B., PLEVA Y.S., SOKOLOV V.E., FURMAN V.I., SCHRECKENBACH K., SHCHERBAKOV O.A. Interference effects in the angular distributions of fragments of heavy-nucleus fission induced by thermal and resonance neutrons.
Physics of Atomic Nuclei **58**, 737-745 (1995)
- ALLANCON C., RODRIGUEZ-CARVAJAL J., FERNANDEZ-DIAZ M.T., ODIER P., BASSAT J.M., LOUP J.P., MARTINEZ J.L. Crystal structure of the high temperature phase of oxidised Pr₂NiO_{4.8}.
Zeitschrift für Physik B **100**, 85-90 (1996)
- ALTORFER F., COOK J.C., COPLEY J.R.D. The multiple disk chopper neutron time-of-flight spectrometer at NIST.
Materials Research Society Symposium **376**, 119-124 (1996)
- ALVAREZ I., MARTINEZ J.L., VEIGA M.L., PICO C. Synthesis, structural characterization, and electronic properties of the LaNi_{1-x}W_xO₃ (0 ≤ x ≤ 0.25) perovskite-like system.
Journal of Solid State Chemistry **125**, 47-53 (1996)
- ANDERSEN K.H. Resolution function of the neutron time-of-flight spectrometer MARI.
Nuclear Instruments and Methods in Physics Research A **371**, 472-479 (1996)
- ANDERSEN K.H., BOSSY J., COOK J.C., RANDL O.G., RAGAZZONI J.L. High-resolution measurements of rotons in ⁴He.
Physical Review Letters **77**, 4043-4045 (1996)
- ANDERSEN K.H., STIRLING W.G. Collective excitations in liquid ⁴He: II. Analysis and comparison with theory.
Journal of Physics Condensed Matter **6**, 5805-5822 (1994)
- ANDERSEN K.H., STIRLING W.G., GLYDE H.R., AZUAH R.T., BENNINGTON S.M., TAYLOR A.D., BOWDEN Z.A., BAILEY I. Final-state effects and momentum distribution in normal liquid ⁴He.
Physica B **197**, 198-205 (1994)
- ANDERSON I.S., SCHÄRPF O., HØGHØJ P., AGE-ROD P. Multilayers for neutron optics.
Journal of Neutron Research **5**, 51-61 (1996)
- ARBE A., BUCHENAU U., WILLNER L., RICHTER D., FARAGO B., COLMENERO J. Study of the dynamic structure factor in the β relaxation regime of polybutadiene.
Physical Review Letters **76**, 1872-1875 (1996)
- ARBE A., RICHTER D., COLMENERO J., FARAGO B. Merging of the α and β relaxations in polybutadiene: a neutron spin echo and dielectric study.
Physical Review E **54**, 3853-3869 (1996)
- ARNAULT J.C., BUBENDORFF J.L., PIMPINELLI A., BUCHER J.P. Transition in the growth kinetics of vacancy islands on NbSe₂.
Surface Science **348**, 185-191 (1996)
- ARRIGHI V., HIGGINS J.S., ABIS L., CIMECIOGLU A.L., WEISS R.A. Characterization of ordering in a main chain liquid crystal polymer by small angle neutron scattering and NMR.
Macromolecular Reports **31**, 1101-1108 (1994)
- AUNEAU I., FRAGA G.L.F., GIGNOUX D., SCHMITT D., ZHANG F.Y. Magnetic phase diagram of TbGa₂.
Physica B **212**, 351-356 (1995)
- BAFILE U., BAROCCHI F., NEUMANN M. Two-body contribution to the density fluctuations in a dilute gas from molecular-dynamics simulations.
Physical Review E **51**, 3756-3759 (1996)
- BAFILE U., BAROCCHI F., NEUMANN M., VERKERK P. Density fluctuations in the quasi-hydrodynamic regime: neutron scattering and molecular dynamics simulations.
Journal of Physics Condensed Matter **6**, A107-A111 (1994)
- BALDINOZZI G., GOUTENOIRE F., HERVIEU M., SUARD E., GREBILLE D. Incommensurate modulated disorder in Ba_{0.85}Ca_{0.15}InO₁₂.
Acta Crystallographica B **52**, 780-789 (1996)
- BALL A.R., GIGNOUX D., RODRIGUEZ FERNANDEZ J., SCHMITT D. Magnetic properties and complex phase diagram of hexagonal NdGa₂.
Journal of Magnetism and Magnetic Materials **137**, 281-292 (1994)
- BALLOU R., LELIÈVRE-BERNA E., FÂK B. Spin fluctuations in (Y_{0.97}Sc_{0.03})Mn₂: a geometrically frustrated, nearly antiferromagnetic, itinerant electron system. [Erratum: Phys. Rev. Lett. **77**, 790 (1996)]
Physical Review Letters **76**, 2125-2128 (1996)
- BALSUNAT D., ASMUSSEN B., MÜLLER M., PRESS W., LANGE W., CODDENS G., FERRAND M., BÜTTNER H.G. Rotational excitations of methane molecules in porous media.
Physica B **226**, 185-188 (1996)
- BALUCANI U., TORCINI A., STANGL A., MORKEL C. Single-particle dynamics in simple liquids.
Physica Scripta **T57**, 13-17 (1995)
- BARGE A., GAGNON J., CHAFFOTTE A., TIMMINS P.A., LANGOWSKI J., RUIGROK R.W.H., GAUDIN Y. Rod-like shape of vesicular stomatitis virus matrix protein - Short communication.
Virology **219**, 465-470 (1996)
- BARTSCH E., FUJARA F., LEGRAND J.F., PETRY W., SILLESCU H., WUTTKE J. Erratum: Dynamics in viscous orthoterphenyl: results from coherent neutron scattering. [Phys. Rev. E **52**, 738 (1995)]
Physical Review E **53**, 2011 (1996)
- BASTIDE J., BOUE F., MENDES E., HAKIKI A., RAMZIA., HERZ J. Swelling and uniaxial extension of polymer gels as seen by small angle neutron scattering. In "Soft Order in Physical Systems", RABIN Y., BRUINSMA R. Eds. (Plenum Press, 1994) pp. 99-102
- BASTIE P., HAMELIN B. La méthode de Laue refocalisée à haute énergie: une technique d'étude en volume des monocristaux.
Journal de Physique IV **6**, C4/13-C4/21 (1996)
- BASTIE P., MANIGUET L., DUPEUX M. Détection et localisation non destructive de l'endommagement par diffraction γ dans un superalliage monocristallin sollicité en cisaillement.
Bulletin du Cercle d'Etudes des Métaux **16**, 15.4-15.10 (1995)
- BASTIE P., MANIGUET L., DUPEUX M. Non-destructive detection and localization of straining by γ-ray diffractometry in a single crystal superalloy submitted to a shear test.
Bulletin du Cercle d'Etudes des Métaux **16**, 15.1-15.3 (1995)
- BATTLE P.D., DAVISON C.M., GIBB T.C., VENTE J.F. Structural chemistry of SrMn_{1-x}Fe_xO_{3.8}, x ≈ 0.3.
Journal of Materials Chemistry **6**, 1187-1190 (1996)
- BATTLE P.D., GORE J.G. Crystal structures and magnetic properties of La₂Zn_{1-x}Mg_xIrO₆.
Journal of Materials Chemistry **6**, 1375-1378 (1996)
- BATTLE P.D., GREEN M.A., LASKEY N.S., MILLBURN J.E., RADAELLI P.G., ROSSEINSKY M.J., SULIVAN S.P., VENTE J.F. Crystal and magnetic structures of the colossal magnetoresistance manganates Sr_{2-x}Nd_{1+x}Mn₂O₇ (x = 0.0, 0.1).
Physical Review B **54**, 15967-15977 (1996)

- BECKER J., EBERT M., GROSSMANN T., HEIL W., HUMBLLOT H., LEDUC M., OTTEN E.W., ROHE D., SCHÄFER M., SIEMENSMEYER K., STEINER M., SURKAU R., TASSET F., TRAUTMANN N. Development of a dense polarized ^3He spin filter based on compression of optically pumped gas. *Journal of Neutron Research* **5**, 1-10 (1996)
- BEE M., COMBET J., GUILLAUME F., MORELON N.D., FERRAND M., DJURADO D., DIANOUX A.J. Neutron scattering studies of linear chains in an organic inclusion compound. *Physica B* **226**, 15-27 (1996)
- BENMORE C.J., SALMON P.S. Structure of fast ion conducting and semiconducting glassy chalcogenide alloys. *Physical Review Letters* **73**, 264-267 (1994)
- BERASTEGUI P., FISCHER P., BRYNTSE I., JOHANSSON L.G., HEWAT A.W. Influence of stacking faults and temperature on the structure of $\text{Y}_2\text{Ba}_4\text{Cu}_7\text{O}_{15}$, investigated by high-resolution neutron diffraction and electron microscopy. *Journal of Solid State Chemistry* **127**, 31-39 (1996)
- BERMEJO F.J., CRIADO A., DE ANDRES A., ENCISO E., SCHÖBER H. Microscopic dynamics of glycerol in its crystalline and glassy states. *Physical Review B* **53**, 5259-5267 (1996)
- BERNHOFER N.R., LONZARICH G.G. Scattering of slow neutrons from long-wavelength magnetic fluctuations in UPt_3 . *Journal of Physics Condensed Matter* **7**, 7325-7333 (1995)
- BERRET J.F., MOLINO F., PORTE G., DIAT O., LINDNER P. The shear-induced transition between oriented textures and layer-sliding-mediated flows in a micellar cubic crystal. *Journal of Physics Condensed Matter* **8**, 9513-9517 (1996)
- BEST S.P., FIGGIS B.N., FORSYTH J.B., REYNOLDS P.A., TREGENNA-PIGGOTT P.L.W. Spin distribution and bonding in $[\text{Mo}(\text{OD})_6]^{3+}$. *Inorganic Chemistry* **34**, 4605-4610 (1995)
- BEZOU C., NONAT A., MUTIN J.C., CHRISTENSEN A.N., LEHMANN M.S. Investigation of the crystal structure of $\gamma\text{-CaSO}_4$, $\text{CaSO}_4 \cdot 0.5\text{H}_2\text{O}$, and $\text{CaSO}_4 \cdot 0.6\text{H}_2\text{O}$ by powder diffraction methods. *Journal of Solid State Chemistry* **117**, 165-176 (1995)
- BIANCONI A., LUSIGNOLI M., SAINI N.L., BORDET P., KVICK Å., RADAELLI P.G. Stripe structure of the CuO_2 plane in $\text{Bi}_2\text{Sr}_2\text{CaCu}_2\text{O}_{8+x}$ by anomalous x-ray diffraction. *Physical Review B* **54**, 4310-4314 (1996)
- BIENFAIT M. Quasi-elastic neutron scattering studies of surface mobilities. In "Proceedings of the EWSSW'94 - Thin Films and Phase Transitions of Surfaces", MICHAÏLOV M., GUTZOW I. Eds. (Bulgarian Academy of Sciences, 1994) pp. 193-208
- BIENFAIT M., ZEPPEFELD P., BOVIE L.J., VILCHES O.E., LAUTER H.J. Structure of mixed $\text{H}_2\text{-D}_2$ adsorbed single layers. *Czechoslovak Journal of Physics* **46**, 447-448 (1996)
- BIEZE T.W.N., TROMP R.H., VAN DER MAAREL J.R.C., VAN STRIEN M.H.J.M., BELLISSENT-FUNEL M.C., NEILSON G.W., LEYTE J.C. Hydration of chloride ions in a polyelectrolyte solution studied with neutron diffraction. *Journal of Physical Chemistry* **98**, 4454-4458 (1994)
- BOISSIEU M., DE BOUDARD M., KYCIA S., GOLDMAN A.L., HENNION B., BELLISSENT R., QUILICHINI M., CURRAT R., JANOT C. Experimental investigation of the dynamics of quasicrystals. In "Proceedings of the Fifth International Conference on Quasicrystals", JANOT C., MOSSERI R. Eds. (World Scientific, 1995) pp. 577-583
- BONGIOVANNI R., OTTEWILL R.H., RENNIE A.R., LAUGHLIN R.G. Interaction of small ions with the micellar surface of an ultralong chain zwitterionic surfactant. *Langmuir* **12**, 4681-4690 (1996)
- BONHOMME F., CERNY R., FISCHER P., GINGL F., HEWAT A.W., HUANG B., STETSON N.T., YOSHIDA M., YVON K., ZOLLIKER M. Powder diffraction as a routine tool for *ab-initio* structure determinations of metal hydrides. *Materials Science Forum* **166-169**, 597-602 (1994)
- BÖNI P. Polarizing supermirrors. *Journal of Neutron Research* **5**, 63-70 (1996)
- BOOTHROYD A.T., MUKHERJEE A., MURANI A.P. Evidence for extreme gap anisotropy in $\text{Ho}_{0.9}\text{Y}_{0.9}\text{Ba}_2\text{Cu}_3\text{O}_7$ from neutron spectroscopy of Ho^{3+} . *Physical Review Letters* **77**, 1600-1603 (1996)
- BORDET P., LE FLOCH S., CAPPONI J.J., CHAILLOUT C., GORIUS M.E., MAREZIO M., THOLENCE J.L., RADAELLI P.G. Gold substitution in mercury cuprate superconductors. *Physica C* **262**, 151-158 (1996)
- BÖTTGER G., MANGELSCHOTS I., KALDIS E., FISCHER P., KRÜGER C., FAUTH F. The influence of a Ca doping on the crystal structure and superconductivity of orthorhombic $\text{YBa}_2\text{Cu}_3\text{O}_{7-\delta}$. *Journal of Physics Condensed Matter* **8**, 8889-8905 (1996)
- BOUCHARD R., SCHNEIDER J.R., GUPTA S., MES-SOLORAS S., STEWART R.J., NAGASAWA H., ZULEHNER W. Distribution of SiO_2 precipitates in large, oxygen rich Czochralski-grown silicon single crystals after annealing at 750°C . *Journal of Applied Physics* **77**, 553-562 (1995)
- BOUDARD M., BOISSIEU M., DE AUDIER M., KYCIA S., GOLDMAN A.L., HENNION B., BELLISSENT R., QUILICHINI M., JANOT C. Modulated phase and diffuse scattering in the AlPdMn icosahedral phase. In "Proceedings of the Fifth International Conference on Quasicrystals", JANOT C., MOSSERI R. Eds. (World Scientific, 1995) pp. 172-175
- BOUDARD M., BOISSIEU M., DE LETOUBLON A., HENNION B., BELLISSENT R., JANOT C. Phason softening in the AlPdMn icosahedral phase. *Europhysics Letters* **33**, 199-204 (1996)
- BOUQUIERE J.P., FINNEY J.L., SAVAGE H.F.J. High-resolution neutron study of vitamin B_{12} coenzyme at 15K: solvent structure. *Acta Crystallographica B* **50**, 566-578 (1994)
- BOURGES P., REGNAULT L.P., SIDIS Y., BOSSY J., BURLET P., VETTIER C., HENRY J.Y., COUACH M. Spin dynamics by inelastic neutron scattering in YBCO . *Journal of Low-Temperature Physics* **105**, 377-382 (1996)
- BRADEN M., WILKENDORF G., LORENZANA J., AÏN M., MCINTYRE G.J., BEHRUZI M., HEGER G., DHALENNE G., REVCOLEVSKI A. Structural analysis of CuGeO_3 : relation between nuclear structure and magnetic interaction. *Physical Review B* **54**, 1105-1116 (1996)
- BRAMWELL S.T., BUCKLEY A.M., DAY P. The magnetic structure of KNiAsO_4 : a two-dimensional honeycomb lattice. *Journal of Solid State Chemistry* **111**, 48-51 (1994)
- BRION S., DE CHOUTEAU G., LEJAY P., CALEMC-ZUK R., CHAILLOUT C., RADAELLI P.G. Magnetic order in $\text{La}_{1-x}\text{MnO}_3$. *Czechoslovak Journal of Physics* **46**, 2123-2124 (1996)
- BROADBENT R.D., NEILSON G.W. The interatomic structure of argon in water. *Journal of Chemical Physics* **100**, 7543-7547 (1994)
- BROWN C.M., BEER E., BELLAVIA C., CRISTOFOLINI L., GONZALEZ R., HANFLAND M., HÄUSERMANN D., KESHAVARZ-K M., KORDATOS K., PRASSIDES K., WUDL F. Effects of pressure on the azafullerene (C_{50}N_2) molecular solid to 22 GPa. *Journal of the American Chemical Society* **118**, 8715-8716 (1996)
- BROWN C.M., CRISTOFOLINI L., KORDATOS K., PRASSIDES K., BELLAVIA C., GONZALEZ R., KESHAVARZ-K M., WUDL F., CHEETHAM A.K., ZHANG J.P., ANDREONI W., CURIONI A., FITCH A.N., PATTISON P. On the crystal structure of azafullerene (C_{50}N_2). *Chemistry of Materials* **8**, 2548-2550 (1996)
- BROWN P.J. Analysing neutron scattering data with the Cambridge Crystallographic Subroutine Library (CCSL). *Journal of Neutron Research* **4**, 25-32 (1996)
- BROWN P.J. Spin-lattice interactions studied by polarised and unpolarised inelastic scattering application to the invar problem. In "New Instruments and Science around SINQ. Lecture Notes of the 4th Summer School on Neutron Scattering" PSI Proceedings 96-02 (PSI, 1996) pp. 329-345
- BROWN P.J., FORSYTH J.B. The crystal structure and optical activity of tellurium. *Acta Crystallographica A* **52**, 408-412 (1996)
- BROWN P.J., ROESSLI B., SMITH J.G., NEUMANN K.U., ZIEBECK K.R.A. Determination of the wavevector and temperature dependence of the 'forbidden' mode in $\text{Fe}_{65}\text{Ni}_{35}$ Invar using inelastic neutron scattering. *Journal of Physics Condensed Matter* **8**, 1527-1538 (1996)
- BRÜCKEL T., PAULSEN C., HINRICHS K., PRANDL W. Ordering due to disorder in an antiferromagnet with continuously degenerate Néel ground state: a combined neutron diffraction and magnetization study of $(\text{Fe,Ga}_{1-x})_2\text{Ca}_2\text{Ge}_2\text{O}_{12}$. *Zeitschrift für Physik B* **97**, 391-401 (1995)
- BUCHENAU U., PECHARROMAN C., ZORN R., FRICK B. Neutron scattering evidence for localized soft modes in amorphous polymers. *Physical Review Letters* **77**, 659-662 (1996)
- BUCHENAU U., WISCHNEWSKI A., RICHTER D., FRICK B. Is the fast process at the glass transition mainly due to the long wavelength excitations. *Physical Review Letters* **77**, 4035-4038 (1996)
- BUCKLEY A.M., BRAMWELL S.T., DAY P., VISSER D. The magnetic properties and structures of the transition metal pyroarsenates $\text{M}_2\text{As}_2\text{O}_7$ ($\text{M}=\text{Ni}, \text{Co}, \text{Mn}$). *Journal of Solid State Chemistry* **115**, 229-235 (1995)
- BURLET P., BOURGES P., BOSSY J., ELKAIM E., HENRY J.Y., LAURIAT J.P., PLAKHTY V.P., REGNAULT L.P., SCHWEIZER J., SIDIS Y., VETTIER C., YAKHOV F. X-ray and neutron scattering studies of $\text{YBa}_2\text{Cu}_3\text{O}_{6+x}$ compounds: oxygen insertion and spin dynamics. *Journal of Superconductivity* **9**, 357-364 (1996)
- BYCHKOV Y.A., MANIV T., VAGNER I.D. Charged skyrmions: a condensate of spin excitons in a two-dimensional electron gas. *Physical Review B* **53**, 10148-10153 (1996)
- BYRNE J. On the neutron lifetime and the weak coupling constants. *Physica Scripta* **T59**, 311-322 (1995)
- BYRNE J., DAWBER P.G., HABECK C.G., SMIDT S.J., SPAIN J.A., WILLIAMS A.P. A revised value for the neutron lifetime measured using a Penning trap. *Europhysics Letters* **33**, 187-192 (1996)
- CAIGNAERT V., MILLANGE F., HERVIEU M., SUARDE, RAVEAU B. The manganite $\text{Nd}_{0.5}\text{Sr}_{0.5}\text{MnO}_3$: a rare distortion of the perovskite. *Solid State Communications* **99**, 173-177 (1996)

- CAIGNAERT V., SUARD E., MAIGNAN A., SIMON CH., RAVEAU B. Neutron diffraction evidence for an antiferromagnetic ordering in the CMR manganites $\text{Pr}_{1-x}\text{Ca}_x\text{SrMnO}_3$. *Journal of Magnetism and Magnetic Materials* **153**, L260-L264 (1996)
- CANNON R.D. Electron transfer reactions: theory. In "Encyclopedia of Inorganic Chemistry, Vol.3", KING R.B. Ed. (John Wiley & Sons, Inc. 1994) pp. 1098-1111
- CANNON R.D., JAYASOORIYA U.A., WU R., ARAPKOSKE S.K., STRIDE J.A., NIELSEN O.F., WHITE R.P., KEARLEY G.J., SUMMERFIELD D. Spin frustration in high-spin triiron(III) complexes: an inelastic neutron scattering study. *Journal of the American Chemical Society* **116**, 11869-11874 (1994)
- CAO Y., CORMACK A.N., CLARE A.G., BACHRA B., WRIGHT A.C., SINCLAIR R.N., HANNON A.C. Points of contact between theory and experiment: a comparison of molecular dynamics and neutron diffraction results. *Journal of Non-Crystalline Solids* **177**, 317-323 (1994)
- CARLING S.G., DAY P., VISSER D. Crystal and magnetic structures of layer transition metal phosphate hydrates. *Inorganic Chemistry* **34**, 3917-3927 (1995)
- CHAHID A., ALEGRIA A., COLMENERO J. Methyl group dynamics in poly(vinyl methyl ether). A rotation rate distribution model. *Macromolecules* **27**, 3282-3288 (1994)
- CHAHIDA A., MCGREEVY R.L., WICKS J., MUTKA H. Critical narrowing of molten $^{7}\text{Li}_{0.62}\text{Na}_{0.38}$ alloy. *Physica B* **226**, 36-40 (1996)
- CHANG L.J., TOMY C.V., PAUL D. MCK., RITTER C. Magnetic structure of $\text{TmNi}_2\text{B}_2\text{C}$. *Physical Review B* **54**, 9031-9034 (1996)
- CHARVOLIN J. Prolamellar bodies in etioplasts: membrane curvature and five-fold symmetry. In "Proceedings of the Workshop Interplay of Genetic and Physical Processes in the Development of Biological Form", BEYSSENS D. et al. Eds. (World Scientific, 1995) pp. 204-210
- CHATTOPADHYAY T., MCINTYRE G.J., KÖBLER U. Antiferromagnetic phase transition in GdAg . *Solid State Communications* **100**, 117-121 (1996)
- CHRISTENSEN A.N., NORBY P., HANSON J.C. A crystal structure determination of HgC_2O_4 from synchrotron x-ray and neutron powder diffraction data. *Zeitschrift für Kristallographie* **209**, 874-877 (1994)
- CICOGNANI G., CONVERT P., OED A., PANNETIER J. Stability of different microstrip plates on ionic and electronic conducting glass. In "Proceedings of the International Workshop on Micro-Strip Gas Chambers", CONTARDO D., SAULI F. Eds. pp. 235-241
- CIPRIANI F., CASTAGNA J.C., WILKINSON C., OLEINEK P., LEHMANN M.S. Cold neutron protein crystallography using a large position-sensitive detector based on image-plate technology. *Journal of Neutron Research* **4**, 79-85 (1996)
- CLARE A.G., WRIGHT A.C. Neutron scattering studies of glasses containing rare earths. *Key Engineering Materials* **94-95**, 141-160 (1994)
- CLARKE S.M., RENNIE A.R., CONVERT P. A diffraction technique to investigate the orientational alignment of anisotropic particles: studies of clay under flow. *Europhysics Letters* **35**, 233-238 (1996)
- CLEMENTS B.E., GODFRIN H., KROTSCHKE E., LAUTER H.J., LEIDERER P., TYMCZAK C.J. Excitations in a thin liquid ^4He film from inelastic neutron scattering. *Physical Review B* **53**, 12242-12252 (1996)
- CLEMENTS B.E., GODFRIN H., KROTSCHKE E., LAUTER H.J., LEIDERER P., TYMCZAK C.J. Theoretical analysis of neutron scattering spectra of ^4He films on graphite - Rapid Communication. *Journal of Low-Temperature Physics* **102**, 1-9 (1996)
- CLEMENTS B.E., KROTSCHKE E., TYMCZAK C.J. Multiphonon excitations in boson quantum films. *Physical Review B* **53**, 12253-12275 (1996)
- COLDEA R., TENNANT D.A., COWLEY R.A., MCMORROW D.F., DORNER B., TYLCZYNSKI Z. Neutron scattering study of the magnetic structure of $\text{C}_{52}\text{CuCl}_4$. *Journal of Physics Condensed Matter* **8**, 7473-7491 (1996)
- COOPER N.R. Theory of exciton recombination from the magnetically induced Wigner crystal. *Physical Review B* **53**, 10804-10812 (1996)
- COSSY C., HELM L., POWELL D.H., MERBACH A.E. A change in coordination number from nine to eight along the lanthanide(III) aqua ion series in solution: a neutron diffraction study. *New Journal of Chemistry* **19**, 27-35 (1995)
- COSTI T.A., KIEFFER C. Equilibrium dynamics of the dissipative two-state system. *Physical Review Letters* **76**, 1683-1686 (1996)
- COULOMB J.P., LARHER Y., TRABELSI M., MIREBEAU I. Neutron diffraction investigation of the structure of the C_2D_2 film physisorbed upon $\text{MgO}(100)$. *Molecular Physics* **81**, 1259-1264 (1994)
- CRANGLE J., NEUMANN K.U., SMITH J.G., ZAYER N.K., ZIEBECK K.R.A. Magnetic phase diagram of Pd_2DySn . *Journal of Magnetism and Magnetic Materials* **140-144**, 919-920 (1995)
- CRISTOFOLINI L., BROWN C.M., DIANOX A.J., KOSAKA M., PRASSIDES K., TANIGAKI K., VAVEKIS K. Interfullerene vibrations in the polymeric fullerene C_{60} . *Chemical Communications*, 2465-2466 (1996)
- CRISTOFOLINI L., VAVEKIS K., PRASSIDES K., DIANOX A.J., KOSAKA M., HIROSAWA I., TANIGAKI K. Molecular dynamics of C_{60} in superconducting $\text{Na}_2\text{CsC}_{60}$. *Physica B* **226**, 41-45 (1996)
- CROOK M.R., COLES B.R., RITTER C., CYWINSKI R. Magnetic order in $\text{Nb}_{1-x}\text{Zr}_x\text{Fe}_2$. *Journal of Physics Condensed Matter* **8**, 7785-7796 (1996)
- CURRAT R. Incommensurate phase transitions. In "New Instruments and Science around SINQ. Lecture Notes of the 4th Summer School on Neutron Scattering" PSI Proceedings 96-02 (PSI, 1996) pp. 265-292
- DABROWSKI B., WANG Z., ROGACKI K., JORGENSEN J.D., HITTERMAN R.L., WAGNER J.L., HUNTER B.A., RADAELLI P.G., HINKS D.G. Dependence of superconducting transition temperature on doping and structural distortion of the CuO_2 planes in $\text{La}_{2-x}\text{M}_x\text{CuO}_4$ ($\text{M}=\text{Nd, Ca, Sr}$). *Physical Review Letters* **76**, 1348-1351 (1996)
- DE TERESA J.M., IBARRA M.R., BLASCO J., GARCIA J., MARQUINA C., ALGARABEL P.A., ARNOLD Z., KAMENEV K., RITTER C., VON HELMOLT R. Spontaneous behavior and magnetic field and pressure effects on $\text{La}_{2/3}\text{Ca}_{1/3}\text{MnO}_3$ perovskite. *Physical Review B* **54**, 1187-1193 (1996)
- DE TERESA J.M., IBARRA M.R., GARCIA J., BLASCO J., RITTER C., ALGARABEL P.A., MARQUINA C., DEL MORAL A. Spin-glass insulator state in $(\text{Th-La})_{2/3}\text{Ca}_{1/3}\text{MnO}_3$ perovskite. *Physical Review Letters* **76**, 3392-3395 (1996)
- DE TERESA J.M., RITTER C., IBARRA M.R., ARNOLD Z., MARQUINA C., DEL MORAL A. The magnetic phase diagram of $\text{Th}_{1-x}\text{Mn}_x$ intermetallics under pressure using neutron diffraction. *Journal of Physics Condensed Matter* **8**, 8385-8396 (1996)
- DECURTINS S., SCHMALLE H.W., PELLAUX R., HUBER R., FISCHER P., OULADDIAF B. Three-dimensional helical supramolecules - Elucidation of magnetic ordering for an antiferromagnetic phase. *Advanced Materials* **8**, 647-651 (1996)
- DENSCHLAG H.O. Status of independent yield measurements. *Journal of Radioanalytical and Nuclear Chemistry* **203**, 319-329 (1996)
- DESCHAMPS P., ENGSTRÖM P., FIEDLER S., RIEKEL C., WAKATSUKI S., HØGHØJ P., ZIEGLER E. A double multilayer monochromator at an ESRF undulator for microbeam experiments. *Journal of Synchrotron Radiation* **2**, 124-131 (1995)
- DESPLAT J., BLEY F., LIVET F., SCHÄRPF O. Short range order and atomic interactions in Al-7 and 17 at% Zn single crystals. *Acta Materialia* **44**, 1849-1856 (1996)
- DIANOX A.J. Application of neutron scattering to investigate diffusion in porous media. *Journal of Chemical Technology and Biotechnology* **65**, 392-393 (1996)
- DOHERTY D.J., CRANGLE J., NEUMANN K.U., SMITH J.G., ZAYER N.K., ZIEBECK K.R.A. Investigation of the effect of heat treatment on the magnetism in Pd_2MnIn . *Journal of Magnetism and Magnetic Materials* **140-144**, 189-190 (1995)
- DOLINO G., BASTIE P. Phase transitions of quartz (α -incommensurate- β). *Key Engineering Materials* **101-102**, 285-308 (1995)
- DÖNNI A., EHLERS G., MALETTA H., FISCHER P., KITAZAWA H., ZOLLIKER M. Geometrically frustrated magnetic structures of the heavy-fermion compound CePdAl studied by powder neutron diffraction. *Journal of Physics Condensed Matter* **8**, 11213-11229 (1996)
- DORNER B. Excitations. In "Introduction to Neutron Scattering. Lecture Notes 1st European Conference on Neutron Scattering" PSI Proceedings 96-01 (PSI, 1996) pp. 69-85
- DORNER B. Identification of different magnetic modes in CsFeCl_3 by polarisation analysis. In "New Instruments and Science around SINQ. Lecture Notes of the 4th Summer School on Neutron Scattering" PSI Proceedings 96-02 (PSI, 1996) pp. 317-327
- DORNER B. Neutronenspektrometrie. "Proceedings of the 27 IFF 'Streuemethoden zur Untersuchung Kondensierter Materie'", B7.1-B7.18
- DORNER B., SCHMID B., KAKURAI K., PETIT-GRAND D. The phase diagram of RbFeCl_3 in a magnetic field perpendicular to the chain direction. *Canadian Journal of Physics* **73**, 800-804 (1995)
- DOSCH H., LIED A., BILGRAM J.H. Disruption of the hydrogen-bonding network at the surface of I_h ice near surface premelting. *Surface Science* **366**, 43-50 (1996)
- DOSTER W., POST F., SETTLES M. Origins of nonexponential relaxation in proteins. In "Disorder Effects on Relaxational Processes Glasses, Polymers, Proteins", RICHERT R., BLUMEN A. Eds. (Springer Verlag, 1994) pp. 615-625
- DROSSLER H., JOSTARNDT H.D., HARNISCHMACH J., KALENBORN J., WALTER U., SEVERING A., SCHLABITZ W., HOLLAND-MORITZ E. Magnetic interactions between copper and RE in RE $\text{Ba}_2\text{Cu}_3\text{O}_{7-\delta}$. *Zeitschrift für Physik B* **100**, 1-11 (1996)

DUBBERS D. Cold neutrons and the fundamental interaction.
In "Proceedings of the 8th International Symposium on Capture Gamma-Ray Spectroscopy and Related Topics", KERN J. Ed. (World Scientific, 1994) pp. 775-783

DUBBERS D. The neutron, and some basic questions. *Neutron News* **5**, 21-24 (1994)

DUPONT-PAVLOVSKY N., ABDELMOULA M., RAKOTOZAFY S., COULOMB J.P., CROSET B., RES-SOUCHE E. Adsorption on pre-plated graphite: displacement transition for the (krypton-cyclohexane) and (methane-carbon tetrachloride) films. *Surface Science* **317**, 388-396 (1994)

DUX C., VERSMOLD H., REUS V., ZEMB T., LINDNER P. Neutron diffraction from shear ordered colloidal dispersions. *Journal of Chemical Physics* **104**, 6369-6374 (1996)

DZYALOSHINSKII I. Extended Van-Hove singularity and related non-Fermi liquids. *Journal de Physique I* **6**, 119-135 (1996)

EBEL C. Characterisation of the solution structure of halophilic proteins. Analytical centrifugation among complementary techniques (light, neutron and x-ray scattering, density measurements). *Progress in Colloid and Polymer Science* **99**, 17-23 (1995)

ECCLESTON R.S., VRTIS M.L., PALMER S.B., MCINTYRE G.J., FORT D. The multicritical region of the Gd-Lu alloy system. *Journal of Physics Condensed Matter* **8**, 3661-3670 (1996)

ECKERT J., ALBINATI A., BUCHER U.E., VENANZI L.M. Nature of the Rh-H₂ bond in a dihydrogen complex stabilized only by nitrogen donors. Inelastic neutron scattering study of TpMe₂RhH₂(η²-H₂)(TpMe₂=hydrotris(3,5-dimethylpyrazolyl)borate). *Inorganic Chemistry* **35**, 1292-1294 (1996)

ECKERT J., NICOL J.M., HOWARD J., TROUW F.R. Adsorption of hydrogen in Ca-exchanged Na-A zeolites probed by inelastic neutron scattering spectroscopy. *Journal of Physical Chemistry* **100**, 10646-10651 (1996)

EGELHAAF S.U., SCHURTENBERGER P. A fiber-optics-based light scattering instrument for time-resolved simultaneous static and dynamic measurements. *Review of Scientific Instruments* **67**, 540-545 (1996)

ELCOMBE M.M., CAMPBELL S.J., HOWARD C.J., BÜTTNER H.G., AUBERTIN F. The crystal structure of Zr₂NiD₄. *Journal of Alloys and Compounds* **232**, 174-179 (1996)

ENSS C., GAUKLER M., HUNKLINGER S., TORNOW M., WEIS R., WÜRGER A. Low-frequency dielectric susceptibility of Li⁺-doped KCl. *Physical Review B* **53**, 12094-12106 (1996)

ESPESO J.I., GARCIA SOLDEVILLA J., GOMEZ SAL J.C., REIFFERS M., BLANCO J.A. Kondo behavior in CeNi_{0.4}Cu_{0.6}. *Journal of Applied Physics* **79**, 6352-6354 (1996)

EWEN B., MASCHKE U., RICHTER D., FARAGO B. Neutron spin echo studies on the segmental diffusion behavior in the different chain sections of high molecular weight poly(dimethylsiloxane) melts. *Acta Polymerica* **45**, 143-147 (1994)

EWEN B., RICHTER D. The dynamics of polymer melts as seen by neutron spin echo spectroscopy. *Makromolekulare Chemie. Macromolecular Symposia* **90**, 131-149 (1995)

EWEN B., RICHTER D., FARAGO B., STUEHN B. Neutron spin echo investigations on the segmental dynamics in semidilute polymer solutions under Θ and good solvent conditions. *Journal of Non-Crystalline Solids* **172-174**, 1023-1027 (1994)

EZEILO A.N., WEBSTER P.S., WEBSTER G.A., WEBSTER P.J. Influence of cyclic loading on residual stress distribution caused by cold hole expansion. In "Proceedings of the 4th International Conference on Residual Stress" (1994) pp. 1275-1284

FARAGO B. Spin echo studies of microemulsions. *Physica B* **226**, 51-55 (1996)

FARAGO B. Static and dynamic neutron x-ray scattering. *Current Opinion in Colloid and Interface Science* **1**, 17-22 (1996)

FATHALLAH R., CAO W., CASTEX L., WEBSTER P.S., EZEILO A.N., WEBSTER G.A., WEBSTER P.J. Comparison of residual stresses determined by x-ray diffraction, neutron diffraction and the hole drilling method in aerospace shot peened materials. In "Proceedings of the 4th International Conference on Residual Stress" (1994) pp. 834-843

FAYOS R., BERMEJO F.J., DAWIDOWSKI J., FISCHER H.E., GONZALEZ M.A. Direct experimental evidence of the relationship between intermediate-range order in topologically disordered matter and discernible features in the static structure factor. *Physical Review Letters* **77**, 3823-3826 (1996)

FERNANDEZ BARQUIN L., BARANDIARAN J.M., TELLERIA I., GOMEZ SAL J.C. Evolution of the electrical resistivity during the crystallization of Co-Si-B glasses. *Physica Status Solidi (a)* **155**, 439-450 (1996)

FILLAUX F., KEARLEY G.J., CARLILE C.J. Inelastic neutron scattering study of isotopic mixtures of lithium acetate with partially deuterated CH₂D groups and sine-Gordon dynamics. *Physica B* **226**, 241-243 (1996)

FISCHER H.E., FISCHER H., DURAND O., PELLEGRINO O., ANDRIEU S., PIECUCH M., LEFEBVRE S., BESSIERE M. Specular and off-specular anomalous x-ray scattering as quantitative structural probes of multilayers. *Nuclear Instruments and Methods in Physics Research B* **97**, 402-406 (1995)

FISCHER H.E., PETROFF F., BELJEN P., LEQUIEN S., VERBANCK G., BRUYNSERAEDY, LEFEBVRE S., BESSIERE M. Interfacial structure and giant magnetoresistance in Fe/Cr superlattices. *Journal de Physique IV* **4**, C9/121-C9/125 (1994)

FITTER J., LECHNER R.E., BÜLDT G., DENCHER N.A. Temperature dependence of molecular motions in the membrane protein bacteriorhodopsin from QINS. *Physica B* **226**, 61-65 (1996)

FLEISCHER G., FUJARA F. NMR as a generalized incoherent scattering experiment. In "NMR basic principles and progress. Vol.30", DIEHL P. et al. Eds. (Springer Verlag, 1994) pp. 161-207

FORET M., COURTENS E., VACHER R., SUCK J.B. Scattering investigation of acoustic localization in fused silica. *Physical Review Letters* **77**, 3831-3834 (1996)

FÖRSTER S., WENZ E., LINDNER P. Density profile of spherical polymer brushes. *Physical Review Letters* **77**, 95-98 (1996)

FORSYTH J.B., WILKINSON C. The spatial distribution of magnetization in cobalt tungstate, CoWO₄. *Journal of Physics Condensed Matter* **6**, 3073-3080 (1994)

FRIEDRICH H., GRIEGER S., GUCKELSBERGER K., SCHERM R., PRESS W. Measurement of total cross-section and spin conversion in solid methane. *Physica B* **226**, 218-220 (1996)

FUESS H. Neutron scattering, neutron diffraction: hydrogen location, cation distribution, magnetic structures.

In "Advanced Mineralogy 2: Methods and Instrumentations", MARFUNIN V. Ed. (Springer Verlag, 1995) pp. 38-49

FULTON S., NAGLER S.E., NEEDHAM L.M.N., WANKLYN B.M. Spin waves and temperature-dependent behaviour of the quasi-two-dimensional antiferromagnet KFeF₄. *Journal of Physics Condensed Matter* **6**, 6667-6678 (1994)

GABRYS B. Long history of short-range order in polymers. *Trends in Polymer Science* **2**, 2-4 (1994)

GABRYS B. Quasi-elastic and inelastic neutron scattering from polymers. In "Scattering Methods in Polymer Science", RICHARDS R.W. Ed. (Ellis Horwood, 1995) pp. 153-192

GARCIA-LANDA B., IBARRA M.R., ALGARABEL P.A., MOZE O. Crystal-electric-field interaction in R₂Zn₁₇ intermetallics. *Physical Review B* **51**, 15132-15145 (1995)

GARCIA-MUNOZ J.L., CYWINSKI R., KILCOYNE S.H., OBRADORS X. Magnetic order and disorder in YBa₂(Cu_{1-x}Fe_x)₂O_{6.45}. *Physica C* **233**, 85-96 (1994)

GEISSLER E., HORKAY F., HECHT A.M. Structure and thermodynamics of flexible polymer gels. *Journal of Chemical Physics* **100**, 8418-8424 (1994)

GIBBS M.R., STIRLING W.G., ANDERSEN K.H., AZUAH R.T., SCHÖBER H., DIANOUX A.J. Temperature dependence of the collective excitations of liquid ⁴He at high pressure. *Journal of Physics Condensed Matter* **8**, 9417-9422 (1996)

GIBSON B.J., KREMER R.K., SCHNELLE W., OULADDIAF B., PÖTTGEN R. Antiferromagnetic ordering of HoAuGe. *Czechoslovak Journal of Physics* **46**, 2113-2114 (1996)

GIRARD P., GUILLAUME F., DIANOUX A.J. Molecular dynamics of guest molecules in the channels of urea inclusion compounds investigated by means of IQNS spectroscopy. *Physica B* **226**, 66-71 (1996)

GLYDE H.R. Deep inelastic neutron scattering and momentum distributions in quantum liquids. *Physica B* **194-196**, 505-506 (1994)

GLYDE H.R. Quasiparticle excitations, Bose condensation, and the f-sum rule. *Physical Review Letters* **75**, 4238-4241 (1995)

GOLDBERG M.E., EXPERT-BEZANCON N., VUILLARD L., RABILLOU T. Non-detergent sulphotetaines: a new class of molecules that facilitate *in vitro* protein renaturation. *Folding and Design* **1**, 21-27 (1995)

GOMEZ SAL J.C., BLANCO J.A., ESPESO J.I., RODRIGUEZ FERNANDEZ J., GIGNOUX D. Enhancement of the localized behavior in CeNi_{0.8}Pt_{0.2} Kondo compound replacing Ce by magnetic ions (Pr,Nd). *Journal of Applied Physics* **76**, 6118-6120 (1994)

GRADZIELSKI M., LANGEVIN D., FARAGO B. Experimental investigation of the structure of nonionic microemulsions and their relation to the bending elasticity of the amphiphilic film. *Physical Review E* **53**, 3900-3919 (1996)

GÜDEL H.U. Magnetic excitations in polynuclear transition metal complexes. In "Proceedings of the Third Summer School on Neutron Scattering. Magnetic Neutron Scattering", FURRER A. Ed. (World Scientific, 1995) pp. 191-200

GÜDEL H.U. Magnetic excitations in transition metal and rare earth metal dimers. *Neutron News* **7**, 24-28 (1996)

- GUILLAUME F. Helical motions of aliphatic chains in molecular crystals. The incoherent quasi-elastic neutron scattering law. *Molecular Physics* **81**, 1411-1423 (1994)
- GUTMANN M., ALLENSPACH P., FAUTH F., FURRER A., HEWAT A.W., ROSENKRANZ S. Neutron investigation of $\text{Nd}_{2-x}\text{Ce}_x\text{La}_y\text{CuO}_4$ ($0 \leq x \leq 0.2$; $y = 0.5, 1$). *Journal of Low-Temperature Physics* **105**, 1487-1492 (1996)
- GUY C.A., WRIGHT A.C., SINCLAIR R.N., STEWART R.J., JANSEN F. A small angle neutron scattering (SANS) study of hydrogen in hydrogenated amorphous silicon. *Journal of Non-Crystalline Solids* **196**, 260-266 (1996)
- GUZIK A., KACZMARSKA K., PIERRE J., MURANI A.P. Spin dynamics in some cerium ternary stannides and antimonides. *Journal of Magnetism and Magnetic Materials* **161**, 103-110 (1996)
- GUZIK A., PIERRE J., KACZMARSKA K., LAMBERT-ANDRON B., OULADDIAF B. Kondo properties of the new compounds $\text{Ce}(\text{Ag}_x\text{Cu}_{1-x})_2\text{Sb}_2$. *Journal of Magnetism and Magnetic Materials* **157-158**, 683-684 (1996)
- HAEN P., MALLMANN F., BESNUS M.J., KAPPLER J.P., BOURDAROT F., BURLET P., FUKUHARA T. Antiferromagnetism and ferromagnetism in $(\text{CeRu}_2\text{Si}_{1-x}\text{Ge}_x)_2$. *Journal of the Physical Society of Japan* **65**, 16-26 (1996)
- HANNON A.C., GRIMLEY D.I., HULME R.A., WRIGHT A.C., SINCLAIR R.N. Boroxol groups in vitreous boron oxide: new evidence from neutron diffraction and inelastic neutron scattering studies. *Journal of Non-Crystalline Solids* **177**, 299-316 (1994)
- HAUER B., HEMPELMANN R., RICHTER D., UDOVIC T.J., RUSH J.J., BENNINGTON S.M., DIANOUX A.J. Ground state and excited state hydrogen tunnelling in $\text{Nb}_{1-x}\text{Ti}_x\text{H}_x$. *Physica B* **226**, 210-212 (1996)
- HAUSS T., BÜLDT G., HEYN M.P., DENCHER N.A. Light-induced isomerization causes an increase in the chromophore tilt in the M intermediate of bacteriorhodopsin: a neutron diffraction study. *Proceedings of the National Academy of Science of the USA* **91**, 11854-11858 (1994)
- HEID C., WEITZEL H., BOURDAROT F., CALEMC-ZUK R., VOGT T., FUESS H. Magnetism in FeNb_2O_6 and NiNb_2O_6 . *Journal of Physics Condensed Matter* **8**, 10609-10625 (1996)
- HELLIWELL J.R., WILKINSON C. X-ray and neutron Laue diffraction. In "Neutron and Synchrotron Radiation for Condensed Matter and Biology - HERCULES. Higher European Research Course for Users of Large Experimental Systems. Vol.3", BARUCHEL J. et al. Eds. (Les Editions de Physique, 1994) pp. 201-219
- HELM L., FOGLIA F., KOWALL T., MERBACH A.E. Structure and dynamics of lanthanide ions and lanthanide complexes in solution. *Journal of Physics Condensed Matter* **6**, A137-A140 (1994)
- HENGGELE W., CHATTOPADHYAY T., ROESSLI B., ZHIGUNOV D.I., BARILO S.N., FURRER A. Dispersion of the $\Gamma^{(1)}_6$ - $\Gamma^{(2)}_6$ Nd crystal field excitation in Nd_2CuO_4 (Rapid Notes). *Zeitschrift für Physik B* **99**, 465-467 (1996)
- HENGGELE W., CHATTOPADHYAY T., THALMEIER P., RÖSSLER B., VORDERWISCH P., FURRER A. Magnetic excitations of Nd in Nd_2CuO_4 . *Swiss Neutron News* **9**, 15-22 (1996)
- HENGGELE W., CHATTOPADHYAY T., THALMEIER P., VORDERWISCH P., FURRER A. Spin wave excitations of Nd in Nd_2CuO_4 . *Europhysics Letters* **34**, 537-542 (1996)
- HENSEL F., HOHL G.F., PILGRIM W.C., WINTER R. Metal-nonmetal transition and the dynamic structure factor of expanded fluid metals. *AIP Conference Proceedings* **309**, 237-240 (1994)
- HEWAT A.W. Crystals, counters and computers - New tools for powder diffraction. *Journal of Neutron Research* **4**, 167-173 (1996)
- HILY L., DUPUY J., JAL J.F., CHIEUX P. From an extended ionic ordering in the pure molten salt KCl to a new and localized ionic ordering in the $\text{K}_{0.3}(\text{KCl})_{0.7}$ mixture. A neutron scattering investigation. *Revue Internationale des Hautes Températures et des Réfractaires* **29**, 1-9 (1994)
- HLINKA J., QUILICHINI M., CURRAT R., LEGRAND J.F. Dynamical properties of the normal phase of betaine calcium chloride dihydrate. II. A semimicroscopic model. *Journal of Physics Condensed Matter* **8**, 8221-8250 (1996)
- HLINKA J., QUILICHINI M., CURRAT R., LEGRAND J.F. Dynamical properties of the normal phase of betaine calcium chloride dihydrate. I. Experimental results. *Journal of Physics Condensed Matter* **8**, 8207-8219 (1996)
- HOCHARD F., JOBIC H., MASSARDIER J., RENOU-PREZ A.J. Gas phase hydrogenation of acetonitrile on Raney nickel catalysts: reactive hydrogen. *Journal of Molecular Catalysis A: Chemical* **95**, 165-172 (1995)
- HOFF R.W., BÖRNER H.G., SCHRECKENBACH K., COLVIN G.G., HOYLER F., SCHAUER W., VON EGIDY T., GEORGI R., OTT J., SCHRÜNDER S., CASTEN R.F., GILL R.L., BALODIS M.K., PROKOFJEVS P., SIMONOVA L., KERN J., KHITROV V.A., SUKHOVOJ A.M., BERSILLON O., JOLY S., GRAW G., HOFER D., VALNION B. Nuclear structure of ^{170}Tm from neutron-capture and (d,p)-reaction measurements. *Physical Review C* **54**, 78-116 (1996)
- HOFSTÄTTER G., PRANDL W., BRÜCKEL T., HILLER W. X-ray and neutron investigation of the structure and disorder in dicalcium barium acrylate. *Acta Crystallographica B* **50**, 448-455 (1994)
- HORDEQUIN C., PIERRE J., CURRAT R. Magnetic excitations in the half-metallic NiMnSb ferromagnet: from Heisenberg-type to itinerant behaviour. *Journal of Magnetism and Magnetic Materials* **162**, 75-84 (1996)
- HOWELL I., NEILSON G.W. Li^+ hydration in concentrated aqueous solution. *Journal of Physics Condensed Matter* **8**, 4455-4463 (1996)
- HOWELL I., NEILSON G.W. The coordination of Ni^{2+} in aqueous solution at elevated temperature and pressure. *Journal of Chemical Physics* **104**, 2036-2042 (1996)
- HOWELLS W.S. The use of Fourier transforms in the analysis of QENS data. *Physica B* **226**, 78-81 (1996)
- HUANG B., FAUTH F., YVON K. Trigonal $\text{Ba}_7\text{Cu}_3\text{H}_{17}$ containing tetrahedral $[\text{Cu}(\text{I})\text{H}_4]^{3-}$ anions. *Journal of Alloys and Compounds* **244**, L1-L4 (1996)
- HUSSAIN A.M., JOENSEN K.D., HØGHØJ P., CHRISTENSEN F.E., LOUIS E., VOORMA H.J., SOONG Y., WHITE N., SERLEMITOS P.J., ANDERSON I. The deposition and characterization of multilayers on thin foil x-ray mirrors for high throughput x-ray telescopes. *Proceedings SPIE* **2805**, 336-342 (1996)
- HUXLEY A., CUBITT R., MCPAUL D., FORGAN E.M., NUTLEY M.P., MOOK H., YETHIRAJ M., LEJAY P., CAPLAN D., PENISSON J.M. A neutron study of the flux lattice in the superconductor CeRu_2 . *Physica B* **223-224**, 169-171 (1996)
- JACOBS W.P.J.H., VAN WOLPUT J.H.M.C., VAN SANTEN R.A., JOBIC H. A vibrational study of the OH and OD bending modes of the Brønsted acid sites in zeolites. *Zeolites* **14**, 117-125 (1994)
- JANOT C. Conductivity in quasicrystals via hierarchically variable-range hopping. *Physical Review B* **53**, 181-191 (1996)
- JANOT C. The properties and applications of quasicrystals. *Europhysics News* **27**, 60-64 (1996)
- JANOT C., BOISSIEU M. DE. Vibrations in quasicrystals: hierarchies and localization. *Physica B* **219-220**, 328-331 (1996)
- JAYASOORIYA U.A., KETTLE S.F.A., MAHASUVE-RACHA S., WHITE R.P. Lattice vibrations in compounds crystallising with the baryte structure. *Journal of the Chemical Society Faraday Transactions* **92**, 3625-3628 (1996)
- JENSEN J., LEASK M.J.M., WELLS M.R., WARD R.C.C., HAYDEN S.M., RAMIREZ A.P. Magnetic properties of the dipole-coupled singlet-singlet system HoF_3 . *Journal of Magnetism and Magnetic Materials* **140-144**, 1191-1192 (1995)
- JENTSCH M., HEINIG K.H., BÖRNER H.G., JOLIE J., KESSLER E.G. Atomic collision cascades studied with the crystal-GRID method. *Nuclear Instruments and Methods in Physics Research B* **115**, 446-451 (1996)
- JOANICOT M., WONG K., CABANE B. Interdiffusion in cellular latex films. *Macromolecules* **29**, 4976-4984 (1996)
- JOBIC H. Applications of neutron scattering to catalysis. In "Catalyst Characterization - Physical Techniques for Solid Materials", IMELIK B., VEDRINE C. Eds. (Plenum Press, 1994) pp. 347-375
- JOBIC H., BEE M. Quasi-elastic neutron scattering study of the dynamics of methane adsorbed in Na-mordenite. *Zeitschrift für Physikalische Chemie* **189**, 179-186 (1995)
- JOBIC H., BEE M., KARGER J., VARTAPETIAN R.S., BALZER C., JULBE A. Mobility of cyclohexane in a microporous silica sample: a quasi-elastic neutron scattering and NMR pulsed-field gradient technique study. *Journal of Membrane Science* **108**, 71-78 (1995)
- JOBIC H., BEE M., KARGER J., BALZER C., JULBE A. Measurement of the diffusivity of benzene in microporous silica by quasi-elastic neutron scattering and NMR pulsed-field gradient technique. *Adsorption* **1**, 197-201 (1995)
- JOHNSON M.R., FRICK B., TROMMSDORFF H.P. A high resolution, inelastic neutron scattering investigation of tunnelling methyl groups in aspirin. *Chemical Physics Letters* **258**, 187-193 (1996)
- JOHNSON M.R., TROMMSDORFF H.P. Rotational tunnelling studied by optical hole burning at high pressure. *Physica B* **226**, 194-198 (1996)
- JONES M.J., GUILLAUME F., HARRIS K.D.M., DIANOUX A.J. Molecular dynamics of tetrakis(trimethylsilyl)silane in the solid state: an incoherent quasi-elastic neutron scattering investigation. *Proceedings of the Royal Society of London A* **452**, 701-714 (1996)
- KAGUNYA W.W. Properties of water adsorbed in anionic clays: a neutron scattering study. *Journal of Physical Chemistry* **100**, 327-330 (1996)
- KAKURAI K., SAKAGUCHI T., NISHI M., ZEYEN C.M.E., KASHIDA S., YAMADA Y. Dynamics of the strain-mediated phase transition in KDCO_3 : a thermal neutron spin-echo study. *Physical Review B* **53**, R5974-R5977 (1996)

- KARAMIAN S.A. Nuclear reactions with high-spin targets. *Acta Physica Polonica A* **26**, 375-381 (1995)
- KEARLEY G.J., BÜTTNER H.G., FILLAUX F., LAUTIE M.F. NH_3 free rotors in Hofmann clathrates. *Physica B* **226**, 199-201 (1996)
- KEARLEY G.J., NICOLAI B., RADAELLI P.G., FILLAUX F. The crystal structure and methyl group dynamics in the room-temperature and low-temperature phases of lithium acetate dihydrate. *Journal of Solid State Chemistry* **126**, 184-188 (1996)
- KHANNA S.N., JANOT C., CYROT-LACKMANN F. Clusters and aggregates: application to quasicrystals. In "Proceedings of the Fifth International Conference on Quasicrystals", JANOT C., MOSSERI R. Eds. (World Scientific, 1995) pp. 401-407
- KHASANOVA N.R., IZUMI F., TAKAYAMA-MURAMACHI E., HEWAT A.W. Crystal structure of the superconductor $\text{Ca}_2\text{Sr}_2\text{Cu}_3\text{GaO}_9$ synthesized at high pressure. *Physica C* **258**, 227-235 (1996)
- KOSTORZ G. Alloy studies with x-rays and neutrons. *Zeitschrift für Metallkunde* **87**, 326-331 (1996)
- KOSTORZ G. Alloys studied with scattering techniques - Invited paper. In "Euromat '94 Topical - Vol. I", VORSATZAND B., SZÖLKE E. Eds. (1994) pp. 21-32
- KOSTORZ G. Decomposition in alloys - Some recent experiments. In "Solid - Solid Phase Transformations", JOHNSON W.C. et al. Eds. (TMS. Minerals-Metals-Materials Society, 1994) pp. 133-152
- KOSTORZ G. Metals and alloys: phase separation and defect agglomeration. In "Modern Aspects of Small-Angle Scattering", BRUMBERGER H. Ed. (Kluwer Academic Publishers, 1995) pp. 255-266
- KOSTORZ G. X-ray and neutron scattering studies of alloys. *Ciencia & Tecnologia dos Materiais* **7**, 13-17 (1995)
- KOSTORZ G. X-ray and neutron scattering. In "Physical Metallurgy: Fourth. Revised and Enhanced Edition", CAHN R.W., HAASEN P. Eds. (North Holland, 1996) pp. 1115-1199
- KRÄMER K., ROMSTEDT H., GÜDEL H.U., FISCHER P., MURASIK A., FERNÁNDEZ-DÍAZ M.T. Three dimensional magnetic structure of ErF_3 . *European Journal of Solid State & Inorganic Chemistry* **33**, 273-283 (1996)
- KUHS W.F., ARCHER J., DORAN D. A closed-shell furnace for neutron single-crystal diffraction - Short communications. *Journal of Applied Crystallography* **26**, 730-733 (1993)
- KULDA J., DORNER B., RÖSSLER B., STERNER H., BAUER R., MAY T., KARCH K., PAVONE P., STRAUCH D. A neutron-scattering study of the over-bending of the [100] LO phonon mode in diamond. *Solid State Communications* **99**, 799-802 (1996)
- KULDA J., SAROUN J. Elastically bent silicon monochromator and analyzer on a TAS instrument. *Nuclear Instruments and Methods in Physics Research A* **379**, 155-166 (1996)
- LAMOREAUX S.K. Ultracold neutrons in superfluid ^4He and $n-\bar{n}$ oscillations: complementarity of cold neutron technology. Proceedings of the « International Workshop on Future Prospects of Baryon Instability Search in p-Decay and $n \rightarrow \bar{n}$ Oscillation Experiments », Ball S.J., Kamyshev Y.A. Eds. (1996) pp. 337-344 (ORNL-6910).
- LANGAN P., DENNY R.C., MAHENDRASINGAM A., MASON S.A., JABER A. Collecting and processing neutron fibre diffraction data from a single-crystal diffractometer. *Journal of Applied Crystallography* **29**, 383-389 (1996)
- LANGAN P., FORSYTH V.T., MAHENDRASINGAM A. Attenuation corrections for x-ray and neutron fibre diffraction studies - Short communications. *Journal of Applied Crystallography* **28**, 49-52 (1995)
- LAPPAS A., PRASSIDES K. Layered cuprates with the T^* structure: structural and conducting properties. *Journal of Solid State Chemistry* **115**, 332-346 (1995)
- LAPPAS A., PRASSIDES K. Magnetic structure of $\text{La}_{1-x}\text{Tb}_x\text{CuO}_4$. *Journal of the Chemical Society Faraday Transactions* **92**, 2151-2153 (1996)
- LARESE J.Z., ASMUSSEN B., ADAMS M.A., CARLILE C.J., MARTIN D., FERRAND M. Rotational tunneling studies of methane films adsorbed on MgO : crossover from two-to-three dimensions? *Physica B* **226**, 221-223 (1996)
- LARTIGUE C., COPLEY J.R.D., MEZEI F., SPRINGER T. Focusing of neutron beams using curved mirrors for small angle scattering. *Journal of Neutron Research* **5**, 71-79 (1996)
- LATROCHE M., PERCHERON-GUEGAN A., CHABREY, BOUET J., PANNETIER J. In situ neutron diffraction study of $\text{LaNi}_{4.5}\text{Mn}_{0.5}$ electrode during electrochemical cyclings. *Progress in Batteries & Battery Materials* **13**, (1994) pp. 225-232
- LAUTENSCHLÄGER G., WEITZEL H., FUESS H., RESSOUCHE E. The magnetic structure of $\alpha\text{-MnMoO}_4$. *Zeitschrift für Kristallographie* **209**, 936-940 (1994)
- LE BAIL A. Modelling the silica glass structure by the Rietveld method. *Journal of Non-Crystalline Solids* **183**, 39-42 (1995)
- LE BAIL A., MARCOS M.D., AMOROS P. Ab initio crystal structure determination of $\text{VO}(\text{H}_2\text{PO}_4)_2 \cdot \text{H}_2\text{O}$ from x-ray and neutron powder diffraction data. A monodimensional vanadium(IV) hypophosphate. *Inorganic Chemistry* **33**, 2607-2613 (1994)
- LEASK M.J.M., WELLS M.R., WARD R.C.C., HAYDEN S.M., JENSEN J. Magnetic excitations in the dipole-coupled singlet-singlet system HoF_3 . *Journal of Physics Condensed Matter* **6**, 505-522 (1994)
- LECHNER R.E. Neutron investigations of superprotonic conductors. *Ferroelectrics* **167**, 83-98 (1995)
- LECHNER R.E. Structural aspects of diffusive proton motion in some complex systems. In "Proceedings of the Quasielastic Neutron Scattering Workshop QENS'93. Quasielastic Neutron Scattering. Future Prospects on High-Resolution Inelastic Neutron Scattering", COLMENERO J. et al. Eds. (World Scientific, 1994) pp. 62-91
- LI J.C., ROSS D.K. Dynamical scaling for spinodal decomposition - A small-angle neutron scattering study of porous Vycor glass with fractal properties. *Journal of Physics Condensed Matter* **6**, 351-362 (1994)
- LI J.C., ROSS D.K., HOWE L.D., STEFANOPOULOS K.L., FAIRCLOUGH J.P.A., HEENAN R., IBEL K. Small-angle neutron-scattering studies of the fractal-like network formed during desorption and adsorption of water in porous materials. *Physical Review B* **49**, 5911-5917 (1994)
- LINE C.M.B., DOVE M.T., KNIGHT K.S., WINKLER B. The low-temperature behaviour of analcime. I: High-resolution neutron powder diffraction. *Mineralogical Magazine* **60**, 499-507 (1996)
- LINE C.M.B., WHITWORTH R.W. A high resolution neutron powder diffraction study of D_2O ice XI. *Journal of Chemical Physics* **104**, 10008-10013 (1996)
- LOEWENHAUPT M., FABI P., HORN S., AKEN P.V., SEVERING A. Low-energy magnetic excitations in $\text{Nd}_{2-x}\text{Ce}_x\text{CuO}_4$. *Journal of Magnetism and Magnetic Materials* **140-144**, 1293-1294 (1995)
- LOEWENHAUPT M., METZ A., PYKA N.M., PAUL D. MCK., MARTIN J., DUUN V.H.M., FRANSE J.J.M., MUTKA H., SCHMIDT W. High resolution neutron scattering study of low-energy magnetic excitations in $\text{Nd}_{2-x}\text{Ce}_x\text{CuO}_4$. *Annalen der Physik* **5**, 197-202 (1996)
- LORENZO J.E., CURRAT R., DIANOUX A.J., MONCEAU P., LEVY F. Phonon density of states and low-temperature specific heat of quasi-one-dimensional $(\text{TaSe}_4)_2\text{I}$ and $(\text{NbSe}_4)_2\text{I}$. *Physical Review B* **53**, 8316-8322 (1996)
- LOSILLA E.R., ARANDA M.A.G., BRUQUE S. Structural features of the reactive sites in $\alpha\text{-M}(\text{DPO}_4)_2 \cdot \text{D}_2\text{O}$ ($\text{M}=\text{Ti, Zr, Pb}$): hydrogen-bond network and framework. *Journal of Solid State Chemistry* **125**, 261-269 (1996)
- LOUREIRO S.M., RADAELLI P.G., ANTIPOV E.V., CAPPONI J.J., SOULETIE B., BRUNNER M., MAREZIO M. The replacement of $[\text{HgO}_3]^{2-}$ by the tetrahedral sulfate anion $[\text{SO}_4]^{2-}$ in the Hg-1201 superconductor. *Journal of Solid State Chemistry* **121**, 66-73 (1996)
- LUTZ H.D., BECKENKAMP K., KELLERSOHN T., MÖLLER H., PETER S. Neutron and x-ray structure determination of laurionite-type $\text{Pb}[\text{O}(\text{H,D})\text{X}]$, with $\text{X}=\text{Cl, Br, I}$. hydrogen bonds to lead(II) ions as a hydrogen-bond acceptor. *Journal of Solid State Chemistry* **124**, 155-161 (1996)
- LUTZ H.D., SCHNEIDER M., WICKEL C. Neutron powder diffraction on monoclinic Li_2CrCl_4 . *Zeitschrift für Kristallographie* **211**, 8-12 (1996)
- MAGERL A. Neutron optics with gradient crystals. *Journal of Neutron Research* **5**, 41-49 (1996)
- MAGLI R., BAROCCHI F., CHIEUX P., FONTANA R. Experimental determination of the long-range potential of argon pairs by means of small-angle neutron diffraction. *Physical Review Letters* **77**, 846-848 (1996)
- MANDAL J.B., BANDYOPADHYAY B., FAUTH F., CHATTOPADHYAY T., GHOSH B. A new mercury-based high-Tc cuprate $\text{Hg}_{0.7}\text{V}_{0.3}\text{Sr}_{2-x}\text{La}_x\text{CuO}_{4+\delta}$. *Physica C* **264**, 145-153 (1996)
- MARET M., LANCON F., BILLARD L. Local symmetries in liquid $\text{Al}_{60}\text{Mn}_{40}$ and $\text{Al}_{71}\text{Pd}_{19}\text{Mn}_{10}$ alloys. *Journal of Physics Condensed Matter* **6**, 5791-5804 (1994)
- MARTIN C., COULOMB J.P., FERRAND M. Direct measurement of the translational mobility of deuterium hydride molecules confined in a model microporous material: $\text{AlPO}_4\text{-5}$ zeolite. *Europhysics Letters* **36**, 503-508 (1996)
- MARTIN T. On the path integral approach to the tunneling time. *International Journal of Modern Physics B* **10**, 3747-3763 (1996)
- MARTIN T. Wave packet approach to noise in N-S junctions. *Physics Letters A* **220**, 137-142 (1996)
- MAYERHOFER U., VON EGIDY T., KLORA J., LINDNER H., BÖRNER H.G., JUDGE S., KRUSCHE B., ROBINSON S., SCHRECKENBACH K., SUKHVOJ A.M., KHITROV V.A., BONEVA S.T., PAAR V., BRANT S., PEZER R. The nucleus ^{198}Au investigated with neutron capture and transfer reactions. I. Experiments and evaluation. *Fizika B* **5**, 167-198 (1996)

- MENDES E., OESER R., HAYES C., BOUE F., BAS-TIDE J. Small-angle neutron scattering study of swollen elongated gels: butterfly patterns. *Macromolecules* **29**, 5574-5584 (1996)
- MERCURIO D., CHAMPARNAUD-MESJARD J.C., FRIT B., CONFLANT P., BOIVIN J.C., VOGT T. Thermal evolution of the crystal structure of the rhombohedral $\text{Bi}_{0.75}\text{Sr}_{0.25}\text{O}_{1.375}$ phase: a single crystal neutron diffraction study. *Journal of Solid State Chemistry* **112**, 1-8 (1994)
- MERMET A., SUROVTSEV N.V., DUVAL E., JAL J.F., DUPUY-PHILON J., DIANOUX A.J. Inelastic neutron and Raman scattering of poly(methyl methacrylate): nanostructure of polymer glasses. *Europhysics Letters* **36**, 277-282 (1996)
- MEYER A., WUTTKE J., PETRY W., PEKER A., BOR-MANN R., CODDENS G., KRANICH L., RANDL O.G., SCHOBER H. Harmonic behavior of metallic glasses up to the metastable melt. *Physical Review B* **53**, 12107-12111 (1996)
- MICHEL A., PIERRON-BOHNE S., LEFEBVRE S., BESSIERE M., FISCHER H.E. Stabilization of the fcc Co structure in Co/Mn multilayers with very thin Mn layers. *Journal of Magnetism and Magnetic Materials* **156**, 23-24 (1996)
- MICHEL C., LETOUZE F., MARTIN C., HERVIEU M., RAVEAU B. Neutron diffraction structure determination of the superconducting copper oxychromate $\text{Ti}_3(\text{CrO}_4)\text{Sr}_2\text{Cu}_2\text{O}_{16}$. *Physica C* **262**, 159-167 (1996)
- MIDDENDORF H.D. Neutron studies of the dynamics of biological water. *Physica B* **226**, 113-127 (1996)
- MILAS M., LINDNER P., RINAUDO M., BORSALI R. Influence of the shear rate on the small-angle neutron scattering pattern of polyelectrolyte solutions: the xanthan example. *Macromolecules* **29**, 473-474 (1996)
- MILLANGE F., CAIGNAERT V., MATHER G., SUARD E., RAVEAU B. Low temperature orthorhombic to monoclinic transition due to size effect in $\text{Nd}_{0.7}\text{Ca}_{0.3-x}\text{Sr}_x\text{MnO}_3$: evidence for a new type of charge ordering (Letter to the editor). *Journal of Solid State Chemistry* **127**, 131-135 (1996)
- MÖLLER H., BECKENKAMP K., KELLERSOHN T., LUTZ H.D., COCKCROFT J.K. Bestimmung der Strukturen von $\text{Ba}(\text{OH})\text{Cl}$, $\text{Ba}(\text{OD})\text{Cl}$ und $\text{Ba}(\text{OD})\text{Br}$ durch Röntgengestrichen- und Neutronenpulver-Messungen. *Zeitschrift für Kristallographie* **209**, 157-161 (1994)
- MURANI A.P., ECCLESTON R.S. High-energy paramagnetic spectral response of CeNi_2 . *Physical Review B* **53**, 48-51 (1996)
- MURANI A.P., RAPHEL R., BOWDEN Z.A., ECCLESTON R.S. Kondo resonance energies in CePd_3 . *Physical Review B* **53**, 8188-8191 (1996)
- MURANI A.P., SEVERING A., MARSHALL W.G. Paramagnetic spectral response of CePd_3 : a comparative investigation of neutron inelastic scattering from single-crystal and polycrystalline samples. *Physical Review B* **53**, 2641-2650 (1996)
- MUTKA H., SACCHETTI F. The focussing monochromator of IN4C. *Journal of Neutron Research* **5**, 103-107 (1996)
- NARDI F., DOSTER W., TIDOR B., KARPLUS M., CUSACK S., SMITH J.C. Dynamics of tRNA: experimental neutron spectra compared with a normal mode analysis. *Israel Journal of Chemistry* **34**, 233-238 (1994)
- NEILSON G.W., ANSELL S., WILSON J. The structural and dynamic properties of some transition metal aqua cations: results from neutron scattering. *Zeitschrift für Naturforschung A* **50**, 247-256 (1995)
- NEILSON G.W., ENDERBY J.E. Aqueous solutions and neutron scattering. *Journal of Physical Chemistry* **100**, 1317-1322 (1996)
- NEOV S., KOZHUKHAROV V., TRAPALIS C., CHIEUX P. Short range order investigation of binary TeO_2 - PbBr_2 and TeO_2 - PbCl_2 glasses. *Physics and Chemistry of Glasses* **36**, 89-94 (1995)
- NEU R., ASMUSSEN K., FUSSMANN G., GELTEN-BORT P.G., JANESCHITZ G., SCHÖNMANN K., SCHRAMM G., SCHUMACHER U., ASDEX Upgrade team - Monitor for the carbon and oxygen impurities in the ASDEX Upgrade tokamak. *Review of Scientific Instruments* **67**, 1829-1833 (1996)
- NEVILLE A.J., RAINFORD B.D., ADROJA D.T., SCHOBER H. Anomalous spin dynamics of CePdSb . *Physica B* **223-224**, 271-274 (1996)
- NIELD V.M., MCGREEVY R.L., KEEN D.A., HAYES W. Structural disorder in CuBr . *Physica B* **202**, 159-166 (1994)
- NORLIDAH M.N., VENTURINI G., MALAMAN B., RESSOUCE E. Magnetic structures of the new TbFeSi_2 -type structure germanides: $\text{RMnCu}_{0.5}\text{Ge}_{1.5}$ (R=La, Ce, Pr). *Journal of Alloys and Compounds* **244**, 121-130 (1996)
- NORWIG J., WEITZEL H., PAULUS H., LAUTENSCHLAGER G., RODRIGUEZ-CARVAJAL J., FUESS H. Structural relations in mixed oxides $\text{Cu}_x\text{Zn}_{1-x}\text{Nb}_2\text{O}_6$. *Journal of Solid State Chemistry* **115**, 476-483 (1995)
- NOZIERES P. The Grinfeld instability of stressed crystals. In "Spatio-Temporal Patterns in Nonequilibrium Complex Systems - NATO Advanced Research Workshop", CLADIS P.E., PALFFY-MUHORAY P. Eds. (Addison-Wesley Publishing Company, 1995) pp. 65-75
- OGANESSIAN Y.T., KARAMIAN S.A., SZEGLOWSKI Z., BRIANCON C., CONSTANTINESCU O., HUS-SONNOIS M., MURADIAN G.V. Resonance neutron capture reaction on isomeric target of ^{178}Hf m2. In "Proceedings of the ISINN-2 Neutron Spectroscopy, Nuclear Structure, Related Topics" (1994) pp.136-144
- OLAZCUAGA R., LE FLEM G., BOIREAU A., SOUBEYROUX J.L. The structure of the high temperature forms of $\text{Cu}^{II}_{0.5}\text{Ti}_2(\text{PO}_4)_3$ and $\text{D}_{0.5}\text{Cu}^{II}_{0.5}\text{Zr}_2(\text{PO}_4)_3$. *Advanced Materials Research* **1-2**, 177-188 (1994)
- OTAKE Y., ZEYEN C.M.E., FORTE M. Dual polarised beam polarimeter: a highly sensitive tool for the detection of very small neutron spin rotation. *Journal of Neutron Research* **4**, 215-219 (1996)
- PAASCH M., MCINTYRE G.J., REEHUIS M., SONN-TAG R., LOIDL A. Neutron diffraction study of $(\text{NH}_4)_2\text{I}_{0.73}(\text{K})_{0.27}$. *Zeitschrift für Physik B* **99**, 339-344 (1996)
- PAASCH M., WINTERLICH M., BÖHMER R., SONN-TAG R., MCINTYRE G.J., LOIDL A. The phase diagram of $(\text{NH}_4)_2\text{I}_{0.73}(\text{K})_{0.27}$. *Zeitschrift für Physik B* **99**, 333-338 (1996)
- PAOLASINI L., LANDER G.H., SHAPIRO S.M., CACIUFFO R., LEBECH B., REGNAULT L.P., RÖSSLER B., FOURNIER J.M. Enhanced exchange in the itinerant ferromagnet UFe_2 . *Europhysics Letters* **34**, 459-464 (1996)
- PAOLASINI L., LANDER G.H., SHAPIRO S.M., CACIUFFO R., LEBECH B., REGNAULT L.P., RÖSSLER B., FOURNIER J.M. Magnetic excitations in the itinerant ferromagnet UFe_2 . *Physical Review B* **54**, 7222-7232 (1996)
- PERRING T.G., TAYLOR A.D., SQUIRES G.L. High-energy spin waves in hexagonal cobalt. *Physica B* **213-214**, 348-350 (1995)
- PETKOV P., ANDREJTSCHIEFF W., BÖRNER H.G., ROBINSON S.J., KLAY N., YAMADA S. Level scheme and electromagnetic transition strengths in ^{177}Lu . *Nuclear Physics A* **599**, 505-544 (1996)
- PRICE D.L., SABOUNGI M.L., HOWELLS W.S. Orientational and translational disorder in semiconducting Zintl compounds. *Physical Review B* **51**, 14923-14929 (1995)
- QUEMERAIS P. Crystallization of polarons in doped ionic materials. *Modern Physics Letters B* **9**, 1665-1672 (1995)
- RADAELLI P.G., MAREZIO M., HWANG H.Y., CHEONG S.W. Structural phase diagram of perovskite $\text{A}_{0.7}\text{A}'_{0.3}\text{MnO}_3$ (A=La, Pr, A'=Ca, Sr, Ba): a new Imma allotrope. (Letter to the editor). *Journal of Solid State Chemistry* **122**, 444-447 (1996)
- RADAELLI P.G., MAREZIO M., HWANG H.Y., CHEONG S.W., BATLOGG B. Charge localization by static and dynamic distortions of the MnO_6 octahedra in perovskite manganites. *Physical Review B* **54**, 8992-8995 (1996)
- RAINFORD B.D., NEVILLE A.J., ADROJA D.T., DAKIN S.J., MURANI A.P. Low temperature excitations in CeRu_2Si_2 , Ce_2 alloys. *Physica B* **223-224**, 163-165 (1996)
- RANDL O.G., VOGL G., KAISERMAIR M., BÜHRER W., PANNETIER J., PETRY W. Unusually high vacancy concentrations in Ni_3Sb . *Journal of Physics Condensed Matter* **8**, 7689-7698 (1996)
- RANDL O.G., VOGL G., PETRY W. Phonons - A diffusion motor in intermetallics? *Physica B* **219-220**, 499-501 (1996)
- RAVEY J.C., STEBE M.J., SAUVAGE S., ELMOUJAHID C. Membrane structures of aqueous fluorinated non-ionic surfactants. *Colloids and Surfaces A* **99**, 221-231 (1995)
- REEHUIS M., DANEBROCK M.E., RODRIGUEZ-CARVAJAL J., JEITSCHKO W., STÜSSER N., HOFMANN R.D. Antiferromagnetic order of the lanthanoid moments in the carbides Ln_2ReC_2 with $\text{Ln}=\text{Tb}$, Dy , Ho and Er . *Journal of Magnetism and Magnetic Materials* **154**, 355-364 (1996)
- RENKER B., SCHOBER H., GOMPF F. Lattice dynamics and electron-phonon coupling in superconducting $\text{HgBa}_2\text{CuO}_4$ investigated by inelastic neutron scattering. *Journal of Low-Temperature Physics* **105**, 843-848 (1996)
- RENKER B., SCHOBER H., GOMPF F., HEID R., RESSOUCE E. Lattice dynamics of RbC_{60} in its rotator, polymer, and dimer phase: a neutron-scattering investigation. *Physical Review B* **53**, R14701-R14704 (1996)
- REQUARDT H., KALNING M., BURANDT B., PRESS W., CURRAT R. Critical x-ray scattering at the Peierls transition in the quasi-one-dimensional system $(\text{TaSe}_4)_2\text{I}$. *Journal of Physics Condensed Matter* **8**, 2327-2336 (1996)
- REZNIK D., BOURGES P., FONG H.F., REGNAULT L.P., BOSSY J., VETTIER C., MILIUS D.L., AKSAY I.A., KEIMER B. Direct observation of optical magnons in $\text{YBa}_2\text{Cu}_3\text{O}_{6.2}$. *Physical Review B* **53**, R14741-R14744 (1996)
- RICHARD D., FERRAND M., KEARLEY G.J. Analysis and visualisation of neutron-scattering data. *Journal of Neutron Research* **4**, 33-39 (1996)

EDITORS: HERMA G. BUTTNER, ALAN J. LEADBETTER
LAYOUT: SOFT OFFICE – E-MAIL: SOFTOFFICE@DIAL.OLEANE.COM
PHOTOGRAPHY BY J.-L. BAUDET, H.G. BUTTNER, S. CLAISSE, J. ITALIA (ILL), STUDIO DE LA REVIRÉE
PRINTING: LA GUTENBERG
APRIL 1997

ACKNOWLEDGEMENT
WE WOULD LIKE TO THANK ALL PEOPLE WHO HELPED MAKE THIS REPORT.

FURTHER COPIES CAN BE OBTAINED FROM:
INSTITUT LAUE-LANGEVIN
SCIENTIFIC COORDINATION OFFICE (SCO)
BP 156 – F-38042 GRENOBLE CEDEX 9 (FRANCE)
TEL: +33 4 76 20 72 40 – FAX: +33 4 76 48 39 06
EMAIL: [KJENKINS@ILL.FR](mailto:kjenkins@ill.fr) OR SCO@ILL.FR
WEB: <http://www.ill.fr>

